Static and Dynamic behaviour of pile supported structures in soft soil

Guillermo Alfonso Lopez Jimenez

Communauté
UNIVERSITÉ Grenoble Alpes

THÈSE

Pour obtenir le grade de

DOCTEUR DE LA COMMUNAUTE UNIVERSITE GRENOBLE ALPES

Spécialité : **Doctorat IMEP2/MATERIAUX, MECA, GENIE CIVIL, ELECTROCHIMIE**

Arrêté ministériel : 25 mai 2016

Présentée par

Guillermo Alfonso LOPEZ JIMENEZ

Thèse dirigée par **Daniel DIAS, Professeur**
et
coencadrée par **Orianne JENCK, Maître de Conférences**

préparée au sein du **Laboratoire 3SR**
dans **l'École Doctorale IMEP2**

Static and dynamic behavior of pile supported structures in soft soil

Thèse soutenue publiquement le **26/06/2019**,
devant le jury composé de :
Mr Luc, THOREL
Directeur de recherche, IFSTTAR Bouguenais (Président, Rapporteur)
Mr Panagiotis, KOTRONIS
Professeur des Universités, Ecole Centrale Nantes (Rapporteur)
Mr Christophe, DANO
Maître de Conférences, Université Grenoble Alpes (Examinateur)
Mr Jérôme, RACINAIS
Menard, (Examinateur)
Mr Cyril, SIMON
EDF, (Examinateur)
Mr Daniel, DIAS
Professeur des Universités, Université Grenoble Alpes (Directeur de la thèse)
Mme, Orianne, JENCK
Maître de Conférences, Université Grenoble Alpes (Co-encadrante)

ABSTRACT

A great amount of earthquakes have caused the collapse of important structures along the history. The design of earthquake-resistant structures depends greatly of the soil-structure interaction. This interaction implies the consideration of relative movements and load transfer mechanism simultaneously. Dealing with liquefiable soils the generation of pore pressure should also be considered.

Pile system constitutes a common foundation of structures resting on soil layers of low stiffness and strength in seismic zones. More recently rigid inclusion systems were utilized. The difference is that in the rigid inclusion systems, the rigid elements are separated from the foundation slab by an earth platform that is able to transfer the surface loads and dissipate energy coming from the seismic loading.

This manuscript studies the behavior, through numerical models, of inclusions systems (soil-inclusion-platform-structure) and pile systems (soil-pile-structure) considering soft soils under seismic loadings. Finite difference numerical models were developed using Flac3D. Several types of soils were utilized in drained and undrained conditions. For the undrained cases, the analyses were carrying out using dynamic coupled fluid-mechanical simulations with accuracy the behavior of soils. The Rayleigh damping approach was applied to provide additional damping in the elastic part when simple elasto-plastic constitutive models were considered.

The objective of the investigation is the identification of the impact of important factors in the response of the analyzed systems. Factor such as the foundation type, the frequency of the input motion, the dynamic characteristics of the structure, the soil profile and the relative density were investigated. Considering the pile and rigid inclusion foundations, the support conditions, the pile group configuration, the pile length, the embedment of the foundation were also examined.

Additional and important aspects of numerical models were also explored like the model geometry, dynamic boundary conditions, element size, interface elements, structural element types, dynamic loading.

Results in terms of movements and stresses in the soil, superstructure and rigid elements were obtained. They show the great influence of some parameters in the response (accelerations, displacements, efforts, strains, pore pressure) of the evaluated systems. Others highlight the importance of a type of failure in the elements of the system.

Keywords: pile; rigid inclusion; numerical modelling; dynamic analysis; soil structure interaction; liquefaction

RESUME

De nombreux tremblements de terre ont provoqué l'effondrement de structures importantes. La conception des structures résistant aux séismes dépend fortement de l'interaction sol-fondation-structure. Cette interaction implique la prise en compte simultanée des mouvements relatifs et des mécanismes de transfert de charge. En ce qui concerne les sols liquéfiables, la génération des pressions interstitielles doit également être prise en compte.

Le renforcement des sols compressibles par des pieux est une solution très utilisée pour supporter les structures dans des zones sismiques. Plus récemment, la technique de renforcement par inclusions rigides a été utilisée. La différence entre les deux techniques réside dans le fait que, dans la technique du renforcement par inclusions rigides, un matelas de transfert de charge est intercalé entre la structure et les têtes des inclusions rigides. L'utilisation du matelas permet la dissipation d'énergie liée au séisme.

Ce travail de thèse étudie le comportement sismique des sols compressibles renforcés par des pieux (système sol-pieux-structure) et des inclusions rigides (système sol-inclusions-matelas-structure). L'étude est effectuée à l'aide d'une modélisation numérique tridimensionnelle par différences finies avec le code Flac3D. Plusieurs types de sol ont été considérés en prenant en compte des états drainés et non drainés. Pour les cas non drainés, les analyses ont été réalisées à l'aide de simulations hydro-mécaniques couplées. Des modèles constitutifs simples et complexes ont été utilisés pour représenter le comportement du sol. Un amortissement de type Rayleigh a été appliqué pour fournir un amortissement supplémentaire à la partie élastique lorsque des modèles constitutifs élastoplastiques simples ont été considérés.

L'objectif de ce travail est d'identifier l'impact des facteurs importants sur la réponse des systèmes analysés. Des nombreux paramètres comme le type de fondation, la fréquence du chargement, les caractéristiques dynamiques de la structure, le profil de sol et la densité relative ont été étudiés. En tenant compte des fondations sur pieux et des inclusions rigides, les conditions aux extrémités des pieux, la configuration du groupe de pieux, la longueur des pieux et l'encastrement des fondations ont également été investigués.

Des aspects importants relatifs aux modèles numériques ont également été explorés tels que la géométrie du modèle, les frontières absorbantes, la taille des éléments du maillage, les éléments d'interface, les éléments structurels et le chargement dynamique.

Les mouvements et contraintes dans le sol, les structures et les éléments rigides de renforcement ont été analysés et ont permis de mettre en évidence l'influence des divers paramètres étudiés. Cette étude a permis de mettre en évidence l'influence de certains paramètres dans la réponse (accélérations, déplacements, efforts, contraintes, pression interstitielle) des systèmes évalués. Le type de rupture dans les éléments des systèmes étudiés ont également été mis en évidence.

Mots-clés: pieux; inclusion rigide; modélisation numérique; analyse dynamique; interaction de la structure du sol; liquéfaction

Dedicated
to
Anahi,
Fernanda and Renata

ACKNOWLEDGEMENTS

First of all, I would like to express my deepest gratitude to my supervisor, Professor Daniel Dias, for giving me the opportunity to develop this thesis under his supervision. Thank you for your support, guidance and constructive suggestions during the development of this work. I would also like to extend my gratitude to my co-supervisor Orianne Jenck for her advices and recommendations on this research work.

I would like to thank you to my friends and colleagues in the 3SR laboratory. Work in this laboratory was a great experience.

I want to express my gratitude to my family in Mexico. Their support in all aspects also contributed to complete this work.

I would like to thank you to my friends in Grenoble, particularly to Clément Lemaignan for all his help and advices.

Finally, I want to express my special thanks to CONACYT for grant me to carry out my PhD studies.

TABLE OF CONTENTS

LIST OF FIGURES

LIST OF TABLES

Chapter 1 BUILDING STRUCTURES ON SOFT SOIL IN SEISMIC AREAS?

1.1. Motivation and Overview

Many buildings, bridges, storage tanks and other type of structures have been critically damaged during severe earthquake events along the history. The damage in these structures has been extensively studied from the structural point of view considering a fixed-base condition, which is reasonable for light structures supported by relatively stiff soil. Various patterns of failure have been observed under these conditions. However, the damage caused by earthquakes suggests that the seismic behavior of structures depends greatly on the response of the structure itself, but also on the foundation and underlying soil. This means that the performance of the structure can be modified due to the soil-structure interaction (SSI) effects, the earthquake characteristics, the travel path of the seismic wave and the nonlinear response of the soil.

The design of structures subjected to earthquakes requires the understanding of the soil-foundation-structure interaction during the seismic loading. The induced motion due to the incident waves during earthquake loading generates inertial forces in the structure which results in stresses in the foundation that are, in return, propagated through the soil. The site effects are function of the mechanical and geometrical characteristics of the subsoil conditions and earthquake motion at its base. The significance of these effects was evident in seismic events such as in 1995 Kobe earthquake, where the liquefaction of soil occurred, or in 1985 during the Mexico City earthquake where the soil amplified the ground motion (Seed et al. 1988).

The densification of cities has rarefied the zones with good quality soils and has pushed the construction of structures in areas seismically active and with low geotechnical conditions. Under these conditions, shallow foundations, compensated raft foundations and pile foundation have been utilized to support structures. However, the pile foundation technique has been the most common systems to support structures in presence of soft soils. More recently, structures founded on rigid inclusions have been constructed. The rigid inclusion system is similar to the pile system with the difference that the inclusions are not connected with the slab foundation. A load transfer platform (LTP) is setup between them. In seismic areas, this platform is very functional because it is considered as a zone of energy dissipation. An effective application of both systems implies the reduction of total and differential settlements in the structure and the increase of the bearing capacity.

Despite the fact that the use of pile foundations is an economic and effective alternative to support structures in soft soils, many structures (bridges, buildings, tanks, and highways) founded with this system have collapsed during important earthquakes such as Niigata 1964, San Fernando 1971, Loma Prieta 1989, Kobe 1995, Mexico City 1985 and 2017. As examples, Fig. 1.1 shows the collapse of two

pile-supported structures. The direct implications of the collapse of structures are the high human and economic costs.

Although the soil-foundation-structure interaction effects have been studied after these earthquake events, the available design procedures have been highly simplified in the codes currently used (Japan Society of Civil Engineers 2005, Caltrana 2006, BSSC 2009, Eurocode 8 1998). These simplified methods consider the response of the structure modelled as a single degree of freedom oscillator and the computation of the impedance matrix permits to represent the soil dynamic response. However, they neglect the presence of the foundation, the nonlinear behavior of the soil and the evolution of the soil stiffness and damping with strain. Hence, it is of high importance to investigate the influence of the SSI in the seismic response of the structures supported by pile foundations.

Numerous studies solved the soil-foundation-structure interaction through experimental, numerical, and semi analytical approaches, varying the degrees of idealization and simplification. Experimental approaches such as shaking tables and centrifuge tests offer the advantage of simulating systems under controlled conditions allowing the understanding of fundamental mechanism in the systems. Dealing with simplified geometries, the Winkler method and the elastic column approach are utilized. However, the use of numerical models becomes an alternative solution when the systems are non-linear or/and have a 3D geometry, for real site conditions simulation or for analyzing a large set of parametric conditions.

This study aims at evaluating the response of systems considering the SSI. The idea is to determinate and to understand the influence of the important factors in the behavior of pile systems (soil-pile-structure) and inclusion systems (soil-inclusion-platform-structure) during earthquake loadings. In dynamic analysis, the response of these systems is the result of complex processes that relates the inertial interaction between the structure and the foundation and the kinematic interaction between the rigid elements and the soil (Wolf 1985).

To achieve this goal, fully coupled three-dimensional analyzes of both systems were developed using the finite difference software Flac3D (Itasca 2012). Different constitutive models with different levels of complexity have been utilized to represent adequately the soil behavior. This has allowed going further in the understanding of this type of systems. The effect of principal aspects such as the pile support conditions, the pile group configuration, the pile length, the dynamic characteristic of the structure, the frequency of the input motion, the soil profile, and the value of relative density in liquefiable soils were investigated. Soils in drained and undrained conditions have been considered.

Additional aspects of the modelling such as the model geometry, dynamic boundary conditions, element size, conditions at the interfaces, structural elements types, damping parameters, dynamic

loading, among others were investigated to get access to the complexity of the systems. Due to the wide spectra of conditions studied the computation time was a limitation for an extensive parametric study.

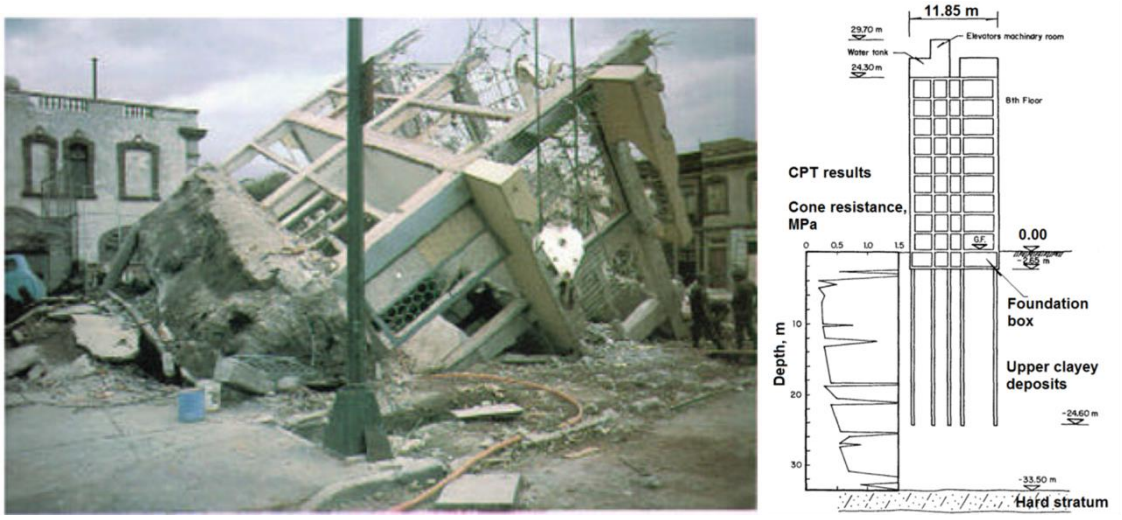

a) Building collapse during the 1985 Mexico City Earthquake. Foundation and geotechnical conditions (Mendoza and Auvinet 1988).

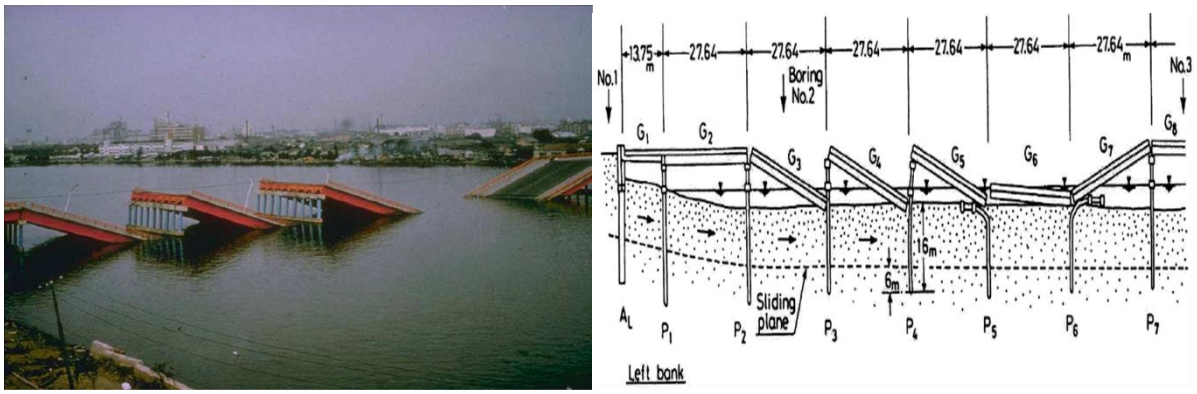

b) Showa bridge collapse during the 1964 Niigata Earthquake. Schematic diagram of the fall-off of the girders in the bridge (Bhattacharya 2003).

Fig. 1.1 Collapse of structures during severe seismic events

1.2. Objectives and Scope of the Study

The main objectives of this work are to investigate the seismic response of soil-foundation-structure systems (pile and rigid inclusion systems) in the presence of softs soils and to analyze the effect of key parameters that can influence the response of the systems using 3D numerical models.

Specifically, the present work has focused on:

- Model the entire three-dimensional soil-foundation-structure systems adopting the direct method. The direct method (Section 2.2.2 Chapter 2) was used to represent in a realistic manner the geometrical complexity and the connection between elements, as well as the material properties.

- Study the soil-foundation-structure systems considering different types of soils in drained and undrained condition. Examine the potential liquefaction phenomena in soils with different relative density values in undrained analyses.

- Investigate the impact of the use of different constitutive models with different levels of complexity to represent the soil behavior on the response of the analyzed systems.

- Examine the effect of the pile type and the fixity conditions. Several pile toe conditions were thus considered, namely the case of the placement of the pile toe on the bedrock, of anchored and of floating piles.

- Explore the effect of the Rayleigh damping parameters in the dynamic response of soil-foundation-structure systems.

- Study the influence of the dynamic characteristics of the structures in the soil-structure interaction phenomenon utilizing different type of structures.

- Analyze the importance of the dynamic loading characteristics on the response soil-foundation-structure systems. The use of different input motion frequencies is investigated in the developed models.

- From these results, develop a better knowledge of the behavior of these systems in order to propose important factors that should be considered for a best design of the soil-foundation-structure systems.

- Develop partial validations of the modelling procedure to show that the results are consistent with the results already known in the literature (experimental tests or analytical procedures).

1.3. Organization of the Thesis

The structure of the thesis is as follows.

Chapter 2 presents a brief literature review relating to the soil-structure interaction theory and the previous research works, the important aspect in the static and dynamic behavior of soil, the theoretical framework for the soil in drained and undrained condition, the liquefaction phenomenon and an overview of the soil constitutive models dealing with dynamic loading.

Chapter 3 is devoted to describe the modelling characteristic using finite difference method (Flac3D). The soil and structural elements, the types of damping boundary conditions, the interfaces and the dynamic analysis utilized in the different developed models are described.

Chapter 4 analyses the dynamic response of soil-pile-structure and of soil-inclusion-platform-structure for different pile types (floating, placed or anchored in a hard soil). The influence of the structural mass, the frequency of the input motion, the soil plasticity, the embedment of slab foundation, the pile flexural rigidity and the pile group configuration were also investigated. The results were presented in terms of surface response spectra. The bending moments, normal forces and displacements along the rigid elements were compared for all cases. Two reference cases were studied to demonstrate that the behavior of the analyzed systems is in accordance with results demonstrated in literature.

Using different values of minimum damping ratio (ξ_{min}) and frequency (f_{min}), and different earthquakes input motions with different predominant frequencies, the effects of the Rayleigh damping parameters in pile and inclusion systems were studied in the second part of Chapter 4.

Chapter 5 investigates the influence of the dynamic characteristics of the structure considering buildings with different heights (3-storeys to 7-storeys) founded on piles or inclusions systems under seismic loading. Values of the maximum lateral displacements, of the inter-storey drifts and of the shear forces distribution in the buildings as well as rocking of the foundation are presented. Considering the foundations, efforts and displacements are compared for the different systems. Two soil conditions are analyzed: drained in Chapters 4 and 5, undrained in Chapter 6.

Chapter 6 analyses numerical models with a 3-storey reinforced concrete frame founded on inclusions systems and pile systems considering a liquefiable soil. The influence of the soil profile, pile length and frequency of the seismic loading were explored. Different relative density values of the liquefiable layer were considered using a model that predicts with accuracy the soil response for various soil densities, stress levels and loading conditions. For each case, the spectrum response, shear

forces in the building and rocking of foundations were obtained. Maximum shear strains and excess pore pressures are presented at different depths. The efforts and displacements in the rigid elements (piles or rigid inclusions) were also compared for the different systems. The bending and buckling failure modes of the pile were examined.

The final part of this work concludes this research and permits to show which parameters are important and indeed controlling the behavior of the analyzed systems. Recommendations are given to designers for building pile-founded structures in soft soil under seismic loadings.

Chapter 2 WHAT WE KNOW AND WHAT WE DON'T

1. Vertical Systems

1.1. Pile System

The pile foundation technique is an efficient alternative to support structures in the presence of soft soil. The loads from the structure are carried through this system and transferred to deeper stiffer soil layers (Fig. 2.1a). The piles elements may be required to resist uplift forces when used to support tall structures that applied great overturning moments on the foundation. The pile elements transfer part of the surface structure loads to the soil by shearing mechanisms generated along their shaft (shaft resistance) and other part by normal stresses generated at their base (base resistance). They are also referred as floating and end-bearing piles respectively.

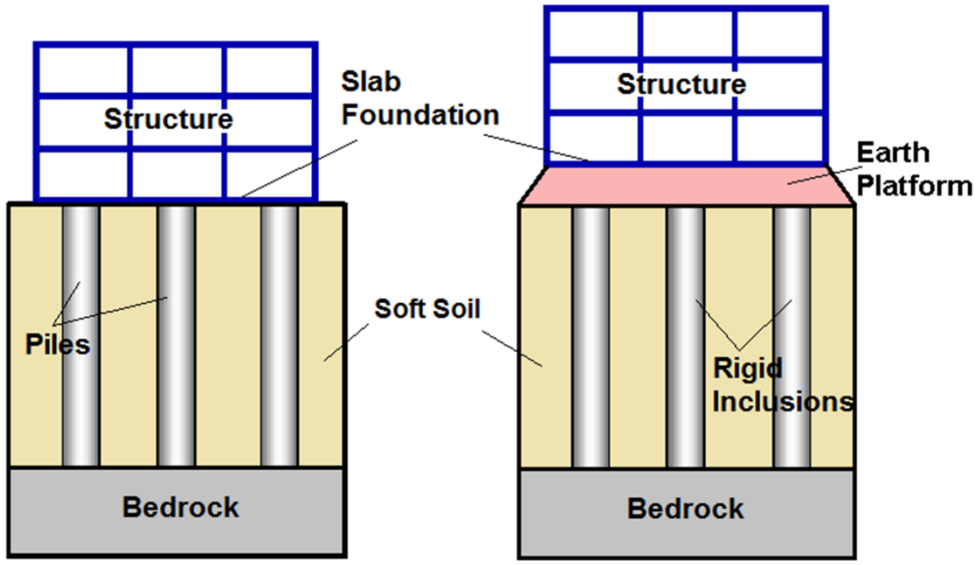

a) Soil-pile-structure system **b)** Soil-inclusion-platform-structure system

Fig. 2.1 Vertical Reinforcement Systems

1.2. Rigid Inclusion System

The rigid inclusion system is considered to be an interesting ground improvement technique in poor soil conditions. This technique allows improving the properties of the ground to support structures using simple shallow foundations. The rigid inclusion system is similar to the pile foundation system with the difference that the inclusions are not connected with the slab foundation (Fig. 2.1b). However, the behavior of these systems is different. In the rigid inclusion system, an LTP is disposed between the compressible layer and the surface structure. The LTP is also referred in this study such as earth platform or mattress. The great advantage of this reinforcement technique in seismic areas is the

fact that the LTP constitutes a dissipation zone of energy between the structure and the vertical rigid elements.

The function of the platform is to transmit surface loads to the head of the rigid inclusions and to uniform the settlements. The arching effect in the platform, caused by shearing mechanisms due to differential settlements of the soil and inclusions, allows a transfer of the load to the rigid elements. Due to the fact that inclusions have a greater stiffness than the surrounding soil, the settlements of the inclusions are smaller than the soft soil, which cause relative displacements of soil in the platform between the zones that are in contact with the heads of inclusions and with the zone between the inclusions. In other words, there is a decrease of the vertical stress acting on the soft soil between the pile head and the inclusions. A schematic diagram of the effect is shown in Fig. 2.2.

The design of LTP consists of the design of its geometry, stability and load transfer mechanism through soil arching. However, most uncertainties of the platform design lie on the load transfer mechanism, which occurs for the arching effect. Several methods to consider the arching effect have been developed dealing with static loadings. These methods can be divided in: Methods based on the equilibrium of a volume of soil in movement (Terzaghi 1943), Methods taking into account an area of influence of soil above the network of inclusions (Guido et al. 1987, Carlsson 1987, SINTEF 2002) and Methods taking into account a transfer of load in the embankment soil (Hewlett and Randolph 1988, BS 8006 1995, Kempfert et al. 1997, Van Eekelen et al. 2013).

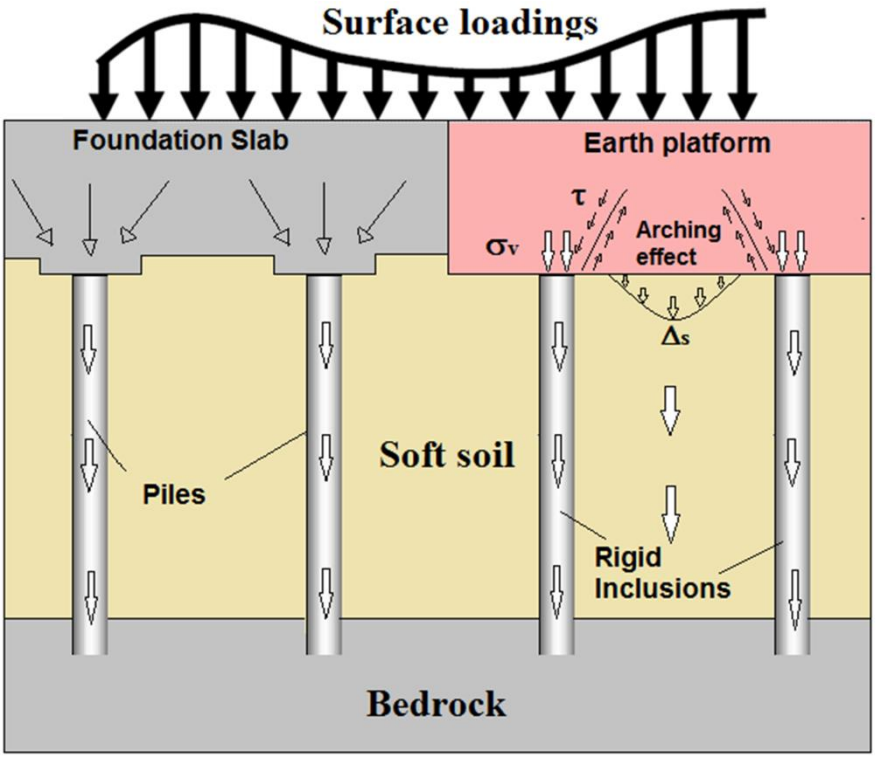

Fig. 2.2 Transfer of load in the soil-inclusion-platform-structure system (Briançon et al. 2004, Deb 2010).

Once loads have been transmitted by arching effect to the head of the rigid inclusions, the set of rigid inclusions embedded in a compressible soil have the function to transfer these loadings to a deeper stratum (Briançon et al. 2004). The amount of load transferred to the rigid inclusions depends on many factors such as the platform thickness, surcharge, compressibility of the underlying soft soil, platform mechanical properties and rigid inclusion group configuration. In a similar way as the piles, the behavior on the end-bearing inclusions depends of the stiffness of the inclusion and the strength of the hard layer, whereas for floating inclusions it depends on the inclusion penetration depth and inclusion stiffness.

The part of load that is not transferred by the arching effect to the rigid inclusions is transmitted to the soft soil underlying the LTP (Fig. 2.2). This causes an increase in the stresses and in the deformation of soil, which generates a relative displacement between the soil and the inclusion. At the top of the inclusions, the compressible soil settles more than the inclusions and induces a negative friction along the inclusion, thus transferring the stresses to the inclusions. Whereas at the bottom part, the inclusions are embedded in a layer that is not perfectly rigid, which induces a positive friction, i.e. the inclusion tends to settle more than the soil around it (Berthelot, Pezot, and Liausu 2003). In that way, the behavior of an inclusion system differs from a pile foundation system, where negative friction would be a parasitic effect.

In order to have a more efficient load transfer mechanism, it can be added the use of geosynthetics (Han and Gabr 2002) and enlarged heads (or caps) to increasing the contact area between LTP and the rigid inclusions (Chen, Ma, and Qin 2011). These elements are not considered in this study.

Here after the term “rigid element” refers to pile elements and rigid inclusion elements. They are called in that way because they have greater stiffness than the surrounding soil. The rigid elements can be prefabricated of made in situ (Briançon et al. 2004). The first ones are driven into the soil with or without previous excavation and their main advantages are that the material and the geometry of the section are controlled during their fabrication, can be produced in series and the implementation in the ground is faster than the inclusion made in situ. They can be of wood, concrete, or steel with a solid or hollow section. The second ones are constructed directly in the soft soil deposit. The implementation of these inclusions into the ground is more flexible than the prefabricated inclusions because they can adapt to the changes in site conditions, however this process makes the risk in local defects. Referring to only inclusions, they can be classified different types: in bored inclusions, vibrocompacted concrete columns, controlled modulus columns and inclusion made by soil mixing with bonding agent (Rodriguez 2001, Balfour 2013, Ménard 2013). Rigid inclusions are usually not made of reinforced concrete, unless horizontal forces are considered which is the case under seismic loading.

1.3. Application of the Pile and Rigid inclusion Systems

The systems describe above have been applied in the foundation of many structures in the presence of soft soils. Examples of these are showed in Fig. 2.3.

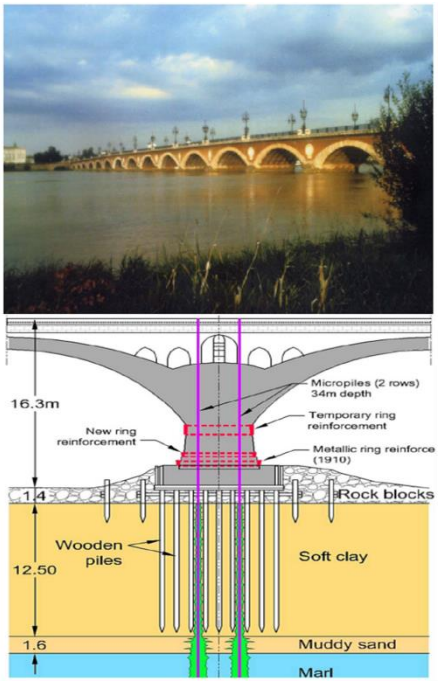

a) Vertical section of Pierre Bridge in Bordeaux. (Frank 2006)

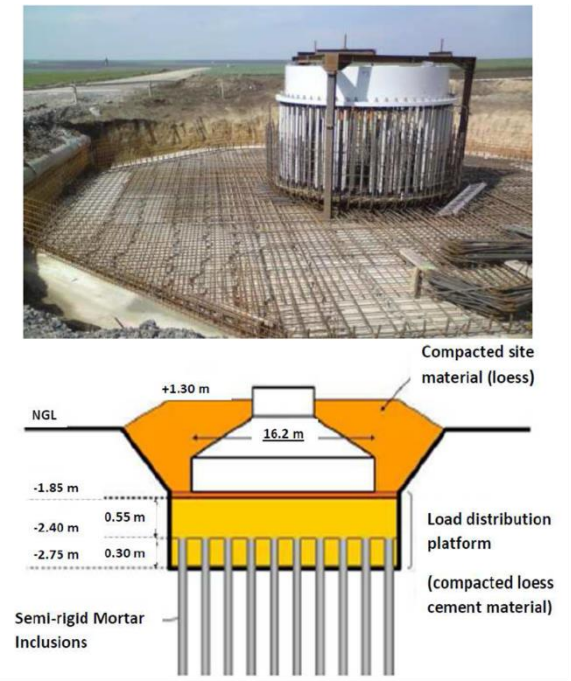

b) Improving section for foundation of wind turbines in the Dobrogea region (Neagoe 2013).

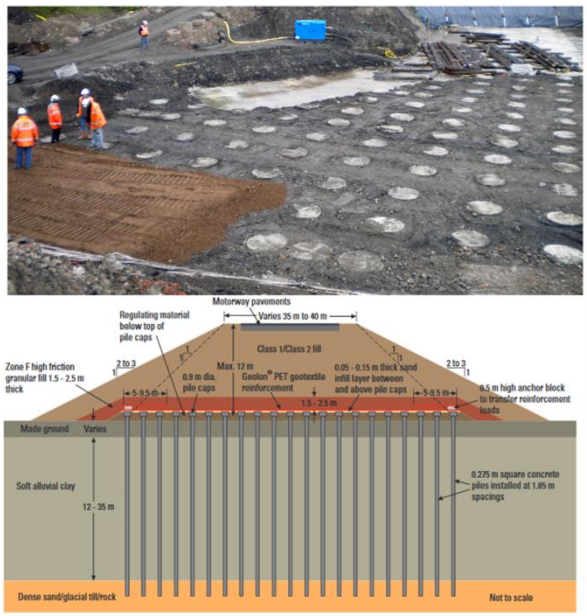

c) Bridge approach embankments, M74 Motorway Completion, Glasgow, UK. (Nowak 2013)

d) Soil Reinforcement for a inclusion bridge Rion-Antirion, Greece. (Combault and Pecker 2000)

Fig. 2.3 Applications of pile and rigid inclusion system

1.4. Damage in Pile and Inclusion Systems under Seismic Loadings

The first pile design processes under dynamic loading were based on experience (Poulos and Davis 1980). The current design codes (Japan Society of Civil Engineers 2005, Caltrana 2006,BSSC 2009, Eurocode 8 1998) apparently provide a high margin of protection using safety factors; however, failure in pile foundations has been observed in important earthquakes. Several authors have reported and analyzed some historical failure cases in their investigations (Berrill et al. 2001, Abdoun and Dobry 2002, Bhattacharya 2003, Hokmabadi 2014, Daftari 2015). Several types of damage in the pile foundations have been presented and analyzed. Table 2.1 presents some cases of damage of collapse in pile-supported structures due to earthquakes. Some of these cases are illustrated in Fig. 2.4.

Table 2.1 Damage or collapse in pile-supported structures

Earthquake	Structure	Pile and structure damage	Reference
Niggata 1964 M=7.5	Showa Bridge	Pile failure due to the lateral spreading of the surrounding soil. Buckling failure in the piles Collapse decks and bent piles	(Hamada 1992) (Ishihara 1993) (Bhattacharya 2003) Fig. 1.1b
	Family Court House building	Exceeded moment capacity at the top and bottom parts in the pile. Excessive settlements in the Building.	(Hamada 1992) Fig. 2.2b
	NHK building	Failure in piles sheared by lateral spreading near pile head and at interface of liquefiable and non-liquefiable soils.	(Hamada 1992)
	Yachiyo Bridge	Pile failure due to lateral spreading, Liquefaction. Numerous horizontal cracks in the piles caused by large bending moments. Damage to the abutment and piers.	(Abdoun and Dobry 2002) Fig. 2.2a
Mexico City,1985 M=8.1	Ten storey Building	Pile failure due to great overturning moments and loss of soil-pile adhesion. Collapse of the Building	(Meymand 1994) Fig. 1.1a
	25 buildings on mat foundation and frictional piles	Reduction in the negative skin friction on the piles due to partial loss of the shear strength of the soil during cyclic loading. Great displacements in the buildings.	(Girault 1986)
Edge-cube, 1987 M=6.3	Landing Road Bridge	Lateral spreading in piles Cracks in the piles and piers	(Berrill et al. 2001) Fig. 2.2c
Loma Prieta, 1989	Highway 1	Excessive lateral pile deflections and flexural or	(Meymand 1994)

M=7.0	Bridge Crossing Struve Slough	shear failures at the connection with the bent. Collapse of the structure	Fig. 2.2d
Kobe, 1995 M=7.2	3-storey Building	Pile failure due to lateral spreading. Building tilted and moved to the sea.	(Bhattacharya et al. 2009) Fig. 2.2e
	Hanshin Expressway	Increments of natural period due to soil-pie-structure interaction. Collapse of the structure	(Gazetas and Mylonakis 1998) Fig. 2.2f

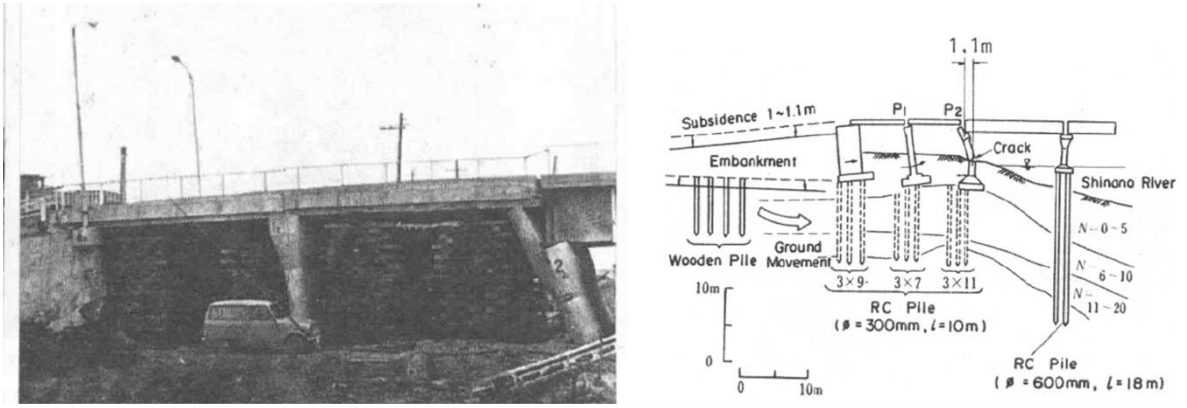

a) Damage of the abutment and piers in the Yachiyo Bridge, 1964 Niigata Earthquake (Abdoun and Dobry 2002).

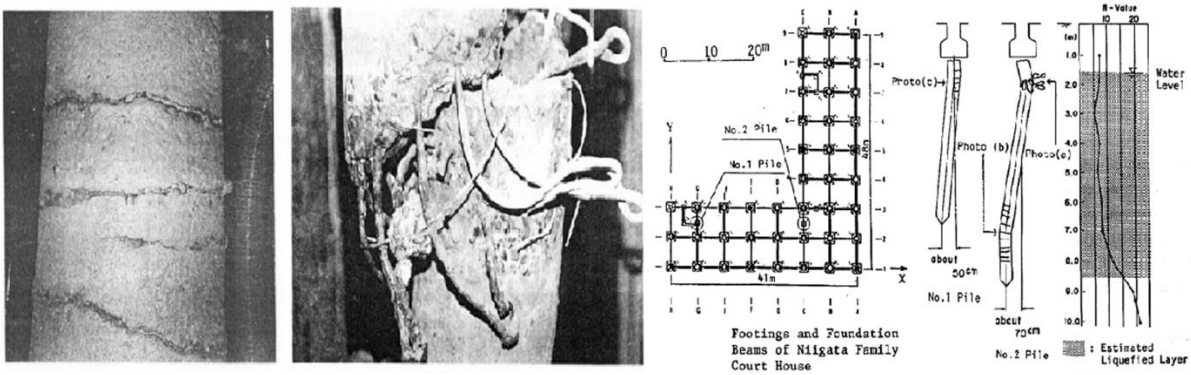

b) Pile failure in Family Court House building, 1964 Niigata Earthquake (Hamada 1992).

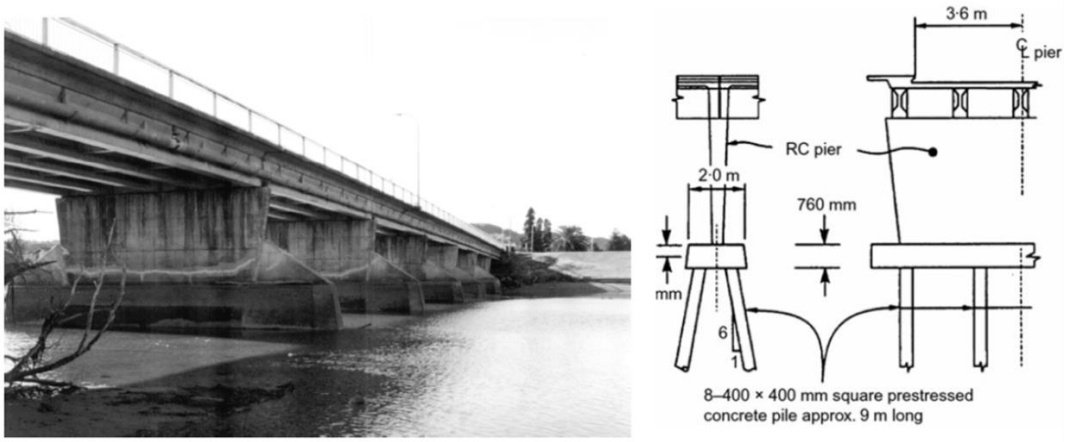

c) Damage in piles and piers in Landing Road Bridge, 1987 Edge-cube Earthquake (Berrill et al. 2001).

d) Highway 1 Crossing Struve Slough Collapsed, 1989 Loma Prieta Earthquake. Gap adjacent to the pile (Meymand 1994).

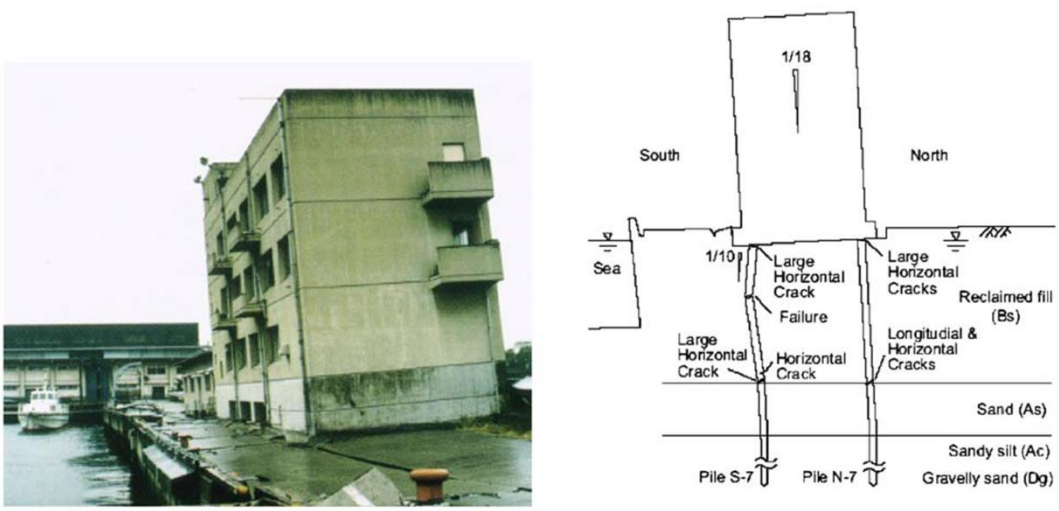

e) Tilting of a pile-supported 3-storey building, 1995 Kobe Earthquake. Formation of cracks in the pile elements. (Bhattacharya et al. 2009)

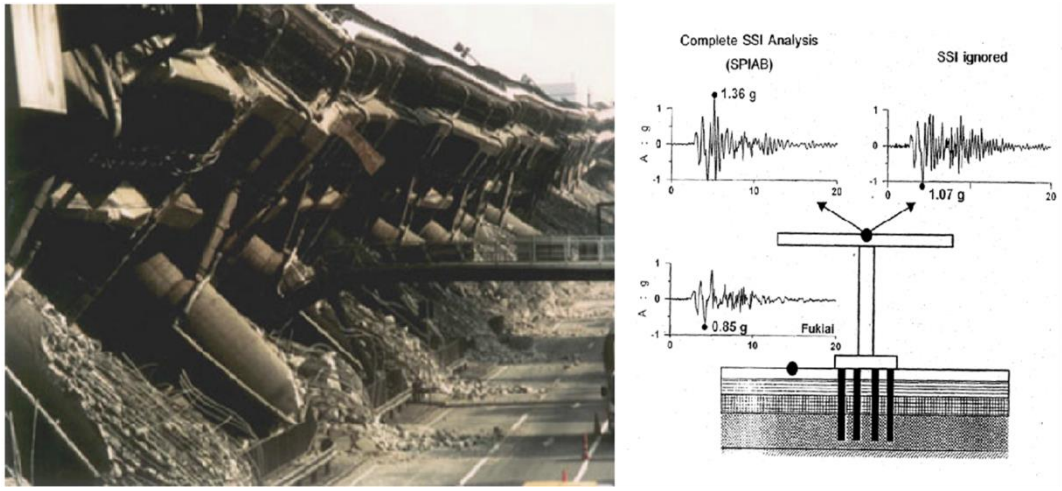

f) Part of the collapsed section of Hanshin Expressway, 1995 Kobe Earthquake. Influence of the SSI in the structure (Gazetas and Mylonakis 1998).

Fig. 2.4 Damage or collapse in pile-supported structures

It is clear from the previous observations that the pile elements have presented different types of damage or failure when subjected to seismic loadings. The potential modes of failure of piles are: 1) pile bending or shear failure due to the stiffness contrast in the soil layers, or in liquefiable and non-liquefiable soils (Fig. 2.5a). 2) Tensile pull-out, settlement or punching failure in the piles due to the loss of bearing capacity caused by liquefaction or strain softening in the soil combined with rocking in the structures (Fig. 2.5b). 3) Pile failure at head level due to excessive displacements and bending moments at the connection with cap or foundation slab mainly with tall structures (Fig. 2.5c). 4) Considering liquefaction phenomenon, other two main failure mechanisms occur: bending and buckling failure. Because these modes of failure were investigated in some sections of this research work, they are described below.

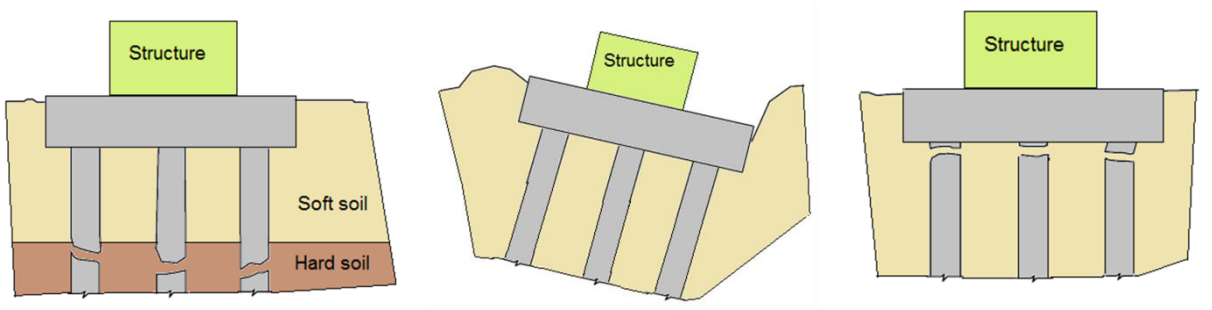

a) Pile failure at stiffness contrast

b) Bearing capacity or tension pull-out failure

c) Pile flexure/shear failure at head

Fig. 2.5 Typical pile failure modes

Bending Failure

The lateral loads may induce bending failure in the pile elements. Inertial forces of the structure and the kinematic effects due to the lateral spreading of the soil are the cause of these lateral loads. The lateral spreading refers to the flow and dragging of the liquefiable soil layer with any overlying non-liquefied layer due to the loss of shear strength. Several authors have considered this type of failure mechanism (Berrill et al. 2001, Sato et al. 2001, Tokimatsu et al. 2001, Takahashi et al. 2002). This mechanism of failure assumes that the soil pushes the pile element. Lateral loads due to the inertia of the superstructure and/or kinematic loads due to lateral spreading of the soil may induce bending failure in piles (Tokimatsu, Suzuki, and Sato 2005). There are two cases that may arise. Due to the earthquake shaking, the soil is subjected to a flow liquefaction at a particular depth which causes a lateral soil flow and the pile bending moments will be developed due to the summation of inertia and kinematic loads (Fig. 2.6). At the end of the shaking, the lateral soil flow will continue until the full dissipation of pore pressures. The bending moment is then only generated due to kinematic forces.

Buckling Failure

The buckling failure occurs when the soil surrounding pile loses its effective confining stress and may not offer sufficient lateral support during earthquake-induced liquefaction (Fig. 2.6). In this case, the pile, that is a slender element behaves as a laterally unsupported column susceptible to axial instability, which may cause that the pile buckles sideways in the direction of least elastic bending stiffness under axial load. This mechanism of failure assumes that the pile pushes the soil. Several authors have considered with this type of failure mechanism (Bhattacharya et al. 2004, Bhattacharya and Tokimatsu 2004, Haldar and Babu 2010).

The buckling load of the pile in absence of the soil may be estimated using the Eq. 2.1 (Euler critical buckling), and represents the maximum axial force at which the pile becomes unstable and the deflection becomes infinitely large (Bhattacharya and Goda 2013).

$$P_{cr} = \frac{\pi^2 EI}{L_{eff}^2} \tag{2.1}$$

where EI is the stiffness of the pile material and L_{eff} is the effective length of the pile, which depends on the fixity conditions of the element ends. In the case of an axially loaded pile in liquefiable soil, $L_{eff} = \alpha_1 (h_L + L_h)$ (Bhattacharya and Madabhushi 2008), where L_h is the length of the pile in free air/water, h_L is the depth of liquefiable soil layer and α_1 is the effective length multiplier which is a function of the boundary condition of the pile at the top and bottom of the liquefiable layer.

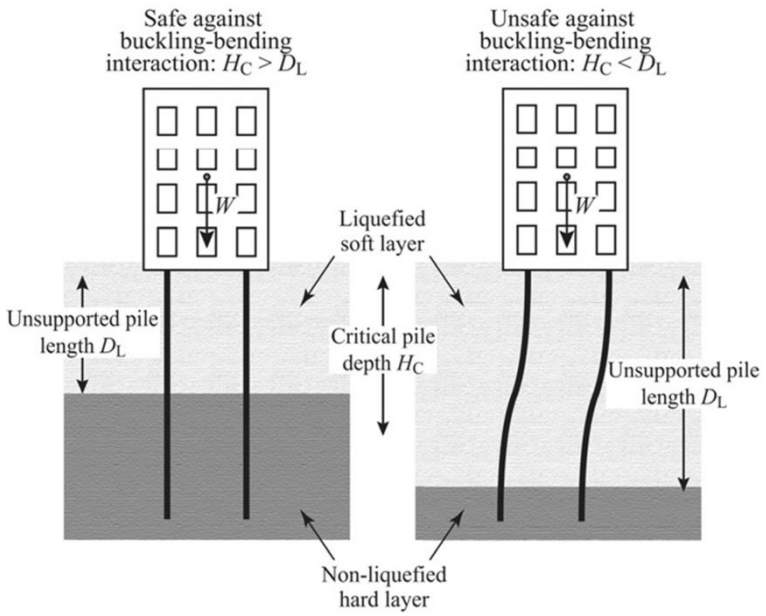

Fig. 2.6 Scheme showing the effect of bending-buckling interaction on the response of pile foundation (Bhattacharya and Goda 2013)

The lateral displacements caused by lateral load get amplified in the presence of axial loads P (Timoshenko and Gere 1961), and are given by the buckling amplification factor which is expressed by the equation

$$\frac{\delta}{\delta_0} = \frac{1}{1 - P/P_{cr}} \tag{2.2}$$

where δ_0 is the maximum lateral displacement in the critical mode shape of buckling and δ is the displacements under the same lateral loads but with the existence of axial loads. The critical load (P_{cr}) of an axially loaded structure is defined as the minimum axial load at which the structure becomes unstable and the deflections indefinitely large. It is consider in this work that the pile starts to deflect abruptly when critical buckling load is almost three times the applied load ($P/P_{cr} < 0.33$) as taken by (Haldar and Babu 2010). Bhattacharya (2003) considers a value of 0.5.

There are cases such as the Rion-Antirion Bridge (Combault and Pecker 2000) or the project of 5-storey building in Mexico City (Rodriguez and Auvinet 2006) where the rigid inclusion system has been effectively utilized in seismic zones. Despite of the fact that there are no examples of real cases in the literature about the failure of rigid inclusions, these elements are susceptible to damage or fail similar to the pile elements (Mayoral et al. 2006, Rangel-Núñez et al. 2008, Hatem 2009, Bohn 2015, Mánica-Malcom et al. 2016) except for the failure mechanism in the connection with the slab foundation. Additionally, in the rigid inclusion cases, the Prandtl's and the punching shear failure are two types of failure mechanisms that can be occurred in the LTP (not treated in this work).

It can be concluded that the pile foundations and the ground improvement by rigid inclusions are two effective systems in the presence of soft soil to transmit the surface loads to deeper resistant soil layer. The transmission of loads and the behavior of in each system are different if a seismic loading is considered.

2. Background of Soil-Structure Interaction (SSI) for seismic loadings

2.1. Concept

In a soil-foundation-structure system, the soil deformation is the result of the incident seismic waves during an earthquake event. This movement is transferred to the structure generating inertial forces that cause stresses at the foundation which in turns are propagated to the supporting soil. The properties of the soil deposits have a considerable influence on the earthquake motions experienced at the base of the superstructure. This interaction called the soil structure interaction (SSI) determines the global behavior of the system, in which the relative movements and load transfer mechanisms should

be studied simultaneously. This important phenomenon can be highlighted in the case of the collapsed section of Hanshin Expressway during the 1995 Kobe Earthquake (Fig. 2.4f). According to Gazetas and Mylonakis (1998), the fundamental period of the bridge was around 0.65 s. Considering the soil-structure interaction, the fundamental period of the system is increased to 0.93 s. It is clear from Fig. 2.7 that this change in period produces a significant increment in the response spectrum and in the response of the structure.

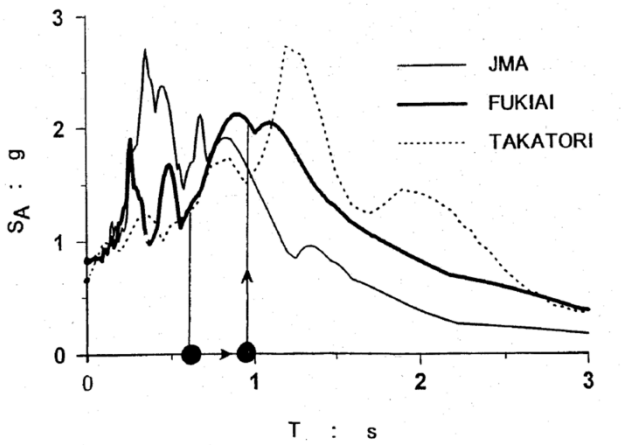

Fig. 2.7 Response spectra of the three accelerogram considered for the analysis of Route 3 section of Hanshin Expressway, 1995 Kobe Earthquake (Gazetas and Mylonakis 1998)

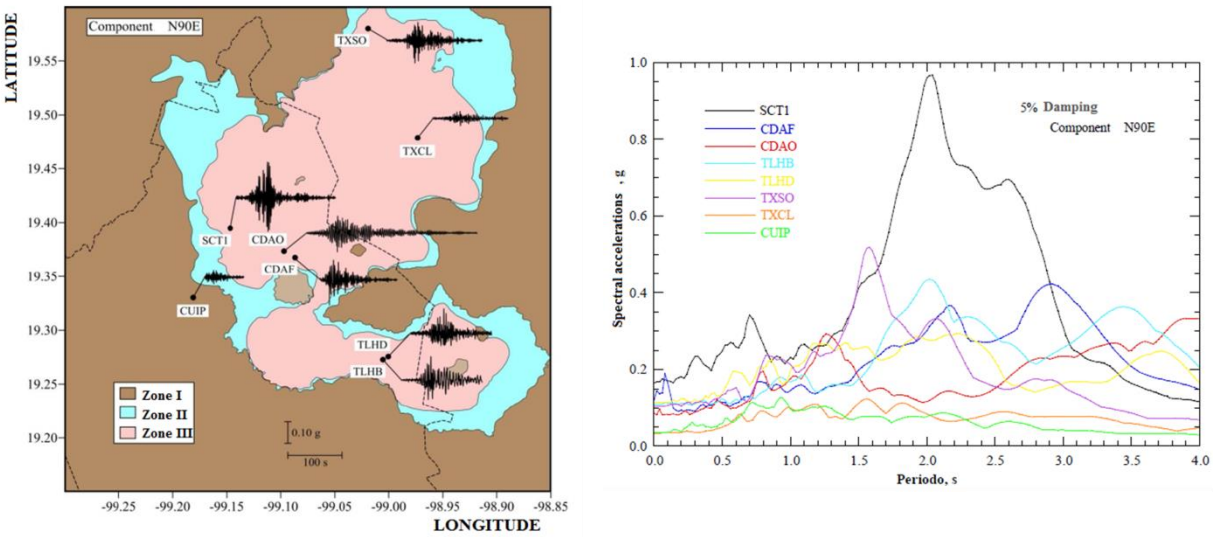

a) Acceleration records **b)** Response spectra

Fig. 2.8 Comparison of recorded motions at different sites during the Mexico City earthquake 1985 (Manica-Malcom 2013)

Another example of the importance of the site effects in the seismic characteristic was evident in the Mexico City Earthquake 1985. Great differences between the intensity and the damage in different parts of the City were observed (Seed et al. 1988). Fig. 2.8a shows the acceleration records in different stations in the City. It is noticeable that the accelerations recorded in the station SCT1at Zone III (soft

clays deposits) are greater than the acceleration in the rock and stiff soil deposits (station CUIP at Zone I). The spectra generated by these acceleration records are presented in Fig. 2.8b. The spectral accelerations in the SCT1 site were amplified around 13 times respect to the CUIP site for periods in the range of 2s.

The response of a structure under a seismic or a dynamic loading depends on the site characteristics, on the loading type, on the soil mechanical properties and on the structure and foundation type. The direct method and the substructure method are two different approaches to evaluate soil-foundation-structure systems. These two techniques are described following.

2.2. Methods of Analysis of the SSI

2.2.1. Substructure Method

In the case of the substructure method, where the principle of superposition is applicable (Kausel and Roesse 1974), the effects of the soil-structure interaction are divided into two subsystems whose response are determined independently. The kinematic interaction effects are separate from those due to the inertial interaction (Stewart et al. 1999). For the use of this method, three steps are necessary. 1) The specification of a Foundation Input Motion (FIM), which is the motion of the base slab that accounts for the stiffness and geometry of the foundation. In this step the condition of structure and base slab having no mass is considered. 2) The determination of the impedance function (stiffness and damping characteristics of the foundation-soil system). 3) The dynamic analysis of the structure supported of a compliant base represented the impedance functions and subjected to the FIM computed in step 1. These steps are represented in Fig. 2.9. The main disadvantage of this method is that it does not work for non-linear systems.

Several authors have studied pile and rigid inclusion systems through this approach. For instance, Han (2001) evaluated the effect of soil-pile-structure interaction comparing the dynamic behavior of a structure on a flexible and fixed piled foundation. Maheshwari et al. (2004) analyzed the seismic response of structures supported on pile foundations. The complete system was divided into structure and pile-foundation subsystems in which the soil nonlinearity was considered. Tokimatsu et al. (2005) studied the inertial and kinematic forces on pile-structure models using shaking table tests and considering dry and liquefiable sand deposits. Wotherspoon and Pender (2011) evaluate the response of 10-storey single framed structure supported by pile foundation under dynamic load. Nonlinear behavior of the structure and of the piles was taken in to account. The Winkler springs approach with a non-linear behavior was used to represents the interface elements in soil-pile. Di Laora et al. (2015) carried out the analysis of a tall building in Naples (Italy) that has recently undergone a seismic vulnerability assessment according to the code requirements. The building is 100 m high and is

founded in a piled raft floating in a soft soil. They used the substructure method to get the kinematic and inertial effects in the system. Messioud et al. (2016) studied the dynamic response of pile-slab, pile-mattress and pile-embankment-slab systems through a 3D finite element analysis. The dynamic impedance functions were calculated.

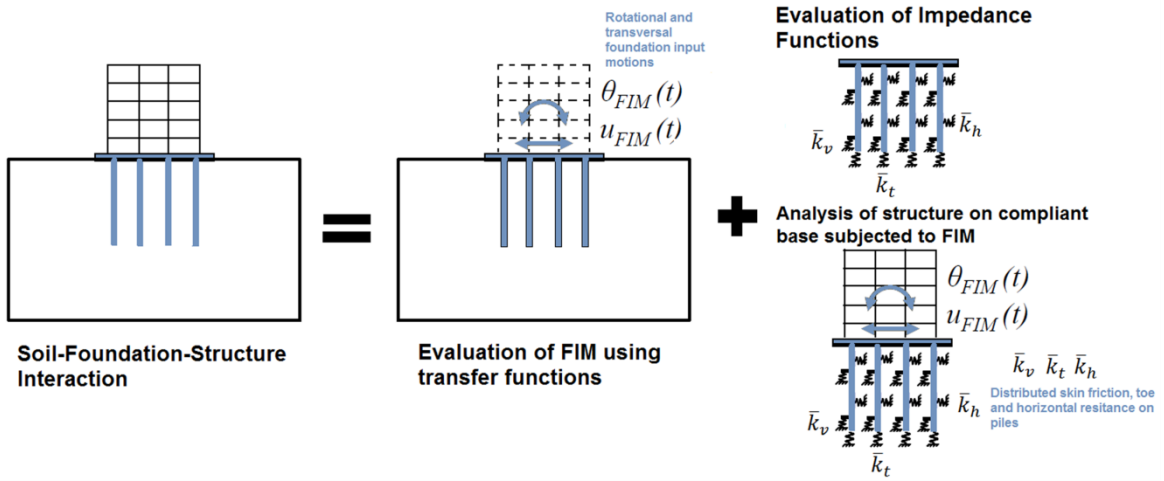

Fig. 2.9 Direct and Substructure methods in soil-pile-structure interaction

2.2.2. Direct Method

In a direct analysis (time domain analysis), the soil and the structure are included within the same model and analyzed as a complete system in a single step accounting for both inertial and kinematic interaction (Wolf, 1985). The soil is discretized in a finite domain limited by artificial boundaries which are formulated with a finite degree of freedom and represent the semi-infinite nature of soil. It is possible to take into account all the elements and their interactions (soil, structure, foundation and connections). The static and the dynamic loading and the soil nonlinear behavior can be introduced. Several researches, (Chu and Truman 2004, Lu et al. 2005, Nghiem and Nien-Yin 2008, Badry and Satyam 2016, Hokmabadi and Fatahi 2016, Mánica-Malcom et al. 2016, Ladhane and Sawant 2012, Tabatabaiefar et al. 2015, Nguyen et al. 2017) have studied the effect of the soil-pile-structure interaction on the behavior of buildings adopting the direct method to get realistic analysis. In this study the direct method was employed because of its adaptability to deal with complex geometries and material properties.

The techniques for analyzing dynamic soil-pile-structure systems include simplified analytical methods based on equivalent soil springs, numerical analyses (based on finite elements/differences or discrete elements), small scale test such as the centrifuge and shaking table and full scale prototypes (Boulanger et al. 1999).

Analytical Methods

In the simplified methods, the piles are connected to ground using non-linear *p-y* springs. Then they are affected by the horizontal movement of ground that is computed in time for the case of ground wave propagation in the vertical direction in the free-field. Examples of these methods are the elastic column, the *p-y* and the Winkler approaches. The Winkler method (Winkler 1876) utilizes a series of unconnected linear springs with stiffness (E_s) to model the soil (Fig. 2.10). With this approach the behavior of a single pile can be analyzed using the equation of an elastic beam supported on an elastic foundation (Hetenyi 1946), which is represented by the 4th order differential beam bending equation.

$$E_p I_p \left(\frac{d^4y}{dx^4}\right) + Q\left(\frac{d^2y}{dx^2}\right) + E_s(y) \quad = 0 \tag{2.3}$$

where E_p is the pile modulus of elasticity, Q is the axial load on pile, I_p is the moment of inertia of the pile cross section, x is the vertical depth and y is the lateral deflection of the pile at point x along the length of the pile.

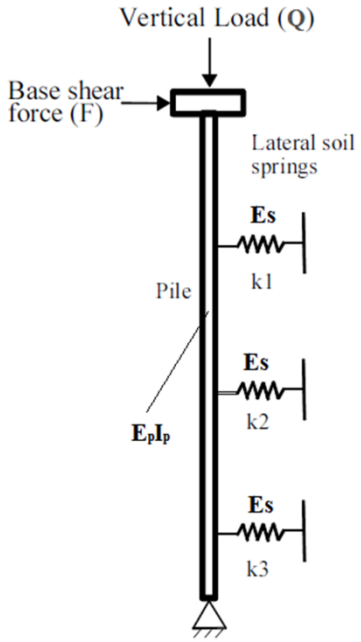

Fig. 2.10 Pile modelling base on Winkler method

Another term utilized usually instead of E_s is the soil lateral subgrade reaction modulus (k_h) which is expressed in units of force per unit volume. The relationship between them is given by $E_s = k_h D$, where D is the pile diameter. The solutions to Eq. 2.3 can be founded doing assumptions to simplify the variation of E_s with depth. The most common assumption is that E_s is constant with depth for clays and E_s varies linearly with depth for sands. As a result of their studies, several authors have

provided tables to obtain moments and deflection in the piles (Poulos and Davis 1980). Some extensions of this method have been developed using *p-y* curves to model nonlinear soil-pile stiffness. Using the modified Winkler method, some characteristics such as cyclic degradation and rate dependency may be considered (Allotey and El Naggar 2008).

The principal limitations of this approach are that the linear elastic springs work separately which means that the displacements in each point are independent from each other. The modulus of the subgrade reaction is not the unique property of the soil since it depends on the pile characteristics and the magnitude of deflection.

Experimental tests

Two experimental tests utilized for modelling SSI problems under dynamic loading are the shaking table and the centrifuge test. Shaking table scale models are conducted under Earth's gravity. This makes it suitable to model cohesive soils in which the stress-strain behavior is independent of the confining pressure. An important disadvantage of this test is related with the reproduction of the actual stresses due to the small size model. This test has been importantly influenced by the boundary effects of the test container, scale modelling techniques and non-adherence to similitude laws (Meymand 1994).

The centrifuge test is another way to analyze soil-foundation-structure problems. A centrifuge apparatus consists of a rotating arm with an experimental package fixed to a swivel at one end. The increase of the gravity force via rotating the model allows modeling the soil stress-strain condition similar to the prototype. This is highly useful dealing with cohesionless soils whose stress-strain behavior is a function of confining pressure. several researchers describe problems such as the difficulty to build complex prototypes, undesirable vertical motions, inability to reproduce with a range frequency as in real earthquakes (Wilson 1998, Jakrapiyanun 2002). Full scale test prototypes can be also utilized to test piles groups under seismic loadings (Lu et al. 2004).

Numerical methods

Due to the quickly advances in computers, the numerical analyses have become a powerful approach in engineering design and research on soil mechanics and geotechnical engineering. The numerical models for the analysis of soil problems give the possibility to describe the soil behavior and failure modes, the pre-existing stress state, the anisotropy and the time dependent behavior caused by creep and plastic deformations. They have the capability of 3D modelling and incorporate the dynamic analysis. Additional challenge is the coupling of the hydraulic process in the analysis of the

mechanical behavior of soils. In this study, finite difference method is utilized and it is described in Section 1.3 Chapter 3.

2.3. Previous Studies Considering SSI Under Dynamic Loading

This part of the study presents the state of art of the soil-foundation-structure systems under dynamic loading in four principal terms: 1) dynamic analyses and pile support conditions, 2) Rayleigh damping, 3) dynamic characteristics of the buildings and 4) impact of liquefaction in soil. Several works performed using analytical, experimental or numerical methods dealing with pile-reinforced systems are presented.

2.3.1. Pile-reinforced System: Dynamic Analysis and Pile Support Conditions

The dynamic behavior of soil-foundation-structure systems is a complex process that involves the interaction between the structure and the pile foundation and the interaction between the pile and the surrounding soil. In addition to this, the type of pile foundation is an essential aspect that can modify the natural frequency and the damping of the soil-foundation-structure system. For these reasons, in Section 1 of Chapter 4 a study was developed on the influence of pile type and other important factors affecting the behavior of the soil-foundation-structure systems under dynamic loadings. Some investigations considering pile- and rigid inclusion-reinforced systems under seismic loading are described and analyzed.

The dynamic behavior of soil-pile-structure interaction has been studied by several authors (Kuhlemeyerr 1979; Gazetas 1984; Trochanis et al. 1988; Brown and Shie 1990; Wu and Finn 1997). More recently, other authors have analyzed this interaction using numerical models considering a single pile. Rovithis et al. (2009) investigated the seismic response of a system with a single pile and a single degree of freedom structure resting on a viscoelastic soil layer over rigid rock (Fig. 2.11a). They found that structural vibrations impose large bending moments in the superior part of the piles when flexible and slender piles are used. On the other hand, with short and stiff piles, the kinematic interaction dominates the pile bending moment at great depths. Cheng and Jeremić (2009) studied the dynamic response of a soil-pile-column-mass system in a liquefiable soil through a 3D finite element model considering different stages of loading (Fig. 2.11b). The soil modelled is a Toyoura sand and its behavior is represented by a bounding surface elasto-plastic model was utilized to model the soil skeleton while a fully coupled formulation (soil-fluid) was used to model the soil and water. The results indicate that the depth at which maximum moments are located in the pile depends on the boundary conditions at the pile head.

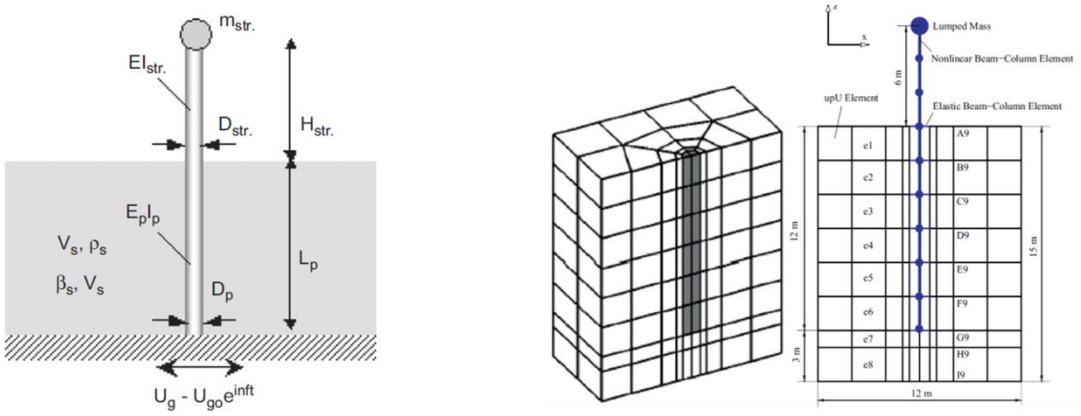

a) Rovithis et al. (2009) **b)** Cheng and Jeremić (2009)

Fig. 2.11 Basic characteristics of the soil-pile-structure considered in previous studies

Other authors have studied the soil-pile-structure interaction considering a group of piles. Chu and Truman (2004) analyzed the seismic response of a soil-pile model with a 3D finite element code and with different pile configurations. Soft clay was assumed with a Young's modulus of 20 MPa and 0.3 of Poisson's ratio. The soil nonlinearity was considered using the Drucker-Prager soil plasticity model. Volumic elements are utilized to represent the piles. The model was validated versus experimental data and existing results of numerical analyses. The study pointed out that the soil properties have a great influence on the pile head response (acceleration and displacement). Elgamal et al. (2008) developed a 3D finite element nonlinear dynamic analysis based on the geotechnical conditions of the Humbold Bay Middle Channel Bridge. Each bridge piers was supported by 16 square or circular piles. The soil profile is idealized in six soil layers. The foundation was modeled as a nonlinear hysteretic material with a Von Mises multi-surface kinematic plasticity model. Undrained soil strength was utilized. The behavior of the bridge superstructure, piers and piles was assumed to be linear elastic. The piles were modeled with beam-column elements. The results showed that the settlements and lateral displacements in the abutments and pile foundations are induced by the permanent ground deformations. Carbonari et al. (2011) evaluated the SSI of a coupled wall-frame structure supported by pile foundations subjected to moderate earthquakes through a 2D linear finite element model (Fig. 2.12a). The superstructure and soil-foundations system responses are derived separately in the frequency domain assuming a linear behavior of the soil and structural elements. Then they were assembled to obtain the whole response of the model. Three soil profiles were considered. They concluded that the internal forces in the piles depend on the structure deformability and that the stresses at the deepest sections are caused by kinematic interactions. Hokmabadi and Fatahi (2016) studied the influence on the seismic performance of a 15-storey building founded on shallow foundations, floating piles and pile-raft foundations through a 3D finite element model. The behavior of the soil is assumed to be linear elastic-perfectly plastic with a Mohr-Coulomb failure criterion. Undrained soil properties were utilized (typical values for clayey soils); however, they do not report of the groundwater level presence. The behavior of the structural elements is considered linear elastic

until it reaches the defined yield stress. A hysteretic damping was considered. Pile elements were modelled with solid elements. The numerical model was verified with experimental shaking table tests. The studies determined that the way that shear forces are distributed in the structure depends of the foundation type. The trend and amount of variation of these forces is not the same at each level. The structure supported by shallow foundations experiences more severe rocking compared to the floating and pile-raft foundation due to the presence of piles. However, the base shear forces are higher.

Dealing with soil-inclusion-platform-structure systems, using a two dimensional model, Mayoral et al. (2006) analyzed the dynamic response of a single inclusion embedded in a soil mass with geotechnical conditions of Mexico City. They concluded that the surface acceleration reduction is essentially due to the presence of the LTP and due to the inclusion reinforcement. Rangel-Núñez et al. (2008) developed a 2D finite element numerical model to study the seismic response of a soft soil (typical clay of Mexico City) deposit reinforced with a group of rigid inclusions taking into consideration the construction stages of the rigid inclusions and different types of fixity conditions. The soil is modelled as a linear elastic material during the application of the undrained seismic loading. No water table is reported. Rayleigh damping formulation was considered. Linear beams were used to model the inclusions. The results showed that the pile support conditions have an important effect in the dynamic response. Hatem (2009) carried out tridimensional finite difference numerical calculations of a soil mass reinforced by rigid inclusions under seismic loads. A soil mass reinforced by a group of 2 x 2 rigid inclusions was considered and compared with a pile system. The properties of soft soil were based in a literature review (Young modulus of 6 MPa, Poisson's ratio of 0.3 and volumic weight of 1700 kg/m^3). The soil behavior is assumed to be linear-elastic perfectly plastic with a Mohr-Coulomb shear failure criterion. The pile behavior was taken as linear elastic. Rayleigh and local damping were respectively assumed for the soil and piles. Solid elements were chosen to model the pile elements. The results show a quantitative and qualitative difference in the seismic forces in the rigid elements for both systems. The forces and bending moments are higher in the piles due to a dynamic amplification compare to the inclusion system. With a 3D finite difference numerical analysis, Mánica-Malcom et al. (2016) investigated how the seismic ground response is affected by inclusions embedded in soft clay deposits of the Mexico City (Fig. 2.12b). Soil was modelled with a linear elastic constitutive model. Rayleigh damping was used to include the energy dissipation. The inclusions were modeled by solid zones. The results indicated that the dynamic characteristics of the structure at the surface mostly affect the ground response of the system. Support conditions, pile length and spacing cause a small variation in this response. The shear forces and bending moments in the inclusions increase in the zones where there is a large contrast in soil stiffness.

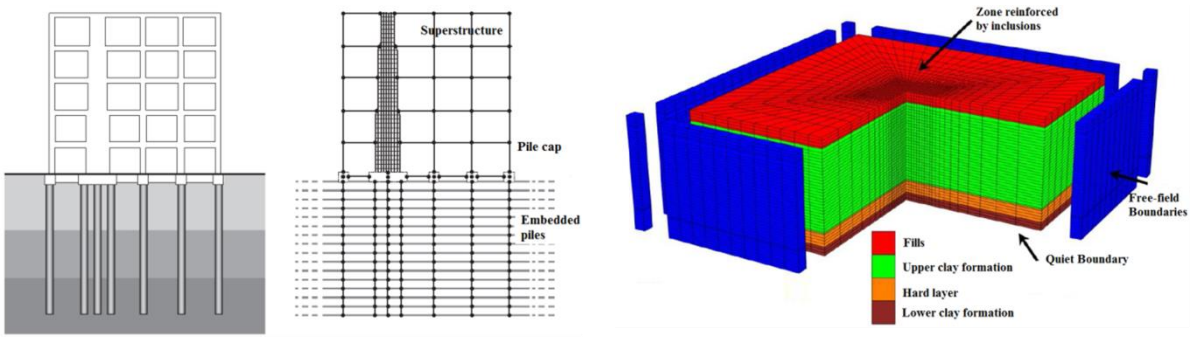

a) Piles system, Carbonari et al. (2011)

b) Rigid inclusion system, Mánica-Malcom et al. (2016)

Fig. 2.12 Characteristics of the soil-foundation-structure models considered in previous studies

Based on the studies presented in this section and although many investigations have focused on pile and rigid inclusion systems considering dynamic analyses, there is still many uncertainties of the effect of some important factors in the response of these systems under seismic loading. For instance, factors such as the soil nonlinearity, pile foundation type, pile group configuration, pile flexural rigidity, frequency of the dynamic loading and embedment of the foundation are not deeply investigated in pile and inclusion systems. These factors are analyzed in this study in Section 1 of Chapter 4.

2.3.2. Pile-reinforced System: Rayleigh Damping

When dealing with dynamic numerical modeling, the damping in a numerical model is an important feature. In numerical models, the soil is usually discretized in a finite domain limited by artificial boundaries which have the ability to dissipate energy. The dissipation of energy in the boundaries is known as the radiation damping and is not an inherent property of the material. The radiation damping is complemented by the material damping that represents the loss of energy within the soil itself, mainly due to microstructural mechanisms such as inter-particle sliding, friction, structure rearrangement and pore fluid viscosity. The material damping has been identified as one of the main factors incorporated into the study of soil-foundation-structure interaction systems (Ambrosini 2006, Wolf 1985) because it depends on the characteristics of the soil and not in the geometry and boundaries of the model.

In dynamic numerical analyses, there are some constitutive models that can simulate the loose of energy. Some of them imply the utilization of many parameters that required advanced laboratory tests to obtain them. Other simple elasto-plastic models need an additional damping for the elastic part of the response, where no energy loss occurs. In this case the additional damping can be introduced by a viscous damping (Rayleigh damping). The main concern in the use of the simplified or the complete Rayleigh damping is the selection of the appropriate target damping ratio (Woodward and Griffith

1996) and the frequency range where the response is frequency independent (Hashash and Park 2002, Hudson et al. 1994, Kwok et al. 2007, Tsai et al. 2014).

The effective results of the Rayleigh formulation (described in Section 1.6 Chapter 3) were proved by some authors. For example, Mánica et al. (2014) developed 3D numerical seismic analysis to show the advantages and drawbacks of different damping formulations (local, Rayleigh and hysteretic) with a typical stratigraphy of the Mexico city (Fig. 2.13a). The soil was modelled with a linear elastic constitutive model. The results were compared with those obtained from the equivalent linear code SHAKE. Showing spectrum accelerations differences, they concluded that the Rayleigh damping is the most suitable alternative to represent the dissipation of energy in seismic analyses considering the appropriate selection of the central frequency. Suwal et al. (2014) developed several linear analyses in an idealized soil profile to explore the influence of Rayleigh damping formulation on site response analysis. Other nonlinear analyses were performed in the Orvieto site in central Italy. The results showed that the full Rayleigh damping formulation is consistent with the response obtained with a frequency-independent analysis; however, the response of the simplified formulation underestimates the response.

Several authors have developed advanced viscous damping formulations in their studies. For instance, Phillips and Hashash (2009) presented two approaches to model the energy dissipation in an one-dimensional site response analysis. The first one constructs a frequency-independent viscous damping matrix which reduces the overdamping at high frequencies (Fig. 2.13b). In the second one, a simplified constitutive model is introduced to match the modulus reduction and the damping curves for nonlinear site response analyses. The proposed method overcomes some longstanding limitations in nonlinear time-domain analysis regarding small and large strain damping. Hashash and Park (2002) developed an extended full Rayleigh damping formulation that represents more accurately the wave propagation in deeper soil columns and improves the non-linear site response analyses for short periods.

The Rayleigh damping type was used for different applications in piled and rigid inclusion systems (Wu and Finn 1997, Lu et al. 2005, Rangel-Núñez et al. 2008, Hatem 2009, Shahrour et al. 2012, Kumar et al. 2016, Luo et al. 2016, Nguyen et al. 2017). However, in most of these studies there is no discussion about the selection of parameters, calibration and influence of them in the response of the systems. A few authors (Hashash and Park 2002, Tsai et al. 2014, Amorosi et al. 2010) have studied through nonlinear site response analysis to select the correct parameters in Rayleigh damping formulation to avoid overdamping or underdamping of the wave propagation. They concluded that the site frequency and the frequency characteristic of the input motion must be taken into account to obtain the frequency-independent range. Other authors (Phillips and Hashash 2009, Phillips et al.

2012, Mánica et al. 2014, Priestley and Grant 2005, Wang 2011, Spears and Jensen 2012) have demonstrated the variations on the seismic response of soil and structures associated to the defective selection of parameters for Rayleigh damping.

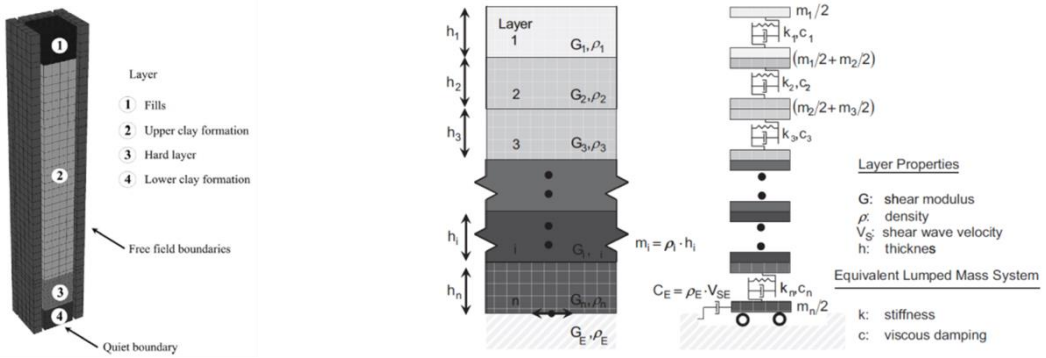

a) 3D models in flac 3D Mánica et al. (2014)

b) Multi-degree-of-freedom lumped parameter model Phillips and Hashash (2009)

Fig. 2.13 Damping formulations in in previous studies

Considering the previous studies, the importance of the correct selection of parameters when the Rayleigh formulation is introduced in dynamic analysis is shown. Besides that, there is an absence of studies that investigate the influence of these parameters for soil-foundation-structure systems. For these reasons and due to the fact that in this work (Chapter 4 and 5) the soil behavior is represented by a simple linear elastic perfectly plastic model with a Mohr-Coulomb shear failure criterion, a detailed study of the influence of the Rayleigh damping parameters in soil-foundation-structure systems is presented in Section 2 of Chapter 4.

2.3.3. Pile-reinforced System: Dynamic Characteristics of the Building

To estimate the accurate response of structures supported on soft soil under seismic loading, it is necessary to consider its interaction with the underlying soil. Dealing with buildings, the role of the SSI can be considered favorable in some cases. However, in other cases the fundamental period of the structure is increased to periods near to the resonant period which can result in increased base shear forces that can produce severe damage or failure of the building.

Several studies have investigated the influence of the SSI on the seismic response of buildings supported by piles through two-dimensional models. For instance, Tabatabaiefar et al. (2013) developed a 2D finite difference model to investigate the lateral seismic response of mid-rise building frames under the influence of SSI. The study considered 5, 10 and 15 storey buildings. Interface elements were considered between the foundation and the soil. The calculation determined that a conventional design procedure which excludes the SSI cannot guarantee the structural safety of mid-

rise building resting on soft soils. It is due to the amplification of the lateral deflection and to the corresponding inter-storey drifts of their flexible base.

Through three-dimensional models, Lu et al. (2005) developed a finite element analysis of a soil-pile-structure system. The adopted structure is a 12-storey reinforced concrete frame building with a single span supported on a group of 9 piles. The soil and piles were meshed with solid elements, and beam and shell elements were utilized for the building columns and slabs respectively. An equivalent linear model is used to simulate the three layers of the Shanghai soft soil behavior and interface elements are considered at the soil-pile connection. A validation versus shaking table tests was developed. The researchers found that the deflections of the structure are composed by the deformation of the structure itself and the ones caused by the rocking and swaying of the foundation. The distribution of the soil-pile contact pressure is more important in both ends of the vertical reinforcement. Nghiem and Nien-Yin (2008) investigated the seismic response of a 33-storey through 3D finite element systems. The building is supported by a sandy clay soil which is a typical profile of the City of Hanoi. Soil, piles and caps were modeled by solid elements. The soil behavior is assumed to be linear elastic perfectly plastic with a Mohr-Coulomb failure criterion. Analyses with a rigid base and flexible base soils were considered in order to examine the evolution of the SSI effects. The findings showed that the shearing of the flexible base is smaller than the one of the rigid base. The building shape irregularity influences importantly the building top deflection. Hokmabadi et al. (2014) studied the seismic response of a 15-storey building supported by shallow foundations and floating piles foundation in soft soil with a 3D finite difference numerical model. The behavior of the soil is assumed to be linear elastic-perfectly plastic with a Mohr-Coulomb failure criterion. An undrained shear strength of 3.1 kPa, a shear wave velocity of 36 m/s, a maximum shear modulus of 1776 kPa and a Plasticity index of 42 are used. They do not report the presence of the ground water level. The behavior of the structural elements is considered to be linear elastic until it reaches the defined yield stress. Hysteretic damping was considered. Pile elements were modelled with solid elements. Interfaces soil-pile and soil-slab foundation were considered. Shaking table tests were developed to validate the numerical results. The results showed that the lateral displacements of the floating pile foundations are greater than the ones of the structure with a fixed-base condition, but are reduced than the shallow foundation case due to the rocking components. Badry and Satyam (2016) analyzed the dynamic response of a 3D nonlinear finite element system that consists of a L-shape 11-storey building supported by a pile foundation with homogeneous sand soil conditions (Fig. 2.14a). The research included the applicability of the equivalent pier method (pile group is represented by a single pier) for the asymmetrical pile groups and the SSI effect of the system. The Drucker-Prager material model is utilized to capture the nonlinearity of the soil. The study pointed out that the displacements in the system response which considers the soil-structure interaction are modified of around 15-20% from the fixed-base analysis. The earthquake magnitude and the soil type have an important impact in

the response of the SSI system. The effect of an asymmetrical structure shows that the response at all points located at the same level is not the same. With the objective to investigate the influence of the type and of the size of the foundation in the seismic response of midrise buildings, Nguyen et al. (2017) developed a 3D finite element numerical model of a 15-storey moment-resisting frame building supported on end-bearing and floating pile foundations. Interface elements were considered between the soil and the piles (Fig. 2.14b). The soil is a soft clayey soil with a unit weight of 14.42kN /m³, a shear velocity of 150 m/s and undrained shear strength of 50kPa. The equivalent linear method is utilized. The ground water level is not mentioned. Solid elements were used to model the pile elements. The pile elements were modeled with solid elements. The results displayed that the lateral deflection of the structure is composed of two components: structural distortion and rocking. The load-bearing mechanism alters the shear forces absorbed by the structure and how they are distributed along the pile elements.

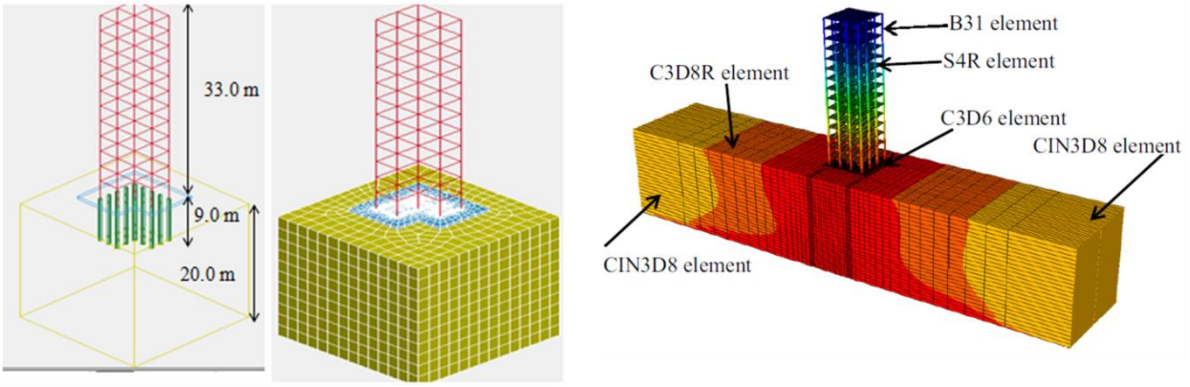

a) Badry and Satyam (2016) **b)** Nguyen et al. (2017)

Fig. 2.14 3D models of the integrated soil-pile-structure systems

Taking into account the previous investigations of the buildings founded on pile systems considering seismic loading, it is clear that the dynamic characteristics of the building have a high effect on the behavior of soil-foundation-structure systems. For this reason, Chapter 5 is dedicated to study this influence of a building with different characteristics.

2.3.4. Pile-reinforced System: Impact of Liquefaction in Soil

The response of a soil-pile-structure system in liquefiable soils considers simultaneously, 1) the dynamic loading acting in the rigid elements (piles/inclusions) due to the surrounding soil and the presence of the structure; 2) the shear strength reduction and the degradation of the soil stiffness due to the soil nonlinearities and the generation of pore pressure (Liyanapathirana and Poulos 2006). The loss of soil strength and stiffness due to excess pore pressure in liquefiable soil may develop large moments and shear forces in the piles.

Due to the fact that bridges, tanks and buildings founded in piles embedded in liquefiable soils have collapsed during important earthquakes (Niiagata 1964, San Fernando 1971, Loma Prieta 1989, Kobe 1995), analysis and design of pile foundations in liquefiable soil have received considerable attention in recent years. Some authors have investigated the soil-pile-structure interaction using experimental test, with centrifuge tests: Abdoun et al. (2003), Abdoun and Dobry (2002), González et al. (2009), Ramirez et al. (2018) and Su and Li (2006); or with shaking table tests: Gao et al. (2011), Haeri et al. (2012), Tamura and Tokimatsu (2006) and Tokimatsu et al. (2005).

Other authors have developed simplified methods to study the soil-pile-structure interaction in liquefiable soils. Ashour and Norris (2003) used a new procedure to analyze the lateral response of a single pile in liquefiable sand under dynamic loading. The procedure involves the degradation of pile response and soil resistance due to the free-field excess pore pressure generated by the seismic loading, along with the near-field excess pore pressure generated by lateral loading from the structure. The results shows a reduction in the capacity and stiffness in the pile head due to the liquefaction compared to the pile response under drained condition. Liyanapathirana and Poulos (2006) utilized a simplified method to analyze pile groups in liquefiable soils (Fig. 2.15a). First an effective stress state (ground response analysis) was developed to obtain the maximum displacements in a single pile, and then a dynamic analysis was carried out assuming that each pile of the group behaves in the same way during seismic loading. They concluded that the method is efficient to compute pile behavior in liquefiable soil subjected to lateral spreading. The results were compared with centrifuge tests. Phanikanth et al. (2013) implemented a seismic-deformation method to check the effects of both kinematic and inertial effects. The soil-pile interaction considers stiffness degradation effects for a range of earthquakes with different amplitudes and durations. It was exhibited that the pile response in liquefiable soils is amplified two times more than for the non-liquefying soils. The depth of liquefied layer has a significant influence on the soil-pile response. The bending moments were maximal in the interface of liquefiable and non-liquefiable soil. Janalizadeh and Zahmatkesh (2015) presented a pseudo-static method for the analysis of piles in liquefiable soil under seismic loadings. First a free-field site response analysis was done using 3D numerical modeling. A dynamic analysis of the pile and structure was performed using the time history of the ground surface. Finally, the 1D Winkler seismic pile analysis was developed. They concluded that the p-y curves with various degradation factors in liquefiable sand produce reasonably results compared to centrifuge tests.

Through a two-dimensional plain strain finite difference model, Haldar and Babu (2010) examined the failure mechanism in piles considering nonlinear constitutive behavior for soil liquefaction, strength reduction and soil-pile interaction (Fig. 2.15b). Loose and dense Nevada sand properties were used for the calculations. The Finn model was utilized to represent the behavior of sand. The water

table was set at the ground surface. The piles were modeled using linear elastic beam elements. The findings show that the failure mode depends greatly in the depth of the liquefiable soil layer. Other factors that affect the pile failure mode are the relative density, the earthquake predominant frequency, the pile material and diameter.

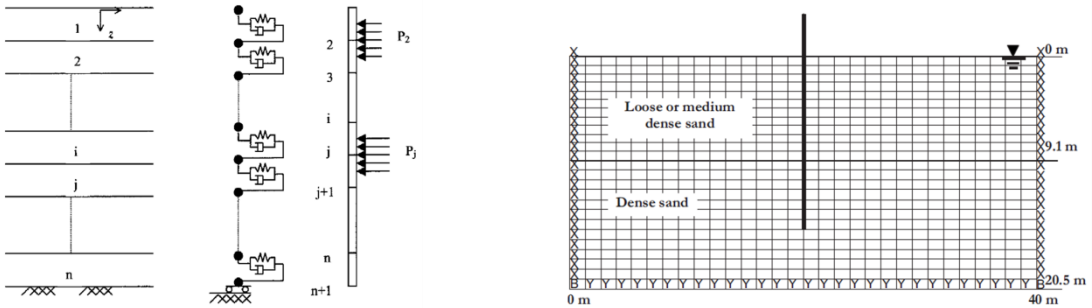

a) Liyanapathirana and Poulos (2006) **b)** Haldar and Babu (2010)

Fig. 2.15 a) Lumped mass representation of the discretized system, b) Schematic diagram of the finite difference model

With the use of three-dimensional models, some authors have carried out analysis of soil-pile-superstructure system considering soil liquefaction. For instance, Ren et al. (2008) considered a group of nine piles supporting a 12-storey concrete frame structure with finite difference analysis. A silty clay layer was modeled over a saturated sand layer. The piles were modeled by beam elements. A coupled mechanical-fluid dynamic analysis was developed. Elasto-plastic and Finn models were used for represent the soil behavior. Nonlinearity of the soil, pore pressure and soil-pile interaction were taken into account. The results were compared with shaking table test showing an agreement. Maheshwari and Sarkar (2011) analyzed with a 3D model developed in a finite element code, a 2 x 2 pile group supporting a 4-storey portal frame structure. A work-hardening plastic cap model was used for the behavior of the loose sand soil. The pore pressure generation for liquefaction was incorporated by a two-constant volume change expression. The soil and pile elements were modeled by using eight-noded solid elements. They deduced that the nonlinearity of the soil medium increases the response of the structure in the low frequency range. The pore pressure generation leading to liquefaction of the soil medium induces a significant increase in structural response. Using the same model but without the structure, Sarkar and Maheshwari (2012) studied the separation and sliding between soil and pile under dynamic condition. Rahmani and Pak (2012) investigated a three-dimensional finite element dynamic analysis of a soil-single pile-structure system in liquefiable soil. Loose and dense Nevada sand were considered. A critical state bounding surface plasticity model was used to model the soil skeleton and a (u-P) formulation was used to analyze the pore pressures and displacements (Fig. 2.16a). The water table was considered at different positions. The piles were modeled by beam-column elements. A lumped mass on the pile head represents the superstructure. Variation of permeability coefficient is considered during liquefaction. The calculations conclude that the bending

moment is the maximum at the head level in fixed-head piles and at 2m in free-head piles. The pile length and the thickness of liquefiable layer have little influence on the maximum lateral displacement during the excitation. The natural frequency of earthquakes has a great influence in the pile performance in these systems. Choudhury et al. (2014) evaluated a 3D finite difference model of a single pile embedded in a homogenous and liquefied soil under dynamic loading. A two-layered soil system composed by a liquefiable layer of loose sand underlain by a non-liquefiable layer of stiff clay was considered. The linear elastic perfectly plastic model with a Mohr-Coulomb failure criteria and the Finn model were used to represent respectively the sand and clay soils. The water table is located at the ground surface. The analysis exposed that the maximum bending moment occurs in the interface of the liquefiable layer and non-liquefiable layer. Moreover the results were compared against combined pile raft foundation with a group of four piles. Wang et al. (2017) studied the seismic pile moments induced by the inertial and kinematic interaction effects (Fig. 2.16b). The soil constitutive model proposed by Wang et al. (2014) was utilized. The model functions within the frameworks of bounding surface plasticity and complies with critical state soil mechanics to achieve a description of the saturated sand for the pre- and post-liquefaction under cyclic loading. Solid elements were utilized to represent the structure, pile and soil. They found that the kinematic interaction dominates the pile moment when the pile head is constrained by the pile cap. When there is no pile cap, the inertial effects dominate the pile moment.

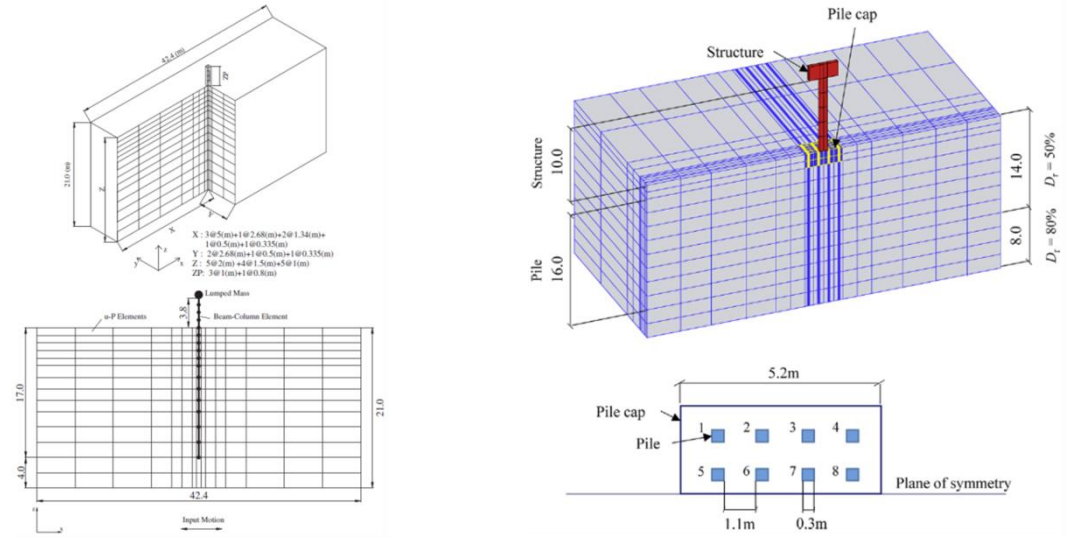

a) Rahmani and Pak (2012) **b)** Wang et al. (2017)

Fig. 2.16 Finite element models with liquefiable soils

It is clear from the previous investigations that the response of the soil-foundation-structure systems is complex when liquefiable soils are considered. Chapter 6 presents a study to better understand the effect of several factors in the response of the soil-foundation-structure systems in the presence of liquefiable soils. Factors such as the relative density, the soil profile and layer thickness

are still not completely studied in the inclusion and pile systems considering liquefiable soils under seismic loadings.

3. Static and Dynamic Behavior of Soil

3.1. Dynamic Loading: Definition and Sources

Although most of the problems in engineering have been devoted to determination of behavior under static load conditions, the presence of dynamic loads is an important factor in many cases. The main difference between static and dynamic loads is that the first do not change (constant load) with time and the second do. The quick rate to apply the loadings is an important characteristic of the dynamic loading (high frequencies). If the load is applied with a slow rate, it is considered as a quasi-static loading.

Dynamic loads vary rapidly in their magnitude, direction, or position with time. The primary objective of study of the effect of dynamic forces acting upon an element is to know the displacements and stresses that are result of those forces, whatever is the nature of the dynamic forces (natural cause or induced on purpose).

The dynamic forces acting on an object or structure have different source of origin, such as, blast loads, wind, wave actions, traffic, operation of machinery and earthquake. It is a fact that the force acting can be the result of different causes. In Fig. 2.17 can see the representation of different types of load according its source.

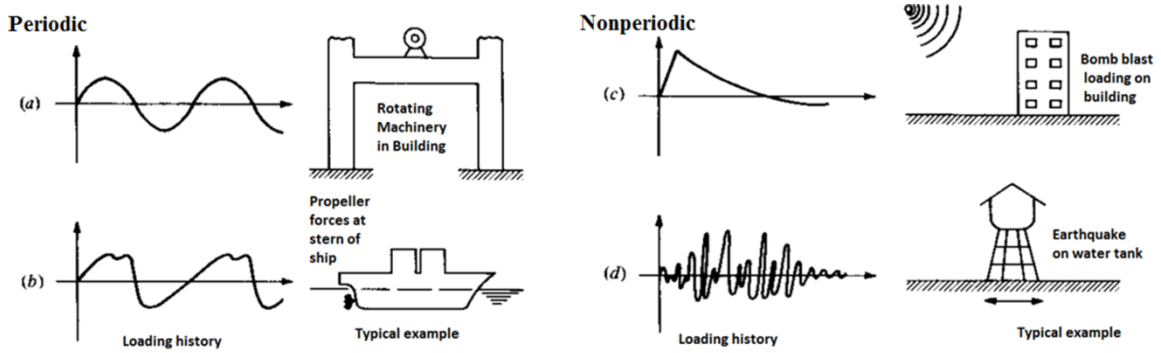

Fig. 2.17 Characteristics and sources of typical dynamic loadings: a) Harmonic load, b) Complex periodic load, c) Transient load, d) Earthquake load (Clough and Penzien 1975).

The primary classification of dynamic loads is in deterministic and nondeterministic loads. The first being specified as definite functions of time and the others being known in a statistical sense.

The deterministic loads can be divided from an analytical standpoint and according to nature of their variation with time in periodic, no periodic and random loads. The periodic loading is a dynamic

load that varies in magnitude with time and repeats itself in regular intervals of time (Fig. 2.17a). The period, the cycle, the frequency and the amplitude are some basic concepts involved with periodic loads. There are forms of periodic loading that are frequently complex like the hydrodynamic pressures generated by a propeller at the stern of a ship (Fig. 2.17b), wave loading on an offshore platform or wind forces induced by vortex on tall structures. These types of complex periodic loads can be represented by the sum of a series of simple harmonic components by means of Fourier analysis (Chopra 1995). The nonperiodic loads are those who do not show any type of periodicity. This type of load may be of a comparatively long duration or short duration (transient). The transient load is often referred to an impulsive load.

An example of this type of load is an impact, blast or explosion. A load that varies in a highly irregular way with time is referred as a random load. Dynamic loading due to an earthquake is considered random in nature. Earthquakes are a result from a fracture in earth's crust due tectonic forces. They can be defined as the vibration of the earth produced by rapid release of energy from within itself. The wave motion of an earthquake is very complex. The ground acceleration resulting from an earthquake provides one example of random disturbance (Fig. 2.17d).

The nondeterministic loads cannot be specified as definite functions of time because of the inherent uncertainty in their magnitude and the form of their variation with time. However, these loads can be defined in a statistical sense only and are described through certain statistical parameters such as mean value and spectral density. Wind loads are also nondeterministic in nature.

Peralta (2010) define a cyclic loading as a load frequency between 0 and 1 Hz. In this cyclic load the inertia forces can be neglected due to the low frequency and the accumulated strain is predominantly plastic. In Table 2.2 is shown the classification of repeated loading soils proposed by Peralta. However, in most of the bibliography there is no clear difference in the use of the terms "cyclic" and "dynamic" when dynamic analyses were carried out. Some authors defined cyclic loading as a period action that when applied to a material body tends to change and usually reverse its stress and strain state over time (Pinto 2012). Rascol (2009) refers the cyclic loading for the system oscillating with constant amplitude and frequency. However, in this study, the cyclic loading is considered as a type of dynamic loading (without any specific characteristic) and both terms are used indistinctly.

In this study the static loadings considered are the gravity and the dynamic loadings are the input motions (seismic records, sinusoidal loadings) applied in the numerical models.

Table 2.2 Approximate classification of repeated loading of soils (Peralta 2010)

Repeated Loading Soils	Cyclic	Cyclic-Dynamic	Dynamic
Frequency	0 – 1 Hz.	1 – 10 Hz.	> 10 Hz.
Inertia	No (negligible)	Yes (relevant)	Yes (relevant)
Strain accumulation	Predominantly plastic	Plastic and elastic	Predominantly elastic

3.2. Theoretical Framework for Soils Behavior in Drained and Undrained Condition.

The soils have different design properties under drained and undrained conditions. In drained condition, the changes in load are slow enough to allow the water flow in or out of the soil. In undrained condition, the changes in load occur rapidly than the water can flow out of soil. Based on the soil profile and its characteristics, the time to dissipate this excess pore pressure can take few minutes or hours. Due to the fact that the time to dissipate the excess pore pressure is larger than the earthquake duration, the seismic analysis of soil should be considered in undrained conditions. In some parts of this study (Chapter 4 and 5) several calculations were developed considering drained condition even for seismic loadings. In other parts (Chapter 6) the analyses consider the behavior of soils in undrained condition because they are more focus in the liquefaction phenomena in soils. In these cases, the water table was considered at ground surface.

Recognizing the importance of characterizing the behavior of soils, the soil behavior in drained and undrained condition (more focus in cohesionless soils because is the type of soil utilized in Chapter 6) under monotonic and dynamic loading is described in the following section.

3.2.1. Monotonic Loading

3.2.1.1. Cohesionless Soils

A sample of soil can be monotonically sheared either under stress or strain control. Fig. 2.18 shows typical stress-strain relationships of cohesionless soils obtained from triaxial test. The peak strength of cohesionless soils is influenced most by density, effective confining pressures, test type, and sample preparation methods.

In drained triaxial test conditions (Fig. 2.18a), there is definite peak strength in the curve for dense soil at a relatively low strain. After reaching the peak value the curve decreases rapidly with increasing strain and deviator stress becomes more or less constant until reach the critical state strength, in which the soil deforms under sustained loading at constant volume. It can be noted that the maximum strength is greater than the critical state strength. When the soil is in loose condition the stress increases gradually with strain until reach the same critical state strength and there is no peak in the stress–strain curve.

In undrained triaxial test conditions (Fig. 2.18b), dense specimens initially get a yield point, after that the state of the soil moves progressively toward the critical state displaying hardening behavior, the stress need to be continually increased in order to produce the plastic deformation. Loose soil samples get the peak strength at small shear stress level and fail rapidly with large strains, to the critical state.

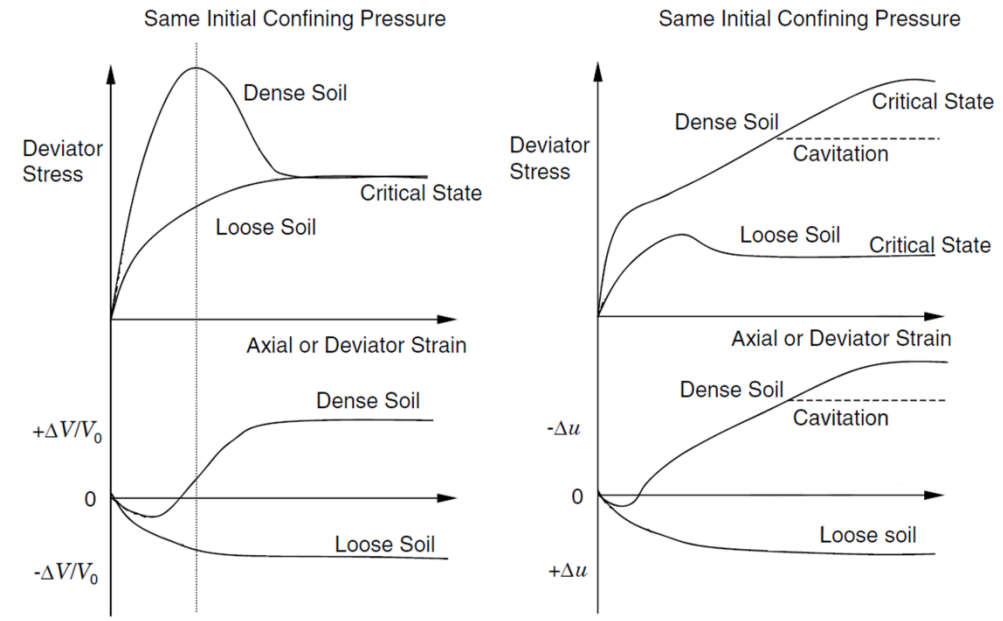

a) Drained conditions **b)** Undrained conditions

Fig. 2.18 Stress–strain relationship of cohesionless soils (Mitchell and Soga 2005)

Fig. 2.18 also displays the relationship between volume change and axial strain. In drained conditions the soils with low densities the soil particles are farther apart on average, in a loose assemblage (Fig. 2.19a). The loading of shear force on loose soils makes particles tend to fall into the gaps between adjacent particles and the volume of the soil decreases (Fig. 2.18a). In dense soils the particles are packed tightly together which cannot move relative to each other unless they ride up over each other (Fig. 2.19b), which cause dilation.

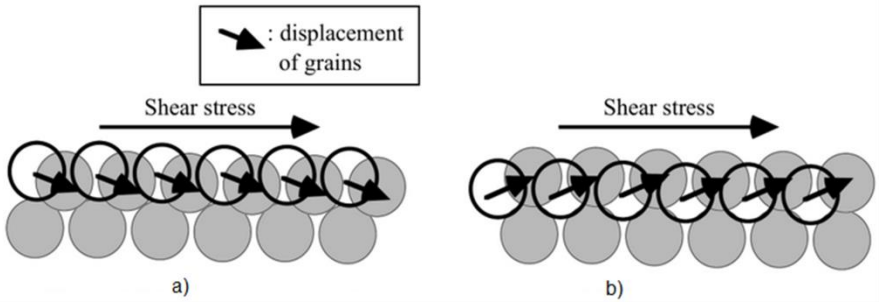

Fig. 2.19 Compression and dilation state (Towhata 2008)

In undrained condition there is a transfer of stress from the soil skeleton to the pore water resulting in pore water increase because no volume change is possible. For dense soils, the tendency for dilation or volume increase results in a decrease in pore water pressure (Fig. 2.18b).

During critical state deformation a soil is completely destructured. The simple concept of the critical state is that under sustained uniform shearing at failure, there exist a unique combination of void ratio (e), mean pressure (p') and deviator stress (q) (Roscoe, Schofield, and Wroth 1958). These stresses are defined by $p' = (\sigma_1' + \sigma_2' + \sigma_3')/3$ and $q = \sigma_1' - \sigma_3'$, where σ_1' and σ_3' are the maximum and minimum principal effective stresses respectively. In the triaxial test is assumed that the intermediate and the minimum stresses are the same. The critical state concept is represented in the p'-q-v space as a line (Fig. 2.20a). Two similar concepts to the critical state line were introduced in the p'-q space by Luong (1980) and Ishihara et al. (1975) though studying the cyclic behavior of drained and undrained soils. These concepts are the Characteristic state line (CSL) and the Phase transformation line (PTL) whose are represented in Fig. 2.20b. When the stress path is below the PTL the soil tends to contract but when it crosses the PTL the soil specimen will attempt to dilate. In undrained condition the compression produce pore pressure increase and suction pressures in dilation.

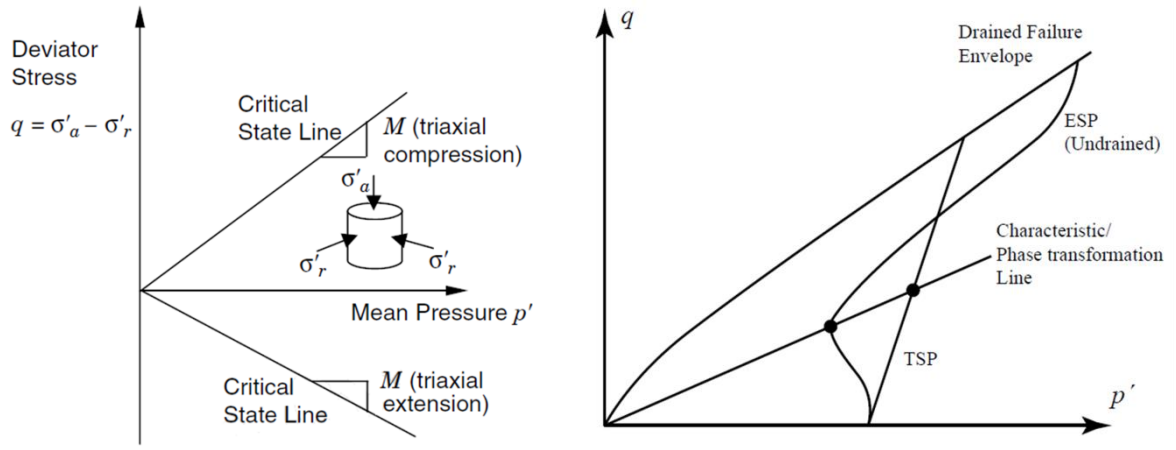

a) Critical state line **b)** Characteristic/Phase Transformation line

Fig. 2.20 Critical state concept (Shajarati et al. 2012)

An example of the undrained behavior of soil in a triaxial test under monotonic load is presented in Fig. 2.21. Loose and dense Shirasu sand are presented (Hyodo, Hyde, and Aramaki 1998). The relative densities are 50% and 90% respectively. Different confining pressures were utilized (50, 100 and 300 kPa). In Fig. 2.21a is shown that the cases with 50 and 100 kPa there is a clear softening behavior. Only contractive behavior was observed in for the case with 50 kPa. For the 100 kPa case a slightly strain hardening was observed at the phase transformation point. Then the steady state condition is achieved. In the case of dense sand, the phase transformation points are reached early following by a strain hardening behavior. After peak the deviator stress is reduced in all cases Fig. 2.21b.

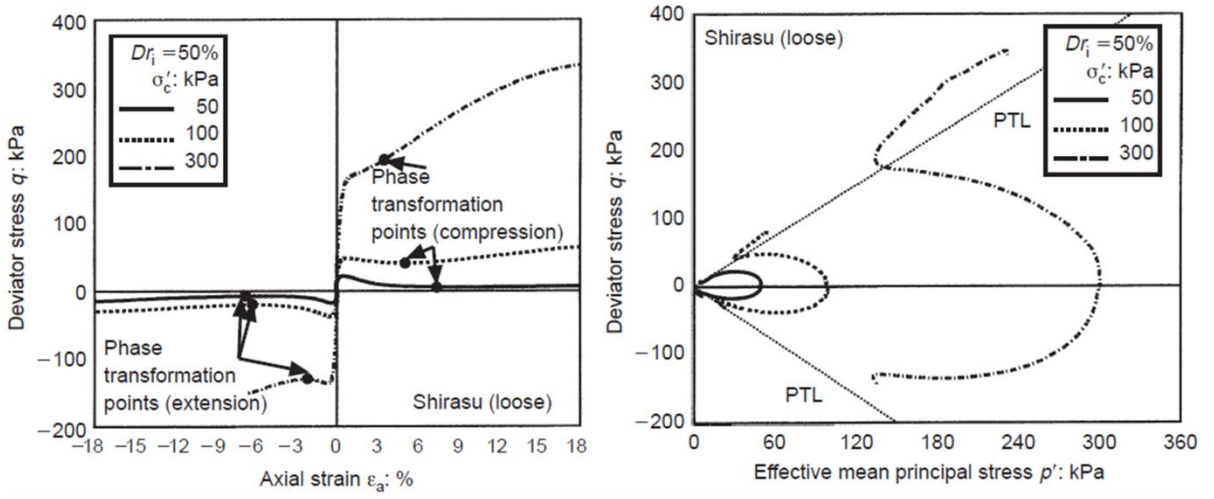

a) Loose condition

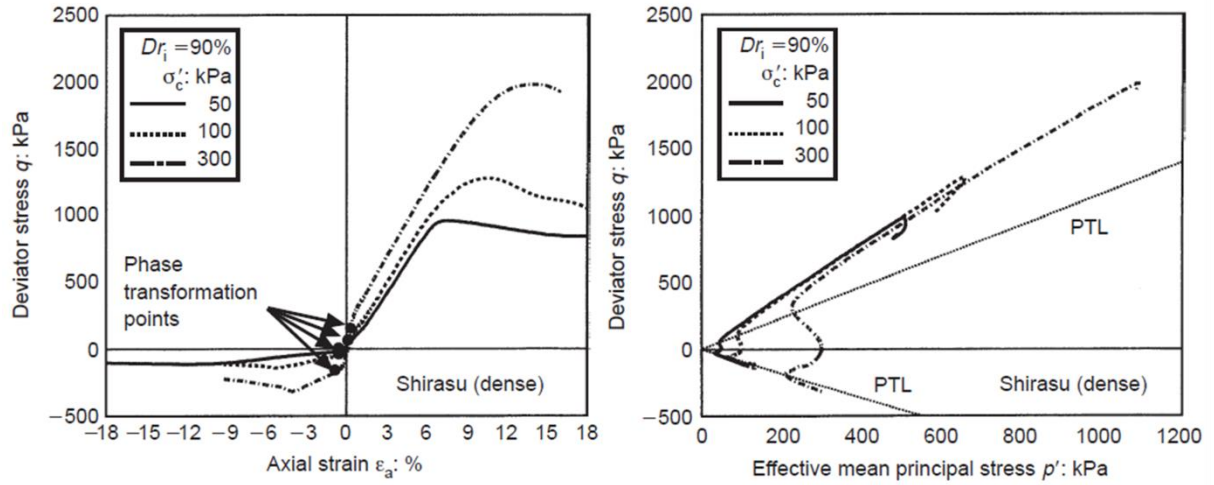

b) Dense condition

Fig. 2.21 Stress-strain curves and effective stress path for Shirasu sand under monotonic loading (Hyodo et al. 1998)

3.2.1.2. Cohesive Soils

In Fig. 2.22 the stress-strain relationships of clay specimens obtained by typical triaxial compression tests (Mitchell and Soga 2005) are presented. They are first normally consolidated (it has not been subjected to an effective stress higher than the present effective stress) and then isotropically unloaded to different overconsolidation ratios (the highest stress experienced divided by the current stress) before shearing. The specimens are consolidated at the same confining pressure p_0' but have different void ratios due to the different stress histories (Fig. 2.22a).

The peak strength of saturated clay is influenced most by overconsolidation ratio, drainage conditions, effective confining pressures, original structure, disturbance (which causes a change in effective stress and a loss of cementation), and creep or deformation rate effects. Overconsolidated clays usually have higher peak strength at a given effective stress than normally consolidated clays.

The differences in strength result from the different stress histories and also the different water contents at peak.

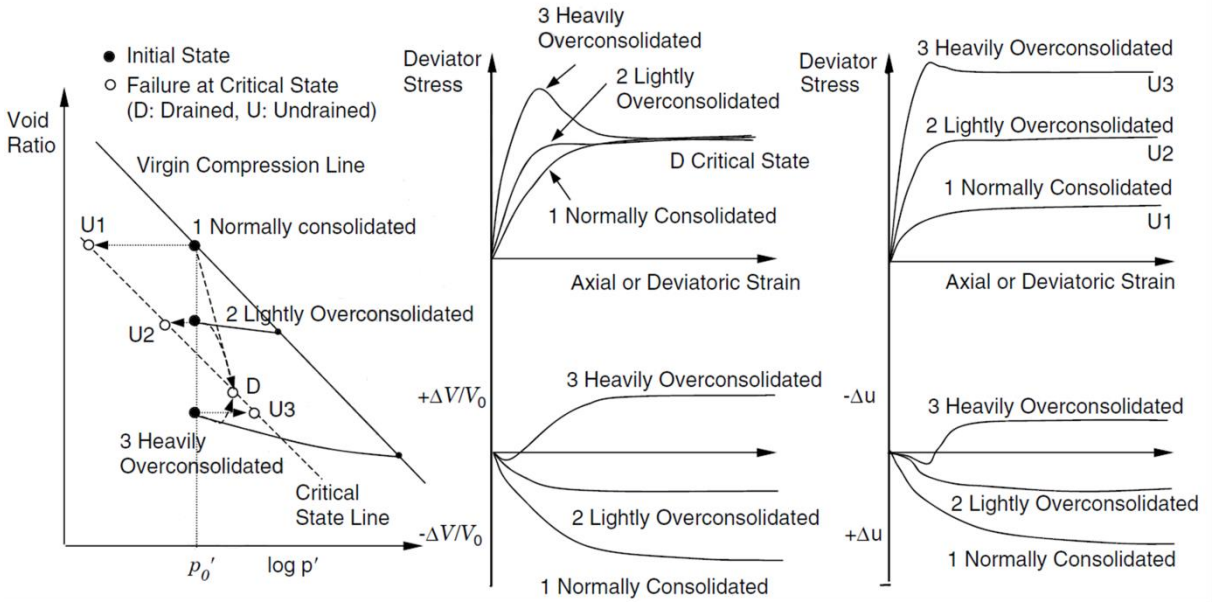

a) p′-ν **b)** Drained condition **c)** Undrained Condition

Fig. 2.22 Stress–strain relationship of normally consolidated, lightly overconsolidated, and heavily overconsolidated clays (Mitchell and Soga 2005)

In drained conditions, heavily overconsolidated clays exhibit a stiff response initially until the stress state reaches the peak strength. The state of the soil then progressively moves toward the critical state exhibiting softening behavior. In the normally consolidated clay, there is no peak in the stress strain curve, the stress increases progressively with strain until reach the same critical state strength. In drained conditions, normally consolidated and lightly overconsolidated clays show volume contraction (Fig. 2.22b). At failure, heavily overconsolidated clays have a greater volume, which is due to its dilative tendency upon shearing.

In undrained condition the stress-strain exposes that the highly overconsolidated clay has a greater strength than the lightly overconsolidated and normally consolidated clays. The difference in undrained shear strength is primarily due to different excess pore pressure development associated with the change in soil fabric. Undrained shearing of normally consolidated and lightly overconsolidated clays generates positive excess pore pressures and negative pore pressure values for heavily overconsolidated clays (Fig. 2.22c).

3.2.2. Cyclic Loading

The stress-strain behavior of a soil element under cyclic loading is shown in Fig. 2.23a. A soil specimen under cyclic loading experiments a cyclic shear strain (γ_{cy}) and a permanent shear strain

(γ_p) after many repetitions of load. The half amplitude of the cycle load is γ_{cy}.The first depends on the cyclic stress and the second is function of the cyclic stress and the number of repetitions. According to Andersen (2009), the failure caused by cyclic loading is defined as either 15% of permanent or cyclic shear strain.

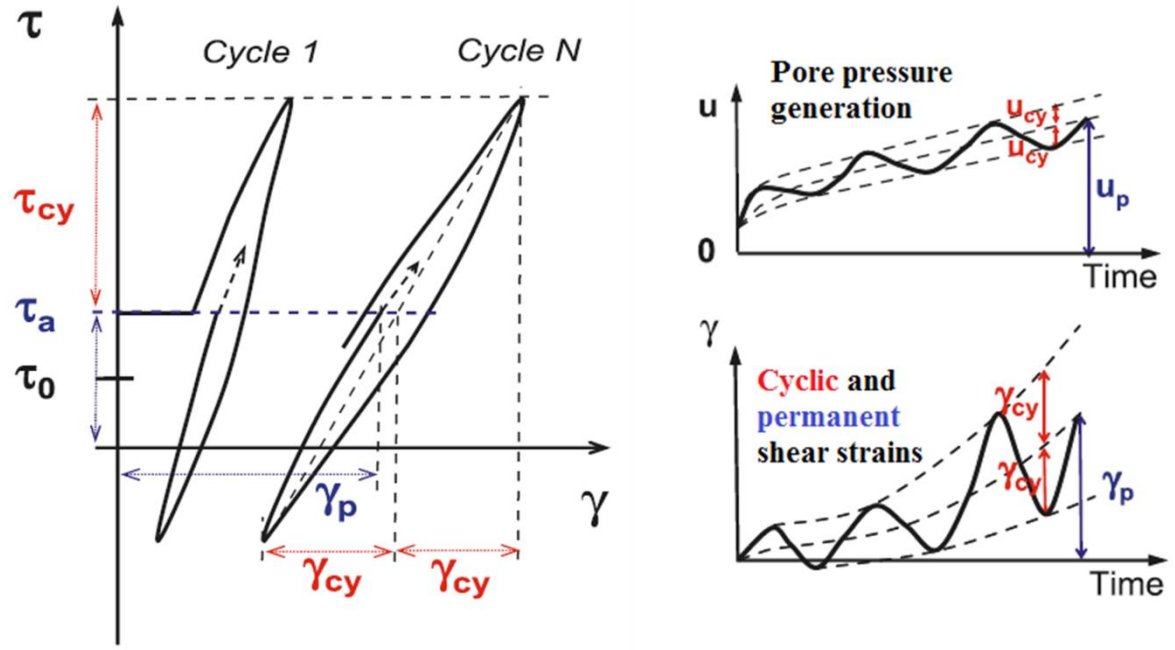

a) Stress-strain behavior

b) Pore pressure and shear strain as function of time

Fig. 2.23 Definition of stress and strain under cyclic loading (Andersen 2009)

Cyclic loading may reduce the bearing capacity of a soil and the bearing capacity under cyclic loading may be lower than the capacity under monotonic loading (Andersen 2009). This happens because the tendency of the cyclic loading to break down the soil structure which results in a tendency of soil contraction. Plastic irrecoverable shear deformations of soils are accompanied by volume changes when drainage is allowed. In undrained conditions this implies a reduction or increase in pore water pressure (u) and a rise or drop in the effective stress (σ') and shear strength as well. As the total stress is the weight of the soil and remains constant, the effective stress is calculating the subtracting the total stress to the pore water pressure (Eq. 2.4).

$$\sigma' = \sigma - u \tag{2.4}$$

In the case of loose soils, the pore water pressures increase progressively with the load, this leads to the transfer of stress from the soil skeleton to the pore water resulting a decrease in effective stress and shear resistance of the soil, which produces that the soil can undergo large deformations (Fig. 2.23b). In some cases this can lead to liquefaction. Dense soil can endure high levels of shear stress due to the

generation of negative excess pore water pressure, in other words the dilation due to the excess pore pressure resulting in an increased shear resistance.

During cyclic or seismic loading, the stress path of a soil element in undrained condition is moving towards the origin until it reaches the characteristic state line due to the increase of pore pressure (Fig. 2.24). When the CL is touched on one side of the p'axis, the strain development and the pore pressure rapidly augmented and the stress path depicts a butterfly wing passing near the origin.

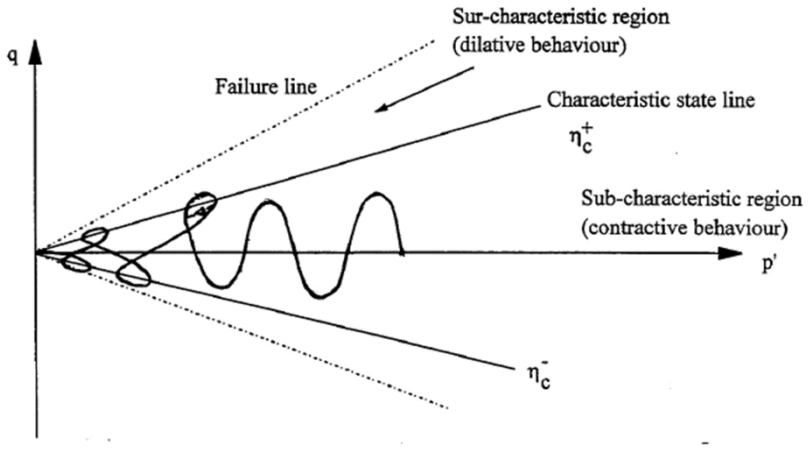

Fig. 2.24 schematic representation of liquefaction (Peiris 1998)

Fig. 2.25 shows the cyclic stress-strain curve with their associated cyclic paths for loose and dense Shirasu sand. These plots correspond to the same cases analyzed with monotonic loading in the previous section. A sinusoidal load with a frequency of 0.1 Hz was utilized in the triaxial tests (Hyodo et al. 1998).

It can be noted that in the case of loose sand the initial cyclic strains were very small and then suddenly they were importantly augmented as p' approached to zero in the last cycles which can trigger liquefaction (Fig. 2.25a). In Fig. 2.25b, is observable that in dense sand the effective stresses are importantly reduced over the 20 cycles and then form a relatively static loop as the cyclic axial strain steadily increments to large values on the extension side (cyclic mobility). The liquefaction and the cyclic mobility are defined and explained in detail in Section 3.3.5.3 of this Chapter.

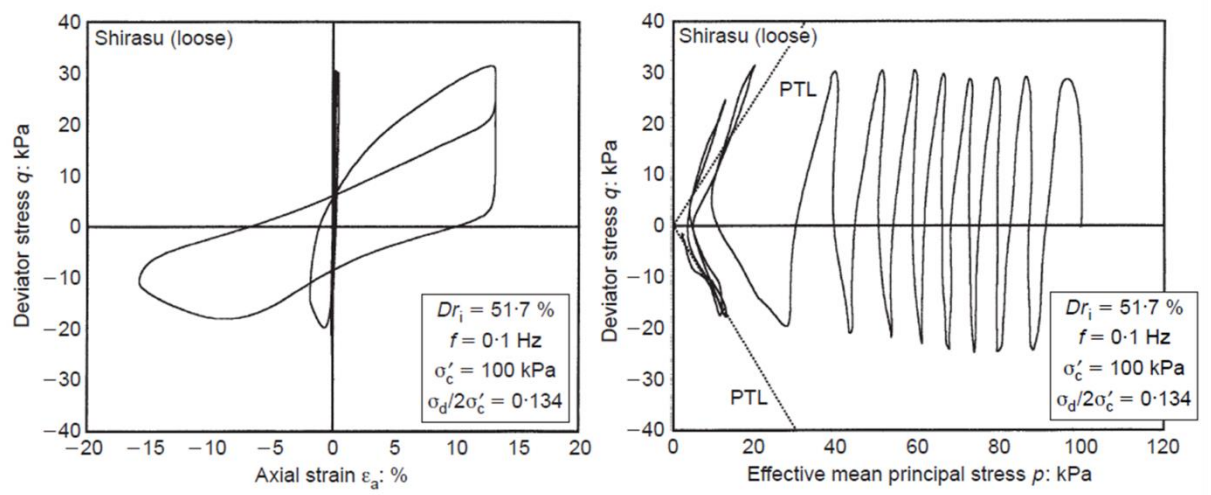

a) Loose condition

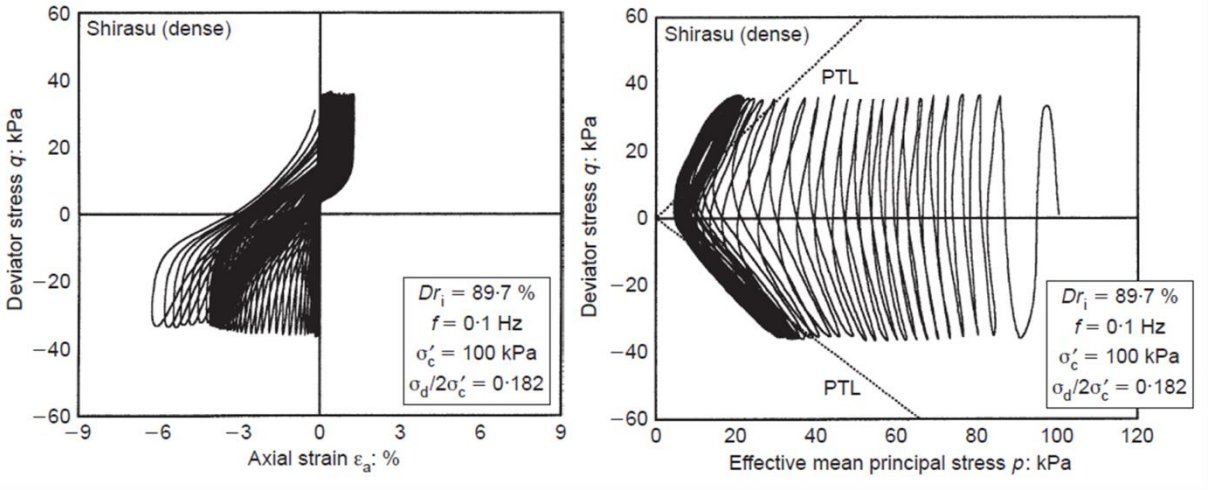

b) Dense condition

Fig. 2.25 Stress-strain curve and cyclic effective stress path for Shirasu sand under cyclic loading (Hyodo et al. 1998)

3.3. Important Aspects in the Dynamic Response of Soil

During an earthquake event, seismic waves coming from an underground source impose movements in the soil (Fig. 2.26). These movements can cause serious damage in structures supported in the shaking affected area. The properties of the soil have an important role on the traveling of seismic waves and vice versa. Shear stresses induced by propagation of shear waves are the main focus in geotechnical earthquake engineering. Thus, the description of the soil response, that is usually described through shear stress and shear strain relationships, is highly important under cyclic or dynamic loading (Ishihara 1996). Fig. 2.27a depicts a stress-strain curve, which exhibits a hysteresis loop. When the soil is in a strain state that has a higher magnitude that the previous maximum attained by the soil, it is in the path of first loading. However, if the soil is in a strain state that has a lower magnitude than its previous maximum the soil is either in an unloading or reloading path (depending on the strain increment or decrement with time). From this information, two important parameters in

the evaluation of dynamic soil behavior are the stiffness properties of soil and the damping characteristics.

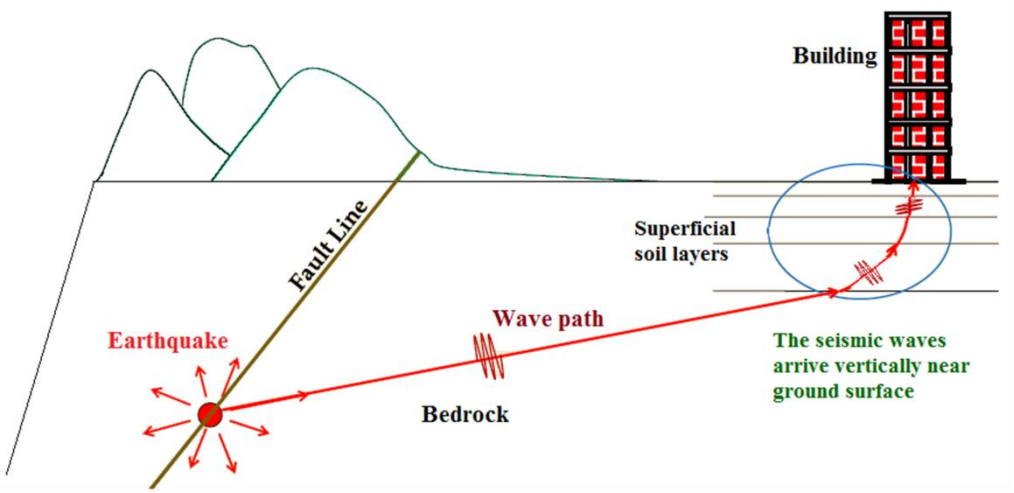

Fig. 2.26 Seismic waves traveling on the soil

3.3.1. Soil Stiffness

The shear strength of a soil in any direction is the maximum shear stress that can be applied to the soil in that direction. It can also be defined as the resistance to deformation by continuous shear displacement of soil particles. The stiffness characteristics of soil govern the material strains which are result of rearranging of particles inside of the soil when the soil is stressed.

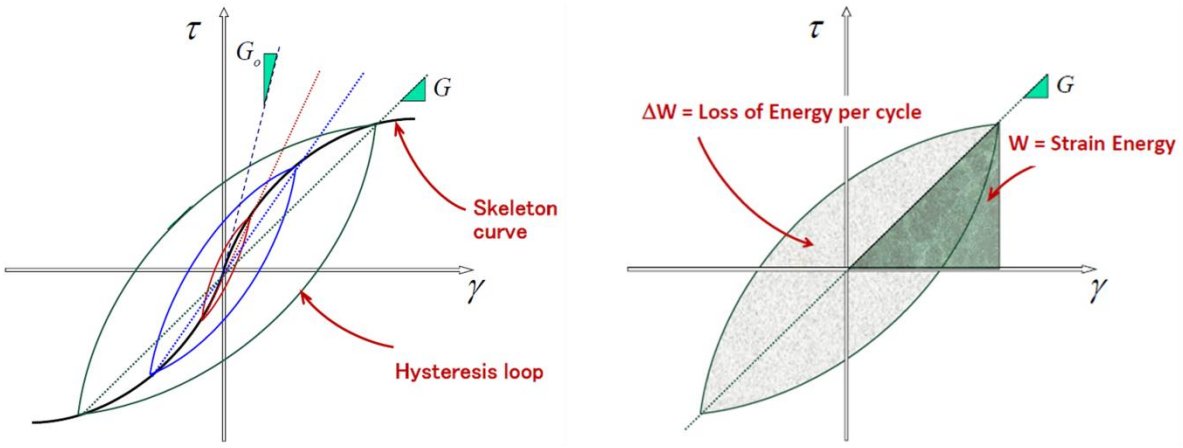

a) Hysteretic loop **b)** Hysteretic damping

Fig. 2.27 Stress-strain relationship of soil under cyclic loading

The stiffness of soil is usually represented by the secant shear modulus (G_{sec}). In this study the G_{sec} is denoted as shear modulus G (Fig. 2.27a).This shear modulus is defined as the ratio of the shear stress to shear strain

$$G = \frac{\tau}{\gamma} \tag{2.5}$$

The maximum value of shear modulus, presented at very small strains, can be related with the shear wave velocity traveling through the soil with the Eq. 2.6 (Kramer 1996).

$$G_0 = \rho v^2 \tag{2.6}$$

where ρ is the bulk density of the soil.

3.3.2. Damping

As mention in Section 2.3.2 of this Chapter, the damping, in the context of dynamic loading, relates to the energy dissipation of energy through the boundaries or by soil itself (radiation and material damping). Material damping is depending on the characteristics of the soil. Soil damping is very significant dealing with seismic loadings because it allows the reduction of an excitation over time and the mitigation of damage in structures. The main way to dissipate energy in soil is though hysteretic damping (Ishihara 1996).

The damping properties of a soil under cyclic loading can be described with the energy dissipated during one cycle of load (Fig. 2.27b). Due to the fact that the energy enclosed in a hysteresis loop (ΔW) is function of the shear amplitude of the considered cycle, a damping factor is utilized (ξ). This parameter is proportional to the energy lost and the maximum elastic energy that can be stored in a unit volume of a viscoelastic body W (Ishihara 1996). This parameter is given by the Eq. 2.7. The quantity W (expressed in Eq. 2.8) is defined as the area of the triangle bounded by a straight line defining the secant modulus.

$$\xi = \frac{1}{4\pi}\frac{\Delta W}{W} \tag{2.7}$$

$$W = \frac{1}{2}\tau_a \gamma_a \tag{2.8}$$

Each elastoplastic constitutive model can produce the shear modulus degradation and dissipate energy through the generation of hysteresis loops (if plasticity is reached).

Although the hysteretic damping is an accurate way to represent the damping behavior of soils, another way to represent the dissipation of energy is through the viscous damping. The principal difference with the hysteresis damping is the fact that the viscous damping is frequency dependent. In this study, two damping formulations (Local and Rayleigh damping) are utilized in all the calculations. These types of damping are explained in Section 1.6 Chapter 3.

3.3.3. Evolution of Dynamic Parameters with Strain

Under cyclic or dynamic loading, the shear modulus ratio is decreased with shear strain or stress level up to peak failure stress. This reduction is represented by the modulus reduction curve. Contrary, the damping is often considered to increase with strain (Kramer 1996). The evolution of the two dynamic parameters is showed in Fig. 2.28.

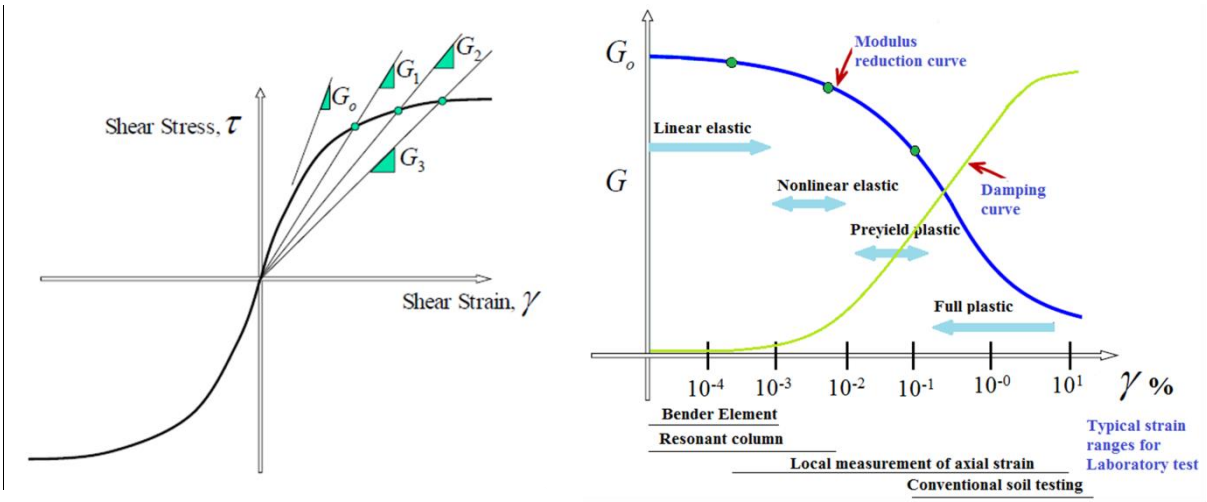

a) Secant shear modulus **b)** Typical stiffness degradation curve

Fig. 2.28 Evolution of dynamic parameters with strain

Laboratory test indicate that the parameters that influence the soil stiffness are the cyclic strain amplitude, the void ratio, the mean effective stress, the plasticity index, the overconsolidation and the number of loading cycles (Kramer 1996, Ishihara 1996). Table 2.3 presents some important parameters that influence the degradation of stiffness with strain. Some of these parameters are exemplified through real studies in Fig. 2.29.

Table 2.3 Important parameters that influence the stiffness degradation curve

Increasing Factor	**G/G0**	**Reference**
Shear strain	Decrease	(Kramer 1996) (Ishihara 1996)
Plasticity index	Decrease	(Vucetic and Dobry 1991) (Ishibashi and Zhang 1993) (Darendeli 2001)
Effective confining pressure	Increase	(Ishibashi and Zhang 1993) (Darendeli 2001)
Void ratio	Increase	(Benz 2007)
Overconsolidation	Increase in cohesive soils Small effect in non-plastic soils	(Darendeli 2001) (Benz 2007)

Number of cyclic loadings	Increase for drained sands Decrease for undrained sand Decrease for clay	(Darendeli 2001)

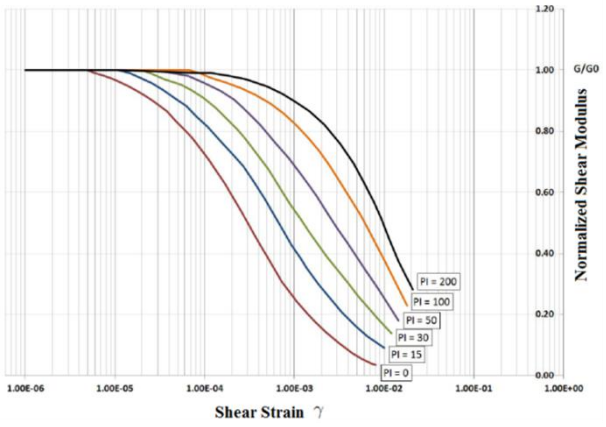

a) Values of plasticity index (Vucetic and Dobry 1991)

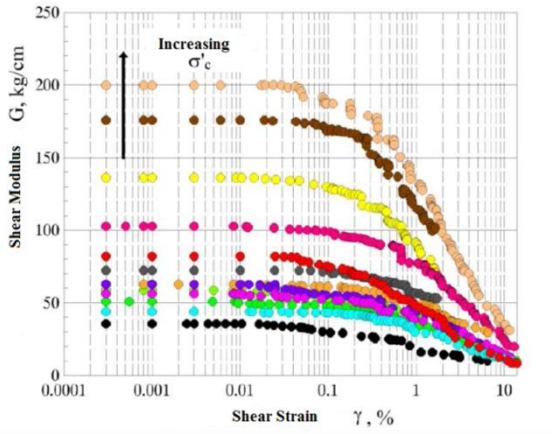

b) Confining pressure (Romo 1995)

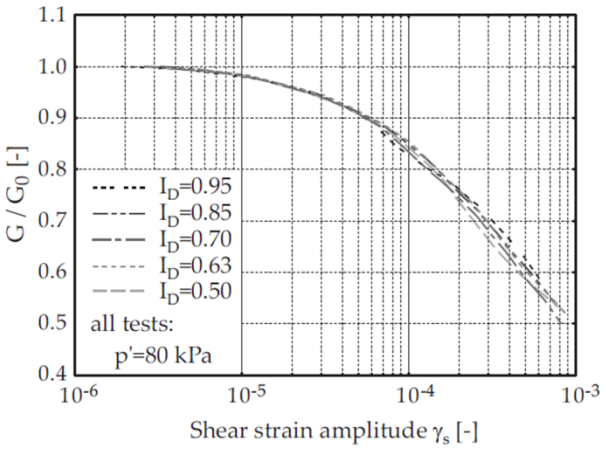

c) Void ratio (Benz 2007)

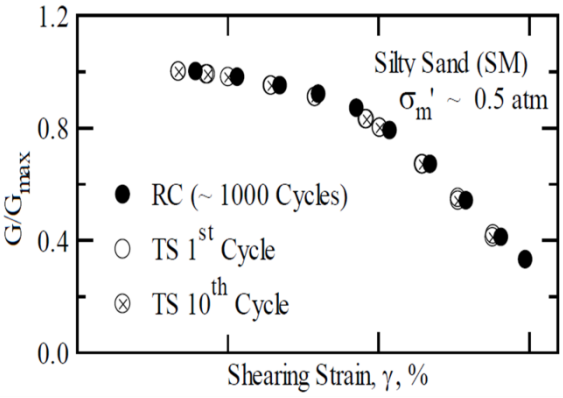

d) Number of cycles (Darendeli 2001)

Fig. 2.29 Evolution of the modulus stiffness with shear strain under the influence of several parameters

Fig. 2.28b shows that in the linear elastic zone, the soil particles do not slide relative to each other under a small stress increment, and the stiffness is at its maximum. The soil stiffness depends on contact interactions, particle packing arrangement, and elastic stiffness of the solids. In this range the behavior of soil is independent of the frequency and the number of cycles.

After that the stiffness begins to decrease from the linear elastic value as the applied strains or stresses increase, and the deformation moves into the nonlinear elastic zone. However, a complete cycle of loading, unloading, and reloading within this zone shows full recovery of strains. In this zone the strain covers a range from $5x10^{-4}$ % for non-plastic soils at low confining pressure conditions to $5x10^{-2}$ % at a high confining pressure or in soils with high plasticity (Santamarina et al. 2001).

In the preyield plastic zone, irrecoverable strains are developed. The soil behavior becomes elastoplastic and the shear modulus tends to decrease as the shear strain increases, and at the same time energy dissipation becomes apparent during cycles of load application. The initiation of plastic strains can be determined by examining the starting of permanent volumetric strain in drained conditions or residual excess pore pressures in undrained conditions after unloading. The equivalent linear method based in the viscoelastic theory is a useful way to represent the soil behavior with a reasonable degree of accuracy. Experimental data suggest that the strain level that initiates plastic strains ranges between $7x10^{-3}$ and $7x10^{-2}$ %, with the lower limit for uncemented normally consolidated sands and the upper limit for high plasticity clays and cemented sands.

The yielding zone is where the full plastics strains are generated. The yield envelope expands, shrinks, and rotates as plastic strains develop. It is usually considered that expansion is related to plastic volumetric strains; the surface expands when the soil compresses and shrinks when the soil dilates. The soil properties tend to change appreciably not only with shear strain but also with the progression of cycles (number of cycles may be of great importance).

Table 2.4 shows a summary of the variation of soil properties with strain. In this table is shown that the effect of repetition begins to appear when the magnitude of shear strain increases above a level of 10^{-1} %.

Table 2.4 Variation of soil properties with strain

Cyclic shear strain amplitude (%)		Associated phenomena	Mechanical characteristics	Behavior	Effect of repetition
Very Small	$< 10^{-3}$	Vibration, wave propagation	Elastic	Practically linear	No (negligible)
Small	10^{-1} - 10^{-3}	Cracks, differential settlements	Elasto-plastic	Non-linear	Yes (relevant)
Large	$> 10^{-1}$	Slide, compaction, liquefaction	Failure	Non-linear	Yes (relevant)

3.3.4. Soil Testing from very small to small strains

The smallest shear strain that can be reliably measured in conventional soil testing without special instrumentation is 10^{-1} % as shown in Fig. 2.28b. However, advanced laboratory test and in situ measurements makes it possible to determinate low strain stiffness values. The principal advantage of quantifying small strain shear modulus is because less conservative geotechnical designs or accurate numerical soil analyses can be made.

3.3.4.1. Laboratory Test

Local transducers

The typical triaxial test and its arrangements do not allow accurate determination of specimen deformation at the small strain level in which the maximum stiffness and strength can be more representative of the in-situ soil response. This is due principally to the system compliance (measure of unrelated movements and deformations), the bedding error and because the friction between the surface of the specimen in contact with the end platens. To overcame these imprecisions local strain measurements can be calculated through placement of axial and radial strain transducers directly on to the test specimen (Seed et al. 2001). The transducers are fixed via two mounting blocks, which displace relative to one another as the specimen deforms (Fig. 2.30a). The deformation of a gauge length can be calculated from measuring the absolute movements of two targets by two independent instruments and subtracting one from the other. Hall Effect displacement transducers or Linear Variable Differential Transformer (LVDT) are usually utilized.

To increase the accuracy of pore pressure measurement during shear, pore pressure transducers may be employed within a triaxial system (Fig. 2.30b). These transducers are fixed and placed in contact with the specimen at mid-height. A hole is cutting in the specimen membrane, allowing a flanged grommet to be slipped between soil and membrane. Inside of this, a porous stone is placed in contact with the soil, permitting the pore pressure to be recorded by movement of the diaphragm. The void between the porous stone and the diaphragm is de-aired to obtain precise pore pressure records.

Resonant column test

Resonant column can load soil samples not only triaxially but also torsionally (Pecker 1984, Ishihara 1996, Kramer 1996). Resonant column test is a cyclic test, in which an axially confined cylindrical soil specimen is set in a fundamental mode of vibration by means of torsional or longitudinal excitation of one of its ends. Once the fundamental mode of resonance frequency is established, the measured resonant frequency can be related to the stiffness of the column using a theoretical elastic solution, which provides satisfactory results in the very small strain range. Resonant column testing can usually be accomplished within a single device.

Bender element test

Using bender element in a triaxial system, the very small strain (below 10^{-1} %) response of a soil can be obtained. With bender elements is possible to obtain the maximum shear modulus of a specimen, which is an important parameter for use in geotechnical design and numerical analyses (Fig.

2.30c). Bender elements are piezoelectric ceramic bimorphs that stand out a small distance into the soil specimen. They can be placed in pairs vertically or horizontally in the test specimen as shown in Fig. 2.30c. During a test, one element generates either a P-wave or an S-wave in the specimen through an excitation voltage. The other element catches the generated wave that propagates through the soil.

To estimate the compression and shear wave velocities (V_p and V_s) with the bender element test, it is necessary to record the time (t) that a generated wave takes to travel from one element to the other one and then divide the distance between the elements by this travel time. It is usually the use of element tip-to-tip distance for this calculation. Subsequently, assuming linear elastic material behavior, elastic stiffness is obtained through the equation 2.5.

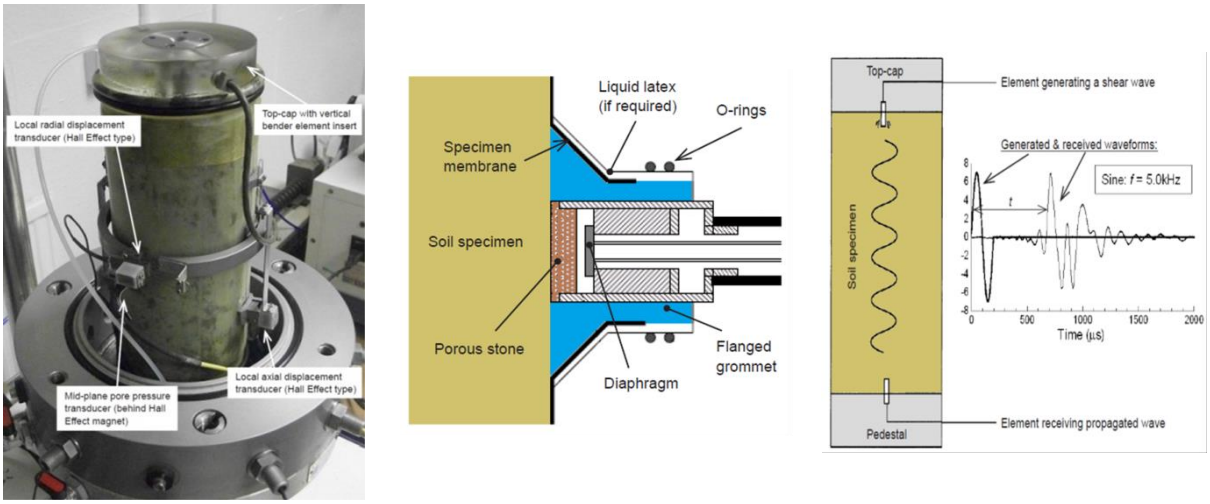

a) Axial and radial transducers **b)** Pore pressure transducer **c)** Bender elements

Fig. 2.30 Advanced laboratory test to measure small strain in soils (Rees 2013)

3.3.4.2. In Situ Measurements

Field or in-situ tests can be used to get the stiffness of soil at very small strain; they are based in geophysical principles, such as, crosshole seismic, downhole seismic and suspension logging.

Crosshole and downhole seismic

In the crosshole technique at least two vertically drilled boreholes are required. In one of them, an energy source is placed at the depth of soil required and in the one receiver is set at the same depth (Fig. 2.31a). The distances between the boreholes must be known exactly, which typically demands inclinometer reading in each borehole. From the source of signal to the receiver device, it is possible to calculate the horizontal wave propagation velocities. From these velocities, maximum soil stiffness is calculated in the same way as in bender element test, but often without knowing the exact density of

the soil. When the readings are taken from different source and receiver depths the propagation velocities can be found for all soil layers. This technique is probably the most efficient to obtain small stiffness values but also the most expensive.

The downhole test requires the drilling of only one borehole, in which a string of receivers are placed (Fig. 2.31b). In this case, the energy source, generally a hammer blow against a steel plank, is situated at the surface. Downhole test is considered an integral measurement over different soil layers. Having receiver recordings from different depths, the initial stiffness of different soil layers can be back-calculated from the recording in the receiver devices at different depths. A disadvantage of this technique is the refraction of waves.

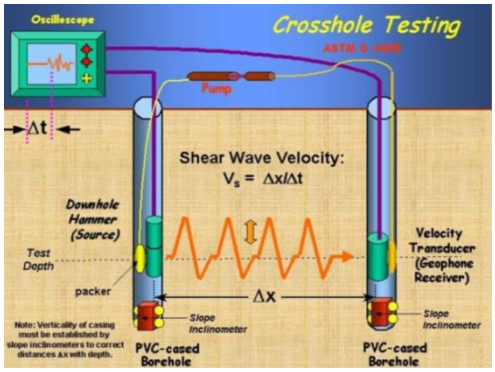

a) Cross Hole seismic test

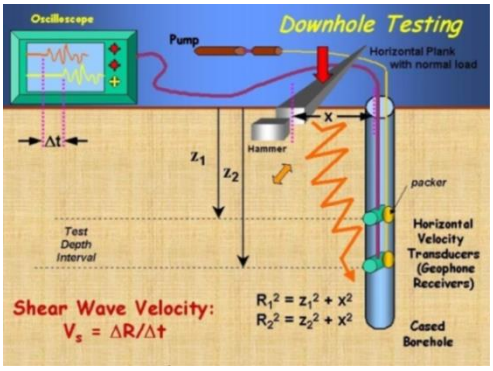

b) Down Hole seismic test

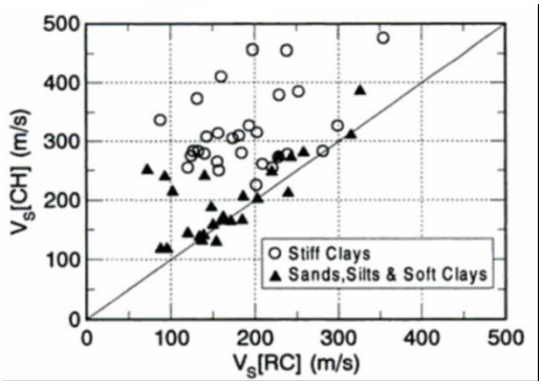

c) Comparison of Vs from crosshole and RC (Pitilakis and Anastasiadis 1998)

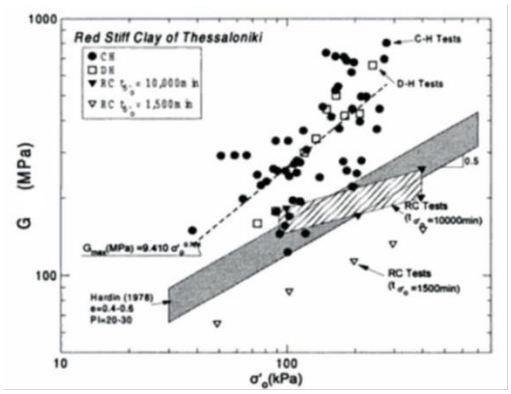

d) Comparison of G values with crosshole and RC (Pitilakis and Anastasiadis 1998)

Fig. 2.31 In situ test to measure small strain in soils

Fig. 2.31c shows a comparison between RC and crosshole/downhole measurements of S-waves velocity. Note that most of the soil tests show generally higher values of Vs in crosshole compared with RC. In Fig. 2.31d are shown the values of shear modulus (G) measured from crosshole and downhole tests at various depths and locations, and from resonant column tests for two confining time pressures for a red stiff clay of Thessaloniki (PI=20, e=0.45). It is noted that the values of G show a

scatter behavior from in situ measurements. Besides that, it can be noted the difference between in situ and laboratory values which are influenced by the confinement time of testing in the RC apparatus.

Suspension logging

A similar way as the downhole, the suspension logging provides velocity data from a single borehole. In this case the source and receivers are situated in the same borehole where they are separated by a few meters drilling suspension only (Fig. 2.32). The propagation of waves along the wall in the borehole is the main purpose of the system. Suspension logging can generate an approximate stiffness profile at very small strain of the borehole's vicinity.

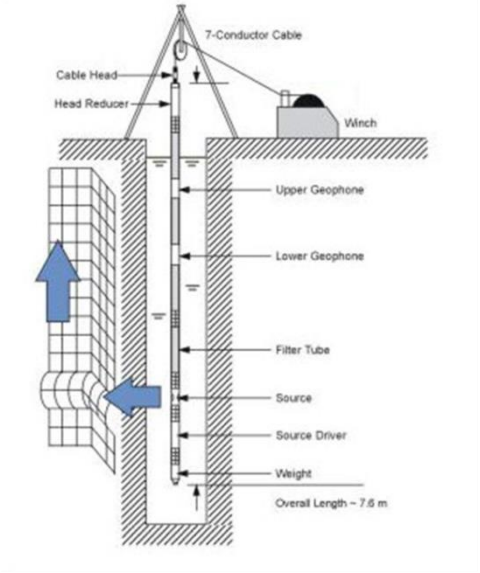

Fig. 2.32 Suspension logging test

3.3.5. Other Significant Characteristics of Soil under Cyclic Loading

Additional important aspects of dynamic cyclic loading that differentiate the soil response from traditional static behavior are rate-dependency of soil response and the reversal of applied stress the when cyclic tests are carried out.

3.3.5.1. Rate-dependency of Soil Response

The response of the soil may be importantly affected by the rate of application of loading. This effect becomes significant once the shear strain of a soil enters the elasto plastic range. This rate-dependency is influenced principally by the inter-particle viscosity and the ability of the soil to dissipate the excess pore pressure. The first one is essential in cohesive soils but in cohesionless soils only the generation of excess pore pressure is important.

The loading rate may highly modify the strength measured in conventional laboratory test usually carried out at slower loading rates than those in shaking during earthquakes. The strength of cohesionless soil is not affected by the loading rate but plastic cohesive soils can display an increment in the strength. For instance, Boulanger and Idriss (2006) founded a strength gain of around 9% per log cycle of loading rate in different types of clays. Romo (1995) obtained increments of 30 to 60% in the strength for clay sample of Mexico City.

3.3.5.2. Reversal of Applied Stress

The reversal stress applied to a soil element signifies the variation in sign of the rate of stress increment. For instance, in triaxial test, this reversing means oscillating between increasing and decreasing values of deviator stress q applied to a soil test sample. If the sign of the applied stress change is referred as a two-way pattern and one-way cyclic loading pattern when the sign does not change (Fig. 2.33). In two-way loaded triaxial tests the soil will be affected of both compression and extension. In this case the soil does not have the same strength when developing negative and positive shear strain, because the extension strength is lower than the compression strength. According to Ghionna and Porcino (2006) and Gennaro et al. (2004), one way loading in compression is more stable than a loading with reversal stress whether they are isotropic or anisotropic.

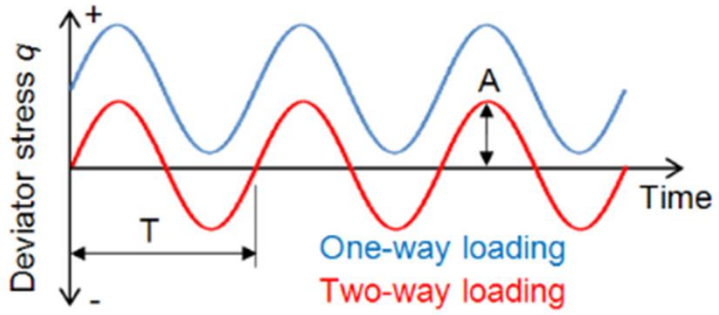

Fig. 2.33 One-way and two-way cyclic loading patterns

Two main characteristics of soil response when undergoing stress reversal are the accumulation of plastic shear strain and the generation of excess pore water pressure. These features only occur once the soil behavior becomes elasto-plastic.

The plastic shear strain is the increment of soil deformation that is permanent or irrecoverable. Although in cyclic loading the increment of plastic strain is small in a single cycle, the accumulative effect from numerous loading cycles may be highly important. Fig. 2.34 shows a typical response during a cyclic undrained triaxial test of Gioia Tauro sand (Ghionna and Porcino 2006). It is noticeable in Fig. 2.34a that the increment of plastic shear strain observed during the first load cycle is in the order of 0.1 %, however, after 22 load cycles the accumulated shear strain applied to the soil

exceeds 6 %. The plastic strain increments tend to reduce as an increasing number of loading cycles are applied to a soil.

The generation of excess pore water pressure in soil is explained in the following section where the liquefaction phenomenon is treated.

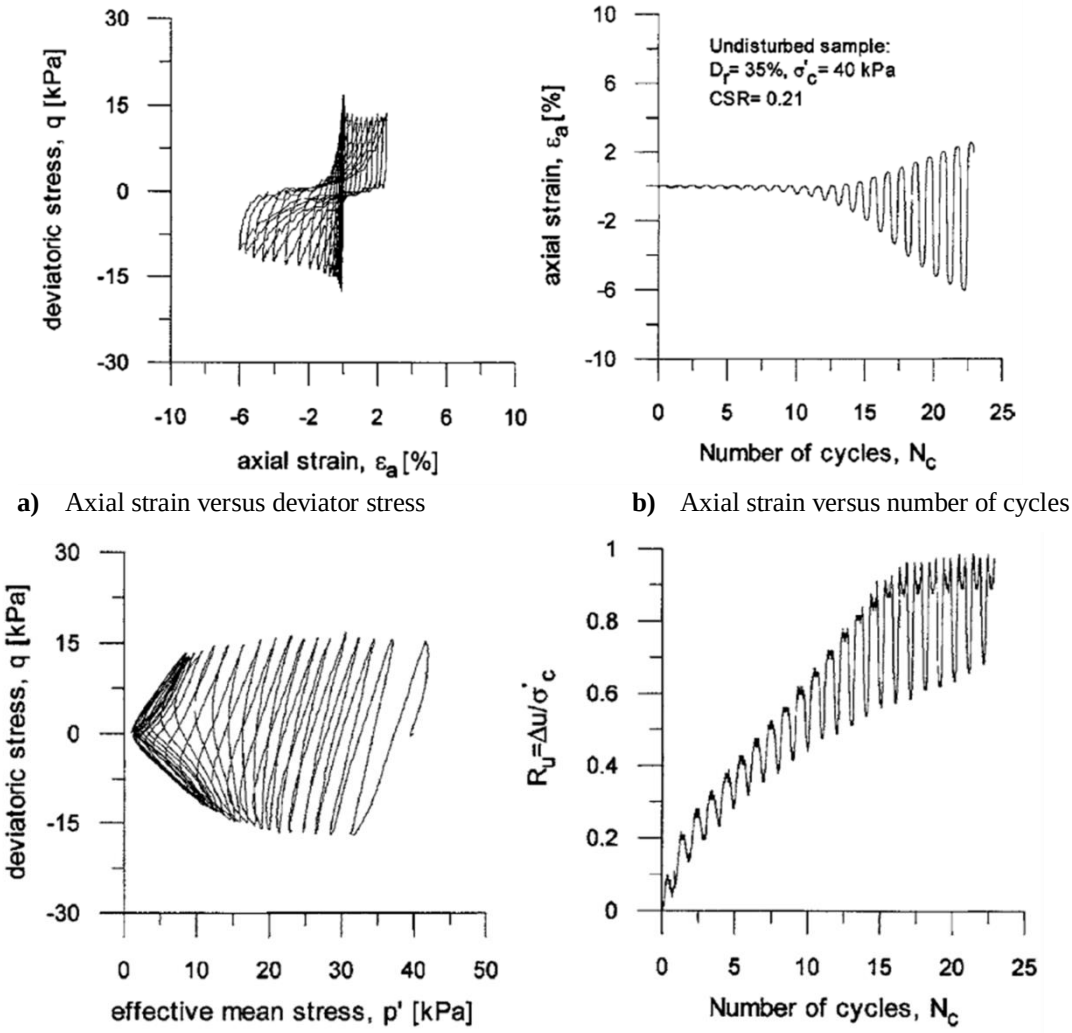

a) Axial strain versus deviator stress

b) Axial strain versus number of cycles

c) Mean effective stress versus deviator stress

d) Excess pore water pressure versus number of cycles

Fig. 2.34 Typical response during a cyclic undrained triaxial test of Gioia Tauro sand (Ghionna and Porcino 2006)

3.3.5.3. Liquefaction Phenomenon

Liquefaction is one of the significant and complex issues in geotechnical engineering because it has been reported as the main cause of damage and failure in buildings and other structures under earthquakes (Niiagata 1964, San Fernando 1971, Loma Prieta 1989, Kobe 1995, Haiti 2010). Fig. 2.35 shows some historic examples of the failure due to liquefaction. Many researchers have shown that

sands in loose assemble are more susceptible to get liquefaction (Kramer 1996, Youd et al. 2001, de Groot et al. 2006).

The term liquefaction was first utilized by Mogami and Kubo (1953). Then many specific and extended definitions have been given by several researchers (Sladen et al. 1985, Ishihara 1993, Idriss and Boulanger 2008).

The liquefaction takes place due to the accumulation of pore pressure in loose saturated sand deposits under dynamic loading, which in turns produce an important reduction in the strength of the underlying soils. The loss of bearing capacity and the foundation settlements are the consequences of this soil strength reduction. Reference studies considering pile foundations in liquefiable soils can be consulted in Section 2.3.4 of this Chapter.

a) Building toppling Niigata 1964 **b)** Quay wall earthfill Kobe 1995

Fig. 2.35 Failure in structures due to liquefaction

The change of pore pressure that occurs within a saturated soil as a load is applied is referred as excess pore water pressure generation. Dealing with cyclic loading, this feature is mainly influenced by the drainage conditions of the soil and the loading rate. The soils with low permeability subjected to faster loading rates are easily prone to develop excess pore pressure.

In practice, a build-up of excess pore pressure reduces the effective stress in the soil, which in some cases implies that the ability of the soil to resist shear loading is lost, resulting in significant soil deformations or complete failure (Seed and Lee 1966). The mechanism of pore pressure rise is illustrated in Fig. 2.36 (Seed 1979). The point A represents the initial state of saturated sand. When sheared the sand tends to contract its volume towards point B. Because the undrained condition, the volume and the void ratio have to keep constant. To remove this volume contraction (AB) unloading of effective stress by swelling (BC) is necessary. In reality the state of the soil moves directly from A to C because the volume contraction and the swelling are superimposed.

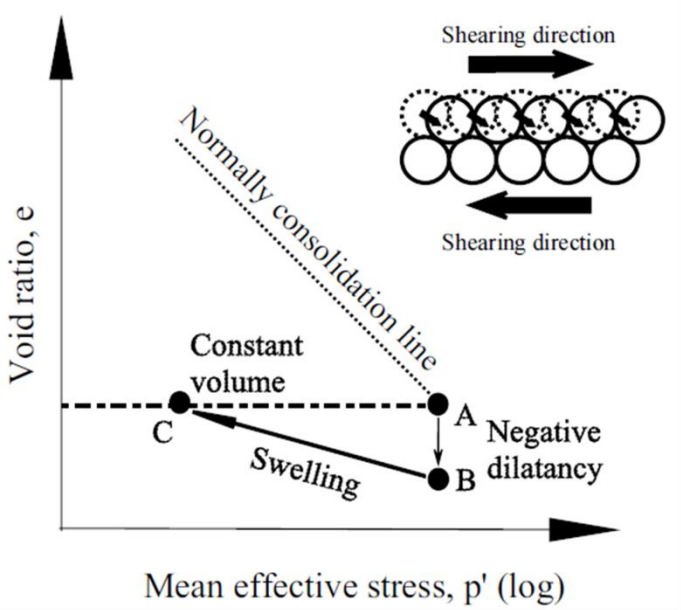

Fig. 2.36 Mechanism of pore pressure increment (Seed 1979)

In this study, the excess pore water pressure ratio (r_u) is defined as the ratio of the difference of pore pressure in a specified stage (u) and initial pore pressure (u_0) over the initial effective stress (σ'_0). When $r_u = 0$, the pore pressure is equal to the applied back pressure. The true liquefaction takes place when the excess pore water pressure ratio is equal to 1 if the total stresses are kept constant during the cyclic loading (Fig. 2.34c). This is applicable for loose to medium sand. However, for dense sand, the onset of liquefaction is defined as the development of 5% double amplitude of the axial strain (Ishihara 1993). An example of generation of excess pore pressure during a cyclic triaxial test under undrained condition is showed in Fig. 2.34d.

The phenomena can be divided into two main categories: flow liquefaction and cyclic mobility. Flow liquefaction occurs when the shear stress required for static equilibrium of a soil mass is greater than the shear strength of the soil in its liquefaction state. The large deformations produced by flow liquefaction are driven by static shear stresses. The cyclic mobility occurs when static shear stress is less than the shear strength of the liquefiable soil. The deformations due to cyclic mobility are caused by static and dynamic stresses that exist during an earthquake. Lateral spreading is a common result of cyclic mobility. Castro and Poulos (1977) described the difference between liquefaction and cyclic mobility using the concept of critical state line (Roscoe et al. 1958) in a diagram with the void ratio (e) and effective minor principal stresses axes (Fig. 2.37). The steady-state line represents the locus of state in which the soil can flow at constant void ratio, constant effective minor principal stress and constant shear stress. They stated that the liquefaction occurs only in contractive soils.

Gennaro et al. (2004) showed that the one-way loading in compression can generate either failure by cyclic mobility or flow liquefaction. However, one-way loading in extension induces more instability and the failure is by flow liquefaction.

In this study it is also considered that when $0.8 < r_u < 1.0$ there is a development of large strains and cyclic mobility occurs (Koutsourelakis et al. 2002, Montoya-Noguera and Lopez-Caballero 2016). For this reason, in this study is considered the liquefaction is triggered when $r_u = 0.8$.

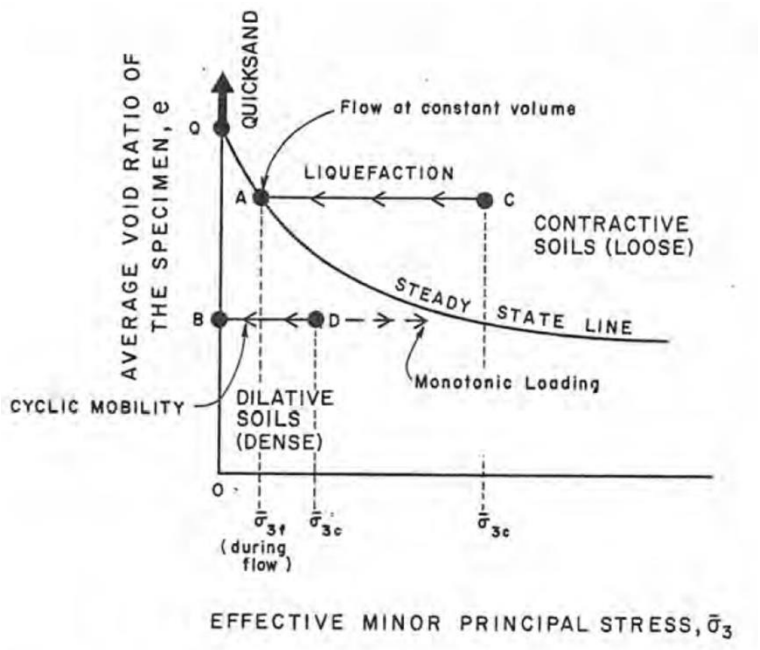

Fig. 2.37 Steady-state line (Castro and Poulos 1977)

Many factors related to the property of the soil can influence liquefaction potential (dynamic shear modulus, relative density, grain size characterization, soil initial state). Others are related with the geological conditions (depth of water table, effective confining pressure, rate of saturation). Also, the characteristics of the dynamic load are important (frequency and amplitude, duration of the shaking).

The evaluation of liquefaction potential can be developed with different methods. For instance, with in situ test such as the Standard Penetration Test (SPT), the Cone Penetration Test (CPT) and in situ shear wave velocity. The data of these tests are generally related with the intensity of the earthquake and the cyclic stress ratio required for liquefaction to develop empirical correlations (Seed et al. 1985). There are also boundary curves to identify the susceptibility to liquefaction based on the grain size distribution.

4. Overview of Soil Constitutive Models with Dynamic Loading

The analyses of SSI problems depend on the representation of the relations between stresses and strains for the materials involved. These relations are represented by a set of mathematical expressions that model the behavior of the soil and they are called constitutive model. Numerous constitutive models have been developed over the past to model the stress-strain behavior of soils. Simple and complex models are formulated on the basis of principles of solid mechanics based on experimental data or theoretical principles. The complexity and capabilities of the models differ and the determination of parameters is not uniform. In this study, to represent the behavior of soil and structural elements simple and complex constitutive models were utilized (linear elastic, elastic perfectly plastic with Mohr-Coulomb failure, Finn and Sanisand model). The characteristics and abilities of each model are explained below.

4.1. Linear Elastic Model

The Linear Elastic model is used to describe materials where the strains in the material are small, the stress is proportional to the strain, the material return to its original shape when the loads are removed and there is no dependence on the rate of loading or straining.

In the linear elastic range, the constitutive equations are represented in Hooke's law. The basic relations between stress and strain are described completely by two elastic constants, Poisson's ratio (ν) and the Young's modulus (E). The generalized Hooke's Law for a three-dimensional state of stress and strain in a homogeneous and isotropic material in index notation is

$$\varepsilon_{ij} = \frac{1+\nu}{E}\sigma_{ij} - \frac{\nu}{E}\sigma_{kk}\delta_{ij} \tag{2.9}$$

or

$$\sigma_{ij} = \frac{E}{1+\nu}\varepsilon_{ij} + \frac{\nu E}{(1+\nu)(1-2\nu)}\varepsilon_{kk}\delta_{ij} \tag{2.10}$$

In geotechnical analysis it is common the separation of the general state of stress and strain in the mean and deviatoric responses:

$$\sigma_{ij} = \frac{1}{3}\sigma_{kk}\delta_{ij} + s_{ij} \qquad \varepsilon_{ij} = \frac{1}{3}\varepsilon_{kk}\delta_{ij} + e_{ij} \tag{2.11}$$

where s_{ij} is the deviator component of stress, e_{ij} is the distortion or shear deformation produced by the stress deviator s_{ij} and δ_{ij} is the Kronecker Delta function, $\sigma_{kk} = \sigma_{xx} + \sigma_{yy} + \sigma_{zz} = 3\sigma_m$ and $e_m = \frac{1}{3}\varepsilon_{kk}$ is the mean component.

The generalized Hooke's Law given in Eq. 2.9 can now be written in terms of deviatoric and mean stresses and strains using Eqs. 2.11, resulting

$$s_{ij} = 2Ge_{ij} \qquad \sigma_{kk} = 3K\varepsilon_{kk} \tag{2.12}$$

In these equations K is the bulk modulus and G is the shear modulus.

$$K = E/3(1-2\nu), \qquad G = E/2(1+\nu) \tag{2.13}$$

This model can be a good approximation to represent the behavior of some structural elements interaction with the soil or in the simulation of the behavior of bedrock layers (Pinto 2012). However, considering soils this model is only valid at very small strain (< 10^{-3}%). This implies that the use of this model requires a previous knowledge of the range of the strain in the soil such as in the study developed by Mánica-Malcom et al. (2016).

Dealing with cyclic loading, this model does not account for the reduction in shear modulus with increasing strain amplitude, the dissipation of energy through damping at any strain amplitude and irreversible strains that occur in the soil for strains at a certain threshold.

4.2. Elastic-perfectly Plastic Model with Mohr-Coulomb Failure Criteria

The elastic-perfectly plastic model with Mohr-Coulomb failure criteria model (termed Mohr-Coulomb model afterwards) is often used to model soil behavior in general and serves as a first-order model. In the area of geotechnical engineering, a number of problems, such as cavity expansion, embankment stability, and footing bearing capacity, can be examined using this model together with the simplifying assumption of plane strain.

The Mohr-Coulomb model assumes that for a given material, the yield will occur when the Mohr's circles of stress reaches the line corresponding to the shear strength (Fig. 2.38). This straight line is based in the Coulomb failure criterion and can be expressed with Eq. 2.14.

$$\tau_f = \sigma_f \tan\phi + c \tag{2.14}$$

where τ_f is the shear strength, σ_f is the normal stress, c is the intercept of the failure envelope with the axis (also called cohesion), and ϕ is the slope of the failure envelope (also called angle of internal friction).

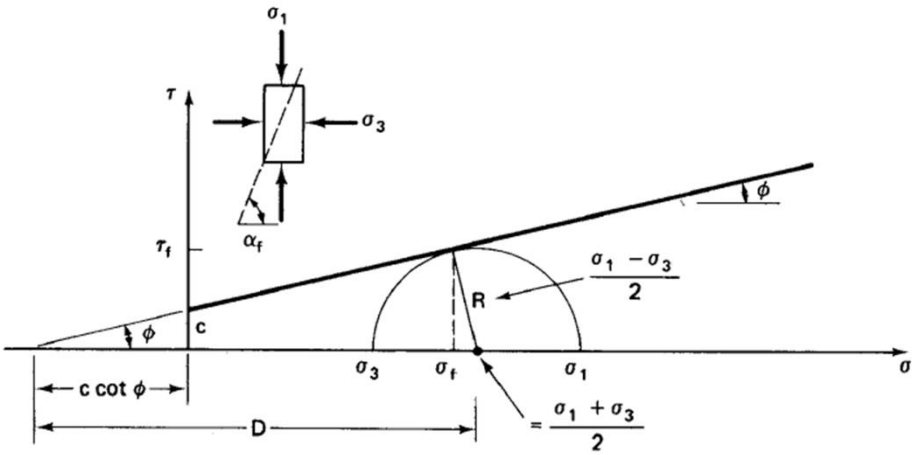

Fig. 2.38 Mohr-Coulomb yield criterion (Labuz and Zang, 2012)

By constructing a Mohr circle tangent to the line (a stress associated with failure) and using trigonometric relations, the Mohr-Coulomb yield criterion can also be given in terms of the principal stresses, as follows:

$$(\sigma_1 - \sigma_3) = (\sigma_1 + \sigma_3)\sin\phi + 2c\cos\phi \tag{2.15}$$

where σ_1 and σ_3 are the major and minor principal stresses respectively.

The yield function of this model is given by Eq. 2.16 and is represented in triaxial stress space in the Fig. 2.39.

$$F(\boldsymbol{\sigma}, \boldsymbol{k}) = (\sigma_1 - \sigma_3) - (\sigma_1 + \sigma_3)\sin\phi - 2c\cos\phi \ = 0 \tag{2.16}$$

The Mohr-Coulomb model is often utilized for the plastic potential definition by the Eq. 2.17

$$P(\boldsymbol{\sigma}, \boldsymbol{m}) = (\sigma_1 - \sigma_3) - (\sigma_1 + \sigma_3)\sin\psi = 0 \tag{2.17}$$

where ψ is the dilatancy angle. If $\psi = \phi$, then the soil material has an associated flow rule ($F(\boldsymbol{\sigma}, \boldsymbol{k}) = P(\boldsymbol{\sigma}, \boldsymbol{m})$).

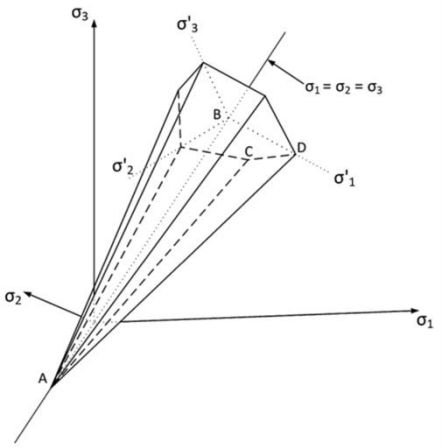

Fig. 2.39 The Mohr-Coulomb yield surface in principal stress space (Kelly 2013)

For this model, Fig. 2.40 shows a typical stress-strain relationship for soils and the evolution of stiffness and damping curves with strain. The behavior of soil is linear elastic until the yield point is reached ($F(\boldsymbol{\sigma}, \boldsymbol{k}) < 0$). In this part, the response is described by the Poisson's ratio (ν) and the Young's modulus (E). Then it is perfectly plastic at strains beyond yield point. Strains in the elastic line are recoverable, but if the material is strained beyond yield point, plastic straining beyond yield point takes place a constant stress and is unrecoverable.

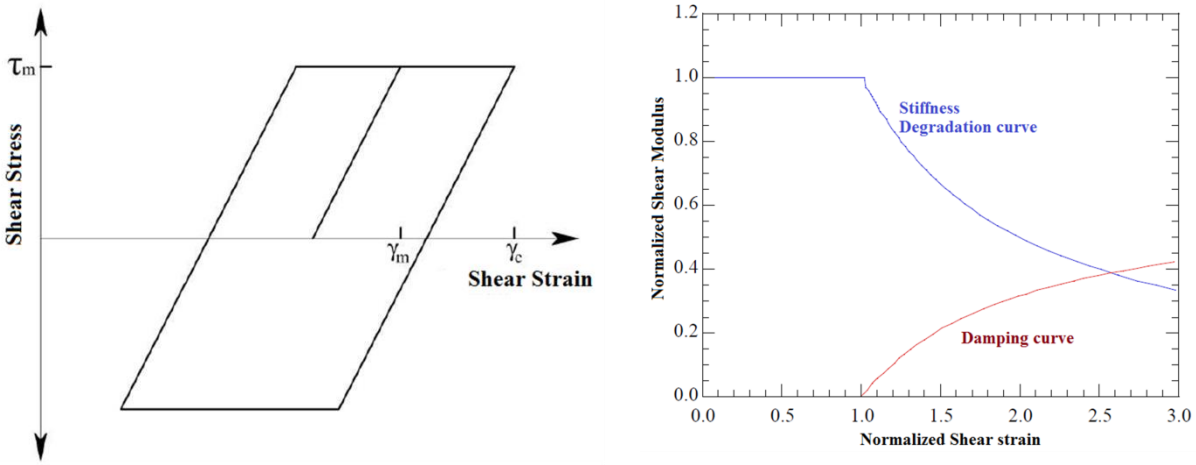

a) Cyclic shear strain relationship **b)** Stiffness and damping curves

Fig. 2.40 Mohr-Coulomb constitutive model with cyclic loading

In the context of the behavior of soil under cyclic loading, this model has several drawbacks:

In the elastic domain, this model does not take into account the reduction in shear modulus (G) with increasing strain amplitude and the dissipation of energy through damping.

Shear modulus reduction and damping only manifest themselves when the soil yields, which is known not to be the case for real soil behavior.

The linear elastic domain of the model has usually a much higher range than what is normally observed in soils.

The shape of the stress-strain curve and hysteresis loops do not correctly reproduce the observed soil behavior under cyclic loading.

The unloading and reloading paths have the same shape as the first loading path, which is known not to be the case for real soils in most circumstances.

4.3. Finn Model

Liquefaction is a process where there is a loss of shear strength of soil under monotonic or dynamic loading, which in turn is due to the tendency of the loose soil to be compacted under shear loading. Although excess pore pressure is generally associated with liquefaction, it is not the direct cause of liquefaction. The main cause is the irrecoverable volume contraction of the matrix of grains when a material is taken through a complete strain cycle under constant confining stress Martin et al. (1975). Due to this rearrangement the volume of void is reduced, which in saturated condition implies an increase of pore pressure. In this case, there is a probability that the effective stresses will reach zero due to pore pressure build-up and the soil will behave as a liquid with no shear strength.

The Finn constitutive model Martin et al. (1975) implemented in FLAC for simulating liquefaction is based on the linear elastic perfectly plastic (with a shear failure criteria of Mohr Coulomb type) constitutive model. Pore water pressure generation is modeled by computing volumetric strains induced by the cyclic shear strains using a formulation given by Byrne (1991). In this formulation the volumetric strain increment ($\Delta\epsilon_{vd}$) occurring in any cycle of loading depends on the shear strain (γ) which occurs during that cycle as well as the previously accumulated volumetric strains (ϵ_{vd}). Eq. (2.18) presents the used relationship to calculate volumetric strain increment:

$$\frac{\Delta\epsilon_{vd}}{\gamma} = C_1^c \exp\left[-C_2^c\left(\frac{\epsilon_{vd}}{\gamma}\right)\right] \tag{2.18}$$

where C_1^c and C_2^c are constants, which can be calculated by

$$C_1^c = 7600\ (Dr)^{-2.5} \quad \text{or} \quad C_1^c = 8.7(N_1)_{60}^{1/2} \tag{2.19}$$

$$C_2^c = {}^{0.4}/_{C_1^c} \tag{2.20}$$

where Dr is the relative density and $(N_1)_{60}$ is the normalized standard penetration test (SPT-N).

Thus, it can be said that the model relates volumetric strain of dry samples subjected to strain-controlled cyclic loading combined with the rebound characteristics of sand to compute residual

excess pore pressure in undrained saturated samples. With cycling loading, the shear modulus is modified for both the current strain and excess pore pressure to allow the computation of the appropriate shear strain for the current cycle. Despite of the simple formulation of the Byrne model, the main mechanisms of liquefaction can be correctly reproduced under dynamic loading. However, the used constitutive model has some limitations. It cannot generate excess pore pressure under monotonic loading. A rapid change in the pore pressures can occur since their values are updated when a half cycle is completed (Dafalias and Manzari 2004). The model cannot predict post liquefaction conditions after shaking compared with other models that use flow rules to predict this condition (Wang et al. 2014). The model cannot reproduce the cyclic-mobility response mechanism and the associated pattern of shear strain accumulation under seismic loading (Elgamal et al. 2002, Tasiopoulou and Gerolymos 2016). The effect of the particles rearrangement during cyclic loading is not considered (Dafalias and Manzari 2004, Boulanger and Ziotopoulou 2013).

Several researchers have implemented more complex constitutive models to better simulate the soil liquefaction under dynamic loading (Elgamal et al. 2002, Dafalias and Manzari 2004, Boulanger and Ziotopoulou 2013, Wang et al. 2014, Tasiopoulou and Gerolymos 2016).

4.4. SANISAND Model

SANISAND represents a family of Simple ANIsotropic SAND constitutive models developed originally by Manzari and Dafalias (1997). The model is based on a bounding surface plasticity and the critical-state soil mechanics concepts. Later extensions of the model were carried out by Dafalias et al. (2004), Dafalias and Manzari (2004), Taiebat and Dafalias (2008), Li and Dafalias (2012). The version of Dafalias and Manzari (2004) is considered in this study for its simplicity because of the few necessary input parameters. One of the distinctions of this model is that one set of material parameters can be applied to different stresses and densities. The model is suitable to simulate monotonic and cyclic loadings.

The stresses are considered as effective stresses. Both stresses and strains are considered positive in tension and pressure is assumed positive in compression. The mean pressure p is defined by $p = -p_{kk}/3$, the deviatoric stress component is $s_{ij} = \sigma_{ij} + p\delta_{ij}$ where δ_{ij} is the Kronecker delta function. The equivalent scalar-valued deviatoric stress q is given by $q^2 = (3/2)s_{ij}s_{ij}$. The superscripts e and p denote the elastic and plastic part.

The SANISAND model utilizes a hypoelastic formulation in which the incremental stress and strain tensors are linearly related through variable material moduli that are functions of the current state of stress or strain (Eq. 2.21).

$$\dot{\epsilon}_{ij}^{e} = \frac{\dot{s}_{ij}}{2G} \qquad \dot{\varepsilon}_{v}^{e} = -\frac{\dot{p}}{K} \tag{2.21}$$

where ϵ_{ij}^{e} is the elastic deviatoric strain and ε_{v}^{e} is the elastic volumetric strain defined by $\epsilon_{ij} = \varepsilon_{ij} - (\varepsilon_v/3)\delta_{ij}$ and $\varepsilon_v = \varepsilon_{kk}$. The hypoelastic shear and bulk moduli (G and K) are given by Eq. 2.22, using a dimensionless constant (G_0), the Poisson's ratio (ν), the void ratio (e) and the atmospheric pressure utilized for normalization (ρ_{at}).

$$G = G_0 p_{at} \frac{(2.97 - e)^2}{1 + e} \left(\frac{p}{p_{at}}\right)^{1/2} \qquad K = \frac{2(1+\nu)}{3(1-2\nu)} G \tag{2.22}$$

The location of the critical state line that defines the critical void ratio e_c is given by the Eq. 2.23 (Li and Wang 1998).

$$e_c = e_{c0} - \lambda_c \left(\frac{\rho_c}{\rho_{at}}\right)^{\xi} \tag{2.23}$$

where e_{c0} is the void ratio at $\rho_c = 0$, λ_c and ξ are dimensionless material constants. The distance between the current and the critical void ratio is given by the state parameter $\psi = e - e_c$ (Been and Jefferies 1985).

The yield surface is defined by Eq. 2.24, representing a cone in a multiaxial space. The parameter m controls the size of the yield surface cone, with a small value to develop plastic strain immediately after the application of shearing.

$$f = \left[(s_{ij} - p\alpha_{ij})\,(s_{ij} - p\alpha_{ij})\right]^{1/2} - \sqrt{2/3}\, mp = 0 \tag{2.24}$$

where α_{ij} is the deviatoric back-stress ratio that characterize the yield surface axis (Manzari and Dafalias 1997, Dafalias and Manzari 2004).

Three concentric and homologous surfaces (dilatancy, bounding and critical surfaces) are considered for the model in the π-plane. The evolution of the dilatant surface is defined by Eq. 2.25 and the evolution of the bounding surface by Eq. 2.26. Both are expressed in terms of the state parameter ψ.

$$M^d = M\exp(n^d \psi) \tag{2.25}$$

$$M^b = M\exp(-n^b \psi) \tag{2.26}$$

where n^d and n^b are positive material constant and M is the ultimate critical state stress ratio. The dilatancy surface defined by the slope of M^d, allows the model to reproduce contractive volumetric soil response if $s_{ij}/p < M^d$ and dilative volumetric soil response if $s_{ij}/p > M^d$. The bounding surface given by the slope of M^b, permits the model reproduce softening if $s_{ij}/p > M^b$. The lines representing

M^d and M^b converge and collapse with the critical surface line M as the sample reaches the critical state and ψ is close to 0.

The Sanisand constitutive model employs a non-associative flow rule to obtain realistic evaluations of plastic strain increments using Eq. 2.27 and 2.28

$$\dot{\epsilon}_{ij}^{p} = \langle L \rangle R_{ij} = \langle L \rangle \left[B n_{ij} + C n_{ik} n_{kj} + (D - C)\, \delta_{ij}/3 \right] \tag{2.27}$$

$$\dot{\epsilon}_{v}^{p} = \langle L \rangle D \tag{2.28}$$

where L is the loading index, $\langle - \rangle$ the MacCauley brackets ($\langle L \rangle = L$ if $L > 0$ and $\langle L \rangle = 0$ if $L \leq 0$). The scalar D associated with the dilatancy is given in Eq. 2.29 and the values of B and C to take into account the effect of Lode angle on the direction of deviatoric plastic strain rate are given in Eqs. 2.30 and 2.31.

$$D = A_d \left(\alpha_\theta^d - \alpha_{ij} n_{ij} \right) \tag{2.29}$$

where A_d is a function of the fabric dilatancy and n_{ij} is the normalized tensor.

$$B = 1 + \frac{3}{2} \frac{1-c}{c} g(\theta,c) \cos 3\theta \tag{2.30}$$

$$C = 3 + \sqrt{\frac{3}{2}} \frac{1-c}{c} g(\theta,c) \tag{2.31}$$

where c is the material constant denoting the ratio of the triaxial extensive strength to compressive strength with θ the Lode angle.

In this study, the behavior of soft soils in drained condition (Chapter 4 and 5) was modeled with the elastic-perfectly plastic model with Mohr-Coulomb failure criteria to consider the soil nonlinearity and possible shear failure in the soil elements during shaking. This model is widely used to simulate the behavior of soft soils deposits under dynamic loadings (Hatem 2009, Choudhury et al. 2014, Hokmabadi et al. 2014, Hokmabadi and Fatahi 2016). Some of these calculations were compared against the response using a linear elastic model. For the LTP, in the rigid inclusions systems, the linear elastic perfectly plastic model with a Mohr-Coulomb shear failure criterion was also considered in all cases. Some authors (Bohn 2015, Rangel-Núñez et al. 2008, Hatem 2009) have typically utilized this model to represent the granular materials in the LTP of the rigid inclusions systems. For the calculations in undrained conditions (Chapter 6), the Finn model and the Sanisand were successively utilized to model the potentially liquefiable sand layers in order to approach to the real behavior of soil during the liquefaction phenomenon. The no liquefiable soil layers were represented by the Mohr-Coulomb model.

The linear elastic model was utilized to represent behavior of all the structural elements considered in this work.

5. Conclusions

This Chapter presents a literature review on the dynamic analysis of soil-foundation-structure systems and the factors that impact greatly their response.

In the first section a description of pile and rigid inclusions systems is given. These techniques are principally utilized for transmission of surface loads to a harder and deeper layer. The primary difference is that the rigid inclusion system has a LTP between the slab foundation and the rigid inclusions. The characteristics, transfer of loading and some real cases using these techniques are shown. Some kinds of failure modes in piles are exhibited.

The Section 2 reports the direct and substructure methods to solve the soil-structure interaction. In this study the numerical approach to model soil-foundation-structure systems is utilized. However, analytical, experimental and numerical approaches to study SSI considering pile foundations are also explained. The previous studies considering pile foundations under dynamic loading are introduced. They were divided in: dynamic analyses and pile support conditions, Rayleigh damping, dynamic characteristics of the buildings and liquefaction. At the final of this section is concluded that there still many uncertainties of the effect of some important factors (pile foundation type, the pile group configuration, the damping parameters in the soil, the dynamic properties of the structure) in the response of pile-supported structures under seismic loading.

The Section 3 mentions important parameters in the static and dynamic behavior of soils. Prior a definition and types of dynamic loading is given. The decrement of stiffness and increase of damping with strain are principal parameters of soils under cyclic or dynamic loading. Laboratory and in-situ test methods to measure low strain stiffness values are described. The rate-dependency, the reversal of stress and the liquefaction phenomenon are essential aspects in the dynamic behavior of soils. The flow liquefaction and cyclic mobility are described.

The Section 4 presents a brief description of the constitutive models utilized in this study: linear elastic model, elastic perfectly plastic with Mohr-Coulomb failure criteria model, the Finn model and the Sanisand model. The two last ones are utilized in the investigation of liquefaction phenomenon in the pile and rigid inclusion systems.

Chapter 3 NUMERICAL MODELING USING FINITE DIFFERENCE METHOD

1.1. General

The Finite Difference Method (FDM) is a technique that allows solving numerically ordinary and partial differential equations. The FDM technique consists in replacing the partial derivatives of the function by the finite differences defined over a certain interval in the coordinate directions. This implies the partition of the domain into grid of nodes among which the finite differences are defined. A system of algebraic equations with unknowns related with the predefined nodes is developed. Then each equation is expressed as a combination of function values at its own and surrounding nodes. Using direct or iterative methods, the system of algebraic equations is solved and the values of the unknowns in each node are founded.

The principal advantages of this technique are that it allows for material deformation and failure, capability of modelling complex behavior and mechanism, faculty of model effect of ground water and pore pressure and the ability to incorporate dynamic analysis as well. The quick advances in computation allow solving problems with these characteristics with a reasonable run time using the FDM method.

One of the most well-known computer programs for solving a variety of soil mechanics problems by FDM, including the direct method to solve soil-structure dynamic interaction, is Flac3D (Fast Lagrangian Analysis of Continua). Due to the fact that this computer program is utilized in this study, the principal characteristics dealing with the modeling in Flac3D of soil-foundation-structures systems under seismic loading are presented in this Chapter.

1.2. Equations of Motion in Soil Structure Systems

As discussed in Section 2.2.2 Chapter 2, the direct method offers the possibility to model and solve SSI dynamic problems accounting for non-linear behavior of the materials. In the direct method, the soil, the foundation and the structure are considered in the same model. The way to study this system is complicated because the difficulty of solve the governing equations of motion for the structure incorporating foundation interaction. The equation of motion of the total system can be represented by the Eq. 3.1 (Kramer 1996).

$$M_t\ddot{u} + C_t\dot{u} + K_t u = -M_t 1\ddot{u_g} + b_t \tag{3.1}$$

where M, C, K are the matrix of mass, damping and stiffness for the structure. u, $\dot{u}$ and $\ddot{u}$ are the displacements, velocities and accelerations vector and $\ddot{u_g}$ is the seismic acceleration. The soil-structure interaction forces are represented by b_t. They are the inertial forces that tend to deform the soil at soil-structure interaction when they are transferred to the base-slab in the form of shear forces and moments. The subscript t refers to all the degree of freedom of the structure. In order to account for the nonlinear behavior, it is necessary to work with the incremental equations rather with the original equations in Eq. 3.1 (Muthucumarasamy 1988).

1.3. Three-dimensional Finite Difference Software (Flac3D)

Flac3D is a finite difference code that uses an explicit numerical scheme which solves the dynamic equations of motion in conjunction with an incremental constitutive law over a small-time step, at discrete points in space. Flac3D ensures that the numerical scheme is stable (even if the situation being modeled is unstable) using full dynamic equations of motion. This method is particularly well adapted for treating nonlinear behavior of soils problems. Because no matrices are formed, large 3D calculations can be made without excessive memory requirements. However, the speed of calculation is a linear function of the number of elements used for calculation. Additional features of Flac3D are that it works in large-strain and small-strain calculation mode, that different built-in constitutive models are available, that interfaces to simulate planes of weakness, that use of structural elements and that analyze fully coupled soil-structure interaction problems.

To obtain a mathematical model description, the mechanics of the medium are derived from general principles (definition of strain, laws of motion), and the use of constitutive equations defining the idealized material (Itasca 2012). The resulting mathematical expression is a set of partial differential equations, relating stress with strain rate or velocity variables, which are to be solved for particular geometries and properties, initial condition and given specific boundary conditions.

The finite difference, the discrete-model and the dynamic-solution are the three approaches that characterize the method of solution in Flac3D. The first one deals with the approximation by finite differences of the first-order space and time derivatives of a variable. The second approach replaces the continuous medium by a discrete equivalent one in which all forces are concentrated at the nodes of a 3D mesh. The third one in which the inertial terms in the equations of motion are utilized as numerical means to reach the equilibrium state of the system under consideration. Using these approaches, the laws of motion of the continuum are transformed into discrete forms of Newton's law at the nodes. The system of ordinary differential equations resultant is then solved numerically using an explicit finite difference approach in time.

The spatial derivatives involved in the derivation of the equivalent medium are those appearing in the definition of the strain rates in term of velocities. To define velocity variations and the corresponding space intervals, the medium is discretized into constant strain-rate elements of tetrahedral shape whose vertices are the nodes of the mesh (Fig. 3.1). These tetrahedral elements have the advantage of not generating hourglass. However, they can produce a stiffer response in the plasticity framework. To deal with this problem a technique of mixed discretization is applied in Flac3D.

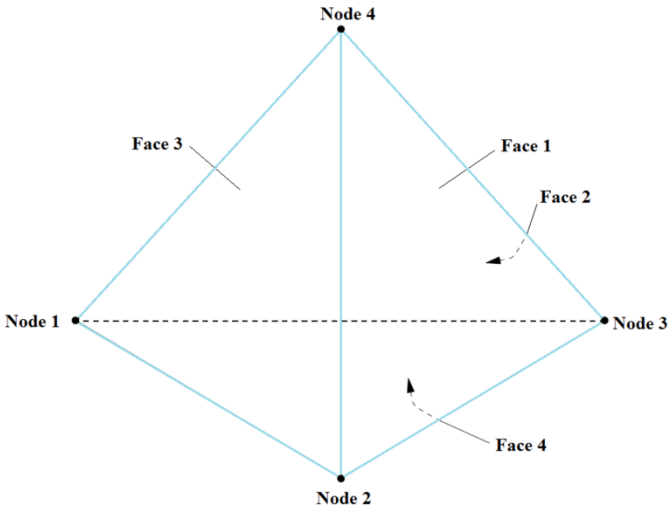

Fig. 3.1 Tetrahedral shape elements used in Flac3D to discretize the continuous medium

1.4. Soil Elements and Structural Elements

In this section the general characteristics of the solid elements and structural elements used in the numerical models are presented. In general, the soil elements are represented by solid elements and the columns, slabs and slab foundation in the buildings by respectively beam, shell and liner elements. The methods to model the rigid elements (piles/inclusions) are described.

1.4.1. Soil Elements

The soil medium is modelled by solid elements. In this study, the soft soil behavior in drained condition (Chapter 4 and 5) was simulated using the linear elastic and the elastic perfectly plastic with Mohr-Coulomb failure criterion to consider nonlinearity and possible shear failure in soil elements. The granular material of the earth platform was represented with the Mohr-Coulomb model. The Finn and Sanisand models were utilized to simulate the behavior of liquefiable sand soils (Chapter 6). The capabilities of each model are explained in Section 4 Chapter 2.

1.4.2. Beam Elements

Beam structural elements (beamSELs) were used in this study to model the columns in the buildings and in some cases to model the piles or rigid inclusions elements. The beam structural elements are two noded, straight, finite elements with six degrees of freedom per node including three translational components and three rotational components. Each beamSEL behaves as an isotropic, linearly elastic material with no failure limit. The 12 active degrees of freedom of the beam finite elements are shown in Fig. 3.2. For each generalized translation or rotation showed in the figure, there is a corresponding generalized force and moment. The stiffness matrix of the beam finite element includes the six degrees of freedom at each node to represent axial, shear and bending action within the beam element.

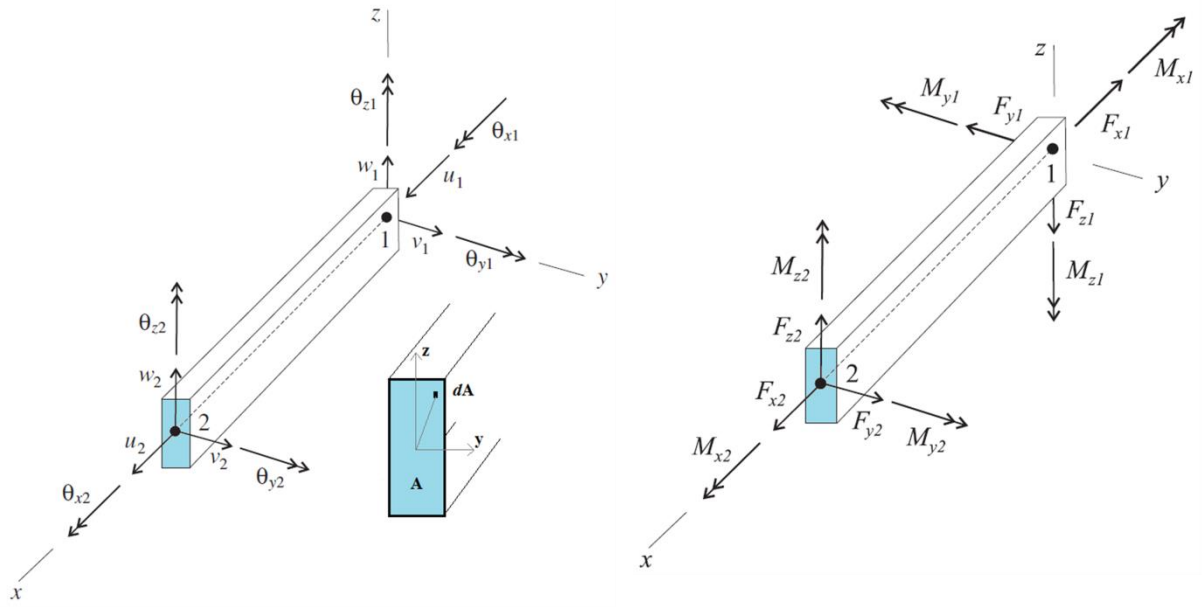

a) Translational components **b)** Rotational components

Fig. 3.2 Generalized displacement and forces at the ends of the beamSELs

The material and geometric properties of the beamSELs are presented in Table 3.1. Flac3D automatically calculate the dimension for the two principal axes beam cross section using the geometric parameters.

Table 3.1 Material and geometric properties of beamSEL

Material Properties		Geometric properties	
ρ	Mass density (kg/m³)	A	Cross-sectional area (m²)
E	Young's modulus (GPa)	I_y, I_z	Second moment of inertia with respect to y- and z-axis (m⁴)
ν	Poisson's ratio	J	Polar moment of inertia (m⁴)

Rigid elements (piles/inclusions) modelling

In three-dimensional numerical analyses, some researchers have modelled piles and rigid inclusions with solid elements (Hokmabadi et al. 2014, Nguyen et al. 2017, Hazzar et al. 2017, Maheshwari and Sarkar 2011). Other authors have considered hybrid methods using beam elements embedded in solid elements with reduced flexural rigidity (Banerjee et al. 2014, Kourkoulis et al. 2012, Goh and Zhang 2017). Rigid elements can also be modeled by beam structural finite elements (Alsaleh and Shahrour 2009, Finn and Fujita 2002, Kitiyodom et al. 2006, Sadek and Shahrour 2004).

In some parts of this work (Chapter 4) a hybrid method to model the rigid elements was utilized (Banerjee et al. 2014, Kourkoulis et al. 2012, Goh and Zhang 2017). This technique consists in modelling the vertical reinforcements as solid elements with the introduction of a beam element in their center axis (Fig. 3.3a). The flexural rigidity of the beam element (EI) was set 10^{-6} times the one of the pile/inclusion flexural rigidity. The efforts in the rigid elements are obtained multiplying the computed efforts in the beam elements by the scaling factor 10^{6}. The use of this method allows determining easily the internal forces in the vertical reinforcements and at the same time considering the physical cross section of the rigid element. It also offers the possibility to capture the sliding and detachments of the rigid elements from the surrounding soil through the use of interfaces elements placed in the periphery of the solid elements.

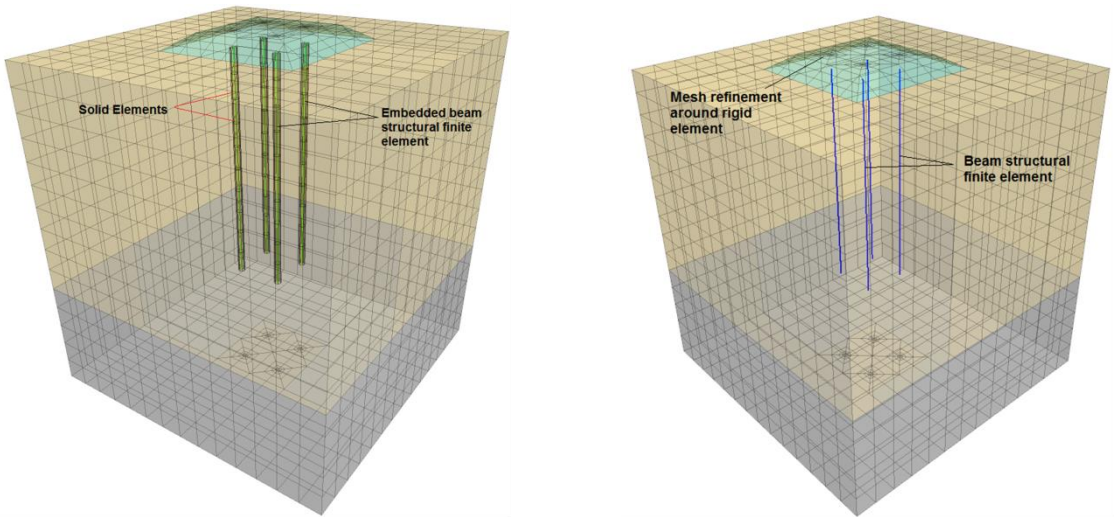

a) Hybrid technique **b)** Beam structural element technique

Fig. 3.3 Piles/Inclusions modeling techniques

In other parts of this study (Chapter 5 and 6), the rigid elements (piles/inclusions) were modeled by beam structural finite elements perfectly bonded with the soil (Alsaleh and Shahrour 2009, Finn and Fujita 2002, Kitiyodom et al. 2006, Sadek and Shahrour 2004). This technique is displayed in (Fig. 3.3b). This technique to model the rigid elements allows reducing the time calculation and directly

gives the pile/inclusion efforts from the numerical simulations. However, this method does not accurately account for the physical rigid element cross section. This results in greater displacements and bending moments along the pile than with the method where the pile is modelled by solid elements (Kitiyodom et al. 2006, Wotherspoon 2006). Mánica-Malcom et al. (2016) compared the response of piles modeled by beam element against solid elements under lateral load. They concluded that beam elements reproduce in an excellent way the flexural rigidity of the pile without excessive time calculations. Contrary, the calculation of slender piles through solid elements requires a smaller mesh and thus results in a larger time calculation. In the analyses, using beam structural finite elements technique, a mesh refinement can be setup around the rigid elements to avoid the loose of accuracy in terms of stresses and displacements in this zone.

1.4.3. Shell Elements

The floor slabs of the buildings were modeled by shell structural elements (shellSELs) which are three noded and flat finite elements. They combine a CST plane element (6 degrees of freedom) to model the bending action and a DKT plate element (9 degrees of freedom) to model the membrane action. The nodal degrees of freedom are shown in Fig. 3.4. The forces for the DKT-CST shell element, whose stiffness matrix in local *xyz* coordinates is called $[k^*]$, is given by

$$[k^*]\{d^*\} = \begin{bmatrix} [k_{CST}] & [0] \\ 6\ x\ 6 & 6\ x\ 9 \\ [0] & [k_{DKT}] \\ 9\ x\ 6 & 9\ x\ 9 \end{bmatrix} \begin{Bmatrix} u_i \\ v_i \\ w_i \\ \theta_{xi} \\ \theta_{yi} \end{Bmatrix} \tag{3.2}$$

where $[k_{CST}]$ is the stiffness matrix of a CST plane stress element, $[k_{DKT}]$ is the stiffness matrix of a DKT plate bending moment and $\{d^*\}$ are the arrangement of the degrees of freedom. In this study each shellSEL behaves isotropic linear elastic material with no failure limit.

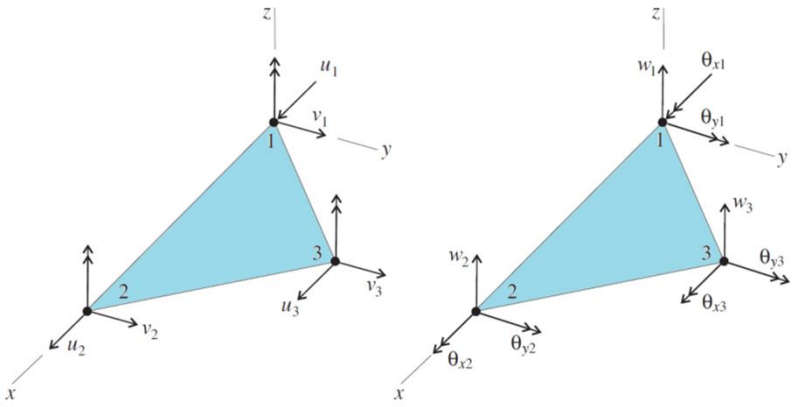

a) CST shell sub-element **b)** DKT shell sub-element

Fig. 3.4 DKT-CST shell element

1.4.4. Liner Elements

Liner elements (linerSEL) were used to model the foundation slab in some analyses (Chapter 5 and 6). The liner element has the same characteristics as the shell element, but additionally, it considers the interface behavior with the soil through linear springs with finite tensile strength in the normal direction and a spring-slider in the tangent plane to the liner surface. This implies that the behavior of the liner element can be divided into the structural response of the liner material itself and the way in which the liner interacts with the soil.

The normal behavior of the liner-zone interface is controlled by the normal coupling spring properties of stiffness per unit area (k_n) and tensile strength (f_t). The shear behavior of the liner-zone interface is cohesive and frictional in nature and is controlled by the shear coupling spring properties of stiffness per unit area (k_s), cohesive strength (c), residual cohesive strength (c_r), friction angle (ϕ) and the interface normal stress (σ_n). These elements are illustrated in Fig. 3.5. The values of k_n and k_s can be obtained with Eq. 3.19.

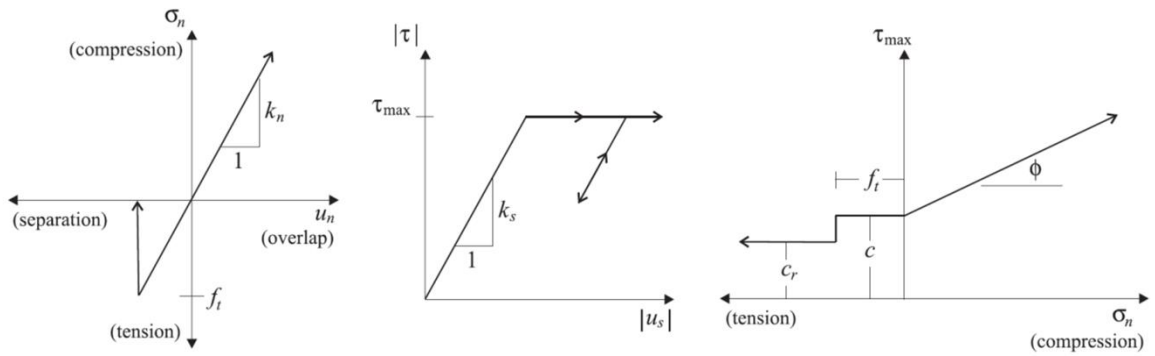

a) Normal **b)** Shear

Fig. 3.5 Interface behavior for linerSELs

1.5. Dynamic Analysis

In general, the procedure of analysis of the numerical models developed in this study consists in a static step calculation followed by a dynamic step computation. However, this procedure is explained in each chapter for each specific model and considerations. Important aspects that must be considered in a dynamic analysis are presented below.

Specification of the appropriate material damping

Although some energy is absorbed by the dynamic boundary conditions, the geotechnical materials have the ability of dissipate energy as mechanical waves propagate through them. This form of energy dissipation is known as material damping. In flac3D this type of damping can be introduced into

formulations for dynamic analyses in different manners. These alternatives are detailed explained in Section 1.6 of this Chapter.

Applying dynamic loading and boundary conditions

The dynamic input loading can be applied in terms of stress, force, velocity or acceleration histories. These histories can be applied to the interior gridpoints or to the model boundaries. When velocity or acceleration histories cannot be applied along the same boundary as a quiet boundary condition since the effect of the boundary would be nullified. In this study because the dynamic loading is applied at the base of the model utilizing acceleration or velocity records, rigid boundary conditions are considered at the base of the models. The boundary conditions utilized in the model during the dynamic loading are explained in Section 1.7 of this Chapter.

The input motions applied horizontally at the base of the models propagate upward through the entire model. Table 3.2 shows a resume of the seismic loadings utilized in this study. They are depicted in Fig. 3.6. Different predominant frequencies of the seismic loading were considered.

Table 3.2 Dynamic base input motions considered (CESMD)

Dynamic loading /Earthquake	Date	Duration (s)	Peak ground acceleration PGA (m/s²)	Magnitude (Mw)	Predominant Frequency (Hz)
Sinusoidal acceleration	----	10	4.00	----	1.25
Loma Prieta, USA	1989/10/17	40	4.69	7.1	1.27
Northridge, USA	1994/01/17	30	8.65	6.7	4.30
Nice, France	2001/02/25	27	3.50	5.1	0.48

When acceleration or velocity histories are applied, the Flac3D model may display continuing velocity or residual displacements after the motion has finished. This is due to the fact that the integral of the complete time history may not be zero. An example is shown in Fig. 3.7 where the velocity and displacement histories (obtained after integration at the final of the analysis) of the Loma Prieta earthquake (part highlighted in Fig. 3.6b) are shown. It is clear that at the final of the calculation, there is a residual displacement of around 1.30 m.

To solve this problem, the applied signals can be treated with baseline correction, which implies the definition of a low frequency wave that when added to the original history, produces a final displacement of zero. In this study, the seismic loading utilized in Chapter 6 was treated with baseline correction and a low-pass filtering (10 Hz). Fig. 3.7 also shows the zero residual displacement obtained after the baseline correction treatment.

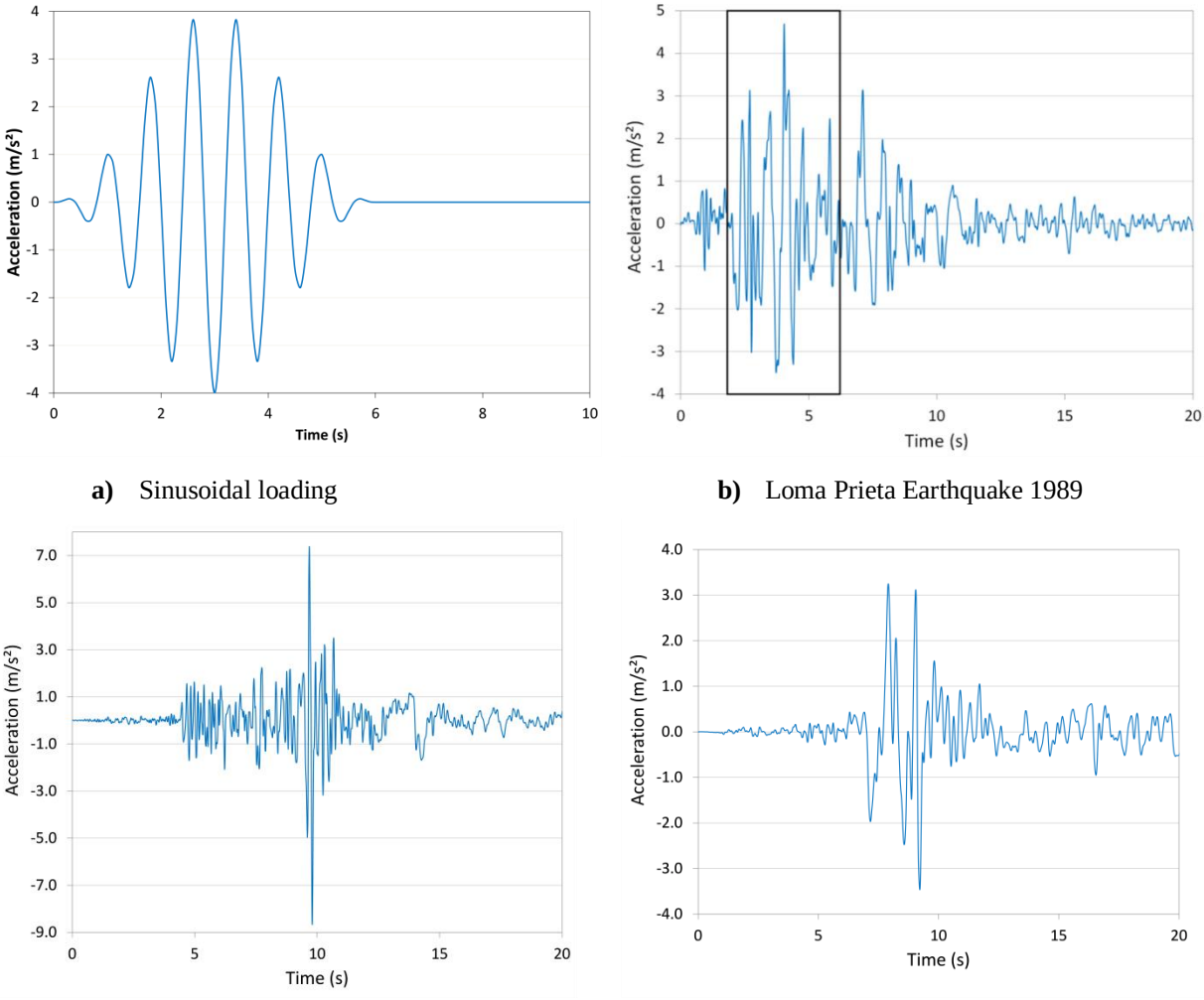

a) Sinusoidal loading **b)** Loma Prieta Earthquake 1989

c) Northridge Earthquake 1994 **d)** Nice Earthquake 2001

Fig. 3.6 Dynamic base input motions considered

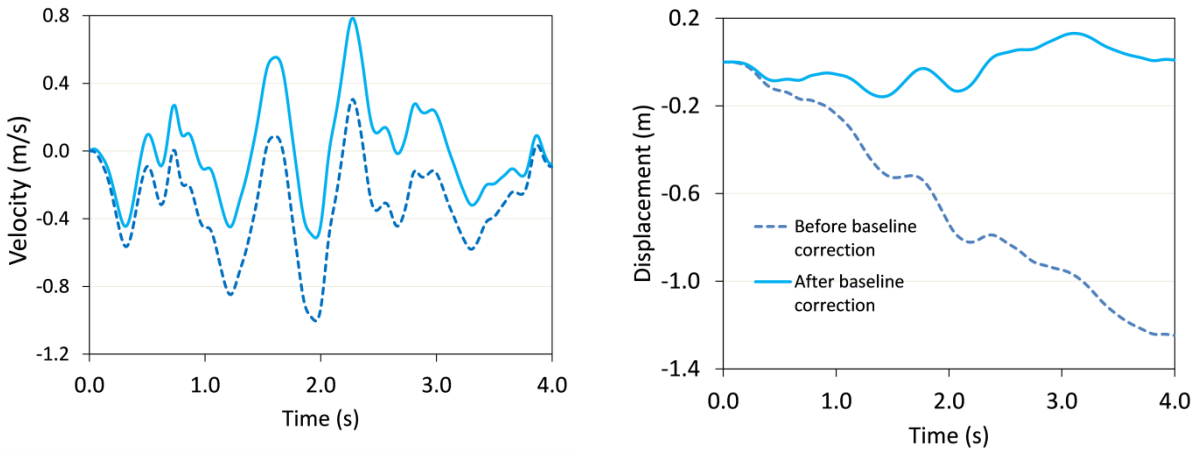

a) Velocities **b)** Displacements

Fig. 3.7 Velocity and displacement time history records for Loma Prieta Earthquake before and after baseline correction

Zone size adjustment

This aspect is considered to ensure that the model conditions satisfy the requirements for accurate wave transmissions. The numerical distortion of the propagating wave can occur as a function of the modelling conditions. The frequency content of the input motion and the wave speed characteristics of the system affect the accuracy of the wave transmission. Kuhlemeyer and Lysmer (1973) suggested that the maximum spatial element size (Δl) must be smaller than the one-tenth to one-eighth of the wavelength associated with the highest frequency component of the input wave.

$$\Delta l = \frac{\lambda}{10} \tag{3.3}$$

where λ is the wavelength associated with the highest frequency component that contains energy, which can be calculated from the wave speed (Eq. 3.4) for elastic continuum systems.

$$f = \frac{V_s}{\lambda} \tag{3.4}$$

For the input motion cases with high frequency, it is necessary the utilization of a fine spatial mesh to get stability condition. This implies small time step which may lead to high time calculation and memory for the analyses. Assuming that most of the power for the input history is contained in lower frequency components, the input history may be adapted by a filtering and removing high frequency components. This allows using a coarser mesh without importantly affecting the results. In this study the maximum size of the elements which constitutes the model is equal to 1 m.

The time step for a dynamic analysis is determined by the largest material stiffness and smallest zone in the model, including structural and interface elements. The time step is an important parameter which corresponds to real seismic loading time per calculation step (Flac3D uses an explicit finite difference solution scheme). The smaller the time step, the longer the calculation time. The computation time is reported for each calculation developed in this study. An example of the time step and time calculation for the analyzed systems is showed in Section 2.5 Chapter 4. All the calculations in this study were developed using a computer with a core i7 3.6GHz 64-bit processor and 8 Gigabytes of RAM.

Dynamic Coupled Mechanical/Groundwater simulations

Flac3D has the capability of model the flow of fluid trough permeable soils. The flow modeling may be done independently of the mechanical calculation or in parallel with the mechanical modeling

(to capture the effects of fluid/solid interaction). In this study, the dynamic pore pressure generation and liquefaction due to dynamic loading was developed by coupled fluid-mechanical analyses. These means that the mechanical response of the soil can be studied under transient fluid flow conditions.

The formulation of the coupling analysis is done within the frame work of the quasi-static Biot theory and can be applied to problems involving single-phase Darcy flow in a porous medium. Important variables describing the fluid flow (pore pressure, saturation and the three components of the specific discharge vector) are related through a fluid mass-balance equation, Darcy's law for fluid transport, a constitutive equation specifying the fluid response to changes in pore pressure, saturation and volumetric strains, and an equation of state relating pore pressure to saturation in the unsaturated range. Pore pressure influence is involved in the mechanical constitutive laws to complete the fluid-mechanical coupling.

1.6. Types of Damping

Due to the fact that the Local and Rayleigh damping were utilized in this study, their formulations are presented in this part of the work.

1.6.1. Local Damping

The simplest damping implementation in Flac3D is the local damping, which operates by adding or subtracting mass from a gridpoint or structural node at certain times during a cycle of oscillation. In order to maintain the overall mass of the system, the mass added is equal to the subtracted mass. When the velocity changes sign the mass is added and subtracted when it passes a maximum or minimum point. This implies that the increments of kinetic energy are removed twice per oscillation cycle. The amount of energy removed (ΔW) is proportional to the maximum transient energy (W). The ratio $\Delta W/W$ can be related to the critical damping (ξ). This damping model is controlled by the local damping coefficient (α_L) which is related to the critical damping ratio by the Eq. 3.5.

$$\alpha_L = \pi\xi \tag{3.5}$$

The local damping is thus frequency independent, which means that the damping ratios are constant during the entire simulation. The local damping in Flac3D is utilized for equilibrating static simulations; however, it can be used for dynamic problems with a damping coefficient appropriate to wave propagation. When the number of frequency components increases the response becomes increasingly unrealistic.

1.6.2. Rayleigh Damping

Another form to introduce damping in Flac3D is through the Rayleigh damping. This damping is expressed in a matrix form and assumed proportional to the mass and stiffness matrices (Eq. 3.6).

$$C = \alpha[M] + \beta[K] \tag{3.6}$$

where C is the damping matrix, M and K are the mass and stiffness matrices respectively and α and β are the mass-proportional and stiffness-proportional damping constants. If the damping ratios (ξ_i-ξ_j) associated with two specific frequencies (ω_i-ω_j) are known, the two Rayleigh damping constants can be evaluated by the following pair of equations:

$$\alpha = \xi\frac{2\omega_i\omega_j}{\omega_i + \omega_j} \quad ; \quad \beta = \xi\frac{2}{\omega_i + \omega_j} \tag{3.7}$$

For a multi degree of freedom system, the critical damping ratio (ξ_i), at any angular frequency of the system (ω_i), can be calculated from the following equation:

$$\alpha + \beta\omega_i^2 = 2\omega_i\xi_i \tag{3.8}$$

Considering Eq. 3.8, Fig. 3.8 represents the curves with only the component proportional to the mass ($\beta = 0$), the part proportional to the stiffness ($\alpha = 0$) and the curve of the sum of both components. It is evident that the curve of the sum of the components has a limited frequency range where an approximately frequency independent response can be obtained. For frequencies outside of this range larger damping values are obtained. This range is limited by a low frequency (f_0) and a large frequency (f_1). It is commonly considered f_0 as the frequency that corresponds to the first mode of the soil column, calculated by

$$f_n = \frac{V_s}{4H} \tag{3.9}$$

where V_s is the elastic shear wave velocity and H is the thickness of the soil column. For larger frequencies, an approach known as the single control frequency considers that f_1 is equal to f_n (Idriss et al. 1975, Suwal et al. 2014). In the two control frequencies approach, there are many approaches to obtain the largest frequency. The simplest considers a larger frequency that corresponds to the predominant frequency (f_p) of the input motion. Kwok et al. (2007) suggest a frequency equal to five times f_n. Other authors suggest a value of $f_1 = nf_n$ with n being the smallest odd integer so f_1 is greater than f_p (Hudson et al. 1994, Rathje and Bray 2001). Park and Hashash (2004) suggest that the

two significant frequencies should be covering a range of frequencies where there is a significant input motion content.

Concerning the target damping, a value between 1-5% is usually considered (Mánica et al. 2014, Suwal et al. 2014, Phillips and Hashash 2009, Hokmabadi and Fatahi 2016, Rangel-Núñez et al. 2008, Shahrour et al. 2012, Kumar et al. 2016).

It is also noticeable from Fig. 3.8 that the curve representing the sum of both components reaches a minimum at

$$\xi_{min} = (\alpha\,\beta)^{1/2} \tag{3.10}$$

$$\omega_{min} = (\alpha\,/\,\beta)^{1/2} \tag{3.11}$$

These two parameters are the input parameters when dealing with numerical modelling for the specification of Rayleigh damping. The frequency is in Hertz (cycle per second). In this work the single control frequency approach is utilized in all calculations which means that the minimum damping ratio (ξ_{min}) is equal to the target damping ratio (ξ_{tar}). Hereafter, both terms are used indistinctly.

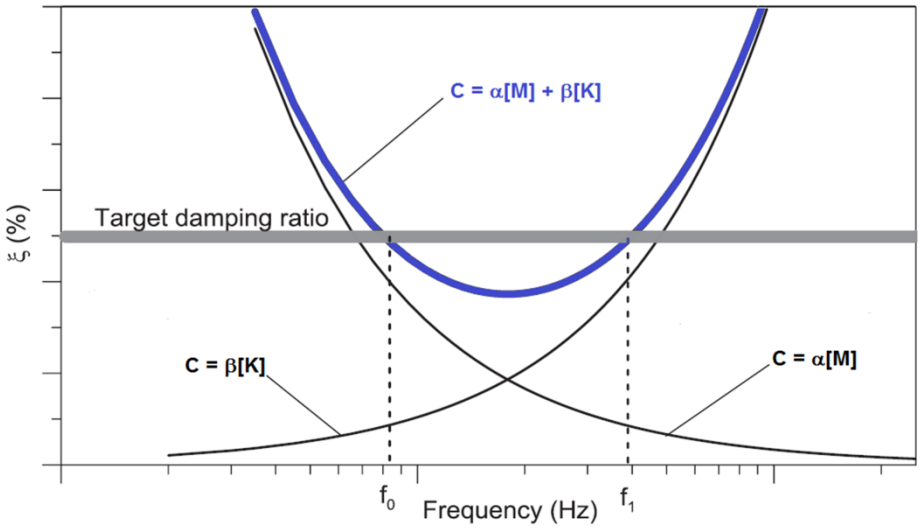

Fig. 3.8 Rayleigh damping formulation

1.7. Boundary Conditions

Due to the fact that the soil of the site extends to a great depth, it is necessary to use artificial boundaries at a certain depth (Okyay 2015). In the calculations developed in this work, during the static analysis step, the side boundaries were fixed in horizontal direction whereas the bottom part was fixed in all directions. However, these preliminary boundary conditions were replaced in the dynamic

analysis, where the base of the model was assumed rigid in order to apply the acceleration input and free-field boundary conditions on the sides to avoid wave reflections (Lysmer and Kuhlemeyer 1969).

1.7.1. Quiet Boundaries

The use of fixed or elastic boundary conditions during dynamic analysis produces the reflection of the outward propagating waves back to into the model and avoids the energy radiation. The use of larger model is a way to overcome this problem; however, it implies a great computational effort because the material damping must absorb most of the energy in the waves reflected from the distant boundaries. The use of quiet boundaries represents a better option. These viscous boundaries developed by Lysmer and Kuhlemeyer (1969) are used in Flac3D. If the body waves approaching the boundaries is greater than 30° there is a completely absorption. They use independent dashpots in the normal and shear direction at the model boundaries (Fig. 3.9a). These dashpots provide viscous normal and shear tractions as follows:

$$t_n = -\rho V_p \nu_n \tag{3.12}$$

$$t_s = -\rho V_s \nu_s \tag{3.13}$$

where ρ is the mass density, V_p and V_s are the velocities of the p-wave and s-wave respectively and ν_n and ν_s are the normal and shear components of the velocity at the boundaries respectively. In the numerical analysis, the tensions are calculated and applied at every time step in the same way boundary loads are applied. These viscous boundaries operate in time domain.

The use of quiet boundaries in dynamic analyses is not recommended when the input motion is applied at the bottom or top of the model because they allow the leakage of the wave energy through the sides. Due to the fact that in this study the dynamic load is applied at the bottom of the model, a free-field boundary condition should be considered.

1.7.2. Free Field Boundaries

The correct numerical analysis of soil-foundation-structure system under seismic loading must account for boundary conditions that simulate the free-field ground motion (absence of structure and rigid elements). This process is considered in Flac3D using free-field boundaries in the vertical sides of the model. After static equilibrium, free-field boundaries are applied to the model for dynamic analysis. These boundaries represent the semi-infinite nature of the ground through plane grids coupled by viscous dashpots to the main grid to simulate a quiet boundary, preventing the distortion of the plane waves propagating upwards (Fig. 3.9b). The unbalanced forces from the secondary grid are applied to the main grid boundary with its normal in the direction of the x-axis are given by the following equations

$$F_x = -\rho V_p\left(v_x^m - v_x^{ff}\right)A + F_x^{ff} \tag{3.14}$$

$$F_y = -\rho V_s\left(v_y^m - v_y^{ff}\right)A + F_y^{ff} \tag{3.15}$$

$$F_z = -\rho V_s\left(v_z^m - v_z^{ff}\right)A + F_z^{ff} \tag{3.16}$$

where ρ is the mass density, V_p and V_s are the velocities of the p-wave and s-wave respectively, A is the area of influence of free-field gridpoint, v_x^m, v_y^m and v_z^m are the *x*, *y* and *z* velocity of gridpoint in main grid at the side boundary respectively, v_x^{ff}, v_y^{ff} and v_z^{ff} are the *x*, *y* and *z* velocity of gridpoint in side free-field and F_x^{ff}, F_y^{ff} and F_z^{ff} are the free-field gridpoint force with contributions from the σ_{xx}^{ff}, σ_{yy}^{ff} and σ_{zz}^{ff} stresses of the free-field zones around the gridpoint respectively. Similar expressions may be obtained on the other sides.

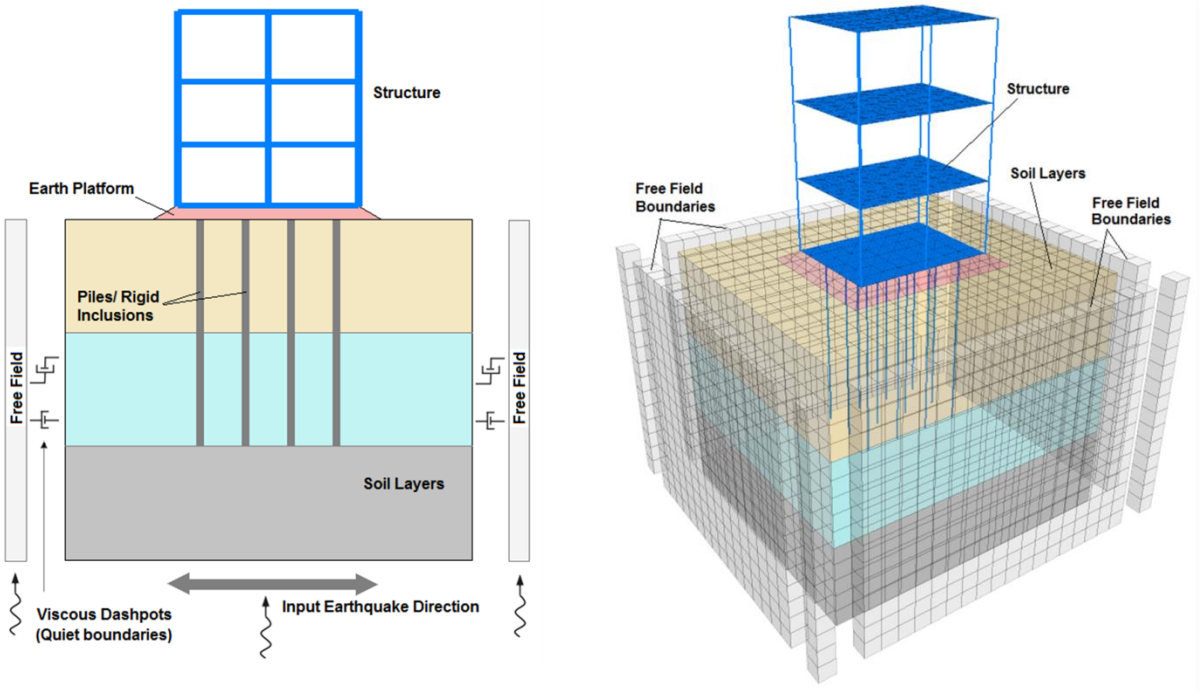

a) Cross section **b)** 3D view

Fig. 3.9 Quiet and Free Field boundaries

1.8. Interfaces

Due to the different properties of the soil and the rigid elements (piles/inclusions), sliding and separation may occur at the soil-pile interfaces (Maheshwari and Watanabe 2006). The interface elements in Flac3D are able to simulate the slip and detachment of these contact surfaces. In general, these elements are not considered in this study; however, in some calculations (Chapter 4) the influence of these elements was checked in the pile/inclusion response considering systems with and without interface elements.

The interface elements in Flac3D are presented by triangular components each one defined by three nodes and are modeled as spring-slider systems as illustrated in Fig. 3.10a. The absolute normal penetration and the relative shear velocity are calculated for each interface node and its contacting target face during each time step. Then these values are utilized by the interface constitutive model to calculate a normal and a shear force vector. The constitutive model of the interfaces is defined by a linear Coulomb shear-strength criterion that limits the shear force acting at an interface node, normal and shear stiffnesses (k_n and k_s), tensile and shear bond strengths (T_s and S_s) and a dilatation angle (ψ) that causes an increase in effective normal force on the target face after the shear-strength limit is reached (Fig. 3.10b).

In the elastic stage, the normal and shear forces at the calculation time $t + \Delta t$ are given by the Eqs. 3.17 and 3.18.

$$\mathrm{F}_n^{(t+\Delta t)} = k_n u_n A + \sigma_n A \tag{3.17}$$

$$\mathrm{F}_{si}^{(t+\Delta t)} = \mathrm{F}_{si}^{(t)} + k_s \Delta \mathrm{u}_{si}^{(t+(1/2)\Delta t)} A + \sigma_{si} A \tag{3.18}$$

In the first equation, $\mathrm{F}_n^{(t+\Delta t)}$ is the normal force at time $(t + \Delta t)$, k_n is the normal stiffness, u_n is the absolute normal penetration of the interface node into the target face, A is the representative area associated with the interface node, σ_n is the additional normal stress added due to interface stress initialization. In the Eq. 3.18, $\mathrm{F}_{si}^{(t+\Delta t)}$ is the shear force vector at time $(t + \Delta t)$, k_s is the shear stiffness, Δu_{si} is the incremental relative shear displacements vector, σ_{si} is the additional shear stress vector due to the interface stress initialization.

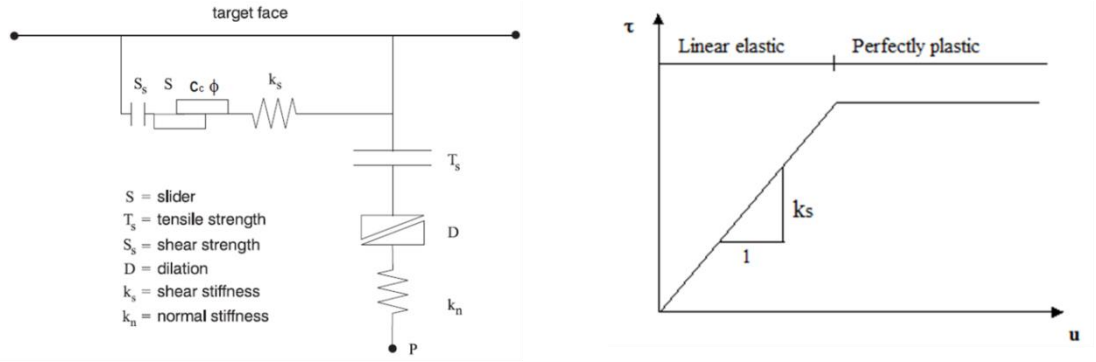

a) Components of the interface constitutive model

b) Relationship between shear stress and shear displacement of the interface element

Fig. 3.10 Interfaces in Flac3D

As recommended by Itasca (2012) the normal and shear stiffness of the interface elements are set ten times the equivalent stiffness of the neighboring zone expressed by Eq. 3.19.

$$\mathrm{k}_n = \mathrm{k}_s = 10\ max\left[\frac{K + \frac{4}{3}G}{\Delta z_{min}}\right] \tag{3.19}$$

where K is the bulk moduli, G is the shear moduli, Δz_{min} is the smallest width of an adjoining zone in the normal direction. The values given by Eq. 3.19 are large enough to avoid the normal penetration and detachment on the pile-soil interface as suggested by Fan et al. (2007) and Rayhani and El Naggar (2008). Other authors suggested that the value of k_n should be on the order of 10^8 N/m³. Some authors (Wu et al. 2016, Xie et al. 2013) state that to correctly simulate the soil-pile interface, a larger value of k_n should be selected. However, the increment of this value is closely related to the time step in Flac3D, which induces an increase of the time calculation.

In the perfectly plastic stage, three types of contact states of the interface are allowed: the bonded interface, slip while bonded and the Coulomb sliding state. The yields relationships in the shear and normal directions are given by Eqs. 3.20 and 3.21.

$$\mathrm{F}_{smax} = cA + \tan\phi(F_n - pA) \tag{3.20}$$

$$\mathrm{F}_n = \sigma_t \tag{3.21}$$

where F_{smax} is the maximum shear strength, c is the cohesion of the interface, ϕ is the friction angle of the interface, F_n is the normal force, p is the pore pressure and σ_t is the normal tensile strength of the interface. The values of the Eqs. 3.20 and 3.21 are automatically set to zero once gap is formed between the soil and the rigid elements and uplift between the foundation slab and soil.

1.9. Conclusions

The principal characteristics of the different components to develop the different numerical models in this study are presented in this Chapter. Prior a description of the numerical formulation utilized by Flac3D is given. Also, a brief coupled fluid-mechanical formulation utilized is presented for the examined cases considering liquefaction. Then, the attributes of the solid and structural elements to model the soil and structural components in the soil-foundation-structure systems analyzed were described.

The aspects to be considered in the numerical modelling of in pile and rigid inclusion systems under dynamic analysis were explained as follows.

- The use of an adequate constitutive model to represent the behavior of the soil (in drained and undrained conditions) and structural elements in soil-foundation-structure systems.

- The consideration of the damping in the numerical model through the boundaries and in the soil itself. The parameters involved in the local and Rayleigh damping formulations

- The formulation of free-field boundary conditions used in dynamic analyses to represent the semi-infinite nature of the soil.

- The rigid boundary condition at the bottom of the model in order to apply the dynamic loading. The process of filtering and baseline correction of the input motion.

- The mesh size to assure an adequately wave transmission in the models, taking into account that the time step in dynamic analysis is determined by the smallest zone and largest stiffness.

- The properties of interfaces to represent the interaction between the soil and the piles and the soil and the slab foundation.

- The consideration of drained or undrained conditions in the calculations. For the undrained case, it is necessary to perform coupled fluid-mechanical analyses.

Chapter 4 SEISMIC NUMERICAL RESPONSE OF PILE AND RIGID INCLUSION SYSTEMS IN SOFT SOIL

1. Dynamic analysis and Pile type

1.1. Introduction

Different types of pile foundation behave differently when shaking during earthquakes. This behavior is highly influenced by the soil-structure interaction (SSI). The dynamic characteristics (damping and natural frequency) of a soil-foundation-structure system can be altered by the properties of the soil, the structural elements and the type foundation. Two key mechanisms are generally involved during a seismic analysis of a soil-foundation-structure system: the kinematic and the inertial interaction (Wolf, 1985). The complexity of modeling this type of system and its entire characteristics require of the consideration of direct method (Section 2.2.2 Chapter 2). Several authors such as Finn and Fujita (2002), Cheng and Jeremić (2009), Carbonari et al. (2011), Hokmabadi and Fatahi (2016) and Mánica-Malcom et al. (2016) have investigated the response of pile and inclusion systems under seismic loading through numerical modelling approaches. A detailed description of these works was presented in Section 2.3.1 Chapter 2.

Due to the fact that there is not a deep understanding of the influence of the different type of pile foundation in the response of the soil-foundation-structure systems under seismic loading, the first part of this Chapter aims at evaluating the effect of the pile fixity conditions in pile groups using tridimensional finite difference (Flac3D) analyses of soil-pile-structure and of soil-inclusion-platform-structure systems under dynamic loading. The profile and properties of soil correspond to an idealized case that considers typical values for the soft soils. The analysis is developed in drained condition without the consideration of water level. The influence of the interfaces in the pile response is also investigated. Different support pile toe conditions are considered including the placement on a hard soil, anchored or floating piles. To represent the soil behavior, the elastic perfectly plastic constitutive model with Mohr-Coulomb shear failure criterion was utilized to consider plasticity and possible shear failure in the soil elements. The influence of the structural mass, the frequency of the input motion, the soil plasticity, the embedment of the slab foundation, the pile flexural rigidity and the pile group configuration were also investigated.

Due to the fact that the considered constitutive model (Mohr-Coulomb constitutive model) in this Chapter induces no energy dissipation at small strains during dynamic analysis, it is necessary introduce additional damping (in this study through the Rayleigh damping formulation). Therefore, in the second part of this Chapter, the influence of the accurately selection of the damping parameters to

avoid overdamping or underdamping of wave propagation in the pile and inclusion systems is investigated. Different range of damping parameters and input motions were selected.

1.2. Characteristics of the Adopted Numerical Model

1.2.1. Soil and Structure Model

In this study, the dimensions of the soil volume were chosen to be 26 m × 24 m × 15 m. A two layered soil model was considered, where a soft soil layer of 10 m thickness is supported on a hard soil layer of 5 m of height (Fig. 4.1). Fig. 4.1a shows the discretization of the system using the finite difference code Flac3D (Marti and Cundall 1982). The numerical model is constituted of 30,624 hexahedral zones to represent the soil mass. In order to simplify the problem, the soil layers were supposed horizontal.

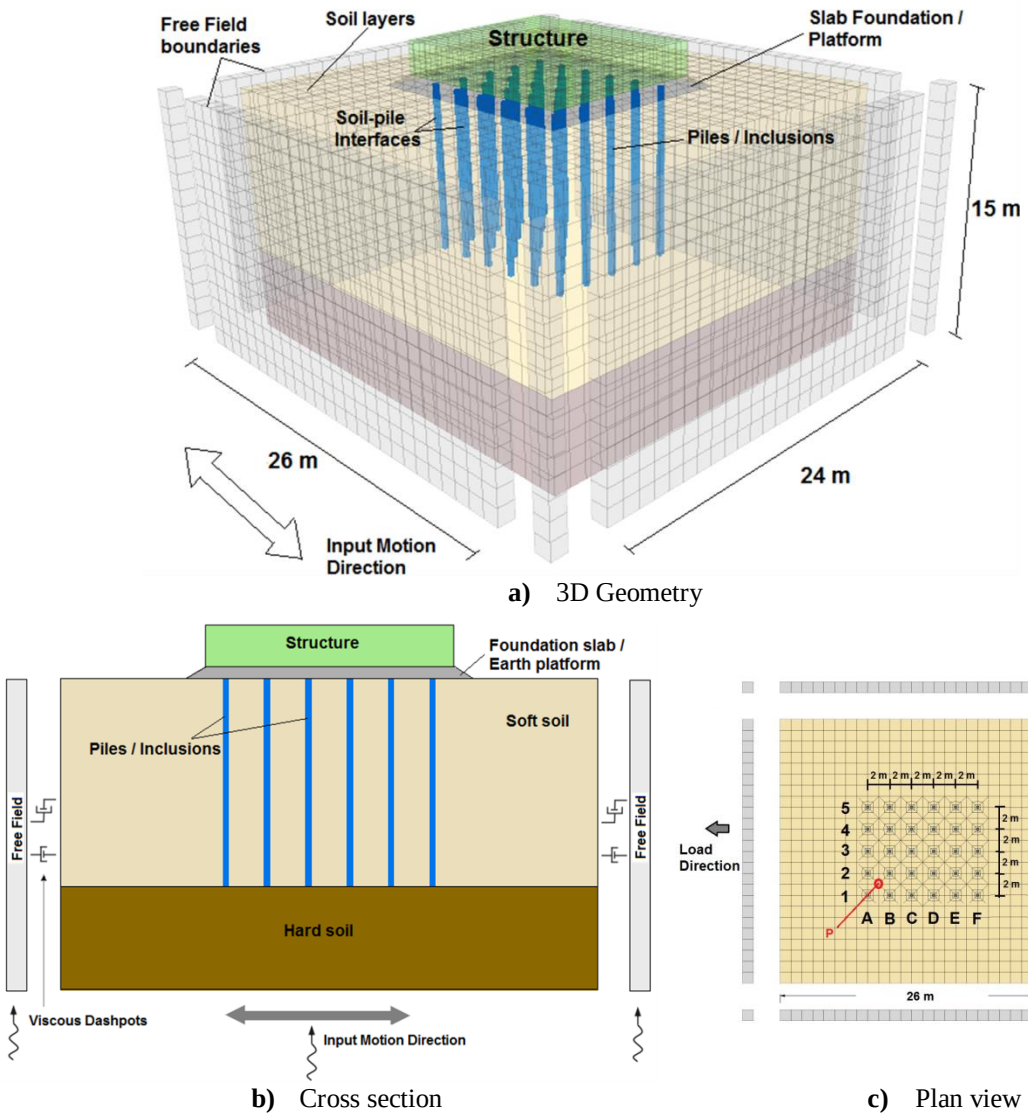

Fig. 4.1 Basic geometry of the numerical model

The choice of the dimensions of the discretized model and of the element size was in agreement with the large wavelength (Kuhlemeyer and Lysmer 1973). In this case, the maximum size of the elements which constitute the model is equal to 1 m, which allows applying frequencies between 0 and 5 Hz without perturbations due to zone dimensions (Section 1.5 Chapter 3).

For the rigid inclusion system, a 0.60 m high earth platform was placed over the rigid inclusions. This height value is considered as in similar studies considering rigid inclusion systems under dynamic loading (Hatem 2009, Messioud et al. 2016, Okyay et al. 2012). This platform thickness allows the adequately transfer of loading to the inclusions and it guarantees that there is no great diminution of the amplification of the input motion at the base of the structure level. In all the rigid inclusion cases analyzed in this study the same high earth platform was considered. The platform applies a supplementary stress of 12 kPa. In the rigid inclusion cases, the head of the inclusions is free. In the pile case, the platform was replaced by concrete slab of 0.6 m thickness perfectly connected to the pile heads (Fig. 4.1b).

A simplified superstructure was placed above the earth platform. The superstructure was modeled by a mass of 2 m of height on a surface of 12 × 10 m². The behavior of the superstructure was considered as linear elastic. The superstructure exerts an average vertical stress of 50 kPa on the mattress. This value remains in the range of the vertical stresses usually applied to vertical reinforcement systems.

Table 4.1 Parameters used for the numerical calculation

Parameter	Pile or inclusion Foundation Slab Superstructure	Earth Platform	Soft soil	Hard soil
Young modulus E (MPa)	30,000	50	10	100
Shear Modulus G (MPa)	12,500	19	3.8	38
Volumic Weight (kg/m³)	2500	2000	1600	2000
Damping Ratio	0.02	0.05	0.05	0.05
Cohesion (kPa)	-	50	5	5
Friction angle (°)	-	25	25	25
Wave velocity (m/s)	2237	160	50	223
Poisson's ratio	0.25	0.3	0.3	0.3

The parameters of the soil and structural elements are presented in Table 4.1. The soil characteristics were taken from Hatem (2009), Okyay et al. (2012) Houda (2016), Messioud et al. (2016) and Rangel-Núñez et al. (2008). Similar ranges of values are considered for the soft soil parameters. The Young modulus of soft soil is usually in the range of 2-50 MPa for soft to medium

clays, of 7-21 MPa for silty sands and of 10-24 MPa for loose sands. The maximum shear wave velocity for the soft soils is around 100 m/s. The water table was not setup in the model and drained conditions are considered for the analysis. Generally, field or in situ geophysical tests (crosshole, downhole, suspension logging test) are used to obtain the dynamic shear moduli at very small strain levels. However, these methods do not permit the evaluation of shear modulus at strain levels produced by strong earthquakes motions. Thus, with the objective to study the behavior at great deformations, static shear moduli are used in the analyses (Shahrour et al. 2001, Chu and Truman 2004, Hatem 2009, Mánica-Malcom et al. 2016, Messioud et al. 2016).

The properties of the earth platform are also shown in Table 4.1. The properties correspond to a treated soil (Okyay 2010) with an important cohesion to work in compression and extension. This cohesion value also allows increasing the strength of the soil and reducing the settlements.

The material properties of all the vertical reinforcements (inclusions/piles) are the same. The Young modulus of the rigid elements considered (30 GPa) has been considered by other researchers (Nghiem and Nien-Yin 2008, Haldar and Babu 2010, Hokmabadi et al. 2014, Badry and Satyam 2016, Nguyen et al. 2017) and remains in the range of values for concrete or reinforced-concrete pile foundation (BSSC 2009, Eurocode 8 1998).

The behavior of the soil layers was considered as linear elastic in a first analysis. However, dynamic loadings can induce large deformations that cannot be considered with an elastic behavior of soil. It is necessary to use a non-linear model to define the soil surrounding the piles. For this reason, a second analysis was carried out using the linear elastic-perfectly plastic constitutive model with a Mohr-Coulomb failure criterion to represent the behavior of the soil and of the LTP. Thus, this model accounts for nonlinearity of soil and possible shear failure in the soil elements. The Mohr-Coulomb model is widely used to simulate the behavior of soft soils deposits under dynamic loadings (Hatem 2009, Choudhury et al. 2014, Hokmabadi et al. 2014, Hokmabadi and Fatahi 2016). Description of these constitutive models can be checked in Section 4 Chapter 2.

The damping of the waves in the soil is due to its characteristics of viscosity, friction and development of plasticity. A linear elastic model cannot represent soil damping due to shearing. The elasto-plastic model used in this study needs also an additional damping for the elastic part of the response, where no energy loss occurs. Consequently, a Rayleigh damping with a factor of 5% was introduced in the soil to avoid pseudo-resonance at low shear deformation. Rayleigh damping give acceptable results for nonlinear dynamic analysis of soil deposits (Park and Hashash 2004). A local damping with a factor of 2% was used for the superstructure. The typical considered values for the damping ratio ranges from 1 to 5% (Mánica et al. 2014, Suwal et al. 2014, Phillips and Hashash 2009, Hokmabadi and Fatahi 2016, Rangel-Núñez et al. 2008, Shahrour et al. 2012, Kumar et al. 2016).

Detail of Rayleigh and local damping can be consulted in Section 1.6 Chapter 3. The use of local damping is simpler than the Rayleigh damping because it does not need the specification of a frequency.

1.2.2. Rigid Vertical Elements

Numerical analyses were developed using a network of 30 rigid inclusions/piles embedded in the soft soil. The reinforced concrete rigid elements were considered with a length from 9 m to 11 m. The diameter of these elements was taken equal to 0.30 m which corresponds to a length/diameter ratio comprised between 30 and 37. The pile/inclusion elements were disposed in a 6 × 5 rectangular grid and the separation between elements in both directions is equal to 2 m (Fig. 4.1c). The number of rigid elements was selected to consider a cover ratio (ratio between the sum of the rigid elements surface areas to the total reinforced area) equal to 1.7%. This cover ratio corresponds to typical values utilized for pile foundation and rigid inclusion improvement. The same cover ratio was considered in all calculations in this study. Similar values were used by some authors (Hatem 2009, Briançon et al. 2015, Houda 2016, Kumar et al. 2016, Mánica-Malcom et al. 2016). The behavior of these elements is considered as linear elastic in all calculations.

The vertical reinforcements were modeled by the hybrid method (solid elements with the introduction of beam elements in their center axis) described in Section 1.4.2 Chapter 3. This technique accounts for the physical cross section of the pile (Banerjee et al. 2014, Goh and Zhang 2017). This technique allows considering the physical cross section of the rigid elements and obtaining pile efforts directly from the beam elements. It also permits the use of soil-pile interfaces.

In the presented numerical model, the structural elements represent zones where the velocity of dynamic wave propagation is very high, this implies a very small time step with the use of Rayleigh damping. For this reason, local damping was also used for the rigid elements. However, the damping in the rigid elements has a negligible influence on the dynamic response in this type of systems.

1.3. Boundary Conditions and Interfaces

Artificial boundaries were used to represent in a correct way the semi-infinite nature of the soil deposits. In the static analysis step, the side boundaries were fixed in horizontal direction whereas the bottom part was fixed in all directions. However, these preliminary boundary conditions were replaced in the dynamic analysis, where the base of the model was assumed rigid in order to apply the acceleration input and free-field boundary conditions on the sides to avoid wave reflections (Fig. 4.1b). Free-field boundaries are described in Section 1.7.2 Chapter 3.

Another important issue in the study of the SSI systems is related with the soil-pile interfaces to represent sliding or separation due to the different properties of the soil and the structural elements (Maheshwari and Watanabe 2006). The interface elements in Flac3D are detailed in Section 1.8 Chapter 3. To verify the influence of the interfaces in the analyzed systems, a preliminary calculation was developed to compare the response of the piles or rigid inclusions with interfaces and without interfaces. Using a model with the characteristics described above, the interface elements were placed around the pile elements and between the slab foundation and the soil as shown in Fig. 4.1a. In this preliminary analysis, the behavior of the soil was considered with a linear elastic-perfectly plastic constitutive model with a Mohr-Coulomb failure criterion. The pile and rigid inclusions are 11 m long. The shear strength was defined with zero cohesion and $2/3$ of the friction angle (Hazzar et al. 2017). As recommended by Itasca (2012) the normal and shear stiffness values of the interface elements are set with Eq. 3.19.

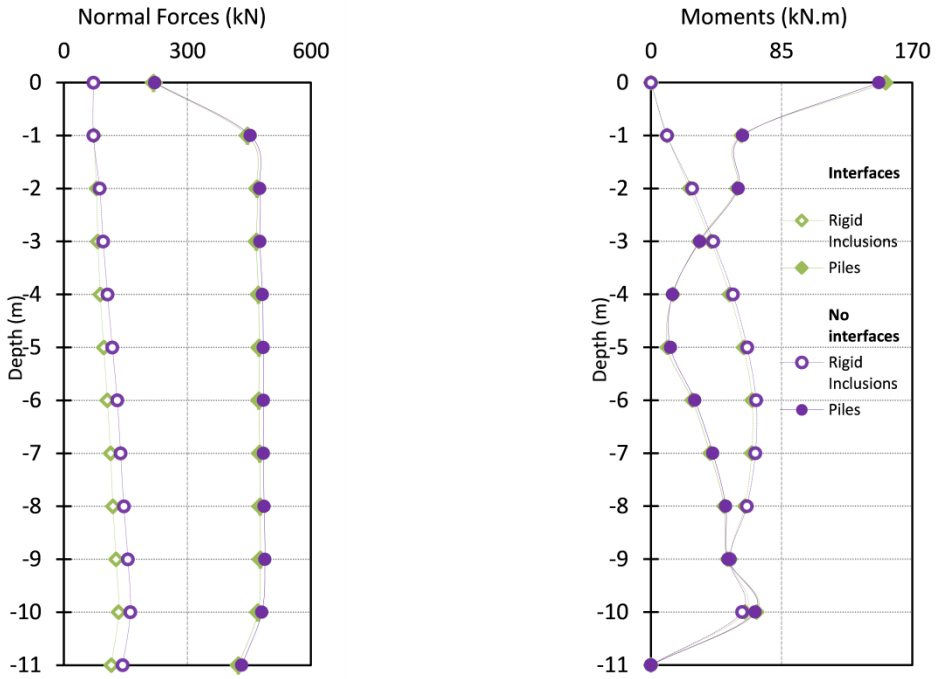

a) Normal Forces **b)** Bending moments

Fig. 4.2 Influence of the soil-pile interfaces on the efforts along the rigid vertical elements.

Fig. 4.2 shows the comparison of the maximal normal forces and bending moments in the rigid inclusion and pile system (from the beginning of the calculation, including forces and moments under initial static loading) with and without interfaces obtained during the dynamic loading. The dynamic loading utilized is described in Section 1.5 of this Chapter. A little reduction is observed for the systems which consider the interfaces. The normal forces in the rigid inclusion case are reduced up to 18% when the interfaces are considered. In the pile case, the reduction is negligible and is equal to

maximum 2% (Fig. 4.2a). Concerning the bending moments, the values for the cases considering interfaces are up to 4% smaller than without interfaces in both rigid inclusion and pile systems (Fig. 4.2b).

Based on these results which show a small difference in the pile and rigid inclusion response with and without interfaces, and considering the fact that interfaces increase the time calculation (approximately 12% of increment of time calculation compare to the case without interfaces), the analyses considered in the following study do not consider interfaces. This implies conservative effort values in the pile response. The time step is an important parameter which corresponds to real seismic loading time per calculation step (Flac3D uses an explicit finite difference solution scheme). The smaller the time step, the longer the calculation. The time step for a dynamic analysis is determined by the largest material stiffness and smallest zone in the model, including structural and interface elements.

1.4. Analyzed Cases

In this part of the study, numerical calculations were conducted for different pile connection and embedment conditions. These support conditions represent typical cases in practical engineering for the vertical reinforcement used (for bridges: Combault and Pecker 2000, Elgamal et al. 2008, for buildings and other structures: Rodriguez and Auvinet 2006, Pinto et al. 2016, for highways and railways: Stewart et al. 2004, Collin et al. 2005). Table 4.2 illustrates the studied cases and the fixity conditions for the pile toe and the pile head for each model. The six cases are described schematically in Fig. 4.3.

The Placed Rigid Inclusions on hard soil (P-RI) are 10 m long and correspond to Fig. 4.3a. They are embedded in the soft soil and are placed on the top of the hard soil. The platform is placed over the rigid inclusion heads and the structure, over the platform.

The Floating Rigid Inclusions (F-RI) are depicted on Fig. 4.3b. They are embedded in the soft soil and have a length of 9 m. The Fig. 4.3c presents the case of the Anchored Rigid Inclusions in the hard soil (A-RI). The anchorage length of the piles in the resistant ground layer is equal to 3 times the diameter of the pile. In this case, the rigid inclusions are 11 m long, with 1 m anchored in the hard soil.

The systems with piles were developed to compare their behavior with the one of rigid inclusions. The Piles placed on the hard soil (P-P), the floating (F-P) and the anchored ones (A-P) are shown in Fig. 4.3d-f respectively. The time calculation for the elastic models was approximately of 50 hours and of 130 hours in the elasto-plastic case. As mention in Section 1.5 Chapter 3, all the calculations of this

work were developed using a computer with a core i7 3.6GHz 64-bit processor and 8 Gigabytes of RAM.

Table 4.2 Cases and fixity conditions for the vertical reinforcement

System	Name of case	Support condition	Connection		Soil behavior
			Head	Toe	
Rigid Inclusion Systems	P-RI	Placed on hard soil	Free	Articulated	Elastic/Elasto-Plastic
	F-RI	Floating	Free	Free	
	A-RI	Anchored	Free	Fixed	
Pile Systems	P-P	Placed on hard soil	Fixed	Articulated	Elastic/Elasto-Plastic
	F-P	Floating	Fixed	Free	
	A-P	Anchored	Fixed	Fixed	

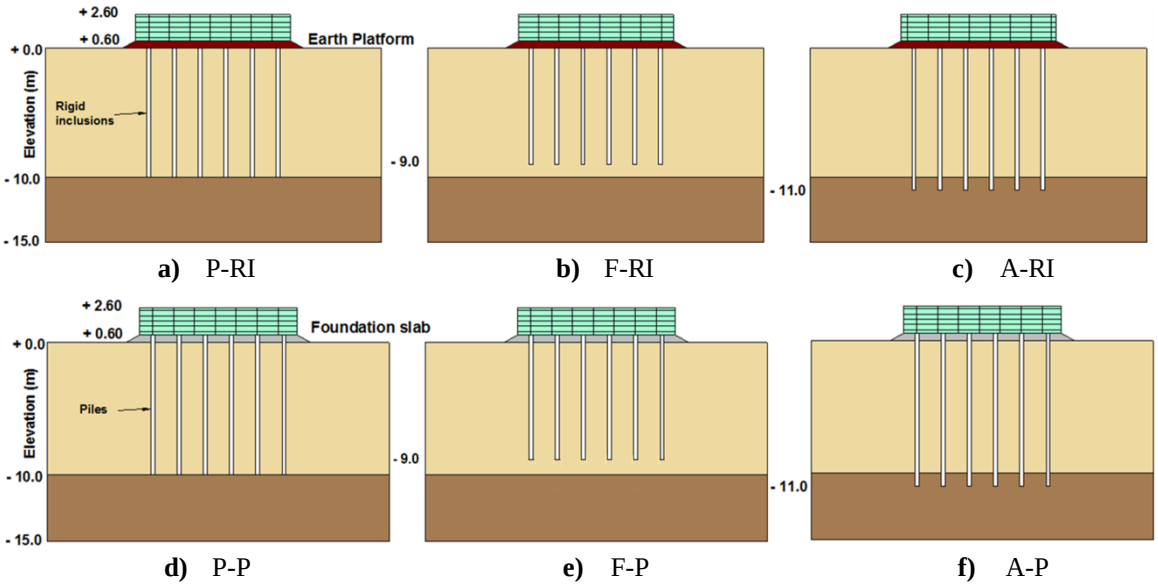

Fig. 4.3 Cases for the numerical calculation

Additional cases were analyzed to study the influence of the structural mass, the frequency of input motion, the embedment of foundation slab, the pile configuration and the pile flexural rigidity. For these analyzes, only the case of anchored piles and rigid inclusion cases (A-RI and P-RI) were considered. Table 4.3 presents the range of values considered for each case. The three pile configurations considered are shown in Fig. 4.4. For the pile configuration study, the cover ratio is kept as a constant equal to 1.7% for all cases. Thus, the pile or rigid inclusion diameter is respectively equal to 0.30, 0.50 and 0.60 m for the 6 × 5, 4 × 3 and 3 × 2 pile groups.

Table 4.3 Considered ranges of values for the additional analyzed cases

Name of case	Structural mass (ton)	Frequency input motion (Hz)	Embedment slab foundation/ platform	Pile group configuration	Pile Young's modulus (GPa)
A-RI	4.08 6.00 8.00	0.75 1.25 1.75	No/Yes	3 x 2 4 x 3 6 x 5	10 30
A-P	4.08 6.00 8.00	0.75 1.25 1.75	No/Yes	3 x 2 4 x 3 6 x 5	10 30

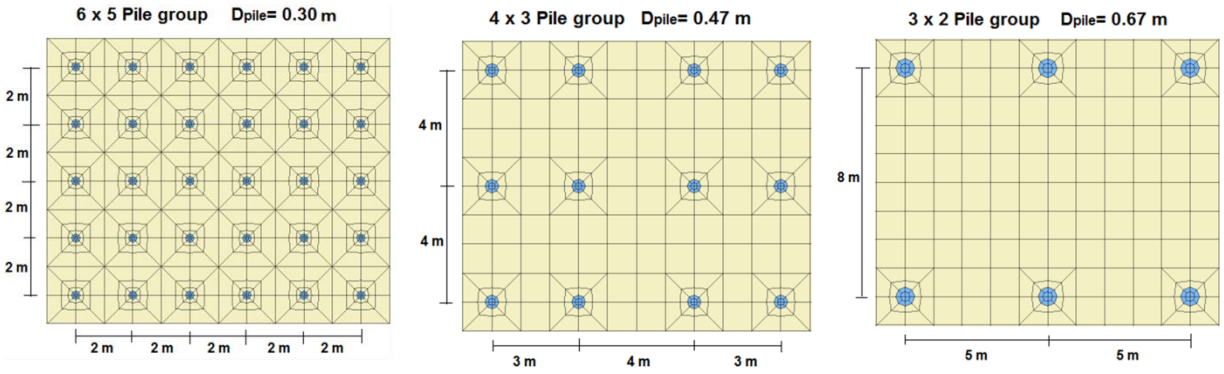

a) 6 x 5 Pile group **b)** 4 x 3 Pile group **c)** 3 x2 Pile group

Fig. 4.4 Pile group configurations

1.5. Dynamic Input Motion

The applied dynamic loading is a sinusoidal acceleration wave (bedrock curve shown in Fig. 4.9) applied at the base of the model in the horizontal direction and is given by the equation $\ddot{u}(t) = \frac{1}{2}\left(1 - \cos\frac{\pi}{3}t\right)A\sin(2\pi ft)$, where $A = 0.4g$ is the amplitude and f is the frequency. As mentioned before different frequency values of the applied loading were utilized in the analyses (0.75, 1.25 and 1.75 Hz). The first term of the equation is an envelope function of 6 seconds duration that provides a gradual build-up and decay of the wave. It means that the acceleration increases during the first three seconds and reaches a maximum of 4 m/s². Then it decreases until the 6th second. In order to get the equilibrium of the system, 4 more seconds were added after the end of the loading.

The fundamental frequency of the soil can be calculated in terms of shear wave velocity with the equation $f_n = (2n-1)V_s/4H$ where Vs is the velocity of the shear waves in m/s, H is the total depth of the layer and n is the mode number (Kramer 1996). For small values of damping, the resonant frequency is almost equal to the natural frequency. For the studied soil profile, the fundamental frequency is deduced from the elastic response in free field and is equal to 1.25 Hz.

1.6. Procedure of Analysis

In the first step, an initial stress state is generated. Then, the vertical reinforcements are installed and the model is equilibrated due to the weight of the vertical elements. The last static calculation step considers the activation of the earth platform and of the surface structure. For the dynamic calculations, the absorbent and free field boundaries are added and the dynamic analyses are executed applying the corresponding horizontal wave using acceleration at the base of the models.

1.7. Verification of the Analyzed Systems

For the cases analyzed in this study there is no simple analytical solution that takes into account all the characteristics of the considered systems. The 3D numerical models developed in this study attended to accurately represent the realistic behavior of the analyzed systems. In order to show that the behavior of the analyzed systems is consistent with results already known and which have been validated through analytical examples or experimental tests in the literature, a brief study of the A-RI and A-P systems (reference cases) is developed. The soil response in terms of accelerations, displacements, settlements, shear stresses and strains and plastic zones were obtained. All these results take into account only the influence of the dynamic loading because the soil values in the initial state (after the implementation of the structure) for all models in elastic and elasto-plastic calculation were initialized before the application of the dynamic loading. This initialization of values was developed in all cases analyzed in this manuscript. The measures presented following were taken in a point P located in between of the rigid elements (Fig. 4.1c).

1.7.1. Soil accelerations and displacements

The maximum accelerations obtained during the whole dynamic loading calculation vertical to the point P (see Fig. 4.1) are shown in Fig. 4.5a. In general, it can be noted that the wave propagation from the input motion acceleration (bottom of the model) to the surface leads, in this case, to a peak acceleration of 0.93 g and 0.84 g for the A-RI and A-P systems respectively. These values implies an amplification factor of 2.3 and 2.1 respectively over the peak input acceleration (equal to 0.4 g). Mánica et al. (2014) and Amorosi et al. (2010) obtained amplification factors around 2.2 and 1.2 respectively. Both authors considered sof clay in their studies.

The soil accelerations in the rigid inclusion systems are close to those of the pile systems except in the depths from 2 m to 8 m, where the acceleration values of the A-RI are 19% greater than the values of the A-P case (Fig. 4.5a). This is due to the difference of the interaction of the pile and rigid inclusion elements with the surrounding soil. In the A-RI case, the acceleration recorded at the earth platform level (0.6 m) are reduced by 9% compared to those in the ground surface. This is due to the

dissipation of energy in the platform which implies a benefit for the structures located in seismic zones Hatem (2009) obtained values around 13 to 15% of acceleration reduction with several platform heights. Mayoral et al. (2006) reported reductions around 2% of the acceleration due to the platform.

The maximum horizontal soil displacements (vertical to point P) are displayed in Fig. 4.5b. The maximum values are obtained in the upper part of the model and decrease with depth for both systems. Similar results have been demostrated by Rahmani and Pak (2012), Kitiyodom et al. (2006) and Liyanapathirana and Poulos (2005). The displacements in the rigid inclusion system are greater from ground surface to 6 m depth. The maximum difference is around 40% at 2 m depth. Contrary, from 6 m depth until the bottom of the model, the displacements in the soil are almos twice the values of the A-RI case (Fig. 4.5b). This variation is due to both the soil energy dissipation and to the soil/vertical element interaction. The displacement at the ground surface is the same for both models (0.16 m).

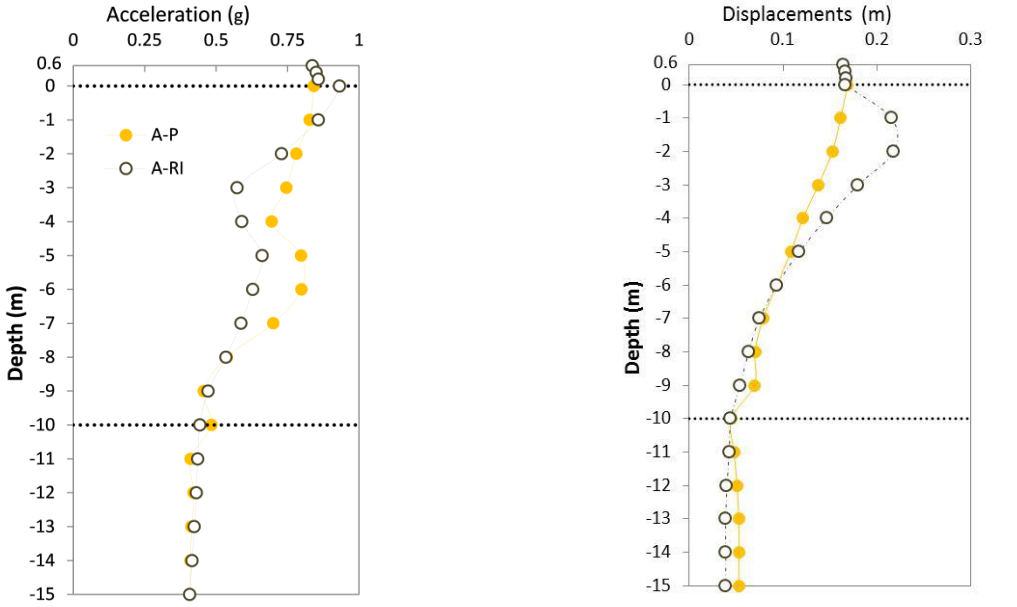

a) Soil accelerations **b)** Soil horizontal displacements

Fig. 4.5 Soil maximum accelerations and displacements

1.7.2. Shear Strains

Fig. 4.6 shows the maximum shear strains obtained after dynamic loading in the soil (vertical to point P) for the rigid inclusion and pile cases. It is clear that the distribution of the maximum shear amplitude is large at the top of the model and small at the bottom. It is in the upper part where the maximum damping ratio and the minimum shear stiffness are attained. This is in agrement with the result shown by Lu et al. (2005), Amorosi et al. (2010), Phillips and Hashash (2009), Tsai et al. (2014) and Mánica-Malcom et al. (2016). The shear strains are larger than the values in the A-RI system at depths from 0 to 6 m. This difference in shear strain values in the upper part of the model is explained

by the influence of the rigid connection of the pile system with the slab foundation or the free condition ar the head of the rigid inclusions. In this case, the shear deformations in the boundary of the hard layer and soft soil are not important; however, they are usually significant when there is a significant rigidity contrast between two consecutive layers (Mánica et al. 2014).

In addition, typical shear-strain curves computed at depths of 3 m and 6 m for both system are presented in Fig. 4.6b, c. It can be noted that the maximum shear stress in both cases is in the order of 40-50 kPa. The shear strains in the A-RI system get values close to 8% and 3.5 % at 3 m and 6 m depth respectively. Larger strains are estimated for small number of cycles at 3 m depth compare to the 6 m depth in the A-RI system. In the A-P case the values reached are lower 3% for the 3 m and 6 m depths.

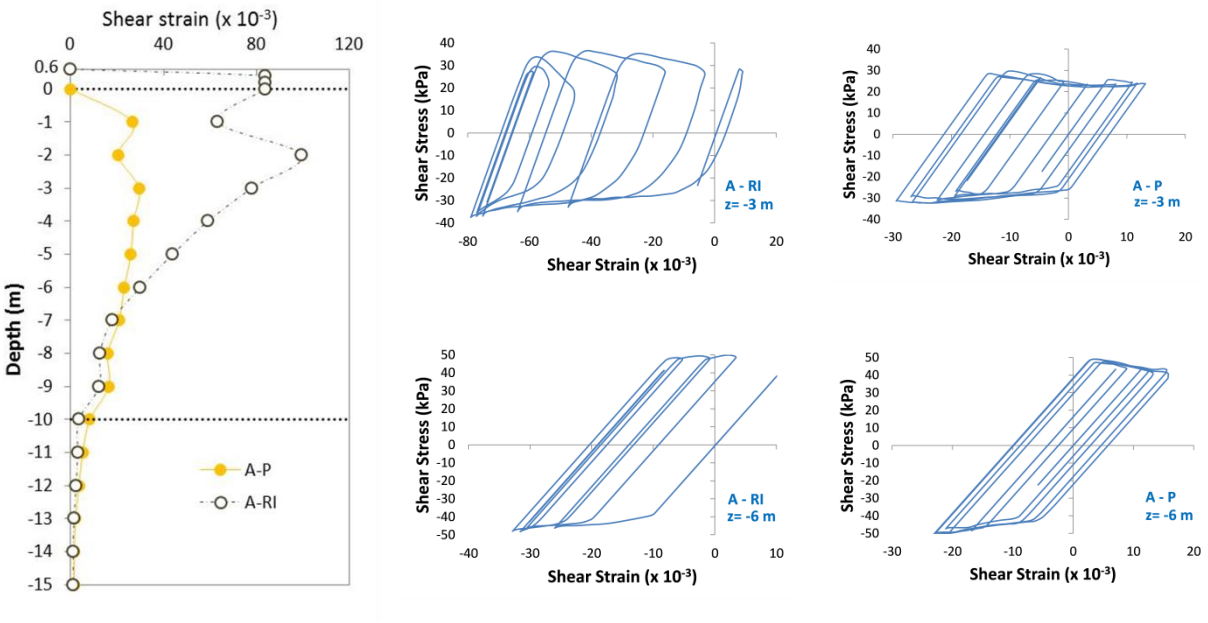

a) Maximum strains **b)** A-RI **c)** A-P

Fig. 4.6 Shear stress and strain in soil

1.7.3. Settlements

The histories of soil settlements at different depths z vertical to point P are displayed in Fig. 4.7. It is noticeable that settlements in the A-RI case are more important than in the A-P. For instance, the settlement at 3 m depth is around 0.065 m in the A-RI case and 0.02 m in the A-P case Fig. 4.7a, b. This can be explained by the way in which each system transmits the surface loadings. In the rigid inclusion systems, there is part of the load that is transmitted to the rigid elements and part to the soft soil. The interaction of the rigid elements with the surrounding soil plays also an important role in the development of these settlements.

The maximum settlements in the A-RI case occur at ground surface and they are reduced with depth (Kitiyodom et al. 2006, Rahmani and Pak 2012, Rahmani et al. 2012). The settlements at 0.6 m (platform level) are 20% lower compare to those in the ground surface Fig. 4.7a. The settlements are importantly reduced in the A-P system respect to the A-RI case. This is explained because the surrounding soil settles together with the pile group indicating that most of the surface load is carried by the slab foundation resistance and the slip between the soil and the pile is minimized (Comodromos, Papadopoulou, and Rentzeperis 2009).

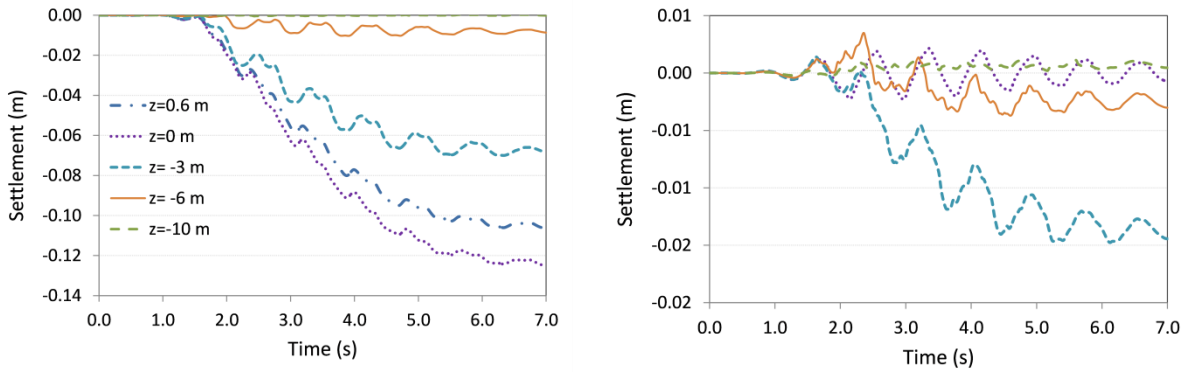

a) A-RI **b)** A-P

Fig. 4.7 Settlements in soil

1.7.4. Shearing Zones

Fig. 4.8 presents the zones where plastic strains appear at the end of the dynamic calculation. In the rigid inclusion systems, the soft soil is shearing. The earth platform and the zones around the upper inclusion parts are shearing and are also in a tension state.

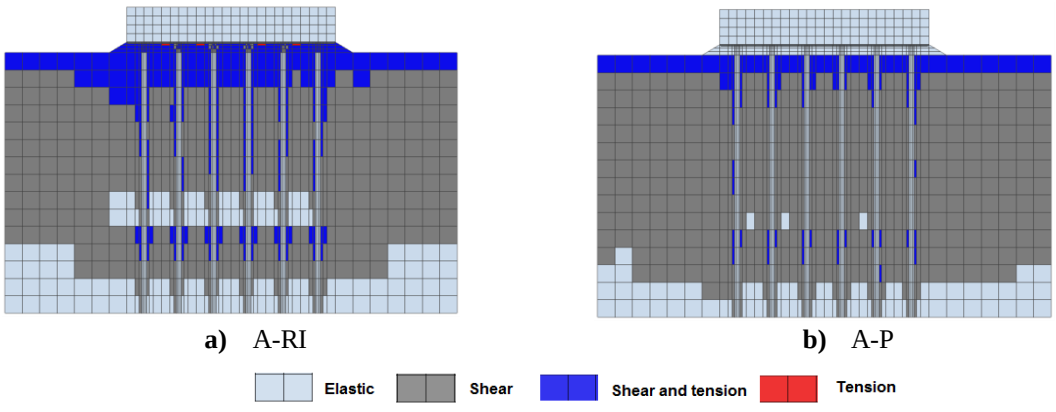

a) A-RI **b)** A-P

Fig. 4.8 Plastic zones in the systems after loading

When the inclusions are anchored (A-RI), the soil under the rigid inclusions (hard soil) is sheared. At the level of the anchorage, the zones around the rigid inclusions are in a shear and a tension limit state (Fig. 4.8a). These zones are not presented in the systems with placed on hard soil and floating

piles. A similar behavior for the rigid inclusion systems is shown in the pile systems (A-P). Two differences can be noted; the first one is that in the pile upper part, there are only shearing zones around the piles until 2 m of depth in the central rigid elements (Fig. 4.8b). The other difference is that there is no shearing of the platform because it is replaced by a slab foundation.

It can be noted from this section that the results from the numerical cases of the reference cases match reasonably well with the results obtained from other studies (Liyanapathirana and Poulos 2005, Lu et al. 2005, Kitiyodom et al. 2006, Phillips and Hashash 2009, Rahmani and Pak 2012, Hokmabadi et al. 2014, Hokmabadi and Fatahi 2016, Mánica-Malcom et al. 2016) which have been confronted with experimental data or analytical solutions. Hence the above finite difference method is used to obtaining the response (soil, rigid element and superstructure) of pile and rigid inclusion systems.

1.8. Results and Discussion

The results of the all the analyzed models are presented below (Table 4.2 and Table 4.3). The results are presented in terms of spectrum response to study the soil-structure interaction effects of each system. The bending moments, normal forces and displacements along the rigid elements are compared for the all cases.

1.8.1. Soil Amplification

The properties of the soil and the foundation type greatly influence the earthquake motions at the base of the structure by altering the inertial and the kinematic interactions. The amplitude and frequency of the ground motion can also be modified by the site effects. The significance of these effects is exemplified in Section 2.1 Chapter 2.

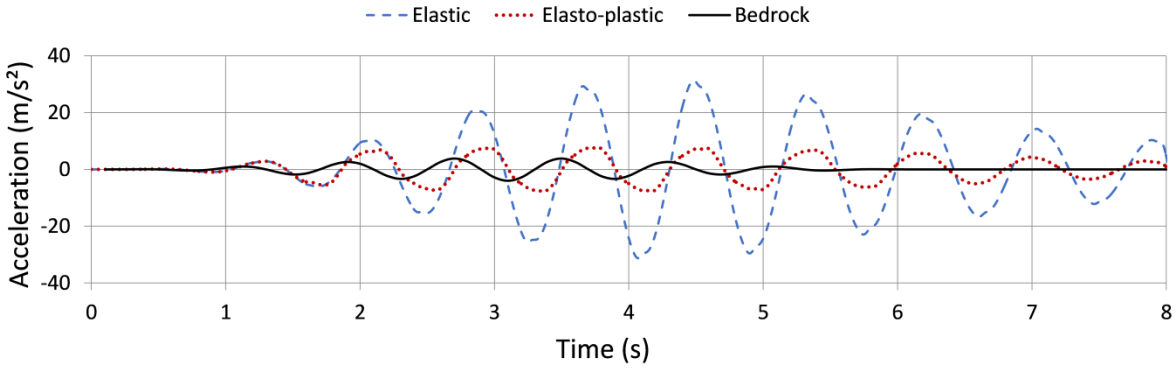

Fig. 4.9 Surface acceleration with elastic and elasto-plastic calculation

Fig. 4.9 compares the surface acceleration curves for the P-RI case (similar results are obtained for the other cases) with elastic and elasto-plastic calculation respectively. The maximal value of the acceleration reaches 31.3 m/s^2 at the surface for the elastic soil condition, which implies an amplification of almost 8 times compared to the input motion (model bottom). However, with the elasto-plastic calculation, the amplification reaches a value of 2. It is noticeable that the acceleration records at the surface are out of phase with the wave applied at the base is due to the kinematic effects of the pile or inclusion groups. This phase lag is not visible in the comparison of the acceleration records with elastic and elasto-plastic calculation.

The induced motion in a soil-foundation-structure system due to the incident waves during earthquake loading generates inertial forces in the superstructure which results in stresses in the foundation that are, in return, propagated through the soil. The soil properties of the underlying soil deposit, the presence of the structure and the foundation type may influence the characteristics of the earthquake motion at the base of the structure modifying the inertial and kinematic interactions. Therefore, the inertial forces generated by the mass of the structure and the foundation may create more motion compared to the free-field motion. On the other side, variations of the base motions are due to the inability of the foundation to match the free-field deformations (kinematic interaction).

The effect of the SSI on the considered systems can be analyzed using the spectrum response obtained from the ground motion at ground surface (base of the structure). A method based on the interpolation of the excitation was used to calculate the acceleration response spectrum. This procedure was utilized to obtain all spectra in this research work. The response spectrum describes the maximum response of a single-degree of freedom system for a specified earthquake ground motion and 5% of damping. Considering the knowledge of structural dynamics, the response spectrums are usually used for the design of structures and calculate the shear forces in building codes in terms of the natural frequency of the system.

In order to investigate the significance of the SSI effects of the considered systems, the acceleration response spectra of the motions recorded at the base of the structure are shown in Fig. 4.10.

It is clear from Fig. 4.10 that assuming linear elastic or elasto-plastic soil conditions, the response is greatly amplified by the soil deposit. The response spectra of all systems are similar with only a small difference in terms of amplitude appears at the peaks. The maximum peak is observed at around a period of 0.8 s (frequency 1.25 Hz) which is equal to the soil fundamental period (Fig. 4.10a). When the plastic soil behavior is considered, the peaks of the spectra decrease importantly in amplitude compared to the elastic response. For instance, the spectrum response of the P-P system with elasto-plastic case is reduced around 3.5 times compared to the elastic one (Fig. 4.10b). This agrees with the studies developed by Kim and Roesset (2004), Maheshwari et al. (2004), Al Fach (2009) and Alsaleh

and Shahrour (2009). These results highlight the importance of the elasto-plastic calculation when the frequency of the loading approaches the soil fundamental frequency in the presence of low soil properties.

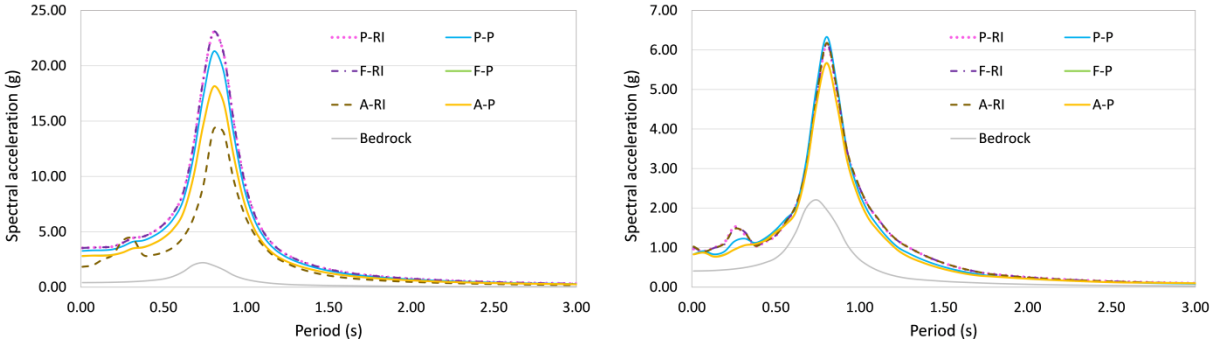

a) Elastic calculation **b)** Elasto-plastic calculation

Fig. 4.10 Acceleration response spectrum for the analyzed cases.

Fig. 4.11 compares the kinematic and inertial effects in the rigid inclusions and piles for all cases with the elasto-plastic conditions. The kinematic effects were evaluated by comparing the response spectra ratio of the motions underneath the structure to the free-field response (Fig. 4.11a). This difference is dependent on the stiffness and geometry of the foundation and the soil properties (Rayhani and El Naggar 2008). It is clear that the spectral ratio curves are not affected by the support type in the pile and inclusion cases. Fig. 4.11a shows that for periods greater than 0.9 s and until 3.7 s, the foundation acceleration is amplified up to respectively 35% and 51% compare to the free-field response for the piles and rigid inclusions systems (independently of the type of pile support). The same comparison of accelerations but for periods around 0.1 to 0.3 s, gives respectively a decrease of the amplification of 30% and 25% for the pile and rigid inclusions cases.

The inertial soil-structure interaction was evaluated by comparing the acceleration response spectra in the upper part of the structure and the one obtained on the side of the foundation (Fig. 4.11b). From this figure, it is noted that the structure experiments higher acceleration up to 20% compared to the response on the side of the foundation over the period range of (0.7-3.7 s) for the pile cases and up to 40% in the rigid inclusion cases for period from (1.15-3.7 s). For smaller periods (0.15 to 0.25 s), the acceleration in underneath the foundation is decreased up to 25% compare to the free-field response in the P-RI and P-P.

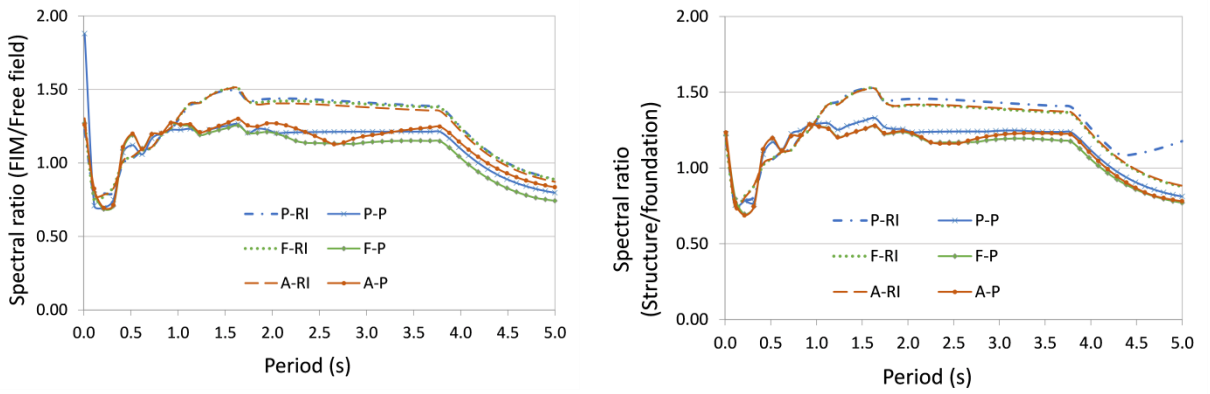

a) Spectral ratio (FIM/Free-field) **b)** Spectral ratio (structure/side of the structure)

Fig. 4.11 Spectral ratios in the rigid inclusion and pile cases placed on hard soil

The response spectra for the systems considering different input motion frequencies are shown in Fig. 4.12a. The consideration of an input motion frequency different of 1.25 Hz (which coincides with the fundamental frequency of the analyzed systems) causes a decrease of the spectral acceleration. For example, for the A-RI case (fundamental frequency equal to 1.25 Hz) the spectral acceleration reached is respectively 6g, 2.7g and 1g when the frequencies of the input motions are 1.25, 0.75 and 1.75 Hz.

It is noted in Fig. 4.12b that kinematic effects reduce the spectral acceleration of the cases considering an embedment of the slab or platform. For instance, the peak acceleration amplitude at 0.8 s decreases respectively of 9% and 7% for the no embedded to embedded condition (A-RI and A-P cases).

The response spectra with different pile group configurations show similar values (Fig. 4.12c). Small differences in the peak values are observed. At periods smaller than 0.5 s, the spectral acceleration is increased for the A-P case compared to the A-RI case for the same pile configuration.

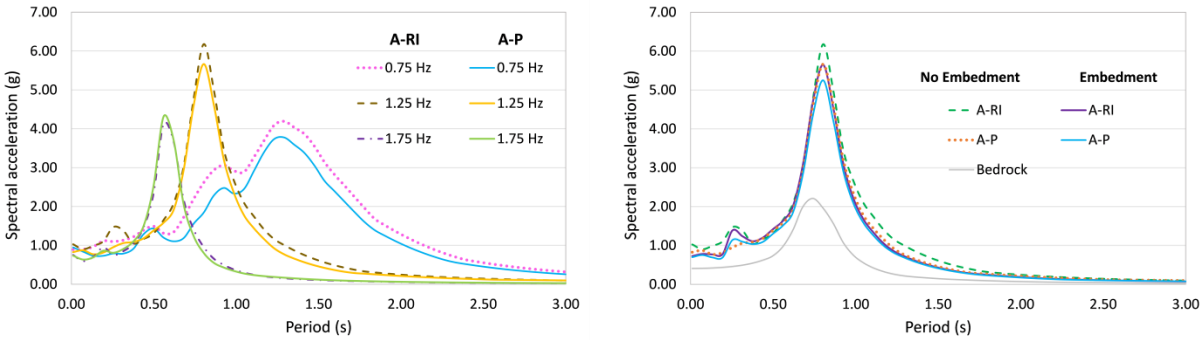

a) Frequency of Input Motion **b)** Embedment effect

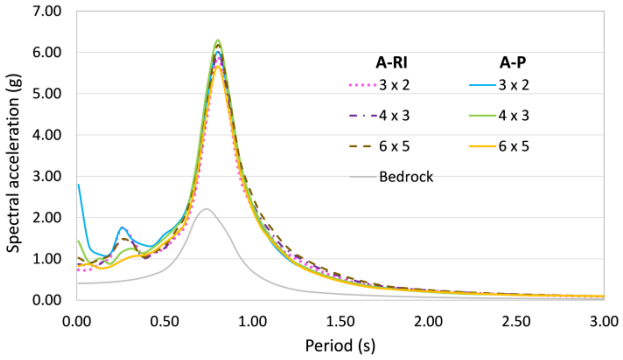

c) Pile group configuration

Fig. 4.12 Acceleration response spectrum for the additional analyzed cases.

1.8.2. Comparison of Efforts and Displacements along the Rigid Elements

The normal forces, the bending moments and the displacements along the vertical elements are compared in this section for the rigid inclusions and piles systems with different support conditions. The values used for the comparison correspond to the element located in axes A-1 (Fig. 4.1c), because it is the element with higher efforts due to the group effects which is in good agreement with the study of Nguyen et al. (2017). The efforts presented correspond to the maximum values recorded during the static and dynamic calculation. However, the initial values in the piles and rigid inclusions (obtained after the implementation of the structure) are negligible (almost zero) for the bending moments, shear forces and displacements. This implies that the efforts and displacements shown in the following part (applied for all results in the thesis) take into account only of the influence of the dynamic loading. Exceptions of this are the normal force values in the rigid elements. Before the application of the dynamic loading, the maximum normal forces obtained along the rigid elements are lower than 160 kN and 127 kN for the pile and inclusions systems.

1.8.2.1. Influence of the Pile Support Condition and Soil Plasticity

Fig. 4.13 shows the curves of normal forces along the inclusions and piles considering different pile support conditions and soil behavior (elastic or elasto-plastic).

In all rigid inclusion cases, the normal forces increase with depth. The normal forces in the rigid inclusion cases are greater in the elastic calculation than in the elasto-plastic calculation. These differences in values are around 117% at 1 m depth and 213% at 5 m depth for all systems. The normal forces in the elasto-plastic cases are lower because the volumetric elements surrounding the elements are plasticized and do not transmit compression forces to the rigid elements. These values are more reliable than those obtained in the elastic case. The normal forces values along the rigid inclusions are similar for the different support type (Fig. 4.13a). At 10 m of depth, the maximum

normal force in the A-RI system is 5% greater than the value of the P-RI model (560 kN) in elastic calculation. In the elasto-plastic case, this ratio is equal to 44%.

In the pile systems, the normal forces are reduced by up to around 60% from elastic to elasto-plastic calculations (Fig. 4.13b). Alsaleh and Shahrour (2009) obtained analogous values.

Comparing both systems, it is evident that the normal forces in the piles are greater than in the inclusions. For instance, at head level, the normal forces are 87% greater in the piles than in the rigid inclusions, for the elastic calculations. The same comparison but for the elasto-plastic case shows 209% of difference, which is comparable to the 180% obtained in the study of Hatem (2009). This takes place because the role of the rigid inclusion system is to limit the transfer of movement towards the superstructure, which in turns reduces the inertial forces. The use of such system thus implies a benefit in seismically active zones. In the rigid inclusion cases the surface loads are transmitted by the rigid elements and the soft soil underlying the LTP.

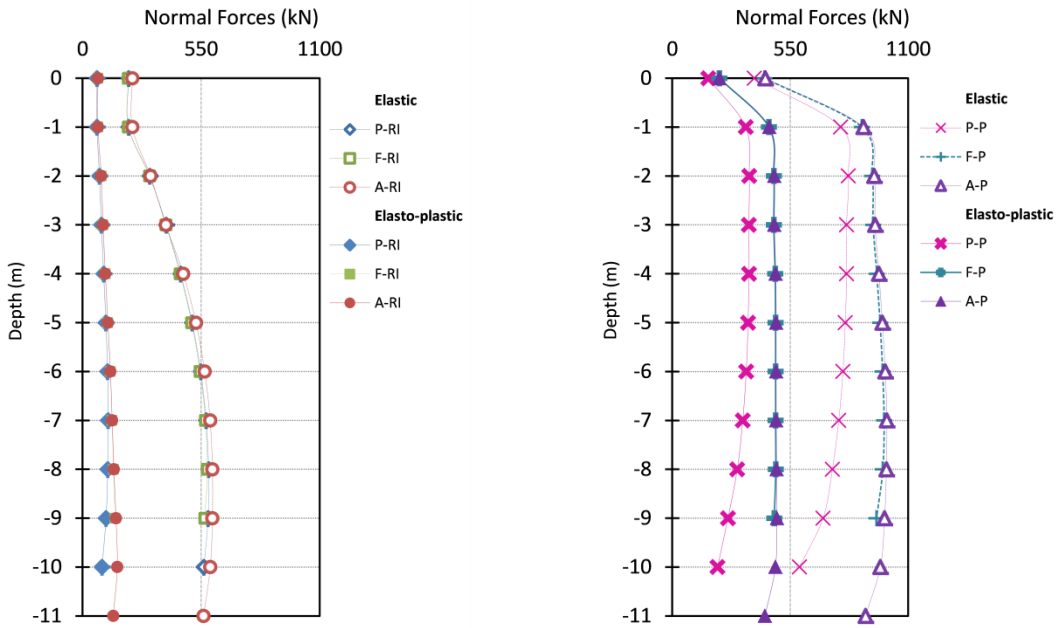

a) Rigid Inclusions systems **b)** Piles systems

Fig. 4.13 Normal forces along elements with elastic and elasto-plastic calculation

In the pile cases, the maximum bending moments are obtained at the element heads, independently of the type of support (Fig. 4.14). The bending moments reached at the pile head with elastic calculations are around 315 kN.m. In the elasto-plastic calculations the values are close to 150 kN.m. These values are due to the rigid connection with the slab that increases the inertial forces at the connection level. However, these inertial forces are decreased by the soil plasticity which in turns causes a decrement of the shear forces and bending in the piles. Parallel results are exhibited by Alsaleh (2007), Al Fach (2009), Alsaleh and Shahrour (2009), Hussien et al. (2011) and Bao et al.

(2012). In the rigid inclusion cases, the bending moments at the rigid inclusion heads are null. This means that the use of the earth platform in the rigid inclusion system reduces the shear forces and bending moments in the head elements, which is useful for structures located in zones with high seismic hazard. The platform limits the movement transferred to the structure, which reduces the inertial forces.

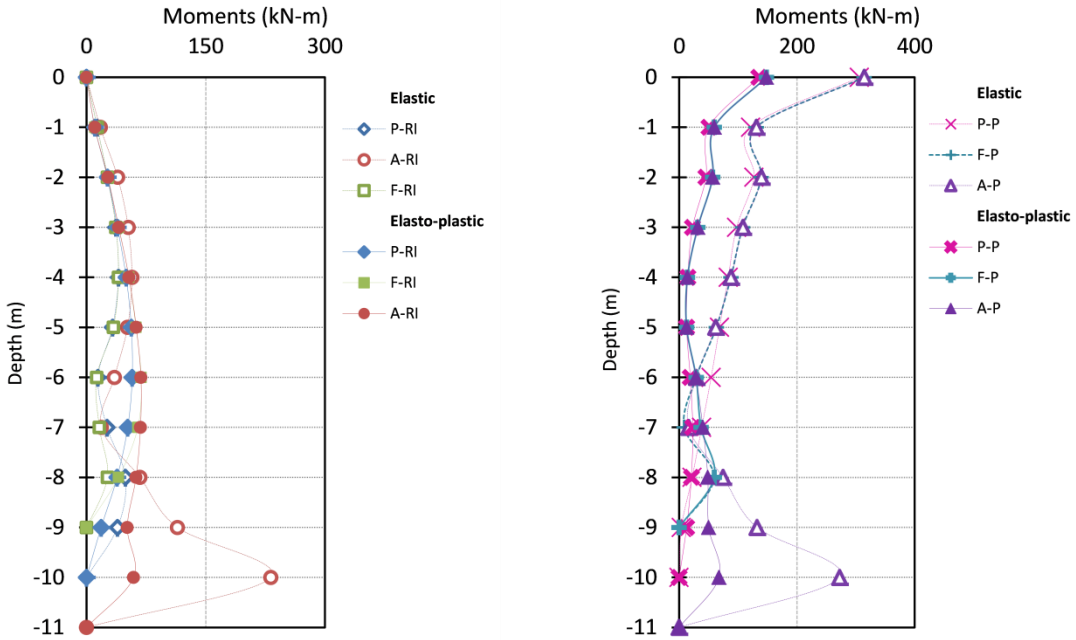

a) Rigid Inclusion systems **b)** Pile systems

Fig. 4.14 Bending Moments along elements with elastic and elasto-plastic calculation

The bending moments in the A-RI and A-P systems are similar to those obtained for the placed and floating systems, with the difference that at the level of the anchorage, the values are more significant (Fig. 4.14). The anchored systems are highly influenced by the lateral deformation of the surrounding soil, which produces extra kinematic forces in the elements and the increase of efforts at the level of the hard soil connection. For instance, in rigid inclusion cases with elastic system, the reached value is equal to 231 kN.m, while in the elasto-plastic case, it is equal to 59 kN.m. In the A-P system, the value with elastic calculation is equal to 111 kN.m and to 26 kN.m in the elasto-plastic case. This is in accordance with the study of Nguyen et al. (2017) where the authors show that the anchored piles experience a great moment at the toe compared to the floating piles. For both system types, a special attention should be paid in the design at the anchorage level to avoid failure in the vertical elements.

The maximum horizontal displacement for all rigid inclusion cases for elastic calculations is almost the same and reaches a maximum of 0.56 m. However, with the use of elasto-plastic behavior, this value is reduced to almost 0.25 m (Fig. 4.15a). Similar displacements are obtained by Luo et al. (2016) with nonlinear soil behavior. This variation is due to both the soil energy dissipation and to the

soil/rigid element interaction. The maximum value is always reached at the element head. The type of support has no influence on the displacements.

The pile systems register a maximum displacement of 0.55 m for the elastic calculation and 0.17 m in elasto-plastic case (Fig. 4.15b). Compared to the rigid inclusions, these values are reduced by 1% and 36% for the elastic and the elastoplastic cases respectively.

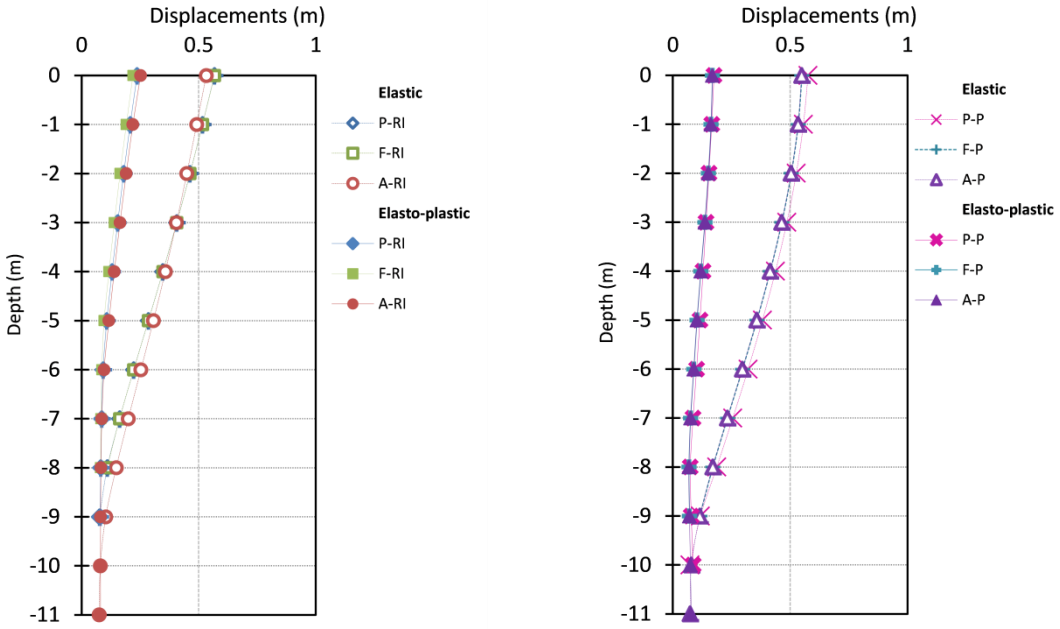

a) Rigid Inclusions systems **b)** Piles systems

Fig. 4.15 Horizontal displacements with elastic and elasto-plastic calculation

1.8.2.2. Influence of Input Earthquake Frequency

To study the influence of the input loading frequency, three different frequencies with identical peak acceleration (equal to 0.4 g) were applied to the A-RI and A-P systems with elasto-plastic calculation. It is noted in Fig. 4.16 that the frequency of excitation has a notable effect on the response of the rigid elements. The normal forces and bending moments are similar for the system analyzed with a frequency loading of 1.25 Hz and 0.75 Hz. However, these values are importantly reduced in the systems with an input frequency of 1.75 Hz. Normal forces are reduced of 38% and bending moments of 25% to 58% for the A-P case. Similar results are obtained for the A-RI system (Fig. 4.16a). These results are in good agreement with the response spectra which indicate that the greatest acceleration occurs when the input motion frequency is close to the system frequency.

The increase of the input motion frequency implies the displacements reduction of the rigid elements. For instance, maximum displacements of 0.43, 0.16 and 0.05 m are respectively obtained for the A-P case for frequencies of 0.75, 1.25 and 1.75 Hz (Fig. 4.16c). The maximum displacement is

located at the head of these elements and is reduced with depth. The displacements of the rigid inclusion cases are larger than the pile ones.

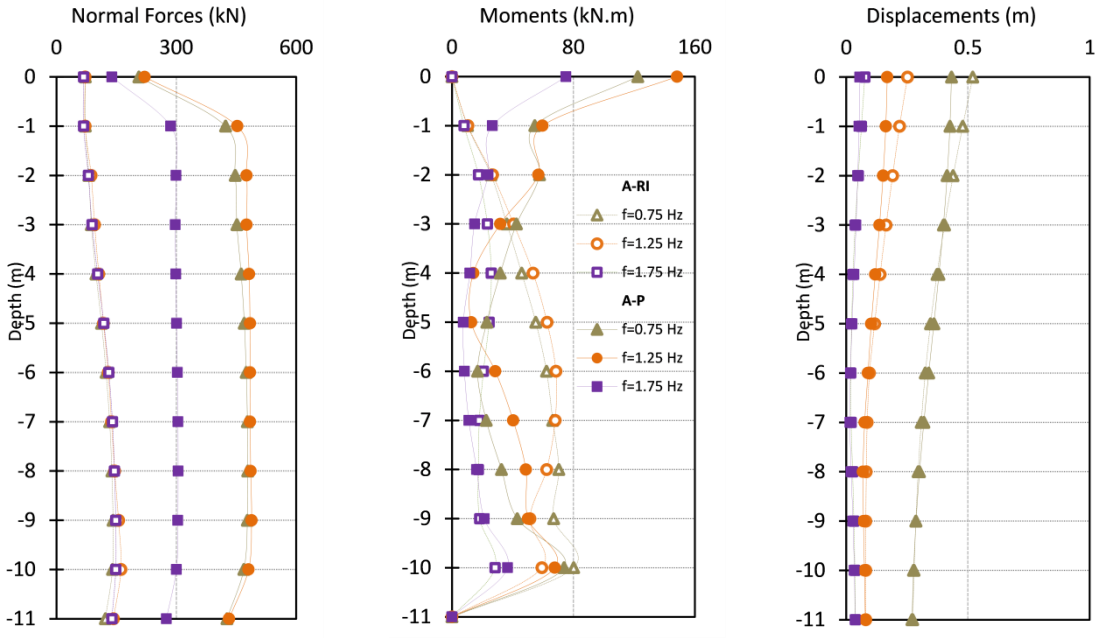

a) Normal Forces **b)** Bending Moments **c)** Displacements

Fig. 4.16 Influence of Input Earthquake frequency in the efforts and displacements along the rigid vertical elements

1.8.2.3. Influence of the Pile Group Configuration and Pile Flexural Rigidity

The influence of the pile group configuration on the seismic response is investigated in this part. Three pile configurations are considered in Fig. 4.17. The cases were only tested for the A-P and A-RI systems with elasto-plastic calculation. Due to the fact that the cover ratio is the same in all the cases, the pile diameter is different. Thus, the normal forces and the bending moments were normalized to consider only the effect of the pile group configuration. The normalized forces are calculated by $\hat{F} = F/\rho_p d^3 a$ and the bending moments by $\hat{M} = M/\rho_p d^4 a$, where ρ_p is the volumic weigth of the pile, a is the peak ground acceleration (PGA) of the applied loading and d is the pile diameter (Xu and Fatahi 2018).

The results indicate that the pile group configurations have an important influence in the dynamic response of the foundation. Fig. 4.17 shows that the bending moments and normal forces developed in the piles decrease with the number of piles reduction. This is due to the kinematic interaction between the piles and surrounding soil. For instance, in the A-P case, the normal forces for the 3 × 2 pile group are 31% and 62% smaller than in the 4 × 3 and 6 × 5 configurations respectively. Concerning the bending moments, they are similar along the piles, except at the pile head where the pile configuration

plays an important role. The same tendency is observed in the A-RI system where the maximum bending moments along the inclusions are respectively reduced of 21% and 45% from the 6 x 5 pile group to the 3 x 2 and 4 x 3 configurations (Fig. 4.17b).

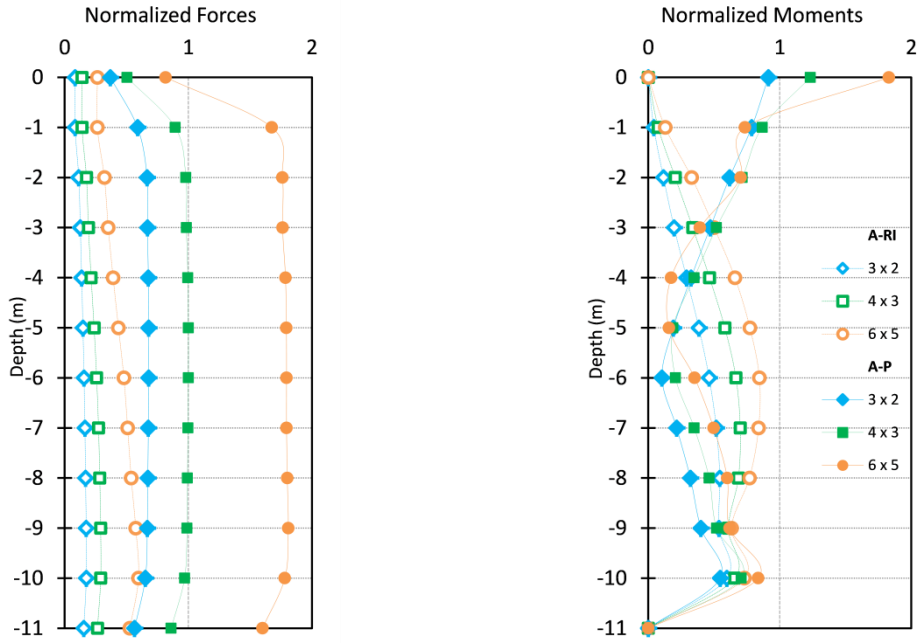

a) Rigid Inclusion systems **b)** Pile systems

Fig. 4.17 Influence of pile configuration in the efforts along the rigid vertical elements

Although the results are not displayed, calculations with the A-P and A-RI systems were carried out with two pile modulus values (10 GPa and 30 GPa). The computed maximum normal forces and bending moments increase with the increase of the pile modulus value. The maximum bending moments in the cases using 30 GPa compared to 10 GPa are respectively lower of 39% and 45% for the A-P and A-RI cases. This is because the soil imposes inertial loading on the stiffer piles instead of giving them a lateral support. In the contrary, even soft soils provide lateral support for flexible piles. Similar results are showed by Banerjee et al. (2014) and Goh and Zhang (2017).

1.8.2.4. Influence of the Structural Mass

Three different structural masses of 408, 600 and 720 tons were considered for using the A-RI and A-P system with elasto-plastic calculation. These masses approximate the mass a 3-storey, 5-storey and 7-storey building with a rectangular geometry of 12 × 10 m. Fig. 4.18 shows the normal forces and bending moments along the rigid elements for the A-RI and A-P cases.

As expected, the normal forces increase almost linearly with increasing the structural mass. This implies that the normal forces in the rigid elements in the A-RI case with 408 t of structural mass are increased of 13% compared to the case with 600 t and 26% compared to the case with 720 t. In the A-

P case the linear difference is around 11%. Similar results have been presented by Goh and Zhang, (2017).

The moments along the rigid vertical elements in the A-RI case with 408 t increase respectively of around 8% and 16% compare to the system with 600 t and 720 t. The moment at the pile head of the A-P case is 22% and 30% greater for the 720 t mass compared to the system with 600 t and 408 t mass respectively (Fig. 4.18b).

The maximum horizontal displacements obtained at the head of the rigid elements in the system with 408, 600 and 720 t are equal to 0.15, 0.16, and 0.17 m respectively.

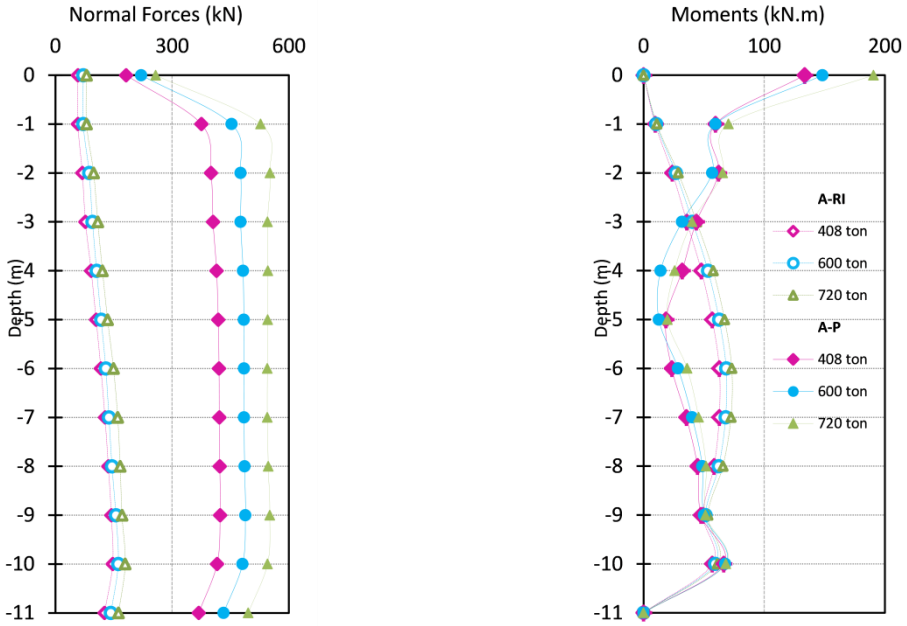

a) Rigid Inclusions systems **b)** Piles systems

Fig. 4.18 Influence of structural mass in the efforts along the rigid vertical elements

1.8.2.5. Influence of the Embedment of the Slab Foundation or Earth Platform

Due to the fact that most of the foundations are partly embedded in the soil, in this part the response with and without embedment of the earth platform for the A-RI case or the slab foundation for the A-P case are compared (Fig. 4.19). Fig. 4.20 shows the maximum normal forces and bending moments for both conditions.

The efforts and displacements obtained are influenced by the embedment in the upper part of the rigid elements. For instance, in the A-P case with embedded slab foundation, the normal forces are reduced from 220 kN to 82 kN, the bending moments from 148 kN.m to 59 kN.m and the displacements from 0.16 m to 0.14 m compared with the system without embedment (Fig. 4.20a-c).

This happens because the embedment of the foundation increases the stiffness and the damping of the system. These results are consistent with the peak acceleration reduction in the response spectra of the embedded and no embedded systems (Fig. 4.12c).

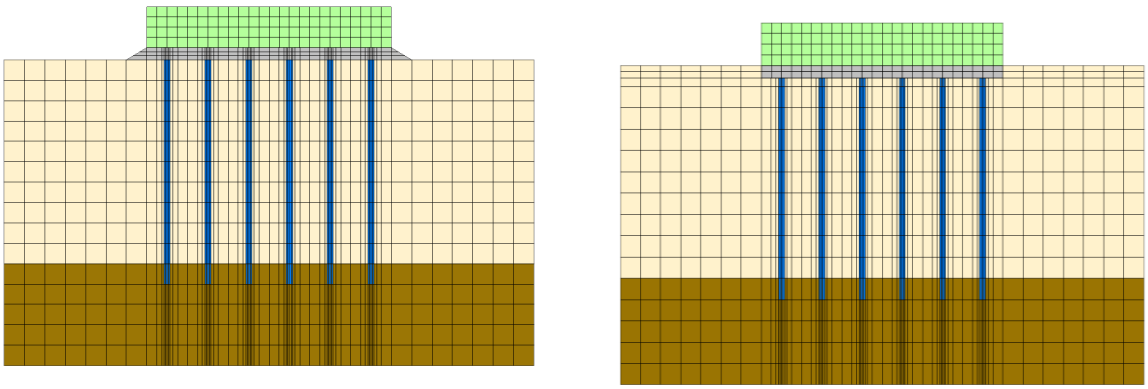

a) Without embedment **b)** Embedded

Fig. 4.19 Embedment of the foundation slab in the A-P case

For the A-RI case, the bending moments and displacements are very similar for the embedded and non embedded conditions. However, the normal forces in the embedded conditions present an increase of 48% compared to the non embedded condition. As mention before, this occurs because the kinematic interaction reduces the amplitude of the foundation motion as a result of the embedment.

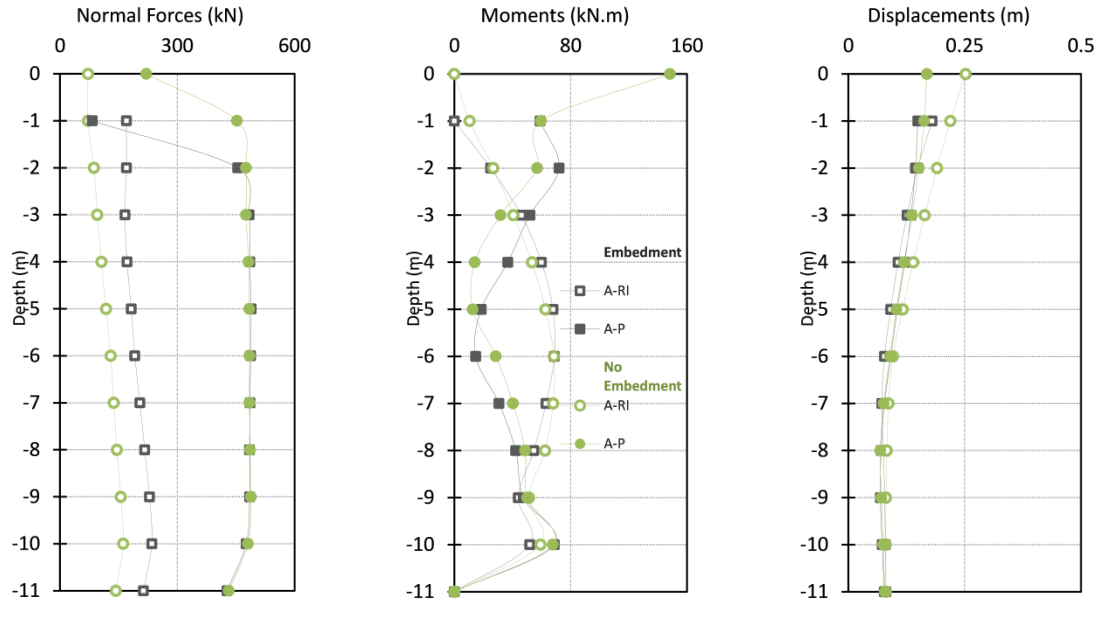

a) Normal Forces **b)** Bending Moments **c)** Displacements

Fig. 4.20 Influence of the embedment of the slab foundation or earth platform in the efforts and displacements along the rigid vertical elements

1.9. Preliminary Conclusions

In the first part of this Chapter, tridimensional dynamic analyses were used to investigate the behavior of soil-pile-structure and soil-inclusion-platform-structure systems. Linear elastic and elasto-plastic constitutive models are successively used to represent the soil behavior. Different pile or inclusion support conditions, pile configurations, structural mass values, frequencies of input motion and pile stiffnesses were taken into account. The 3D numerical models presented were developed to accurately represent the realistic behavior of the analyzed systems.

The response spectra of all systems are greatly amplified compared to the response of the input motion. The peaks of the spectra importantly decrease in amplitude when the nonlinear soil behavior is considered, compared to the elastic condition. The energy transferred to the superstructure is reduced due to the plasticity of soil, leading to a decrement of normal forces, shear forces and the bending moments along the rigid elements with elasto-plastic soil condition compare to the elastic calculations.

The toe fixity conditions have a small influence on the normal forces developed in the rigid inclusion systems for both elastic and elasto-plastic calculations. The maximum bending moments in the pile cases are always obtained at the elements head, whatever the type of support. This is due to the fixed-head connection with the slab foundation that increases the inertial forces. The improvement with rigid inclusions allows reducing these efforts at the head level with the use of a LTP between the structure and the rigid inclusions. This reduction is beneficial in the design of structures in seismic regions.

The systems in which the rigid elements are anchored in hard soil are greatly affected by the lateral deformation of the surrounding soil, which produces extra kinematic forces in the elements and thus bending moments increase at the connection level with the hard soil.

The frequency of the input motion is a significant parameter in the response of the analyzed systems. When the frequency of the dynamic loading is close to the system frequency, the amplification of the response spectra is higher. This increment in spectral acceleration generates an increase of the normal forces, moments and displacement along the rigid elements.

Significant effect in the pile and rigid inclusion systems is evident considering different pile group configuration with the same cover ratio. Despite a similar response spectrum in all configurations, the bending moments and normal forces in the rigid elements augment with the number of piles increment. This is due to the kinematic interaction between the piles and the surrounding soil.

Stiffer piles and rigid inclusions acquire more lateral forces from the soil that results in a rise of efforts and displacements in the rigid elements.

As expected, the bending moments and normal forces along the rigid inclusions and piles are enlarged with the structural mass increase.

The embedment of the foundation slab (for the pile cases) or the platform (for the rigid inclusion cases) produces an important decrease of the efforts and displacements values in the rigid elements compared with the ones in the systems without embedment. A reduction in the acceleration in the response spectrum is observed in the embedded cases against to the not embedded cases.

Due to the fact that the Rayleigh damping formulation is introduced to account the dissipation of energy in the soil in the analyzed systems of Section 1, the following section presents the influence of the appropriate selection of damping parameters in the soil-foundation-structure systems.

2. Effect of the Rayleigh Damping Formulation Parameters

2.1. Introduction

The dissipation of energy in soil-foundation-structure system can be given by two sources: the dissipation of energy in the boundaries (radiation damping) and the loss of energy within the soil itself (material damping). The material damping has been identified as an significant parameter in the analysis of soil-foundation-structure systems (Ambrosini 2006, Wolf 1985). When the soil behavior is described by a comprehensive constitutive model, the loss of energy is inherently simulated, however, with simple constitutive models such as those considered in this Chapter, it is needed to model additional damping in the elastic part where there is no energy loss possibility. In this study, additional damping was introduced by a viscous damping (Rayleigh damping). Several studies considering the Rayleigh damping formulation are described in Section 2.3.2 Chapter 2.

Despite the Rayleigh damping formulation has been utilized by many authors with soil-foundation-structure systems, there is no sufficient examination about the selection and influence of the parameters on the systems. The differences on the seismic response of soil and structures associated with the correct selection of parameters (target damping ratio and the frequency-independent range) in the Rayleigh formulation is the main concern (Hashash and Park 2002, Tsai et al. 2014, Phillips and Hashash 2009). Hence, the objective of this part of the study is to investigate the effect of Rayleigh damping parameters in soil-pile-structure and soil-inclusion-platform-structure systems in the presence of soft soil under seismic loading. Three-dimensional analyses of both systems were carried out using the finite difference software Flac3D. The same soil profile and properties of soil describe in Section 1.2.1 of this Chapter are considered. The analyses were developed in drained condition and without considering the water level. Different values of target damping ratios and minimum frequencies were utilized. Several earthquakes were used to study the influence of the different excitation frequencies of the systems.

2.2. Characteristics of the Adopted Numerical Model

2.2.1. Soil and Structure model

The analyses were carried out using the same soil profile and properties described in Section 1.2.1 of this Chapter. However, in this case a reduced model was utilized. The dimensions of the volume of soil are 14 m x 14 m x 15 m. The model is constituted by 5,600 hexahedral zones. The discretization of the system using Flac3D (Itasca 2012) is depicted Fig. 4.21.

The material properties of all the elements are presented in Table 4.1. The behavior of the different soils is represented by the linear elastic-perfectly plastic constitutive model with a Mohr-Coulomb

shear failure criterion. The behavior of the superstructure, foundation slab and piles or inclusions is considered as linear elastic. These constitutive models can be consulted in Section 4 Chapter 2.

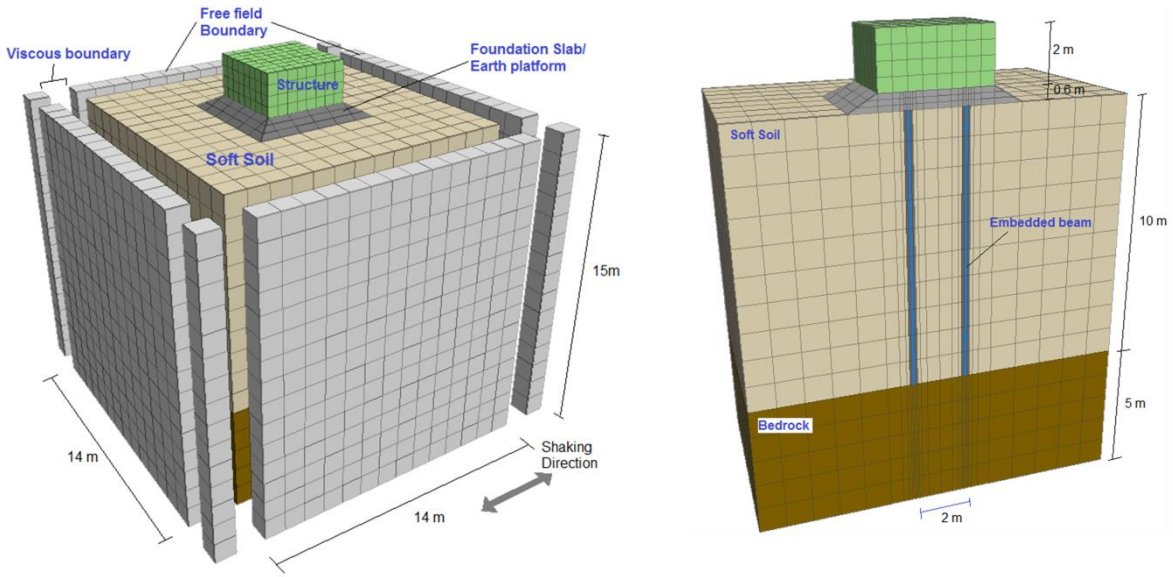

a) 3D Model **b)** Embedded beam

Fig. 4.21 Basic geometry of the numerical model

2.2.2. Vertical reinforced elements

Four piles were installed in the soft soil with a distance separation of 2 m in both directions (Fig. 4.21b). The reinforced concrete rigid elements were considered of 10 m length. The diameter of these elements was taken equal to 0.30 m. The cover ratio was set to 1.7%. The piles or inclusions were represented by the hybrid technique described in Section 1.2.2 of this Chapter.

A preliminary analysis was carried out to compare the pile response considering each pile modelled as solid elements combined with a beam element and considering only beam elements embedded in soil (Sadek and Shahrour 2004, Alsaleh and Shahrour 2009). In this preliminary analysis, a target damping ratio of 5% and a $f_{min} = 1.25$ Hz under the Loma Prieta earthquake is considered (Fig. 4.27a).

Fig. 4.22 shows how the shear forces and the bending moments in the rigid inclusion and pile systems are reduced for the combined system (solid elements and beam element) compare to the case where the piles are modelled using beam elements. The results indicate that there is a reduction from 57 to 61% of the maximum bending moments for the rigid inclusion case and from 38 to 53% for the pile case (Fig. 4.22a). The shear forces are very similar along the elements. Only a considerable reduction is observable in the three first depth meters (Fig. 4.22b).

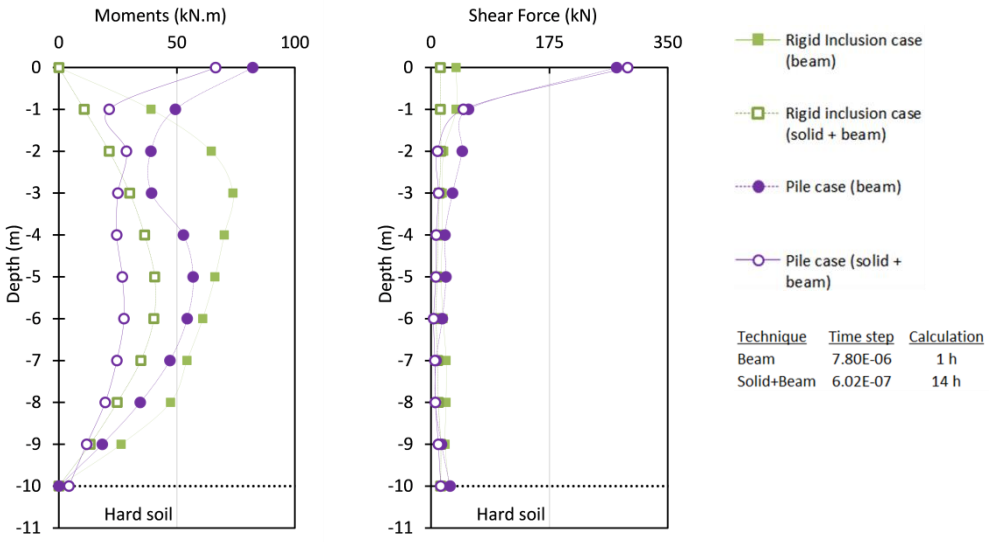

a) Bending moments **b)** Shear Forces

Fig. 4.22 Efforts in the pile and inclusion systems with different modelling technique

The consideration of this technique (solid elements with beam element embedded) implies a reduction of the time step that results in a larger computation time. The time step and time calculation for both systems are also showed in Fig. 4.22.

2.3. Boundary conditions and interfaces

Artificial boundaries were utilized as in Section 1.3 of this Chapter and are depicted in Fig. 4.1b.

Using the same preliminary model as in the previous section (Section 2.2.2), Fig. 4.24 shows the comparison of the maximal normal forces and bending moments in the rigid inclusion and pile systems with and without interfaces. It is clear that the normal forces and bending moments are reduced when considering interfaces. The normal forces in the pile cases are reduced by 24% at 2 m depth when the interfaces are considered. However, this difference is reduced with depth. In the rigid inclusions case, the reduction is smaller and equal to up to12% (Fig. 4.24a). For the bending moments, the differences are respectively of 8% and 12% for the pile and rigid inclusion systems (Fig. 4.24b).

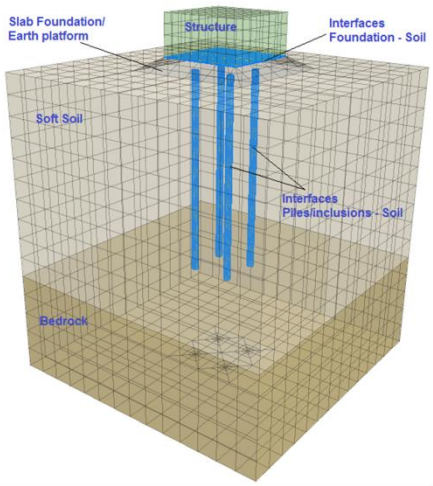

Fig. 4.23 Interfaces in the numerical simulation

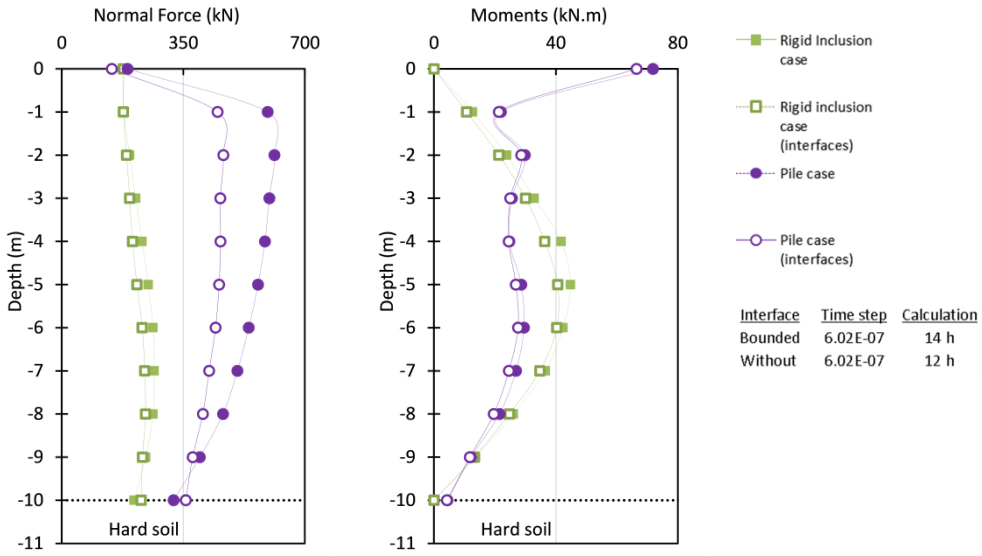

a) Normal Forces **b)** Bending Moments

Fig. 4.24 Efforts in the pile and inclusion systems with and without interfaces

Concerning the interface parameters, the influence of the normal stiffness (k_n) and shear stiffness (k_s) is showed in Fig. 4.25 and Fig. 4.26. Generally high values of stiffnesses should be provided to avoid movements at the interface (Fan et al. 2007, Xie et al. 2013, Wu et al. 2016). Fig. 4.25 and Fig. 4.26 show the influence of the normal and shear stiffness respectively. In Fig. 4.25, the normal forces and moments in the rigid elements were obtained varying the value of k_n and keeping constant the k_s value ($1.7\ 10^8$ Pa/m). Then, in Fig. 4.26, the value of k_n was constant ($1.7\ 10^8$ Pa/m) and the k_s value was variable.

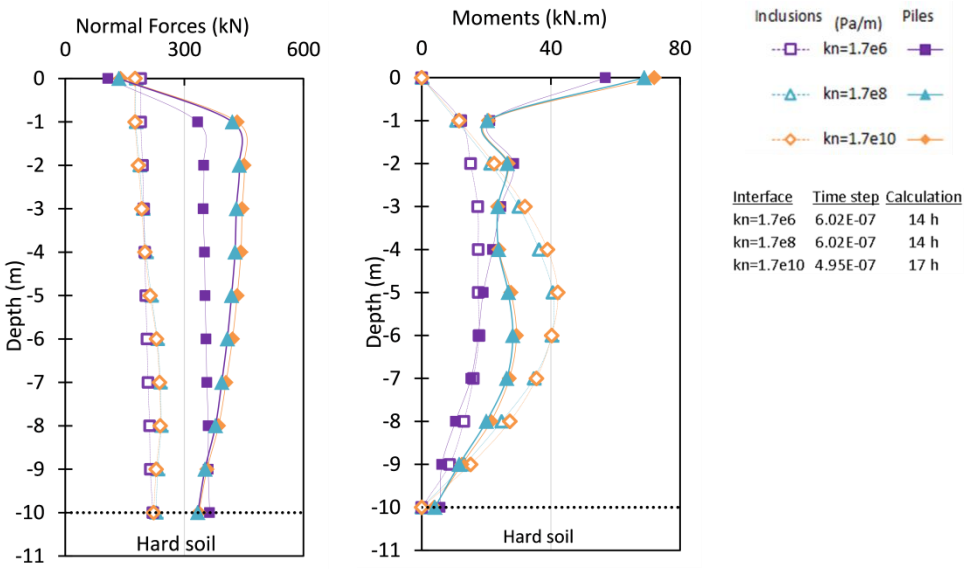

a) Normal Forces **b)** Bending moments

Fig. 4.25 Efforts in the pile and inclusion systems for different $\mathbf{k_n}$

It can be noted from Fig. 4.25 that the larger the value of k_n, the greater normal forces and bending moments in the rigid elements. For the pile case, the normal forces obtained with a value of k_n = 1.7e8 Pa/m are 3% smaller than the values with k_n = 1.7e10 Pa/m. However, when a value of k_n = 1.7e6 Pa/m is utilized the normal forces are reduced 22%. In the rigid inclusions, these forces are close, only a small decrease is observable considering the lowest value of k_n (Fig. 4.25a).

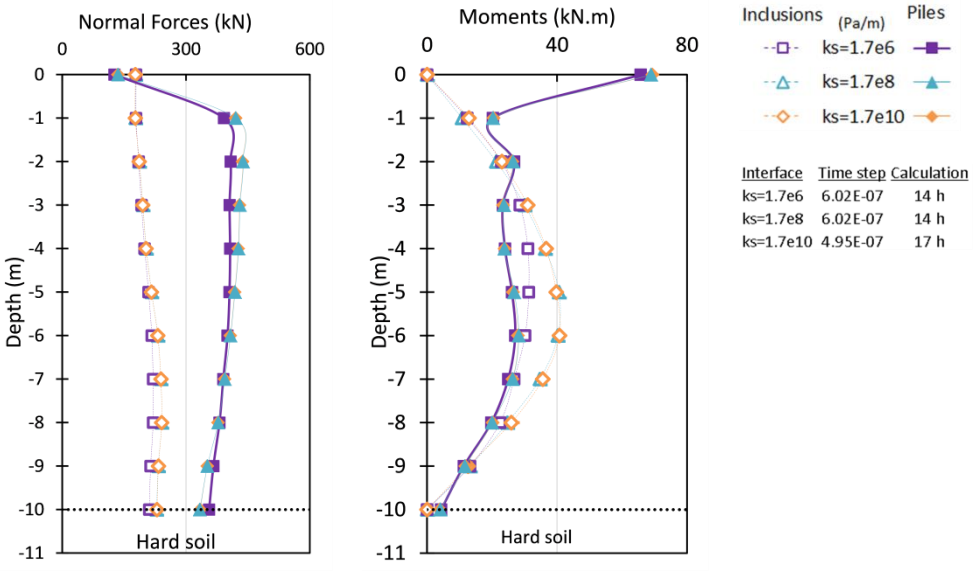

a) Normal Forces **b)** Bending moments

Fig. 4.26 Efforts in the pile and inclusion systems with different $\mathbf{k_s}$

About the bending moments, the values in the rigid inclusions are almost the same for the systems analyzed with k_n = 1.7e8 Pa/m and k_n = 1.7e10 Pa/m. These values are decreased around 54% for the system with k_n = 1.7e6 Pa/m. While in the piles the values are practically the same, only in the pile head there is a difference of 4% for the system analyzed with smaller k_n value.

The influence of k_s is lower than the influence of k_n (Fig. 4.26). The normal forces and moments in the piles and rigid inclusion system are practically the same. In the pile case there is a difference of 5% for the system with k_s = 1.7e6 Pa/m. The bending moments along the rigid inclusions are reduced of 30% for the case with lower k_s value (Fig. 4.26b).

2.4. Seismic Input Motion

The Loma Prieta earthquake was utilized to perform the former dynamic analyses. However, to study the influence of the input motion frequency in the systems, the Northridge and Nice earthquakes were also considered. They were scaled to the same acceleration amplitude of the Loma Prieta earthquake. The original records of each earthquake are displayed in Fig. 4.27. The characteristics of each earthquake are presented in Table 4.4. Only the highlighted 5 seconds of each accelerogram were used for the calculation.

Table 4.4 Earthquake base motions considered (CESMD)

Earthquake	Date	Duration (s)	Peak ground acceleration PGA (m/s²)	Magnitude (Mw)	Predominant Frequency (Hz)
Loma Prieta, USA	1989/10/17	40	4.69	7.1	1.27
Northridge, USA	1994/01/17	30	8.65	6.7	4.30
Nice, France	2001/02/25	27	0.35	5.1	0.48

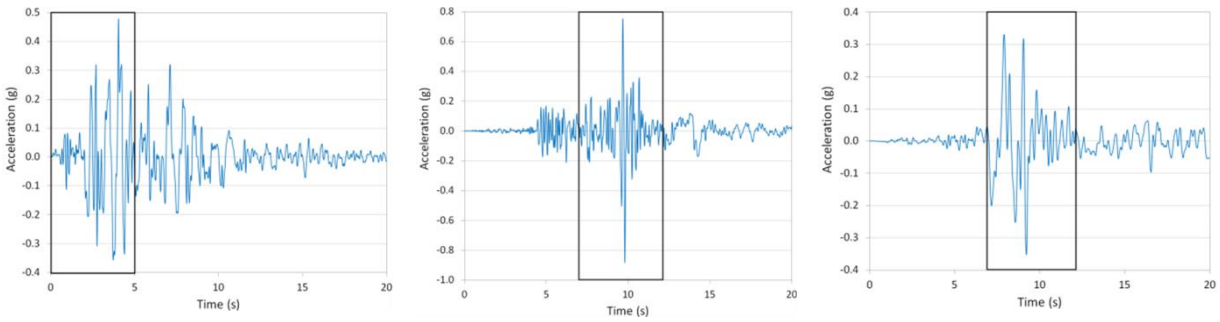

a) Loma Prieta **b)** Northridge **c)** Nice

Fig. 4.27 Original earthquakes considered in the analyses.

2.5. Analyzed cases

The considered cases in this study permit to illustrate the effect of the damping parameters in the seismic response of the soil-pile-structure and soil-inclusion-platform-structure systems. To achieve this goal, values of 1%, 3% and 5% of the minimum damping ratio (ξ_{min}) and values from 0.3 Hz to 4 Hz of minimum frequency (f_{min}) were utilized. In the case of the minimum frequencies, the considered values range permits to cover the range of predominant frequencies of the earthquakes used in the calculations. The damping ratios considered are values commonly used in this type of systems under dynamic loadings (Shahrour et al. 2012, Kumar et al. 2016, Luo et al. 2016, Nguyen et al. 2017). Table 4.5 shows the numerical cases developed.

In the numerical model, the structural elements represent zones where the velocity of the dynamic wave propagation is very high, this implies a very small time step when using the Rayleigh damping. For that reason, a local damping with a factor of 2% is used for the superstructure and for the rigid elements. The use of local damping is simpler than the Rayleigh damping because it does not need the specification of a frequency. However, the damping in rigid elements has a negligible influence on the dynamic response in this type of systems (Hatem 2009). Damping types can be consulted in Section 1.6 Chapter 3. Fig. 4.28 shows the time step and time calculation for each case with different values of ξ_{min} and f_{min}.

Table 4.5 Characteristics of the analyzed cases

System	Damping ratio ξ_{min}	Minimum frequency f_{min}	Earthquake
Rigid Inclusions	1%	0.3, 0.75, 1.25, 2.0, 4.0 (Hz)	Loma Prieta
	3%		
	5%		
	5%	1.25 (Hz)	Northridge, Nice
Piles	1%	0.3, 0.75, 1.25, 2.0, 4.0 (Hz)	Loma Prieta
	3%		
	5%		
	5%	1.25 (Hz)	Northridge, Nice

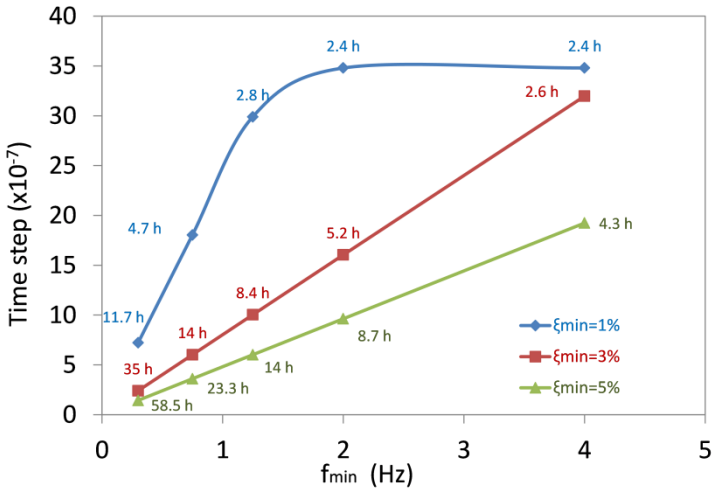

Fig. 4.28 Time step and calculation time for different ξ_{min} and f_{min} values.

2.6. Results and Discussion

The results of the analyses are presented below. The variation of the Rayleigh damping formulation, acceleration response spectra and shear strains in the soil are given. The bending moments and normal forces along the rigid inclusions and piles are compared.

2.6.1. Variation of the Damping Ratio with Frequency

The frequency dependency of the Rayleigh damping formulation in the analyzed cases is highlighted in Fig. 4.29. In this figure, the variation of the damping ratio is presented for different values of f_{min} and ξ_{tar}. The Fourier spectrum of the Loma Prieta earthquake is also displayed. The Fast Fourier Transform is used to calculate the Fourier response spectrum. It is clear that the damping ratio is close to the target damping ratio when the frequency of the system is close to f_{min}. This highlights the importance of selecting carefully the position of the central frequency to capture the ground motion in the desired frequency range (frequency independent) and avoid overdamping.

For instance from Fig. 4.29a, when considering the system with 1% as the target damping and a f_{min} of 0.75 Hz, the damping ratio is close to 1%. If the minimum frequency stated is changed to 1.25, 2.0 and 4.0 Hz, the damping ratio increases from 1% to 1.1%, 1.5% and 2.7% respectively. Similar behavior is displayed in Fig. 4.29c, when assuming $\xi_{tar} = 5\%$ and f_{min} equal to 1.25 Hz, the damping ratio is 5%, however, if the minimum frequency is modified to 2 Hz the damping ratio reaches 5.6% and 9% when the curve of f_{min} is equal to 4 Hz.

For the systems analyzed in this study, the fundamental frequency of the input motion applied at the bottom is equal to 1.27 Hz. Due to the characteristics of the soil profile, this frequency is modified

from a range of 1.13 Hz to 1.24 Hz for the surface response in the analyzed cases when 5% was set as the target damping ratio. For the cases with 1% and 3% of target damping ratio, this range is from 1.18 Hz to 1.22 Hz.

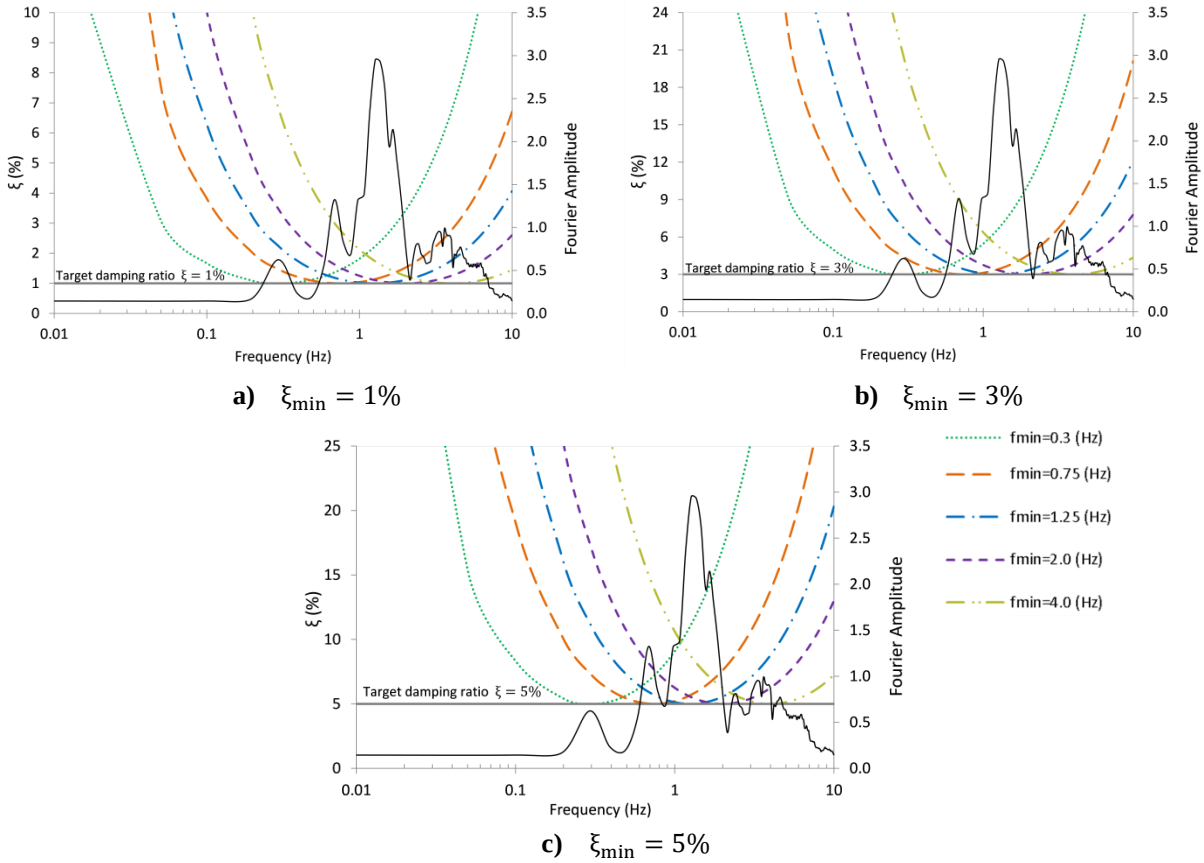

a) $\xi_{min} = 1\%$ **b)** $\xi_{min} = 3\%$

c) $\xi_{min} = 5\%$

Fig. 4.29 Rayleigh damping formulation for different ξ_{min} and f_{min} values.

2.6.2. Acceleration Response Spectra

Fig. 4.30 shows the maximum accelerations in-depth along a vertical line that corresponds to the center position of the reinforced area, in the soil, mid-span between the 4 piles or inclusions. As expected, the accelerations are greater for the systems with lower damping ratio. For instance, in the pile analyzed cases with $f_{min} = 4.0$ Hz and 1% of damping ratio, the accelerations are respectively reduced of 11% and 20% for the cases with 3% and 5% of damping ratios. For the rigid inclusions case, the same comparison gives acceleration reduction equal to 8% and 19%respectively.

It can be noted that the accelerations of soil along the rigid inclusion system are greater when compared with the pile system for all the analyzed cases. This is clearer in the case where $f_{min} = 0.3$ Hz, the accelerations are 5% to 19% greater than the respective pile system with the same target damping ratio. In the cases where $f_{min} = 1.25$ Hz and $f_{min} = 4.0$ Hz, this difference range is reduced

to 5% to 13%. This can be explained by the difference of the interaction of the pile and rigid inclusion elements with the surrounding soil in each system.

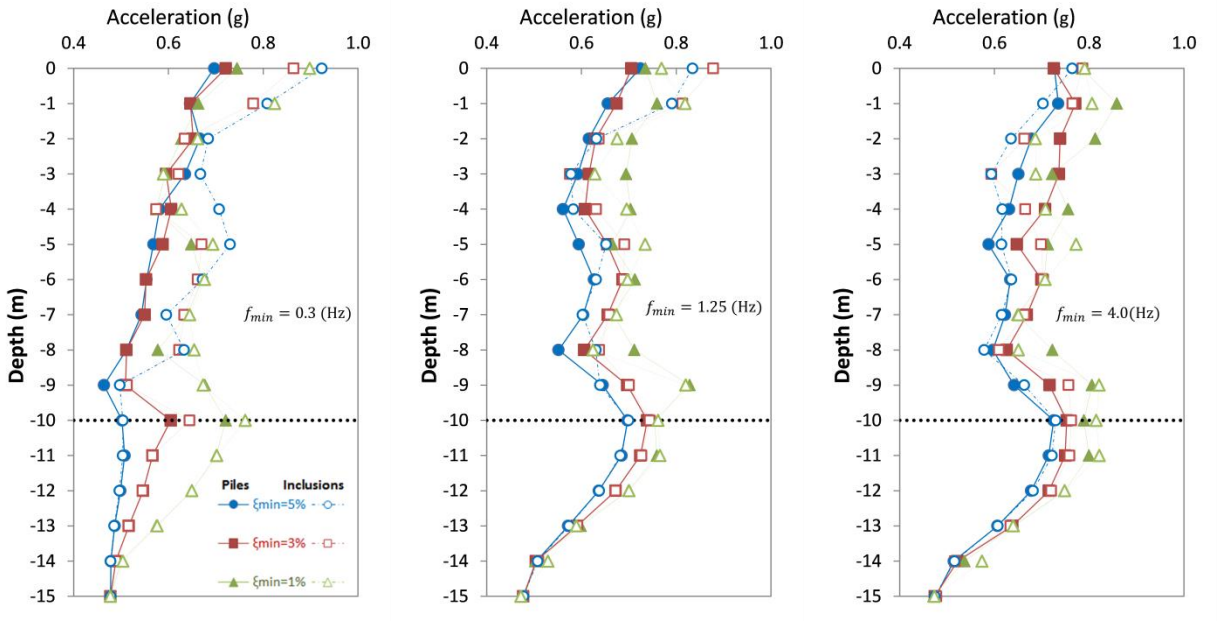

a) $f_{min} = 0.3$ (Hz) **b)** $f_{min} = 1.25$ (Hz) **c)** $f_{min} = 4.0$ (Hz)

Fig. 4.30 Maximum in-depth acceleration in the pile and inclusion systems

To examine the soil-structure interaction effects in the analyzed systems, the acceleration response spectra of the motions recorded at the soil surface (base of the structure) are shown in Fig. 4.31. In all cases, the spectral acceleration increase compared to the acceleration reached in the spectrum of the input motion. This is significant when the period of the ground motion matches the period of the superstructure as presented by Seed et al. (1988) when they compare the relationships between the soil conditions and the ground motions during the Mexico earthquake 1985.

Fig. 4.31a illustrates the response spectrum of the analyzed systems with 1% and 5%. For the pile cases with 1% target damping ratio, it is clear that the impact of the f_{min} is important for periods smaller than 0.2 s. For greater periods, the response is independent of the f_{min}. In the system with 5% damping ratio (Fig. 4.31b), it is noticeable that the response amplitude is greater with the increase of f_{min} for periods between 0.2 s and 0.4 s. The maximum response is presented for the system with $f_{min} = 1.25$ Hz. This response is reduced of around 1% for the systems with f_{min} equal to 0.75 Hz and 2.0 Hz and 6% with f_{min} equal to 0.3 Hz and 4.0 Hz.

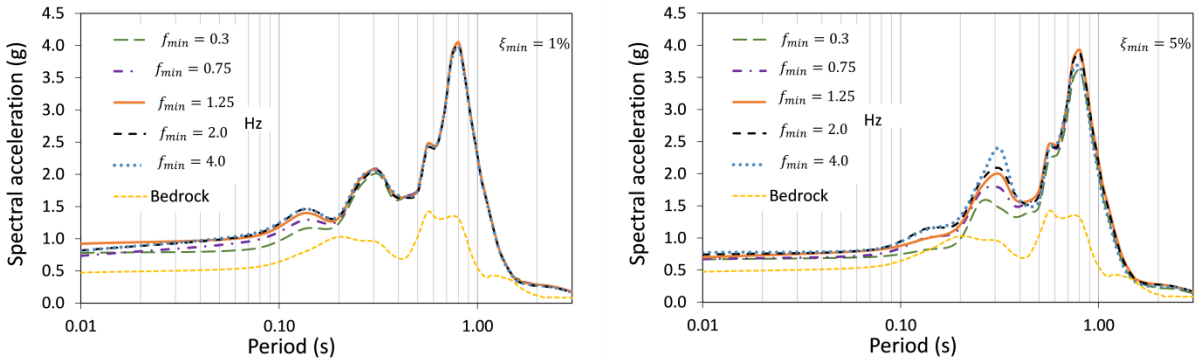

a) $\xi_{min} = 1\%$ **b)** $\xi_{min} = 5\%$

Fig. 4.31 Surface response spectrum in the pile systems for different $\mathbf{f_{min}}$ values.

Concerning to the rigid inclusion systems, the response spectra for different values of f_{min} is similar to the pile case. However, the spectral acceleration in the rigid inclusion systems is greater than in the pile case with the same damping ratio and f_{min} (Fig. 4.32). This is due to the inertial interaction of the complete system and of the vertical elements kinematic interaction. In the case of rigid inclusions, the response spectrum was established with the surface acceleration recorded at the top of the earth platform. The acceleration at the top of the soft soil is slightly higher. This highlights the advantage of the earth platform which dissipates energy and then reduces the inertial forces in the structure during the seismic loading.

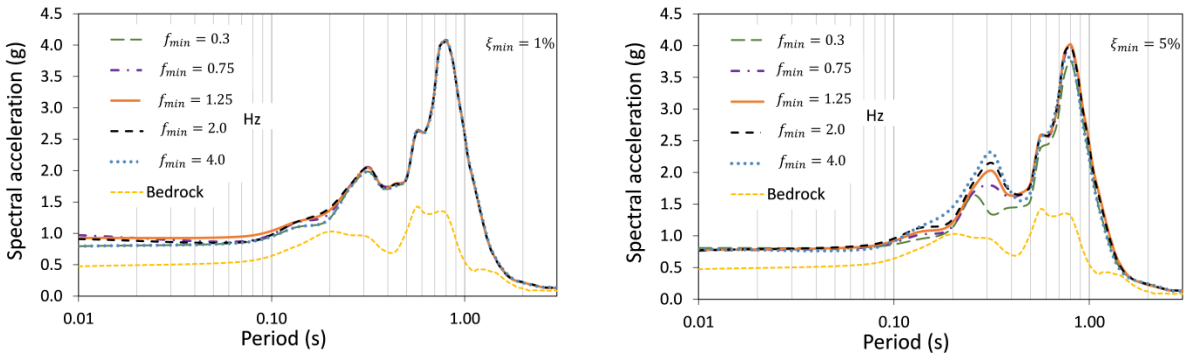

a) $\xi_{min} = 1\%$ **b)** $\xi_{min} = 5\%$

Fig. 4.32 Surface response spectrum in the rigid inclusions systems for different $\mathbf{f_{min}}$ values.

2.6.3. Soil response

The maximum shear strains values recorded in the center of the reinforced area in all analyzed cases at different depths are presented in Fig. 4.33. The strain values are importantly increased in the layer of soft soil compare to hard soil. The maximum shear strain values in the pile systems are independent of the damping ratio. However, in the rigid inclusion system the influence of the ξ_{min} and f_{min} is important. For example, in the case where $f_{min} = 4.0$ Hz, the values with 1% of minimum damping ratio are reduced in a range from 2% to 13% compared to the values of $\xi_{min} = 3\%$. The

strains at the surface with 5% of damping ratio increase respectively of 80% and 200% compared to the cases where $\xi_{min} = 3\%$ and $\xi_{min} = 1\%$.

It is obvious that the shear strains in the pile system are lower than the values in the rigid inclusion system at depths from 0 m to 7 m. The rigid connection of the piles with the slab foundation or the free condition in the head of the inclusions seem to have a great influence on the shear strains developed at the upper part of the models. An interesting phenomenon is observed at 2 m depth where the shear strains are importantly reduced. This can be explained by the attenuation of accelerations at this depth due to the damping ratio overestimation.

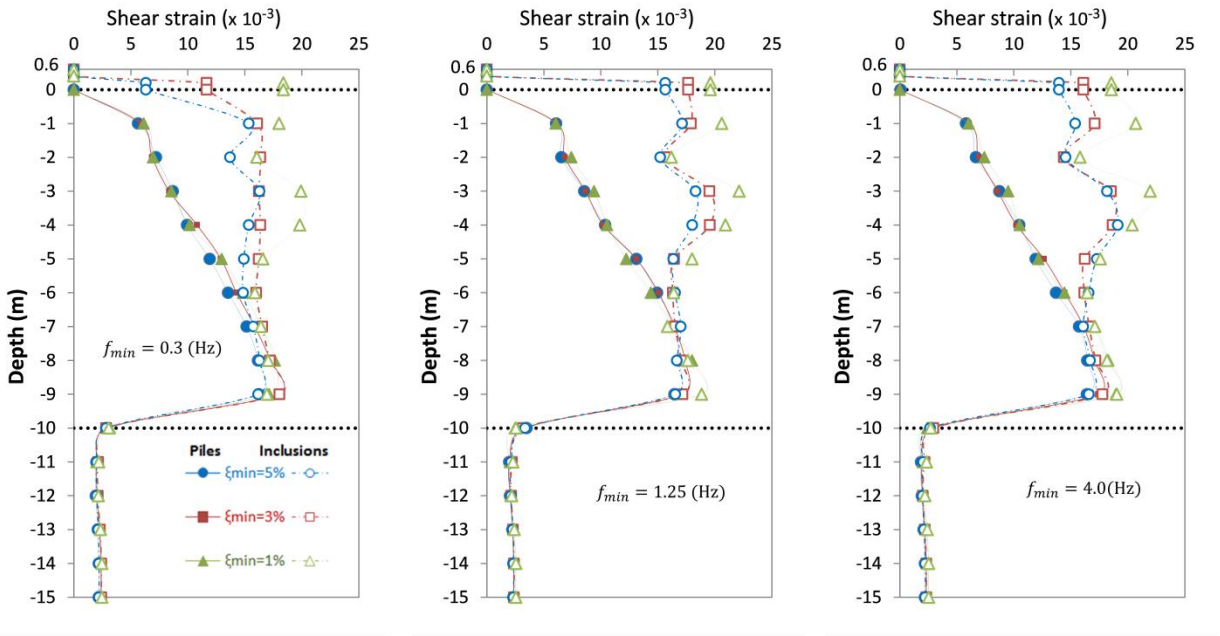

a) $f_{min} = 0.3$ (Hz) **b)** $f_{min} = 1.25$ (Hz) **c)** $f_{min} = 4.0$ (Hz)

Fig. 4.33 Maximum in-depth shear strain for the pile and rigid inclusion systems

The sketch of the stress-strain behavior computed for the cases where $f_{min} = 0.75$ Hz and $f_{min} = 2.0$ Hz for different target damping ratios are shown in Fig. 4.34. These diagrams were obtained at 1 m depth. It can be noted that the maximum shear stress in pile and rigid inclusion systems is in the range of 20 kPa for all the cases. At the same time, the strains in the pile system are around 0.6% while in the rigid inclusion systems are greater than 1.5%.

As shown in Fig. 4.34, there is clearly more energy dissipation for the systems with lower target damping ratio. In the analyzed systems with the same target damping ratio, larger strains are estimated for the cases analyzed with $f_{min} = 2.0$ Hz than for cases with $f_{min} = 0.75$ Hz. This is because there is in the last one less damping ratio overestimation.

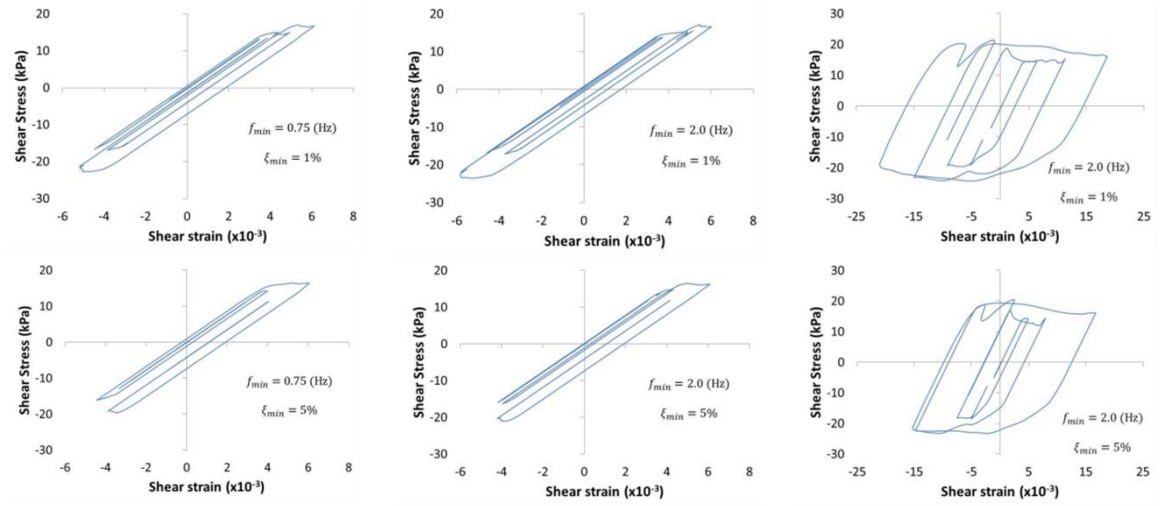

a) Pile systems **b)** Rigid inclusion systems

Fig. 4.34 Stress strain loops in the analyzed systems with different $\mathbf{f_{min}}$ and $\boldsymbol{\xi_{min}}$

2.6.4. Bending Moments and Normal Forces in the Rigid Vertical Elements

In this section, the maximum bending moments and normal forces are presented along the piles and inclusions. In general, the maximum value in the rigid inclusion cases is reached in the middle depth of the elements (5 m) and is null in the top and bottom part of the vertical elements. The moments along the piles are smaller compared to the rigid inclusion values for depth up to 3 m. However, the values at the elements head are higher in the pile case due to the rigid connection with the foundation slab.

As expected, the moments along the vertical elements are reduced with the increase of the target damping ratio for both pile and rigid inclusion systems (Fig. 4.35). For example, there is a reduction of about 10% of the moment values from $\xi_{min} = 5\%$ to 1% in the rigid inclusion system with $f_{min} = 1.25$ Hz. In the analyzed cases with $f_{min} = 0.3$ Hz and $f_{min} = 4.0$ Hz, the same comparison induces a decrease of 26%. These values are in accordance with the results presented in Section 2.6.1 which show the damping ratio overestimation for different values of ξ_{min} and f_{min}. For instance, the maximum bending moment of 44 kN.m in the rigid inclusions system with a target damping ratio of 5% and $f_{min} = 1.25$ Hz is reduced to 36 kN.m when the f_{min} is modified to 0.3 Hz due to the damping ratio increase from 5% to 11% (Fig. 4.29). Similar comparisons can be made in the system with a 3% damping ratio. However, in the systems with a 1% damping ratio, these differences are almost negligible. This means that the differences caused by the damping parameters decrease when the target damping ratio decreases.

In the pile systems, the bending moments in the cases of a 5% damping ratio are 16% smaller than in the case where $\xi_{min} = 3\%$, whatever the frequency. At the same time, the bending moments of the

case with $\xi_{min} = 3\%$ are reduced up to respectively 22% and 36% compared to the case with $\xi_{min} = 1\%$ for the $f_{min} = 0.3$ Hz and $f_{min} = 4.0$ Hz. As in the rigid inclusion cases, the values in the piles are influenced by the damping ratio in the system. For example, the maximum bending moment of 66 kN.m at the pile head with a damping ratio of 5% and $f_{min} = 1.25$ Hz is reduced to 57 kN.m when the f_{min} is modified to 4.0 Hz. This is due to the damping ratio increase from 5% to 8.5% (Fig. 4.29).

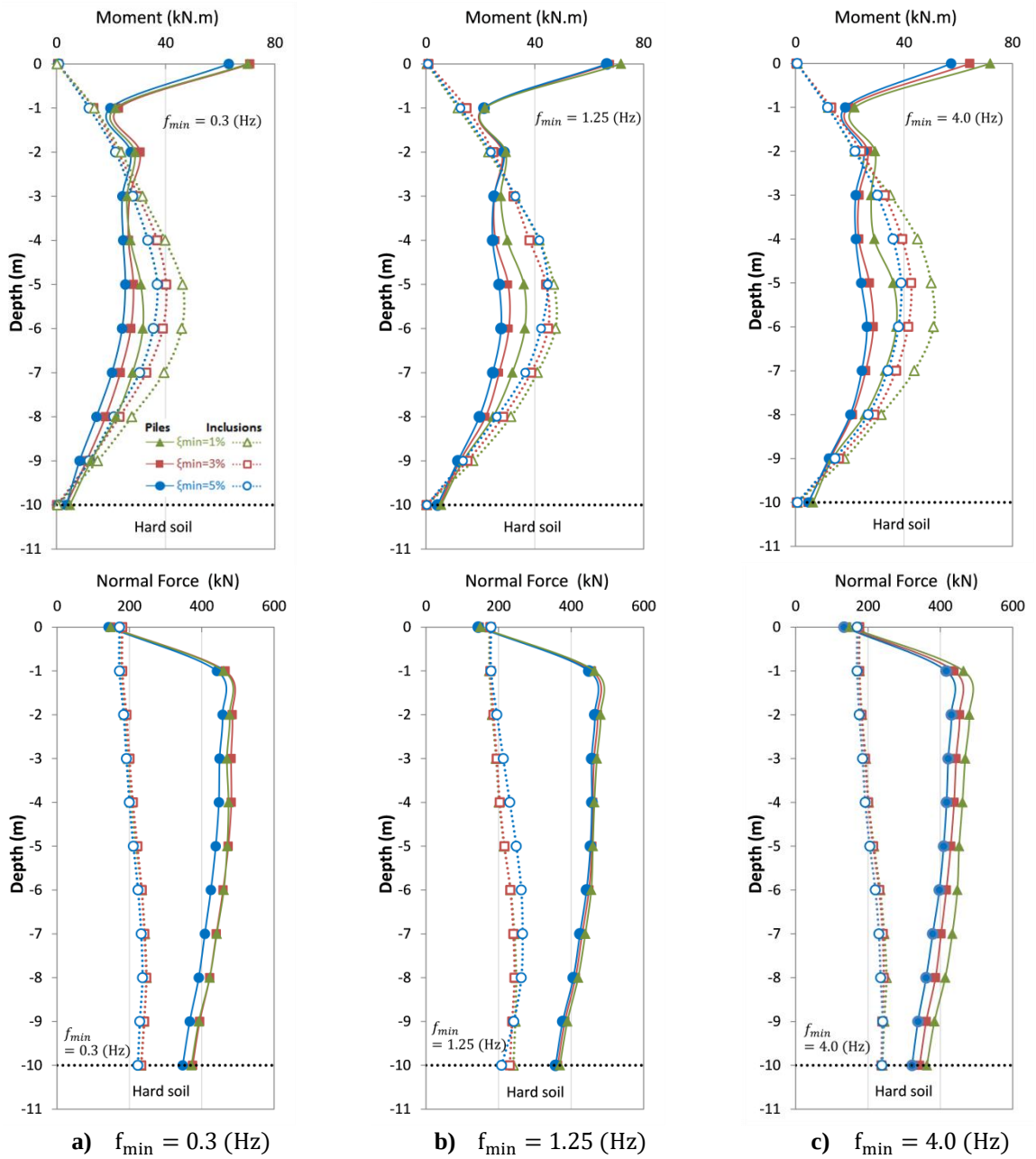

a) $f_{min} = 0.3$ (Hz) **b)** $f_{min} = 1.25$ (Hz) **c)** $f_{min} = 4.0$ (Hz)

Fig. 4.35 Maximum bending moments and normal forces in-depth in the pile and rigid inclusion systems for different f_{min} and ξ_{min}

From Fig. 4.35, it can be also noted that the normal forces in the piles are greater than in the rigid inclusions. The role of the rigid inclusion system is to limit the movement transfer towards the superstructure, which in turns reduces the inertial forces. The variation of the ξ_{min} and f_{min} values in

the rigid inclusion cases has a small effect in the normal forces along the elements. Concerning the pile cases, the values in the case with $f_{min} = 1.25$ Hz are almost equal whatever the damping ratio. However, the normal forces in the piles for the system with 1% damping ratio are reduced of 6% compared to the values with 5% damping ratio for the same f_{min} (0.3 Hz). The same comparison but considering a $f_{min} = 4.0$ Hz, gives 10% of decrement of the normal forces.

2.6.5. Influence of the Input Motion Frequency

To study the influence of the frequency on the pile and rigid inclusion systems, the case with $\xi_{min} = 5\%$ and $f_{min} = 1.25$ Hz was analyzed with the Loma Prieta, Northridge and Nice earthquakes. The predominant frequency of each earthquake is shown in Table 4.4. All the earthquakes were scaled to the same peak ground acceleration to only consider the effect of the frequency input motion in the analyses.

Fig. 4.36 shows that the response spectrum of the rigid inclusion and pile systems excited with Loma Prieta earthquake are greater in periods from 0.3 to 1.0 s compared to the response obtained with the Northridge and Nice earthquakes. Out of this range, the response of the Nice earthquake is larger. The responses of the rigid inclusion systems are greater than the pile cases.

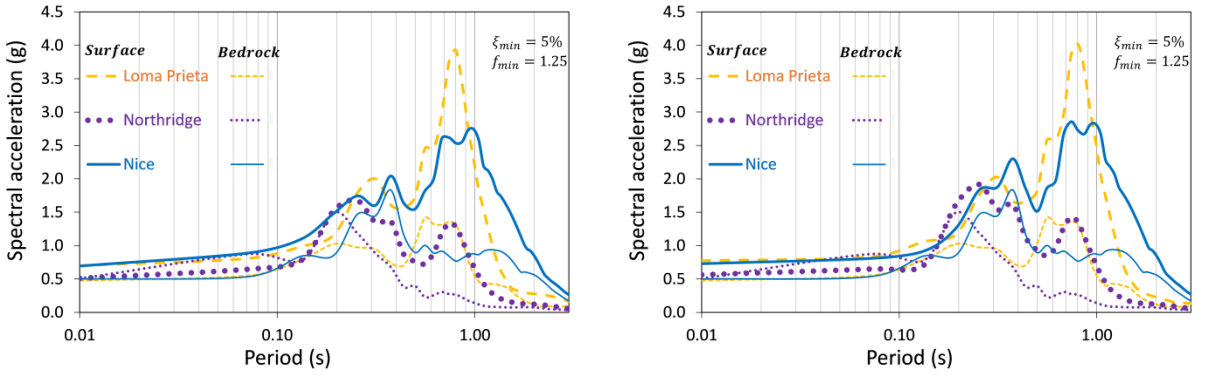

a) Pile system **b)** Rigid Inclusion system

Fig. 4.36 Surface response spectrum using Rayleigh damping for different f_{min} values.

Fig. 4.37a illustrates that the system analyzed with the Loma Prieta earthquake (1.27 Hz) produces the greater bending moments in the pile and rigid inclusion system. This happens because the damping ratio is equal to 5%, but increases to 8.3% and 9.3% under the Nice (0.48 Hz) and Northridge (4.3 Hz) earthquakes respectively (Fig. 4.29). In the rigid inclusion cases, the maximum bending moments (at 5 m depth) are reduced 11% and 58% for the Loma Prieta earthquake if they are respectively compared with the ones of the Nice and Northridge earthquakes. The same comparisons at the pile head give 14% and 36%. These results demonstrate that when the frequency of the input motion is near the f_{min} value, there is less overdamping because the damping ratio is near to the target damping.

Fig. 4.37b shows that the normal forces in the systems with the Loma Prieta and Northridge earthquakes are almost the same (5% of difference). In the rigid inclusions systems, the values are similar until 6 m depth for all three earthquakes, after that depth, the values of the Northridge are reduced of 5%.

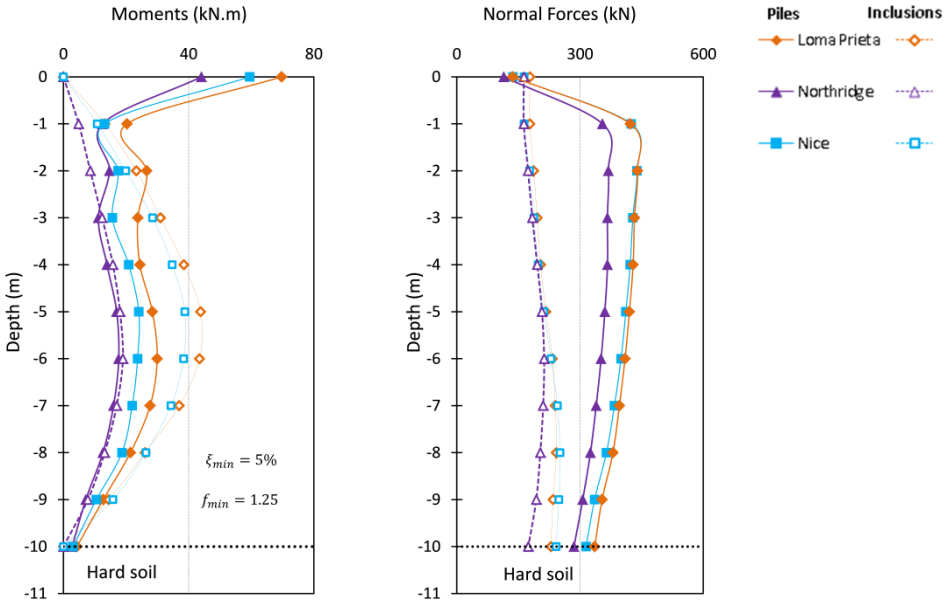

a) Bending moments **b)** Normal Forces

Fig. 4.37 Bending moments and normal forces along elements with elastic and elasto-plastic calculation

2.7. General Conclusions

This chapter tries to provide better insight into the performance of soil-pile-structure and soil-inclusion-platform-structure systems under dynamic loadings. The soil behavior was described by the linear elastic and the Mohr-Coulomb constitutive models. Different pile or inclusion support conditions were taken into account. The 3D numerical models analyzed were developed to accurately represent the realistic behavior of the systems. To study the effect of the Rayleigh damping formulation parameters in the analyzed cases, different values of ξ_{min} and f_{min} were considered. Several earthquakes were used to study the influence of different excitation frequencies of the systems.

The results of the numerical simulations show that the motion experienced at the base of the structure is notably changed by the properties of soil, structure and foundation. For the analyzed cases, the spectral accelerations recorded at the ground surface (base of the structure) are greater compared to the ones of the input motion (bottom of the model).

The fixity conditions highly affect the efforts along the rigid elements. In pile systems, the moments and shear forces are important because the link of the piles head with the slab foundation. However, in the rigid inclusion systems, these efforts are not presented because the free-head condition. The rigid elements anchored also show an increment of the bending moments and shear forces at the interface of the soil and hard layers due to the kinematic interaction.

For all cases, the application of an input motion with a frequency close to the fundamental frequency of the system implies an amplification of the spectral acceleration.

When other factors such as the number of piles in a configuration (same cover ratio), the structural mass and the pile stiffness increase, the normal forces and bending moments displayed in the rigid elements are amplified. Contrary, the consideration of an embedded foundation slab or earth platform reduce the efforts in the piles and rigid inclusions.

The use of the Rayleigh formulation induces a time step decrease and thus a time calculation increment when compared to other damping models implemented in Flac3D. When the single control frequency approach is utilized in the Rayleigh formulation, it is important to correctly select the position of the central frequency (f_{min}) to avoid overdamping. The damping ratio should stay close to the target damping ratio.

The peak spectral acceleration is greater for the systems where the input motion frequency is near to the f_{min} with the same target damping ratio. However, this difference is negligible when the target damping is reduced. Due to the kinematic interaction, the spectral acceleration in the rigid inclusion systems is larger than in the pile systems, with the same target damping ratio and f_{min}.

The impact of the ξ_{min} and the f_{min} in the shear strains is more evident in the rigid inclusion system than in the pile system. Due to the kinematic interaction and the free condition at the rigid inclusion head level or the rigid connection in pile systems, the shear strains in the rigid inclusion systems are larger (from 0 to 7 m depths) than for the pile cases.

Notable reduction is observed in the bending moments and normal forces along the vertical elements with the increment of target damping ratio for both pile and rigid inclusion systems. However, in the systems with 5% and 3% of target damping ratio, the increase is more evident than for the systems with a damping ratio of 1%. This indicates that the overdamping caused by a change in the damping parameters decreases with the reduction of the target damping ratio.

When the frequency of the input motion is close to the f_{min}, the amount of overdamping is reduced and the surface spectral acceleration of the analyzed systems is increased. Thus, the bending moments and normal forces along the piles and inclusions are also incremented.

From the results obtained in this Chapter is noticeable that the dynamic characteristics of the superstructure have an essential impact in the SSI analysis. For this reason, the following Chapter is dedicated to study the effect of these dynamic characteristics considering buildings with different heights.

Chapter 5 SEISMIC RESPONSE OF MID-RISE BUILDINGS FOUNDED ON PILE AND INCLUSION SYSTEMS: Effect of the dynamic characteristics of the Structure

1.1. Introduction

Under seismic loading, the effects of the SSI are generally considered as beneficial to the structure due to the fact that they increase the natural period and damping of the structure compared to the corresponding rigidly supported structure. This implies the reduction in the structural demand of the structure (reduction of the base shear) and an increase of displacements. However, there are some cases where the role of the SSI may lead to an unsafe design for both the superstructure and the foundation. For instance, the 1985 Mexico earthquake was particularly destructive to 10 to 12-storey buildings (supported in soft clay) whose period increase due to the SSI from about 1.0-1.5 s to nearly 2.0 s, which corresponds to the resonant period (Gazetas and Mylonakis 1998). Because the dynamic characteristic of the building play an important role in the response of the soil-foundation-structure systems (Maheshwari and Sarkar 2011, Mánica-Malcom et al. 2016, Hokmabadi and Fatahi 2016, Badry and Satyam 2016, Nguyen et al. 2017), this Chapter is dedicated to examine the influence of these characteristics considering mid-raise buildings founded in pile and inclusions systems under seismic loading.

To fully achieve this goal, coupled three-dimensional analyzes of pile and rigid inclusion systems were developed using the finite difference software Flac3D considering 3, 5 and 7-storey frame buildings. Additionally, the influence of the foundation type (floating, placed or anchored on the hard soil) is considered for both systems. The soil profile and properties are the same as in Chapter 4. Drained analyses were developed assuming that the water level is very deep and do not affects the soil surface. The elastic perfectly plastic model with a Mohr-Coulomb failure criterion is used to represent the behavior of the soil. Other investigations considering behavior of the building on pile foundations under a seismic loading are described in Section 2.3.3 Chapter 2.

1.2. Characteristics of the Adopted Numerical Model

1.2.1. Building

The structure considered for the study is a concrete frame building with respectively three and two spans in the x and y directions. The structure has a rectangular geometry of 12 x 10 m (Fig. 5.1). A 5-storey building is considered for the reference case. However, in order to study the influence of the dynamic characteristics of the structure, 3-storey and 7-storey are also considered. The storey height is equal to 4 m. This structure represents a simplification of a conventional frame buildings. Table 5.1

shows the sections used for the structural elements in the building. The installation of the building is done in a single phase after the equilibrium of the model.

Table 5.1 Structural sections considered for the building

Section	Notation	Length (m)	Width (m)	Thickness (m)
Floor slab	h_{fs}	12	10	0.28
Foundation slab	h_s	12	10	0.28
Columns	a_c	0.4	0.4	4

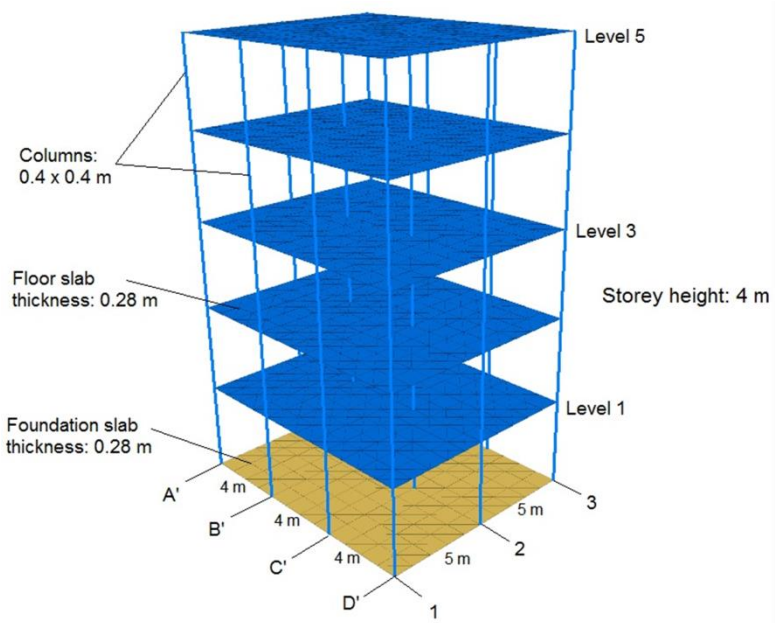

Fig. 5.1 Columns and slabs sections in the 5-storey concrete frame building

The columns and slabs of the structure are considered made of reinforced concrete with a linear elastic behavior. The material properties are summarized in Table 5.2. The columns and floor slabs were modeled with beam and shell elements respectively. The foundation slab is considered using a liner element. The characteristics of these structural elements are described in Section 1.4 Chapter 3.

Table 5.2 Material properties considered for the structural elements in the building.

Parameter	Notation	Columns and Slabs
Young modulus (GPa)	E	30
Shear Modulus (GPa)	G	12.5
Volumic Weight (kg/m³)	ρ	2500
Poisson's Ratio	ν	0.2
Damping Ratio	ξ	0.05

The behavior of the structural elements is considered as linear elastic. A structural Rayleigh damping (Section 1.6 Chapter 3) ratio of 5% was assigned for all the elements in the concrete frame building.

In this study, the damping constants used to simulate the structural damping were calculated based on the first and second mode of frequencies of the structure and, are shown in Table 5.3 for the three buildings. The fundamental periods of the fixed-base (representing the condition excluding SSI) and the total weight of the buildings are also displayed.

Table 5.3 Dynamic properties of the considered buildings.

Building	Number of storey	Fundamental Period (s)	Weight (kN)	Rayleigh damping constants	
				α	β
B3	3	0.478	3936	0.7225	0.0034
B5	5	0.791	6000	0.4363	0.0056
B7	7	1.112	8064	0.3109	0.0079

1.2.2. Soil Mesh

The above 5-storey building is setup on a soil volume of dimension 26 x 24 x 15 m^3 as shown in Fig. 5.2. The soil mass is composed by a layer of soft soil (10 m) supported by a hard soil layer (5 m). The soil model corresponds to the same soil profile and dimensions as in Section 1.2. Chapter 4. The layers of soil are considered horizontal. With this model, the maximum frequency that can be properly modeled by an element of the mesh, and with the hypothesis of shear waves propagating in vertical direction (Kuhlemeyer and Lysmer 1973) is 5 Hz. In the soil-inclusion-platform-structure system, a 0.60 m earth platform is placed over the rigid elements. However, in the case of pile systems, the rigid elements are perfectly connected with the foundation slab of the building.

Free-field boundary conditions (Section 1.7 Chapter 3) are applied on the sides of the soil mesh. They were to avoid wave reflections at the boundaries of the model (Lysmer and Kuhlemeyer 1969). They are displayed in Fig. 5.3a. A rigid condition is applied at the base in order to apply the earthquake input motion.

The behavior of soil layers and earth platform is considered using a linear elastic perfectly plastic constitutive model with a Mohr-Coulomb failure criterion (Section 4.2 Chapter 2). The material properties of the layers of soil and mattress are the same as those showed in Table 4.1 of Chapter 4.

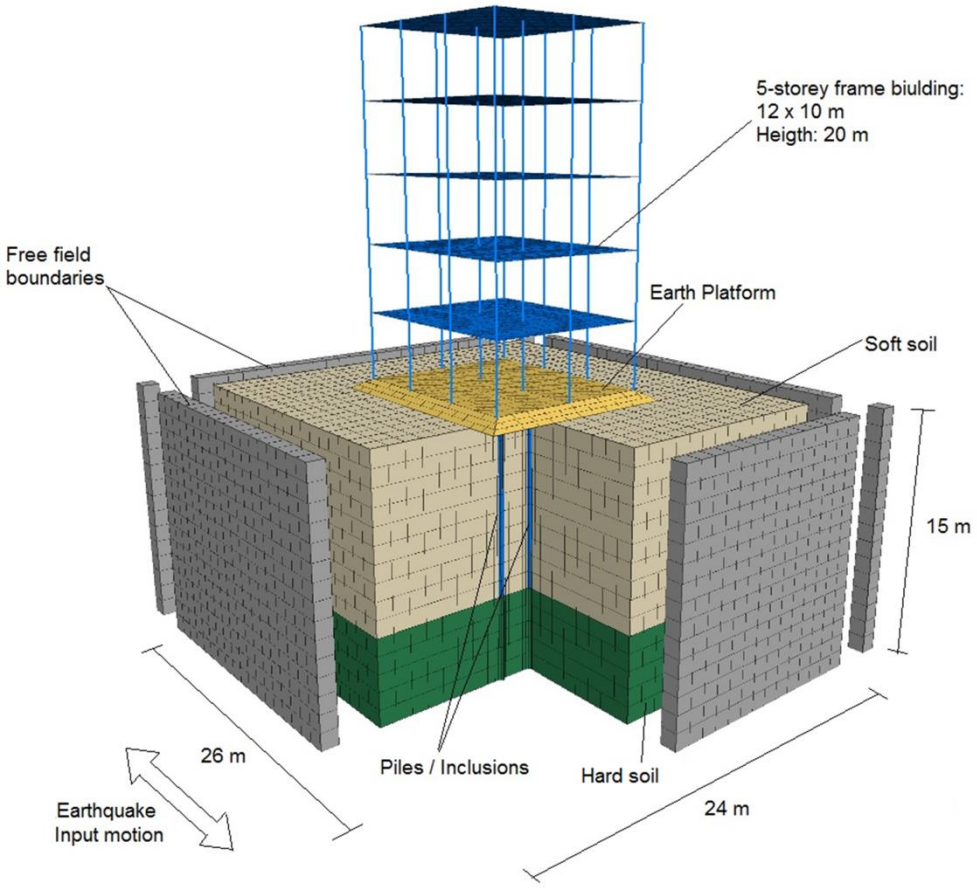

Fig. 5.2 Geometry of the numerical model

1.2.3. Vertical Reinforced Elements

This study includes the analysis of both rigid inclusion and pile systems. A group of 30 rigid elements are considered in the analyses to support the structure. These elements are separated of 2 m in both directions. The coverage ratio is equal to 1.7%. Depending on the support type different lengths for the rigid elements are considered: 9 m for the floating ones, 10 m and 11 m for the placed and anchored ones on the hard soil respectively.

Using three dimensional analyses, some researchers have modelled piles and rigid inclusions with solid elements (Hokmabadi et al. 2014, Nguyen et al. 2017, Hazzar et al. 2017, Maheshwari and Sarkar 2011). Other authors have considered hybrid methods using beam elements embedded in solid elements with reduced flexural rigidity (Banerjee et al. 2014, Kourkoulis et al. 2012, Goh and Zhang 2017). Both methods implies an important computation time. In the following analyzed systems, rigid elements are considered by using beam structural finite elements perfectly bonded with the soil (Alsaleh and Shahrour 2009, Finn and Fujita 2002, Kitiyodom et al. 2006, Sadek and Shahrour 2004). A mesh refinement is done around the rigid elements to avoid the loose of accuracy in terms of stresses and displacements in this zone. This technique to model the rigid vertical elements permits reducing the time calculation and directly gives the pile efforts from the numerical simulations.

However, this method does not accurately account for the physical rigid element cross section. This results in greater displacements and bending moments along the pile than with the method where the pile is modelled by solid elements. For instance, Kitiyodom et al. (2006) and Wotherspoon (2006) respectively showed that the maximum horizontal displacement along piles can be 15% and 45 % smaller when piles are modelled with solid elements than with beam elements.

The behavior of the rigid vertical elements is considered as linear elastic in all calculations. The material properties of the rigid elements are the same as the concrete columns and slabs in the superstructure (Table 5.2). Fig. 5.3b shows the plan view with the localization of the vertical elements.

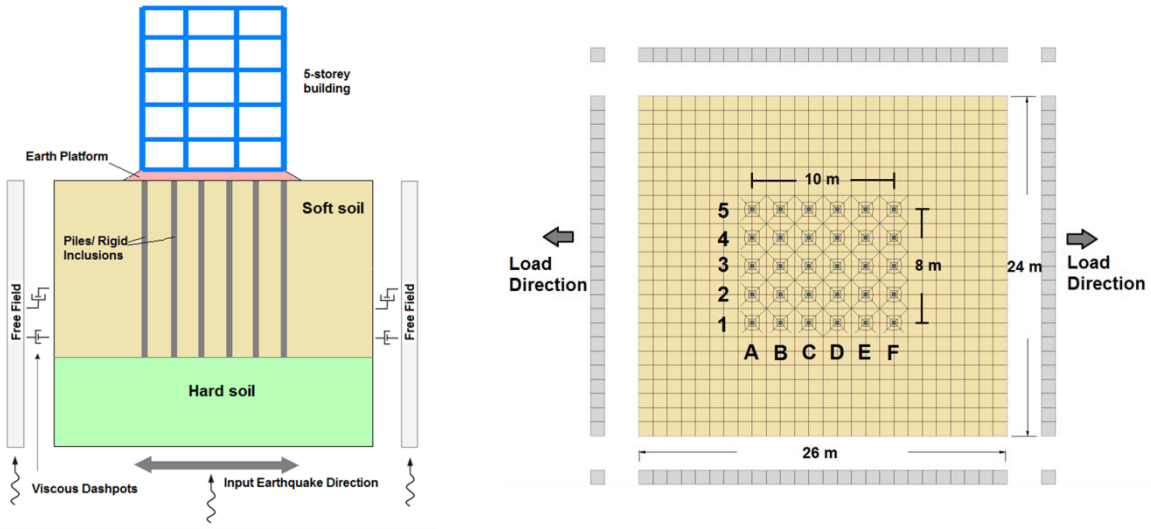

a) Cross section **b)** Plan view and location of the vertical reinforcements

Fig. 5.3 Schematic representation of the analyzed systems

1.3. Seismic Input Motion

A Nice earthquake (France) is imposed to the numerical model (Do et al. 2014,Grange 2008) The characteristics of this 2001's earthquake are shown in Table 5.4.

Table 5.4 Earthquakes base motions considered

Earthquake	Date	Duration (s)	PGA (m/s^2)	Magnitude (Mw)
Nice, France	2001/02/25	27	0.350	5.1

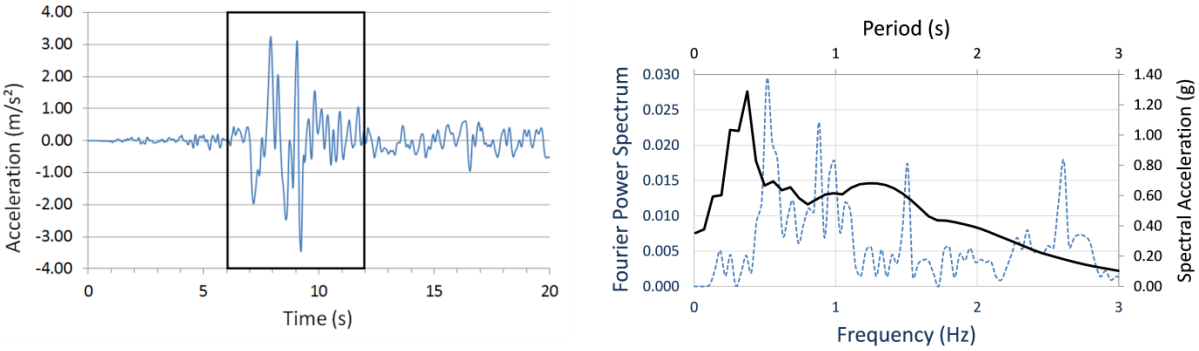

a) Earthquake record

b) Fourier amplitude and acceleration response spectrum

Fig. 5.4 Nice 2001 Earthquake

The acceleration time-history of 20 seconds duration is presented in Fig. 5.4a. This record is applied in the horizontal direction to all nodes in the bottom part of the model. Due to time calculations consideration, only 6 seconds of the earthquake record are applied (between 6 and 12 seconds). The spectrum of the corresponding Fourier amplitude and the response spectrum are shown in Fig. 5.4b.

1.4. Analyzed Cases

The soil-inclusion-platform-structure and soil-pile-structure systems analyzed in this paper are respectively presented in Fig. 5.5 and Fig. 5.6. It can be noted that both systems are analyzed with floating, placed or anchored on hard soil rigid elements supporting the 5-storey building. A resume of the systems and fixity conditions for each case is presented in Table 5.5. The time calculation was approximately 192 hours for each case. Reference of the computer characteristics are displayed in Section 1.5 Chapter 3. The procedure of analysis is similar to that described in Section 1.6 of Chapter 4.

Table 5.5 Cases and fixity conditions for the vertical reinforcement

Fixity conditions		CASE	Name of the case	Building storey		
Head connection	Toe connection					
Soil-inclusion-platform-structure systems						
Free	Articulated	Rigid inclusions placed on the hard soil	P-RI	B3	B5	B7
Free	Free	Floating rigid inclusions	F-RI		B5	
Free	Fixed	Anchored rigid inclusions	A-RI		B5	
Soil-pile-structure system						
Fixed	Articulated	Piles placed on the hard soil	P-P	B3	B5	B7

Fixed	Free	Floating piles	F-P	B5
Fixed	Fixed	Anchored piles	A-P	B5

* B3: 3-storey building; B5: 5-storey building; B7: 7-storey building

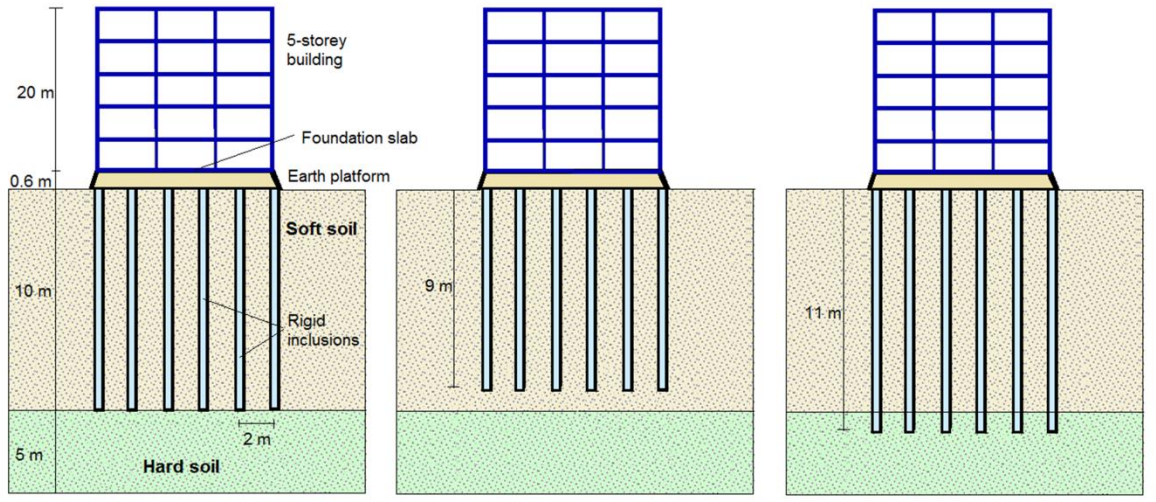

a) P-RI **b)** F-RI **c)** A-RI

Fig. 5.5 Soil-rigid inclusions-structure analyzed systems with different support conditions

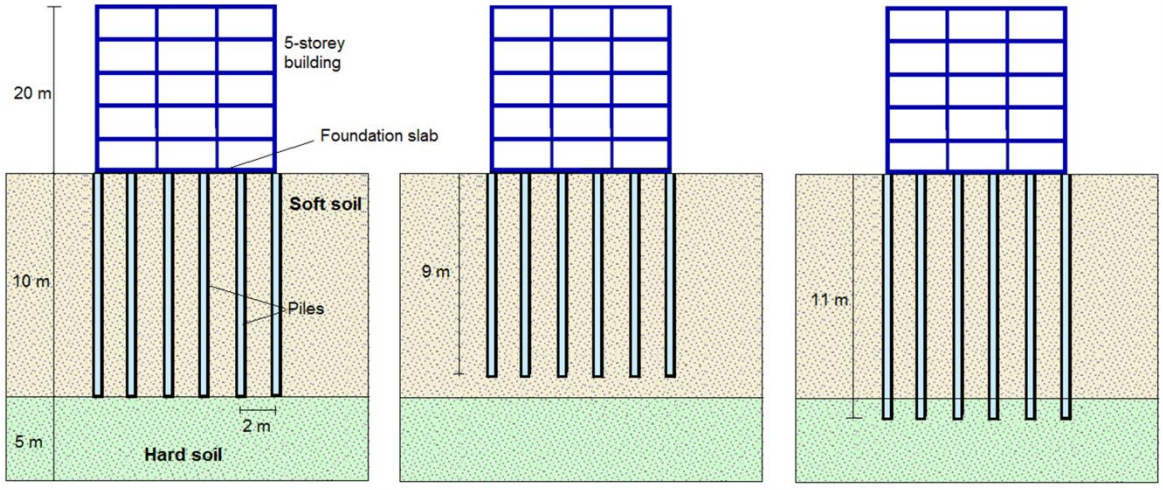

d) P-P **e)** F-P **f)** A-P

Fig. 5.6 Soil-piles-structure analyzed systems with different support conditions

1.5. Results and Discussion

The results are presented in this section in terms of response spectrum of the different systems, lateral displacements, inter-storey drifts and shear forces in each building level and rocking of the foundation. All these values are the maximum values recorded during the seismic loading. In order to check the influence of the earthquake in the response of the building, the efforts and displacements at

the initial state were subtracted from the obtained values. In the piles and the rigid inclusions normal and shear forces, bending moments and displacements are presented.

1.5.1. Effect of the SSI in the Analyzed Systems

The earthquake motions experienced at the base of the buildings depend importantly in the mechanical and geometrical characteristic of the subsoil and of the input motion. Besides this, the kinematic and inertial interactions may be modified by the foundation type and the attributes of the building. The effect of the SSI is examined through the acceleration response spectrum of the motions recorded at the surface of soil (base of the structure). The spectra (Fig. 5.7) were calculated in the same way as in Section 1.8.1 Chapter 4.

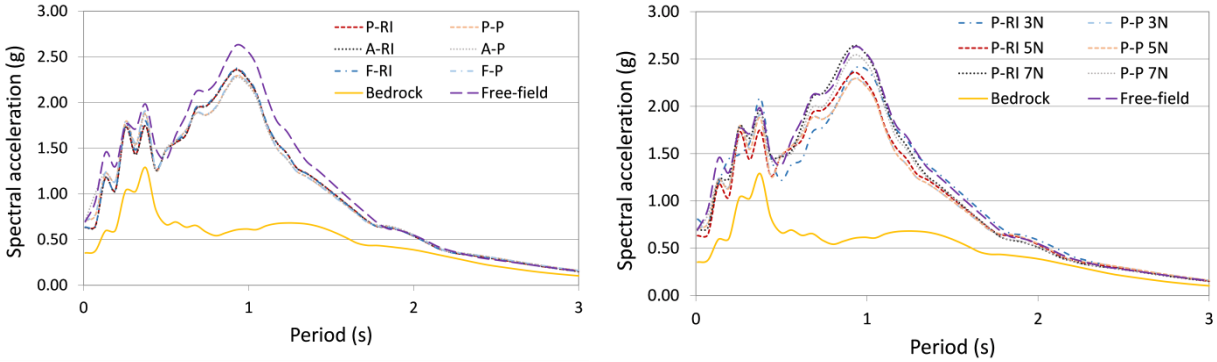

a) 5-storey Building **b)** 3, 5 and 7-storey Buildings

Fig. 5.7 Acceleration response spectrum of the 5-storey building with different support conditions.

Fig. 5.7a illustrates the response spectrum of the systems with a 5-storey building with placed, floating and anchored vertical reinforcements. The response spectrum of the systems with vertical reinforcements is smaller than the free-field motion one. The kinematic interaction reduces the foundation motion relative to the free-field motion because the stiffness of the foundation and the surrounding soil differs. The response of both the rigid inclusion and the pile systems are independent of the support condition. However, the response of the piles is lower than the one of the rigid inclusion systems. This is due to the inertial interaction of the complete system and of the piles kinematic interaction. In the case of rigid inclusions, the response spectrum was established with the surface acceleration recorded at the top of the earth platform. The acceleration at the top of the soft soil was slightly greater. The energy dissipation in the earth platform reduces the inertial forces in the buildings located in seismic sites.

Comparing the response spectrum for the P-RI and P-P systems in Fig. 5.7b, it is highlighted that the response of the rigid inclusion and of the pile systems with the 7-storey building induces higher amplitudes (similar to the free field case) than the systems with 3 and 5-storey buildings. A greater

motion is produced at the base of the building due to the inertial forces. The spectral accelerations values in the systems with the 3 and 5-storey buildings are closer in all cases, only the P-RI 3N (rigid inclusion system placed on the hard soil with the 3-storey building) is different and presents a small amplification and reduction for some range periods.

1.5.2. Shear Forces in the Structure

The impact of the SSI on the shear forces of the 5-storey building system is presented in Fig. 5.8a. During the time history analysis, the shear forces generated in every column in each level were summed up in order to determine the maximum shear force in that level. Then the absolute maximum value of the shear force in each level was registered. Considering the SSI reduces the base shear forces compared to the fixed-base case. The maximum base shear force of the fixed-base condition is equal to 2423 kN. This value respectively decreases by 3%, 5% and 7% for the A-P, P-P and F-P systems. Considering the A-RI, P-RI and F-RI cases, the decreases are respectively equal to 14%, 13% and 15%.

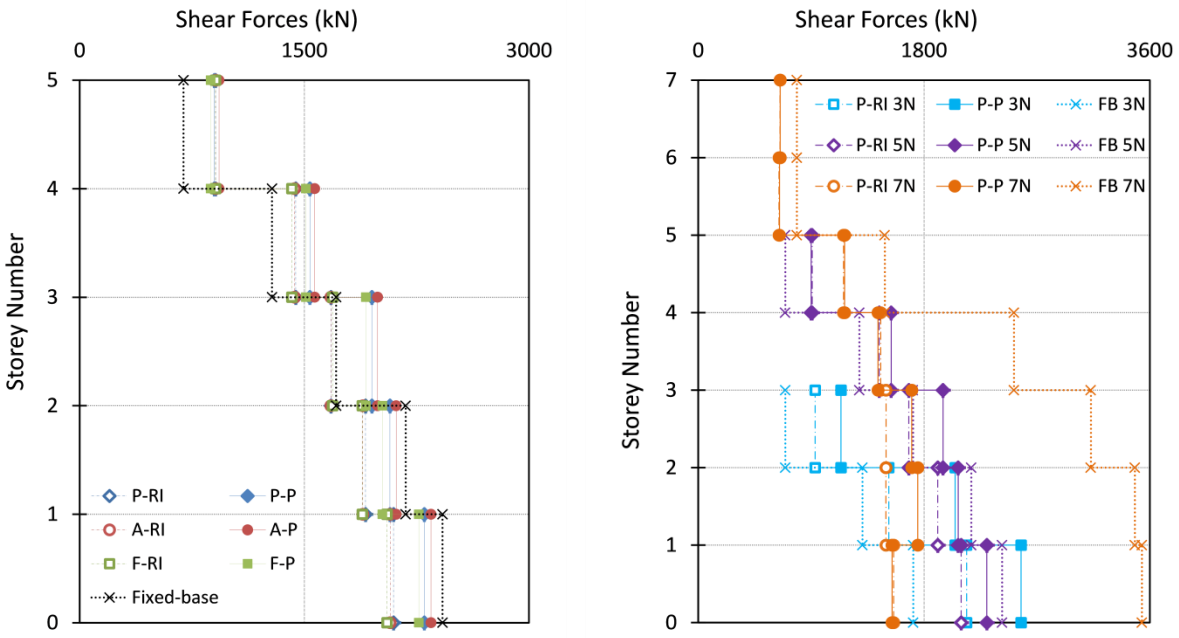

a) 5-storey Building **b)** 3, 5 and 7-storey Buildings

Fig. 5.8 Maximum shear force distribution on the analyzed systems with different support conditions

The shear forces along the building with pile cases are greater than with the rigid inclusion systems in all levels. The fixed connection of the pile head and the foundation slab increase the inertial forces. However, this difference is reduced in the upper levels. For instance, the A-P case give shear forces respectively higher of 13%, 18% and 2% for the A-RI system in the first, third, and fifth levels (Fig. 5.8a). The distribution and the value of shear forces differ with the level number of the building (Hokmabadi and Fatahi 2016, Nguyen et al. 2017). For both pile and rigid inclusion systems with the 5-storey building, the anchored systems induce higher shear forces than placed and floating pile

systems. The rigid elements absorb the inertial forces from the toe (connection of the element on the hard soil). While the floating systems exhibit the lower shear forces values.

As expected, the shear force values in the fixed-base case with the 7-storey building (FB 7N) are greater than the ones of the fixed-base cases with the 3 and 5-storey building. The three systems present similar spectral acceleration with different building mass and height (Fig. 5.8b). The base shear forces of the P-RI 7N are 56% smaller than the FB 7N case (3538 kN). For the P-P 7N this difference is the same. The base shear forces in the P-RI 3N and P-P 3N systems are equal to respectively 2139 kN and 2574 kN. It corresponds to an increase of 24% and 50% considering the fixed-base condition. However, considering the SSI, the shear forces of both pile and rigid inclusion systems with the 3 and 5-storey buildings are greater than the ones of the 7-storey building case. The fundamental period of the systems with the 3 and 5-storey buildings lies in a response spectrum region where the acceleration is close to the resonance. It is not the case for the 7-storey building.

1.5.3. Rocking of the Foundations

During strong seismic excitations, rocking takes place due to the generated inertial forces in the superstructure, which cause compressions in one side (settlements) and tensions (uplifts) in the other side of the foundation.

The rocking can affect the stability of the building due to the lateral displacement increase. On the other hand, some of the seismic energy can be dissipated due to the rocking-dissipation which reduces the shear forces in the structure. The amount of rocking depends on the foundation type supporting the superstructure. When placed or anchored on the hard soil, the axial deformation of the elements and the deformation of the surrounding soil are the main factors which can cause rocking. Additionally, when the system is composed of floating reinforcements, the settlements are also significant. There is no rocking in the fixed-base structure (F-B) because it is assumed that there is not rotation of the foundation slab.

Fig. 5.9a displays the maximum rocking in the systems with the 5-storey building. In general, the rocking values in the rigid inclusions cases are lower than in the pile systems with the same type of support. The inertial forces acting in these systems are lower and due to the presence of the earth platform, it reduces the total and differential settlements. The maximum rocking values in the P-RI, A-RI and F-RI systems are respectively equal to 0.52° and 0.51° and 0.53°. In the pile cases, these values are respectively equal to 0.56°, 0.55° and 0.57° for the P-P, A-P and F-P cases. It can be noted that the systems with placed and anchored elements induce a lower rocking compared to the floating systems The connection with the hard soil reduces the foundation uplift and the settlements values when the compression forces act on the other side of the foundation.

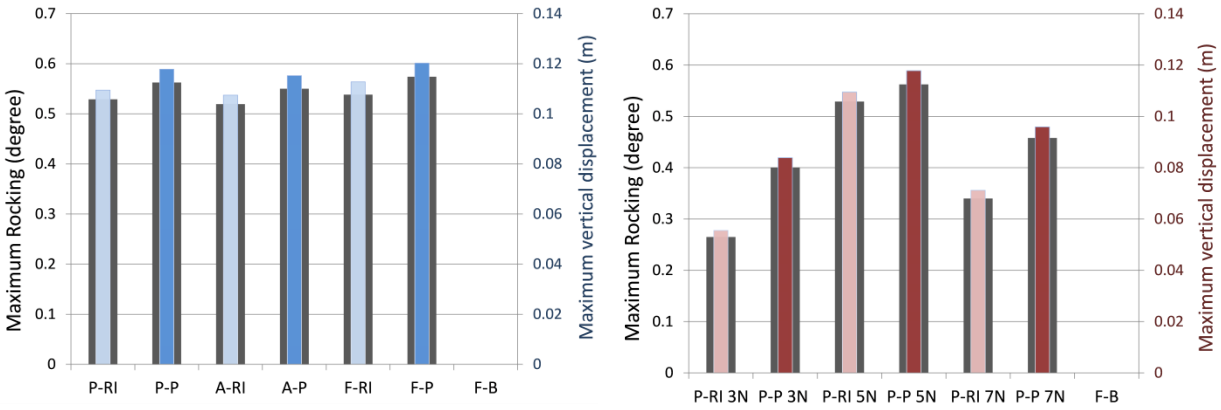

a) 5-storey Building **b)** 3, 5 and 7-storey Buildings

Fig. 5.9 Maximum rocking and vertical displacement in the analyzed systems with different conditions

In Fig. 5.9b, the rocking values in the P-RI and P-P systems are compared with the 3, 5 and 7-storey buildings. The maximum rocking is presented in the systems with the 5-storey building. The P-RI 5N is 99% and 56% greater than the P-RI 3N and P-RI 7N cases. The same comparison but with piles cases gives an increment respectively equal to 40% and 22%. This is mainly because the amount of seismic energy absorbed by the 5-storey building (shear forces) is greater compared to the other building heights. The earth platform seems to have an effect in the reduction of the settlements of the slab foundations which in turns diminish the rocking values.

1.5.4. Lateral Displacements and Inter-storey Drifts

The displacements of the analyzed systems which consider the SSI are amplified compare to the fixed-base condition. This is due to the translation (directly related to the shear forces generated in the building) and to the rotation of the foundation system. Due to these displacements increase, the structures have to be more ductile to undergo these large deformations without collapsing. In order to have a reasonable pattern of deformation, the values reported in this study correspond to the displacement at each level when the maximum displacement occurred at the top level. The displacements of the foundation are subtracted from the storey displacements, which mean that the values are referred to the translation of the foundation at the surface level. The translation at the base of the structure in the rigid inclusions cases is equal to 0.24 m and 0.06 m for the pile cases.

Fig. 5.10a shows that the maximum displacement at the top level of the rigid inclusion systems with the 5-storey building is almost equal (0.35 m) for any support type. This value denotes an increase of 118% compared to the fixed-base condition. When the 5-storey building is founded with the F-P system, the maximum lateral deformation displacement reaches 0.49 m, which corresponds to an increase of 40% compared to the rigid inclusion systems. This increase in the lateral displacements is related to energy absorbed from the earthquake by the rigid elements having contact with the surrounding soil and then transferred to the building.

Comparing the three model structures, the increment in the maximum lateral displacements is more severe for the 5-storey cases than the 3-storey and 7-storey systems. This is in accordance with the shear forces developed in the superstructure (greater spectral acceleration in the systems with 5-storey building) and the rocking values in the different systems. It can be noticed from Fig. 5.10b, that the maximum displacement at the top level of the P-RI 5N case is respectively higher of 169% and of 6% considering the P-RI 3N and P-RI 7N cases. In the pile systems, the P-P 3N and P-P 7N cases are 53% and 47% smaller than in the P-P 5N one.

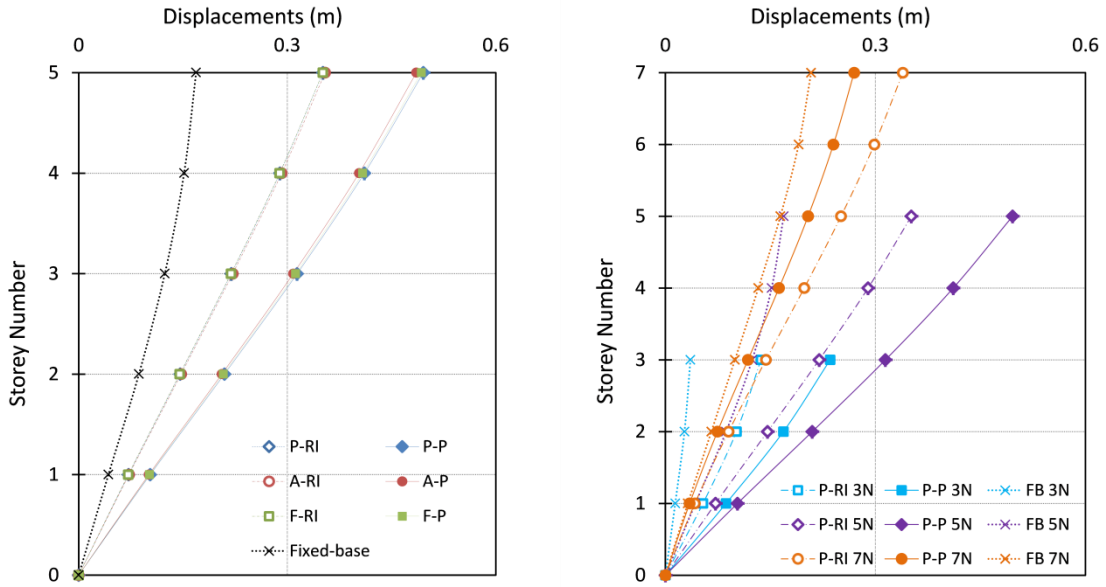

a) 5-storey Building **b)** 3, 5 and 7-storey Buildings

Fig. 5.10 Maximum lateral displacement on the analyzed systems with different support conditions

The ratio of the successive floors displacement difference to the height of the floor is known as the inter-storey drift. This quantity is an important indicator of the performance of the buildings because most of the seismic design codes establish limits for these values. Besides, this is an important indicator of the structural behavior in performance-based seismic analysis. In this study the maximum recorded inter-storey drift in the rigid inclusion systems with the 5-storey building is equal to 1.87% and is independent of the support type. In the pile foundation cases, the maximum inter-storey drift (2.66%) is obtained for the P-P 5N case. The maximum inter-storey drift in the P-RI 3N and P-P 3N cases are respectively equal to 1.34% and 2.16% (Fig. 5.10b). For the P-RI 7N and P-P 7N cases the corresponding values are respectively equal to 1.36% and 1.10%.

1.5.5. Efforts and Displacements in the Vertical Reinforcement Elements

The results obtained in the rigid elements (piles or inclusions) are presented in terms of normal and shear forces, bending moments and displacements for all cases. The displayed results correspond to

the rigid elements situated in the axes A-3 and/or F-3 in the system configuration shown in Fig. 5.3b. The rigid elements located in these axes are where maximum efforts and displacements took place.

1.5.5.1. Normal Forces

The maximum normal forces are reached at the head of the rigid elements. They decrease with depth in all the analyzed cases. The values at the head in the A-RI, P-RI and F-RI systems with the 5-storey building are respectively equal to 125 kN, 133 kN and 96 kN (Fig. 5.11a). The normal forces along the elements in A-RI and P-RI systems are similar. However, these values are 56% greater than the F-RI case. In the cases with floating rigid inclusions, the transfer of stress between soil and the rigid elements occur mainly through the element shafts while in the placed or anchored cases the connection of the element toe in hard soil dominates the load transfer mechanism.

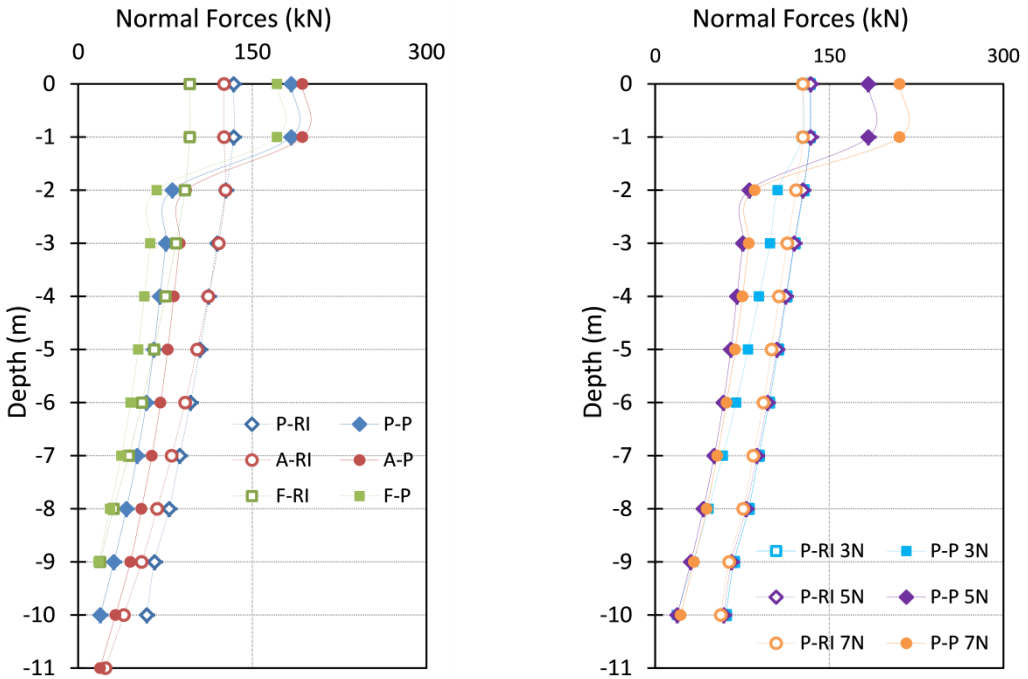

a) 5-storey Building **b)** 3, 5 and 7-storey Buildings

Fig. 5.11 Normal Forces in rigid inclusion and pile systems with different support conditions

In the A-P, P-P and F-P systems, the maximum normal forces (at the head element) increase by 54%, 37% and 78% compare to the rigid inclusion systems with the same support type. This increase is due to the higher compression and tension forces (increased by the inertial forces in the building) in the piles at the link with the slab foundation. In the rigid inclusion systems, these values are lowered because only compression forces can be developed by the existence of the earth platform between the piles and the foundation slab. Besides this, the transmission of surface loads in the rigid inclusion system is share by the inclusions and the soft soil underlying the platform. The normal forces in the pile systems are reduced at a depth of 2 m from the head position.

Fig. 5.11b shows that the normal forces values in the head (133 kN) and along the rigid inclusions are not influenced by the different building heights. However, in the pile cases, the P-P 7N one is the system with higher normal forces at the pile head (210 kN). This value decrease respectively of 12% and 40% compared to the P-P 5N and to the P-P 3N cases. This can be related to the weight difference of the buildings.

1.5.5.2. Shear Forces and Bending Moments

The maximum shear forces and bending moments in the rigid elements for the systems with the 5-storey building are respectively presented in Fig. 5.12a and Fig. 5.13a. In all pile or inclusion cases, the inertial forces are mainly responsible of the maximum moment and shear forces near the pile head (Ishihara 1997). These inertial forces are strongly dependent on the dynamic characteristics of the buildings.

In the rigid inclusion cases, the maximum shear force value reached is equal to 33 kN in the head of the element and until 1 m of depth independently of the support condition. The bending moment at this level is null. However, the maximum bending moment reached is 50 kN.m at 3 m of depth for all types of support. Along the rigid inclusions, the shear force distribution varies from 15 kN at 2 m to 10 kN at 9 m of depth. In the rigid inclusions anchored (A-RI case), the shear forces and bending moments are increased at the anchorage level and reach respectively a value of 17 kN and 23 kN.m. The values at this level are due to the lateral deformations of the surrounding soil in the rigid elements (kinematic forces).

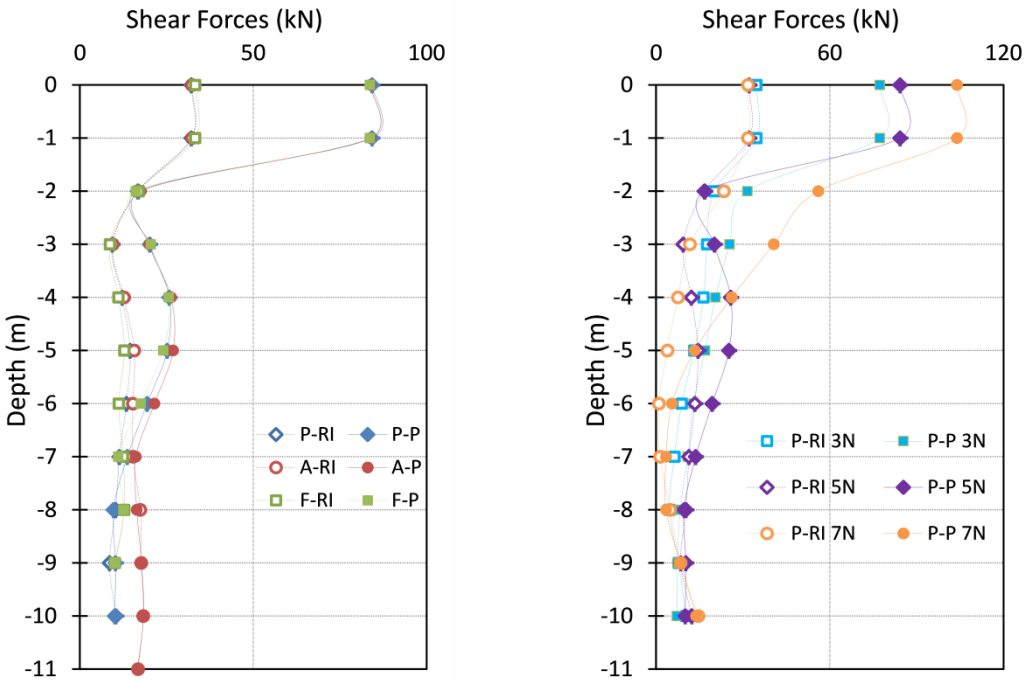

a) 5-storey Building **b)** 3, 5 and 7-storey Buildings

Fig. 5.12 Shear Forces in rigid inclusion and pile systems with different support conditions

In the pile cases, the maximum shear forces are also located at the pile head with a value of 84 kN, which means an increment of 154% in respect to the rigid inclusion cases. The maximum bending moment value reached is equal to 145 kN.m. The fixed connection of the piles with the foundation slab which amplifies the inertial forces at this level. For the rigid inclusion improvement, the earth platform permits to decrease the efforts at the head of the reinforcements which can be useful under earthquake loadings. The shear forces along the pile cases are greater than in the rigid inclusion systems from 2 m to 9 m of depth. As in the rigid inclusion cases, the shear force (19 kN) and moment (16 kN.m) in the anchored system are amplified at the interface of the soft and hard soil layers.

The comparison of shear forces in the P-RI and P-P systems with the 3, 5 and 7-storey buildings is illustrated in Fig. 5.12b. The maximum shear force value at the head (32 kN) and at the toe (14 kN) of the rigid inclusion systems is almost the same for the three building heights. In the pile cases, the values (at head level) of the P-P 5N are 9% higher than for the P-P 3N but 18% smaller than the P-P 7N. These shear forces are importantly reduced at 2 m depth. For both pile and inclusion cases, the maximum shear forces are lower 25 kN from 3 to 10 m depth.

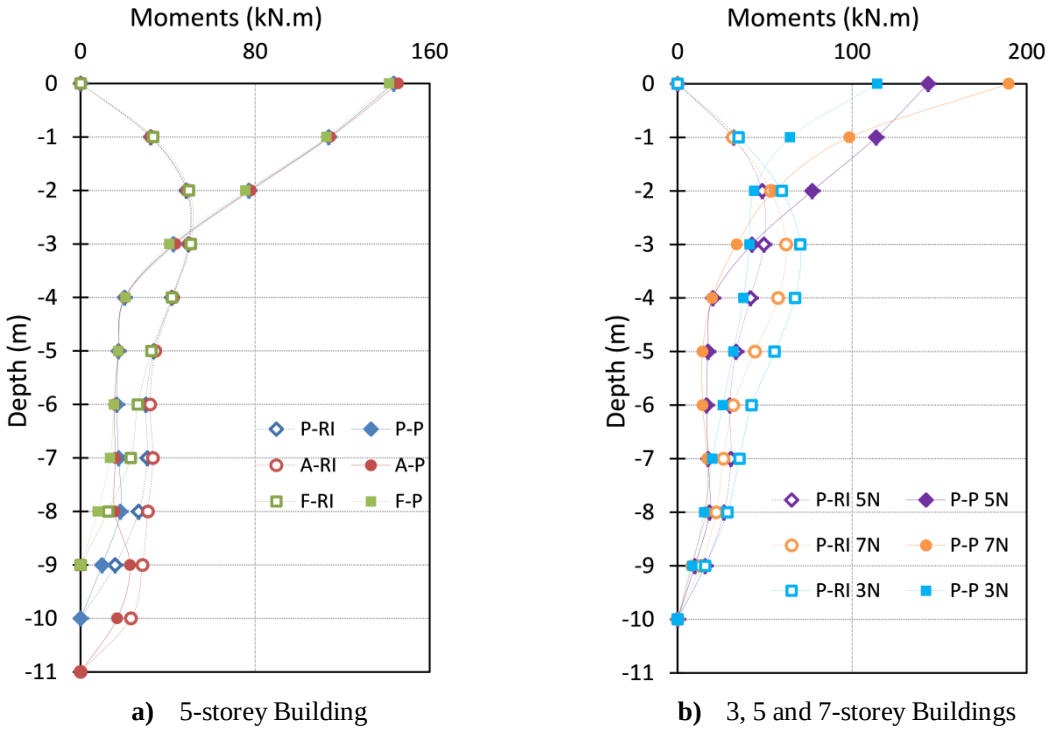

a) 5-storey Building **b)** 3, 5 and 7-storey Buildings

Fig. 5.13 Bending moments in rigid inclusion and pile systems with different support conditions

The maximum moment (always located at 3m depth) of the P-RI 3N is equal to 70 kN, which corresponds to an increase of 13% compare to the P-RI 7N and 42% against the P-RI 5N case (Fig. 5.13b). In the pile cases, the maximum bending moments is attained at the connection with the foundation slab. These moments are respectively equal to 189, 145 and 114 kN.m for the P-P 7N, P-P

5N and P-P 3N. The maximum shear forces and bending moments in the inclusion and pile cases strongly depend on the dynamic characteristics of the buildings and the energy absorbed from the foundation.

1.5.5.3. Displacements

Fig. 5.14a indicates that the displacements of the rigid inclusions and of the piles systems are not influenced by the support condition. The maximum displacement occurs at the head of the vertical elements. The maximum displacement in the rigid inclusions system is equal to 0.39 m. In the piles, this value reaches 0.35 m, which implies a reduction of 10% respect to the rigid inclusions. The displacement at the pile toe for all systems is almost the same (0.27 m). Fig. 5.14b shows that the rigid elements in the P-RI 3N system present the greater displacement at the head of the elements (0.44 m). This value decreases respectively of 11% and of 15% for the P-RI 5N and for the P-RI 7N systems. In the case of piles, the maximum displacement is equal to 0.37m for the P-P 3N system.

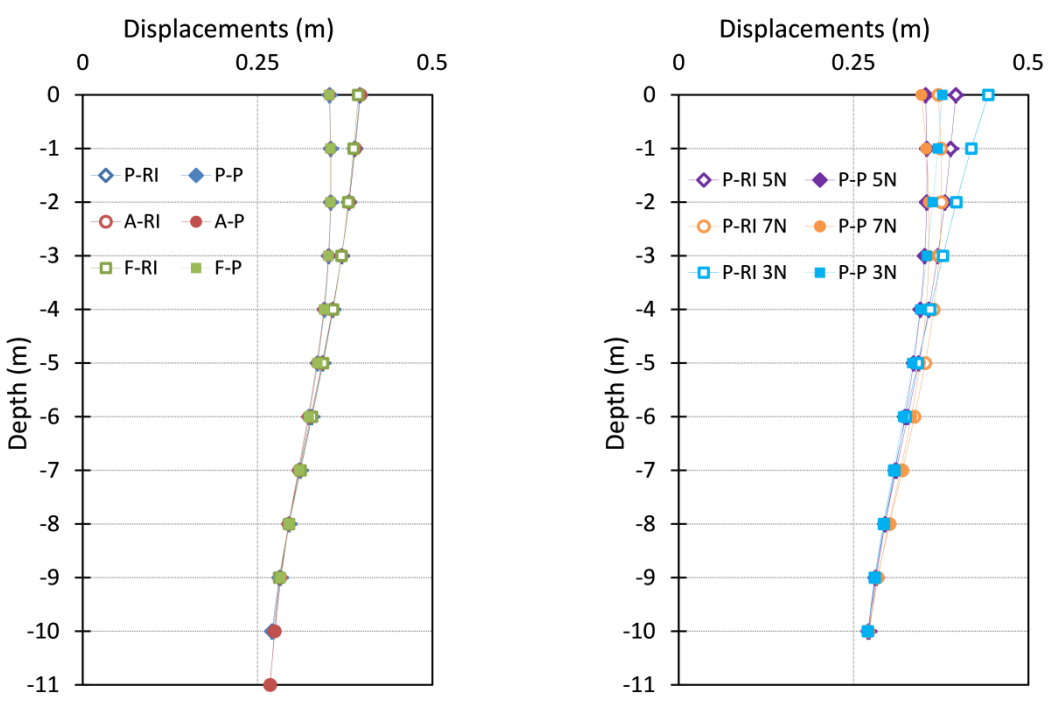

a) 5-storey Building **b)** 3, 5 and 7-storey Buildings

Fig. 5.14 Displacements in rigid inclusion and pile systems with different support conditions

1.6. General Conclusions

In this chapter, fully coupled three-dimensional analyses of both soil-inclusion-platform-structure and soil-pile-structure systems are developed with different foundation types under a seismic loading. Floating, placed and anchored on hard soil rigid elements are considered. Buildings with different

heights (3, 5 and 7-storey) are modelled over the pile and rigid inclusion foundation to gain insight of the effects of the dynamic characteristics of the superstructure on the response of the systems.

The results of the numerical analyses show that the soil properties and the dynamic characteristic of the building and foundation cause an amplification of the fundamental period of the building and the spectral acceleration in the soil surface response spectrum (compare to the input motion) in all analyzed cases.

The shear forces distribution along the building considering pile foundations are greater than the ones for the rigid inclusion systems. The inertial forces increase in the pile cases due to the fixed-head connection with foundation slab. Considering the SSI, the shear forces of both pile and rigid inclusion systems with 3 and 5-storey buildings are greater than the ones of the 7-storey building case. The fundamental period of the systems with the 3 and 5-storey buildings lies in a response spectrum region where the acceleration is higher (close to the resonance) than for the 7-storey building.

The systems with placed or anchored elements induce a lower rocking compared to the floating system. The connection with the hard soil reduces the uplift in one side of the foundation and reduces the settlements values when the compression or tension forces act on the other side of the foundation. The rocking values are lower in the systems that consider 3 and 7-storey building compare to the case with 5-storey building.

The displacements and inter-storey drifts when considering the SSI are amplified compare to the fixed-base case. This increase in the lateral displacements is related to the amount of inertial energy absorbed by the soil-pile/inclusion-structure system. The maximum displacement at the top level of the rigid inclusion and pile systems with the 5-storey building is almost equal for any type of support. In agreement with the shear forces and rocking in the systems, the maximum displacements are greater in the pile or inclusion systems with 5-storey building than in the 3 and 7-storey cases.

In the systems with the 5-storey building, the maximum normal forces in the piles systems are greater than in the rigid inclusion systems. This increase is due to the high compression and tension forces in the piles at the connection with the slab foundation. In the rigid inclusion cases the earth platform allows only compression forces in the elements.

The maximum shear forces are more important at the rigid inclusions heads and decrease with the depth. The maximum bending moment in the rigid inclusion systems is reached at 3 m of depth and is null at the head. Because of the fixed connection with the foundation slab, in the pile cases, the bending moments and the shear forces at the pile head are high independently of the type of support.

The anchored systems induce an increase of the moments and of the shear forces at the interface of soft and hard soil layers. This is due to the extra kinematic ground forces in deeper areas. This important factor should be considered in the design of the rigid element to avoid failures at this level.

Chapter 6 SEISMIC RESPONSE OF INCLUSION AND PILE-REINFORCED SYSTEMS IN LIQUEFIABLE SOILS

1. Effect of the Soil Profile, Pile Length and Input Motion Frequency

1.1. Introduction

The behavior of pile foundations in soft soils is related to the pile-soil interaction, the failure mechanisms and the pile response, which in turns depends greatly of the soil type, characteristics of the earthquake and pile strength. In the presence of liquefiable soils, the response of these foundations is more complex. There are dynamic loads acting on piles due to the structure and the surrounding soil, and simultaneously there is a shear strength reduction and a significant degradation of the stiffness of the surrounding soil over time due to the nonlinear behavior of soil and also to the pore pressure generation. Several previous investigations considering the SSI in the presence of liquefiable soils are described in Section 2.3.4 Chapter 2.

This Chapter presents a study to understand deeply how some factors (soil profile, relative density, pile length and frequency of the seismic loading) influence the response of the soil-foundation-structure systems in the presence of liquefiable soils under seismic loadings. The investigation was made into numerical models considering a 3-storey reinforced concrete frame founded on inclusions systems (soil-inclusion-platform-structure) and pile systems (soil-pile-structure). The constructed finite difference numerical models were analyzed using coupled mechanical-fluid calculations. Different soil profiles were contemplated in the analyses. The analyses were developed in undrained conditions. The water table is considered to be present at the ground surface level.

In the Section 1 of this Chapter, a simple constitutive model for the liquefaction analysis that relates to the volumetric strain increment in relation with the cyclic shear strain amplitude was utilized to represent the sand behavior. The effects of the soil profile, pile length and earthquake frequency on the response of the systems were examined. The bending and buckling failure modes in the rigid elements were also studied. Using the comprehensive Sanisand constitutive model, the Section 2 of this Chapter, investigates the influence of the soil relative density and the input motion frequency in the seismic analysis of the systems.

The Mohr-Coulomb constitutive model (Section 4.2 Chapter 2) was used to represent the behavior of the non-liquefiable soil layers and earth platform. Two typical strong-motion earthquakes events that correspond to the Loma Prieta (1989) and Northridge (1994) were used to study the influence of different frequencies of excitation of the systems.

1.2. Characteristics of the Adopted Numerical Model

1.2.1. Soil Mesh

Fig. 6.1 shows one of the structured finite-difference meshes implemented to represent the subsoil conditions, where a total of 13,300 Flac hexahedral zones were employed. The mesh was extended downward to -15 m, where the input motion was applied. The maximum spatial element size utilized in the modelling (1 m) allows applying frequencies between 0 and 6 Hz without the distortion of the propagate wave in the model by the choice of zone size (Kuhlemeyer and Lysmer 1973). After a static equilibrium, free-field boundaries are applied to the model for the dynamic analysis (Section 1.7 Chapter 3).

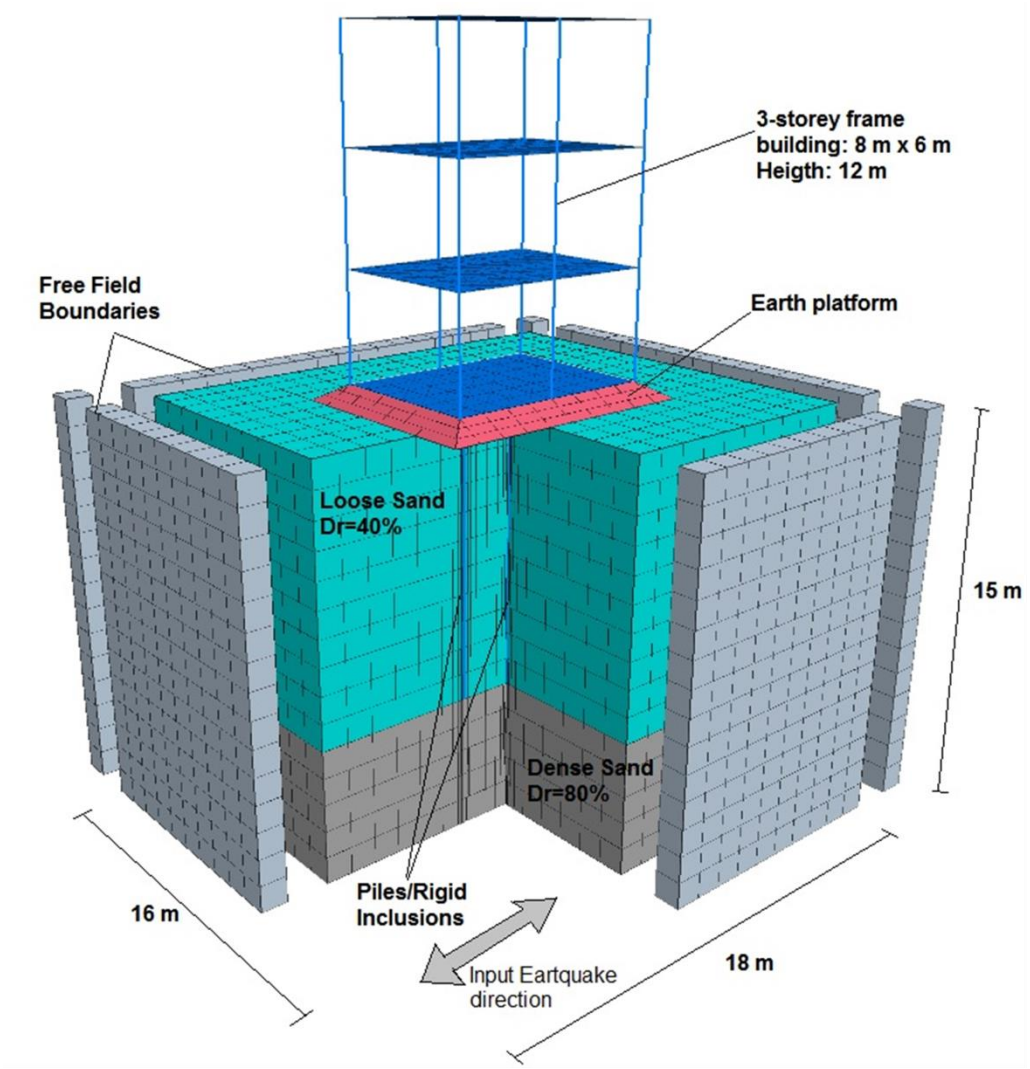

Fig. 6.1 Geometry of the numerical model

Two soil profiles are analyzed. The first is a 2 layers soil profile that consists in an horizontal 10 m thick loose sand layer (liquefiable soil) over a 5 m thick dense sand layer (non liquefiable soil). The second profile is composed of 3 layers of 5 m, where the layer in between corresponds to a liquefiable

soil and the other layers not (Fig. 6.2). In all profiles, the water table is located at the surface ground level. The properties of the Nevada sand (Haldar and Babu 2010) are used in the numerical modeling and are presented in Table 6.1. The loose and dense sand are 40% and 80% relative density (Dr) respectively. The behavior of sand layers is simulated with the Finn model (Martin et al. 1975) described in Section 4.3 Chapter 2.

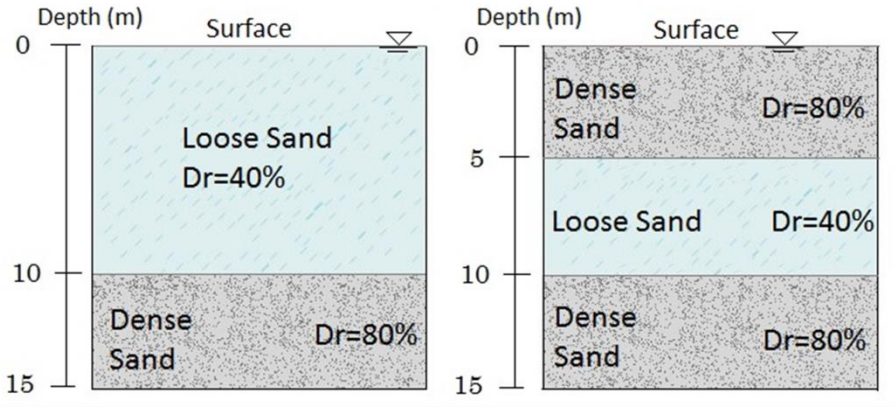

a) 2 layer soil profile (LD) **b)** 3 layer soil profile (DLD)

Fig. 6.2 Considered soil profiles

Table 6.1 Nevada Sand properties (Haldar and Babu 2010)

Properties	Unit	Dr=40%	Dr=80%
Poisson's ratio, ν	----	0.45	0.45
Mean effective vertical stress, σ'_{vo}	kPa	167	167
p_0	kPa	100	100
K_0	----	0.5	0.5
Shear modulus, G	kPa	2.7×10^4	4.47×10^4
Bulk modulus, K	kPa	2.16×10^5	4.32×10^5
$(N_1)_{60}$	----	7.2	30
Permeability, k	m/s	6.6×10^{-5}	3.7×10^{-5}
Porosity	----	0.424	0.373
Friction angle, ϕ	°	33°	39.5°
Bulk modulus of water, k_w	kPa	2.51×10^6	3.67×10^6
Soil density (ρ_{sat})	kg/m³	1962	2047
C_1^c	----	0.7376	0.1239
C_2^c	----	0.5422	3.2284

As in the previous chapters fixed-head elements with the slab foundation are considered in the pile systems and free-head when the analysis considers rigid inclusions cases because the presence of the 0.60 m thick earth platform between the soil and the rigid elements. The material properties of the

mattress are showed in Table 6.2. The linear elastic perfectly plastic constitutive model with a Mohr-Coulomb failure criterion is utilized to represent the behavior of the earth platform. An additional damping is introduced in the elastic part of the response where there is no soil energy loss during the dynamic analysis. This was done using the frequency dependent Rayleigh damping (Section 1.6 Chapter 3) with a ratio of 5%.

Table 6.2 Material properties considered for the earth platform.

Properties	Young modulus (MPa)	Shear Modulus (MPa)	Volumic Weight (kg/m³)	Damping Ratio	Cohesion (kPa)	Friction angle (°)	Wave velocity (m/s)
Platform	50	19	2000	0.05	50	25	160

1.2.2. Vertical Reinforced Elements

This study is developed with 12 rigid vertical elements embedded in the soil profiles described above. The distribution of the rigid elements is showed in Fig. 6.3. Each circular concrete element is 0.30 m in diameter. The coverage ratio is equal to 1.7%. The length of the vertical rigid elements varies in each model and it can vary between 10 m and 14 m.

As in the previous Chapter, the rigid elements were modeled by using beam structural finite elements perfectly bonded with the soil (Finn and Fujita 2002, Sadek and Shahrour 2004, Kitiyodom et al. 2006, Alsaleh and Shahrour 2009). The advantages are the computation time efficiency and obtaining the pile efforts directly from the simulations. The use of these beam elements results in greater efforts in the piles because the physical rigid element cross section is not considered (Section 1.2.3 Chapter 5). Reinforced concrete rigid elements are considered. The material properties of the rigid elements are displayed in Table 6.3. The behavior of the rigid elements is considered as linear elastic in all calculations.

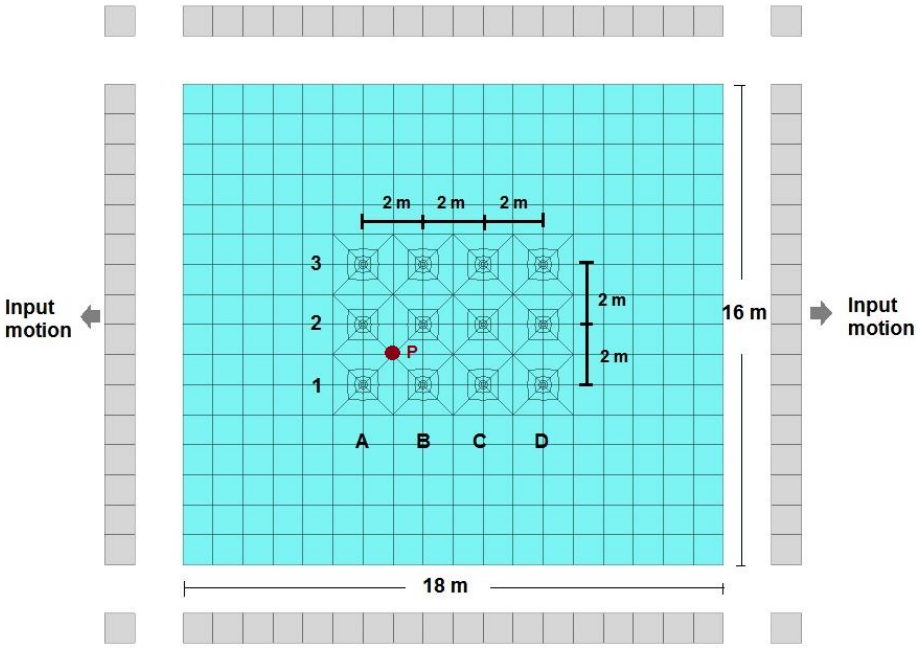

Fig. 6.3 Plan view and location of the rigid elements

Table 6.3 Rigid element properties.

Properties	Diameter (m)	Cross-sectional area (m^2)	Moment of inertia (m^4)	Young's modulus (GPa)	Shear Modulus (MPa)	Volumic Weight (kg/m^3)	Damping Ratio
Rigid elements	0.30	4167	2500	30	4167	2500	0.05

1.2.3. Superstructure

All the calculations cases consider the modelling of a 3-storey reinforced concrete building over the earth platform for the inclusion systems and over the foundation slab for the pile systems. The frame is composed of two bays and one span. The in plane dimensions are 8 m x 6 m (Fig. 6.3). The storey height is equal to 4 m. The sections of the structural element utilized are shown in Table 6.4. The columns and slabs are considered made of reinforced concrete with the same material properties as the vertical reinforcement elements (Table 6.3). The behavior of the structural elements is considered as linear elastic.

Table 6.4 Sections considered in the building

Section	Notation	Length (m)	Width (m)	Thickness/height (m)
Floor slab	h_{fs}	8	6	0.25
Foundation slab	h_s	8	6	0.25
Columns	a_c	0.4	0.4	4

The columns, floor slabs and foundation slab were respectively modeled by a collection of beam structural, shell and liner elements (Section 1.4 Chapter 3). The installation of the superstructure is considered in a single phase after the model equilibrium. A Rayleigh damping with a factor of 5%. The model coefficients $\alpha = 0.6583$ and $\beta = 0.0037$ are based on the first and second mode frequencies of the superstructure. They are used to simulate the structural damping. The fundamental period of the structure is equal to 0.493 s.

1.3. Seismic Input Motion

The Loma Prieta 1989 and Northridge 1994 earthquake motions are imposed to the numerical model. The characteristics of these two benchmark earthquakes are showed in Table 6.5. The predominant frequency is different in order to verify its influence in the analyses.

Table 6.5 Earthquake base motions considered (CESMD)

Earthquake	Date	Duration (s)	Peak ground acceleration PGA (m/s²)	Magnitude (Mw)	Predominant Frequency (Hz)
Loma Prieta, USA	1989/10/17	40	4.69	7.1	1.35
Northridge, USA	1994/01/17	30	8.65	6.7	4

The original acceleration time-histories of 20 seconds duration are presented in Fig. 3.6b, c (Chapter 3). In order to reduce the time calculation, only 4 seconds of each earthquake record are applied (between 2 and 6 seconds for the Loma Prieta earthquake and between 7 and 11 s for the Northridge earthquake). Fig. 6.4 shows the records, which were scaled to the same peak acceleration value (0.75g) with the idea of a rapid liquefaction. Then they were applied in the horizontal direction to all nodes in the bottom part of the model. The applied signals were treated with a baseline correction (Section 1.5 Chapter 3) and a low-pass filtering (10 Hz).

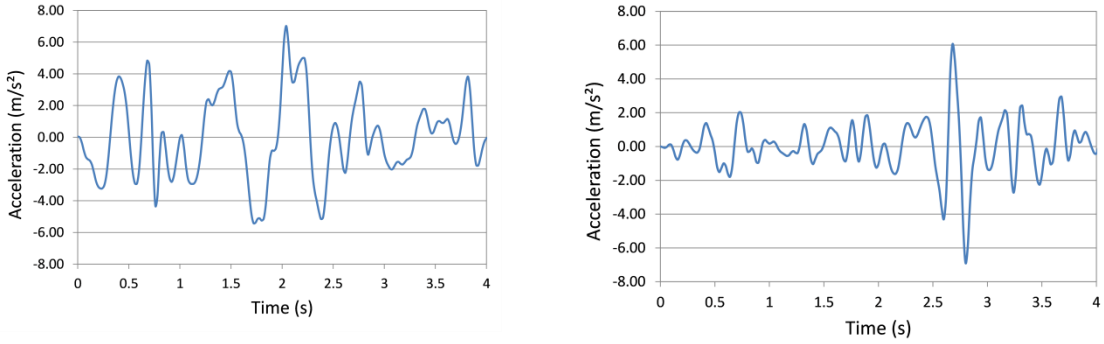

a) Loma Prieta 1989 **b)** Northridge 1994

Fig. 6.4 Earthquake records considered

1.4. Numerical Cases

The soil-pile-structure and soil-inclusion-platform-structure cases analyzed are represented schematically in Fig. 6.5 and Fig. 6.6. These cases present different soil profiles, pile length and input earthquakes (Table 6.6). The name or the case has three terms, the first term (RI or P) refers to Rigid Inclusion or Pile case, the second one (2layers or 3layers) indicate the soil profile considered and the third term is the rigid element length (10 m or 14 m). The term w/S in two cases means without structure. For instance, the case RI-2layers-10m correspond to the rigid inclusions system with 2 layer soil profile and 10 m pile length. The time calculation for the models was approximately of 195 hours for each case. The characteristics of the computer to develop the analyses can be consulted in Section 1.5 Chapter 3.

Table 6.6 Characteristics of the analyzed cases

Rigid elements	Name of Case	Pile Length (m)	Soil profile	Structure	Earthquake
Rigid inclusions systems	RI-2 layers-10m	10	LD	Yes	Loma Prieta
	RI-2 layers-14m	14	LD	Yes	Loma Prieta
	RI-2 layers-14m w/S	14	LD	No	Loma Prieta
	RI-3 layers-14m	14	DLD	Yes	Loma Prieta/Northridge
Pile systems	P-2 layers-10m	10	LD	Yes	Loma Prieta
	P-2 layers-14m	14	LD	Yes	Loma Prieta
	P-2 layers-14m w/S	14	LD	No	Loma Prieta
	P-3 layers-14m	14	DLD	Yes	Loma Prieta/Northridge

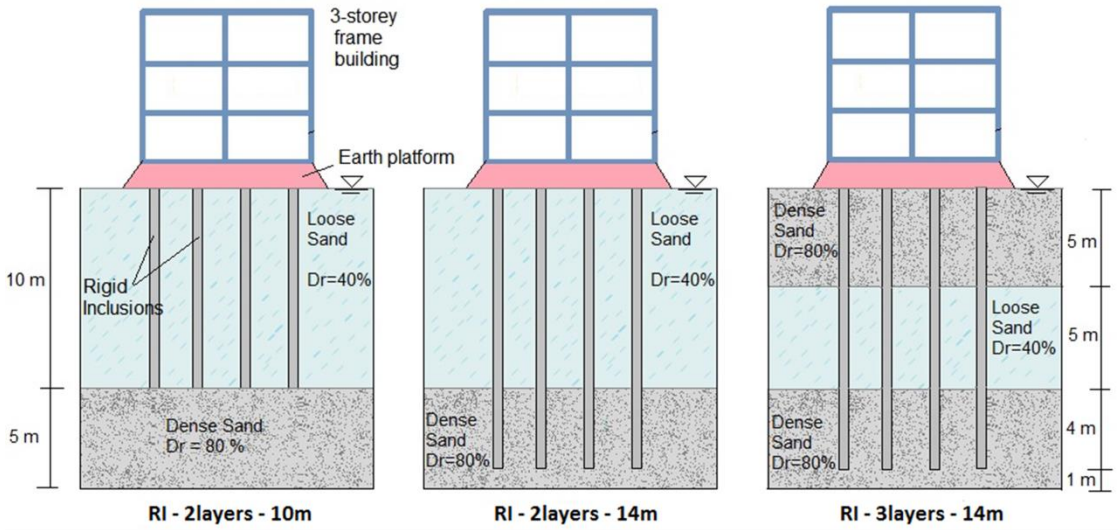

Fig. 6.5 Soil - rigid inclusions - earth platform - structure analyzed systems

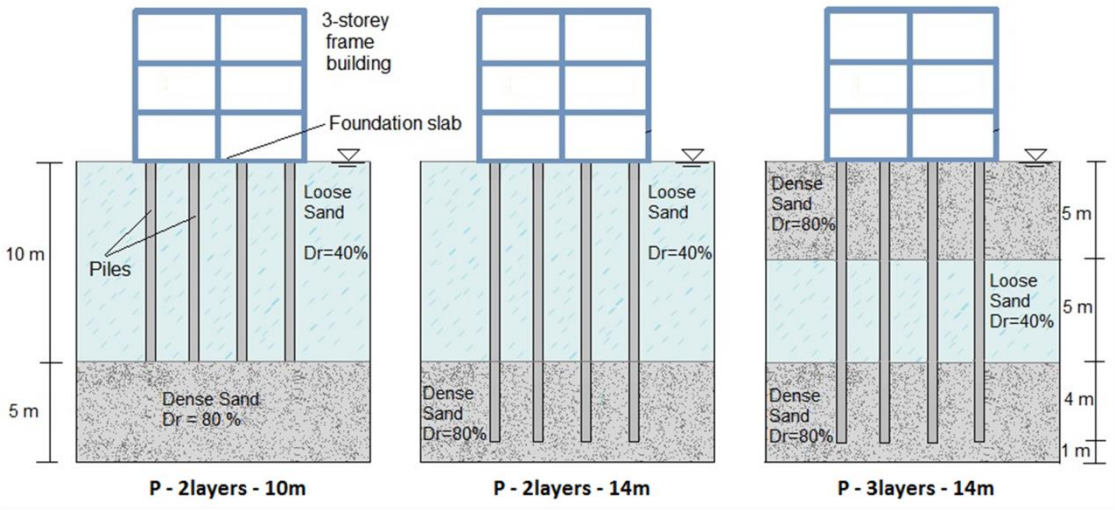

Fig. 6.6 Soil - piles - structure analyzed systems

1.5. Procedure of Analysis

First a mechanical equilibrium state is obtained with the groundwater level present at the soil surface. Then, the vertical reinforcements are installed. The last static calculation step considers the activation of the earth platform and of the surface structure. In all these preliminary steps, no fluid flow is considered to obtain a faster solution. After that, a flow calculation is carried out to determine the steady flow condition. Then a final mechanical calculation is done subsequently. The fluid flow is prevented since the consolidation process is not the main concern.

The dynamic analysis is then performed as a coupled simulation, in which changes in deformations and volumetric strains induced by seismic excitation causes the pore pressure to evolve. The formulation of the coupling analysis is done within the frame work of the quasi-static Biot theory (single-phase Darcy flow in a porous medium). For the dynamic calculations, the absorbent and free field boundaries are added and the dynamic analyses are executed applying the corresponding horizontal wave using acceleration at the base of the models.

1.6. Results and Comparisons

In this section, the results of the structure response in terms of shear forces in the building and spectrum response are presented. The soil response is displayed through pore pressure and strains in point P (Fig. 6.3) at different depths. The bending moments, normal forces and displacements are exhibited to evaluate the response of the rigid vertical elements. Considering these efforts, the bending and buckling failure in the rigid elements can be obtained. All the values presented correspond to the maximum values measured during the seismic loading in the calculations in the axes A-1 (Fig. 6.3), which is the element where higher efforts are present. As mention in Chapter 4, after the

implementation of the building, the soil values were initialized to account only the effect of the dynamic loading.

1.6.1. Structure Response

1.6.1.1. Response Spectrum

A seismic soil-structure interaction analysis evaluates the overall response of the superstructure, the foundation and the soil underlying and surrounding the foundation, for a specific ground motion. The impact of the SSI on the soil movements is illustrated using the response spectrum at the base of the structure (ground motion at the ground surface) in the analyzed models as showed in Fig. 6.7. The spectra were calculated similarly as in Section 1.8.1 Chapter 4. It describes the maximum response of a single-degree of freedom system for a specified earthquake ground motion and 5% of damping. In all analyzed cases, the spectra are reduced because the surface accelerations records are lowered compared to the input record (applied at the model bottom). This decrement is due to the fact that a liquefied layer attenuates the energy as the motion propagates at the surface, which prevents the liquefaction in superficial soil. Similar results are obtained by Tokimatsu et al. (2005), Popescu et al. (2006), Taiebat et al. (2010), Wang et al. (2013), Montoya-Noguera and Lopez-Caballero (2016).

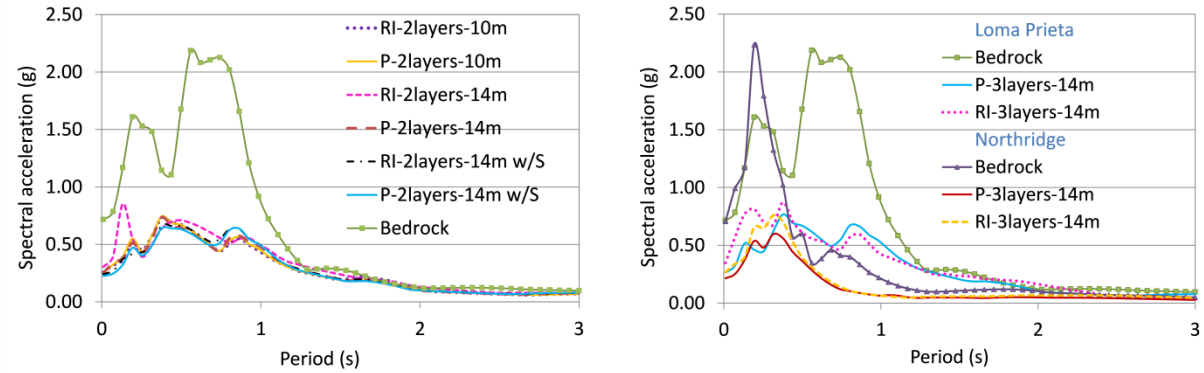

a) 2 layer soil profile **b)** 3 layer soil profile

Fig. 6.7 Acceleration response spectrum of the analyzed systems with different soil profiles and earthquakes.

The spectrum responses in the 2 layers soil profile are independent of the pile length (Fig. 6.7a). However, there are some cases where the length of the rigid elements influences the seismic motion characteristic at the base of the structure by altering the kinematic and inertial interaction. For instance, the spectrum response (mainly at short periods) is increased in the rigid inclusion system compare to the 10 m pile length. The spectrum response lightly increases with the consideration of the superstructure. This is in accordance with the results obtained by Maheshwari and Sarkar (2011).

Fig. 6.7b shows that the response spectrum of the RI-3layers-14m and P-3layers-14m systems excited with the Loma Prieta earthquake. They are greater compared to the response obtained with the

Northridge earthquake. This means that the response increases when the frequency of the excitation decreases. The responses of the rigid inclusion systems are greater than the pile cases considering the 3 layers soil profile.

1.6.1.2. Shear Forces in the Superstructure

In accordance to the spectrum response in the previous section and with the purpose to investigate the seismic energy absorbed by the structure, Fig. 6.8 shows the comparison of the shear forces developed in the building for the different cases. The maximum shear forces in the building were found in the same way as in Section 1.5.2 Chapter 5. The response of the fixed-base case (F-B) is also displayed. The F-B case refers to the case where the superstructure is analyzed with fixed support conditions and without soil. It is noticeable that the consideration of the SSI reduces the shear forces in the superstructure compare to the fixed-base case. The shear forces in the building with pile systems are greater than in the rigid inclusion systems considering the same soil profile and pile length. The fixed connection of the pile head to the foundation slab increases the inertial forces.

In the systems with 2 layers soil profile, the shear forces in the cases with 14 m pile length are greater than the cases with 10 m pile length. This happens because the longer piles are subjected to inertial forces from the embedded part in the non-liquefiable soil layer. However, considering the rigid inclusion cases, the RI-10m system shows slightly larger shear forces compared to the RI-14m one. This can be explained because there is no connection of the rigid inclusions with the slab foundation.

Due to the fact that the fundamental period of the RI-3layers-14m and P-3layers-14m systems induced by the Northridge earthquake lies in a response spectrum region where the spectral acceleration is lower than the acceleration with the Loma Prieta earthquake, the shear forces in the building are reduced.

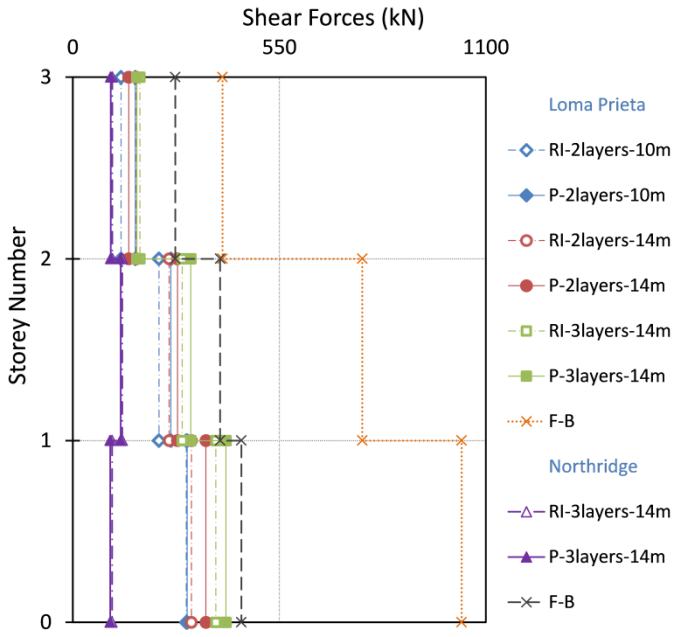

Fig. 6.8 Maximum shear force distribution on the analyzed systems with different soil profiles and earthquakes

1.6.2. Soil Response

1.6.2.1. Pore Pressure

In practice, excess pore pressures reduce the soil effective stresses, which in some cases implies that the ability of the soil to resist to shear loading can be lost, resulting in significant soil deformations or a failure.

The excess pore water pressure ratio (r_u) is defined as the ratio of the difference of pore pressure in a specified stage (u) and initial pore pressure (u_0) over the initial effective stress (σ'_0). When $r_u = 0$, the pore pressure is equal to the applied back pressure. The true liquefaction takes place when the excess pore water pressure ratio is equal to 1 if the total stresses are kept constant during the cyclic loading. It is also considered that when $0.8 < r_u < 1.0$ there is a development of large strains and cyclic mobility occurs (Koutsourelakis et al. 2002, Montoya-Noguera and Lopez-Caballero 2016). As mentioned before (Section 3.3.5.3 Chapter 2), in this study the liquefaction is triggered when $r_u = 0.8$.

Fig. 6.9 exhibits the excess pore pressure time histories computed at point P (Fig. 6.3) at two depths (5 m and 9 m) to check the effect of the soil response surrounding the piles. In general, the values of the excess pore water pressure ratio of the systems with rigid inclusions are greater than with the pile systems (Fig. 6.9a, d). The r_u values that do not consider the structure are lower than in those where it is considered (Fig. 6.9a, b). This happens because the inertial forces generated in the superstructure produce larger soil shear strains in the top section of the model. However, this difference is reduced with the depth. It means that the effect of inertial forces in the superstructure is

less perceptible in the deeper areas. This is in accordance with the results founded by Rahmani and Pak (2012).

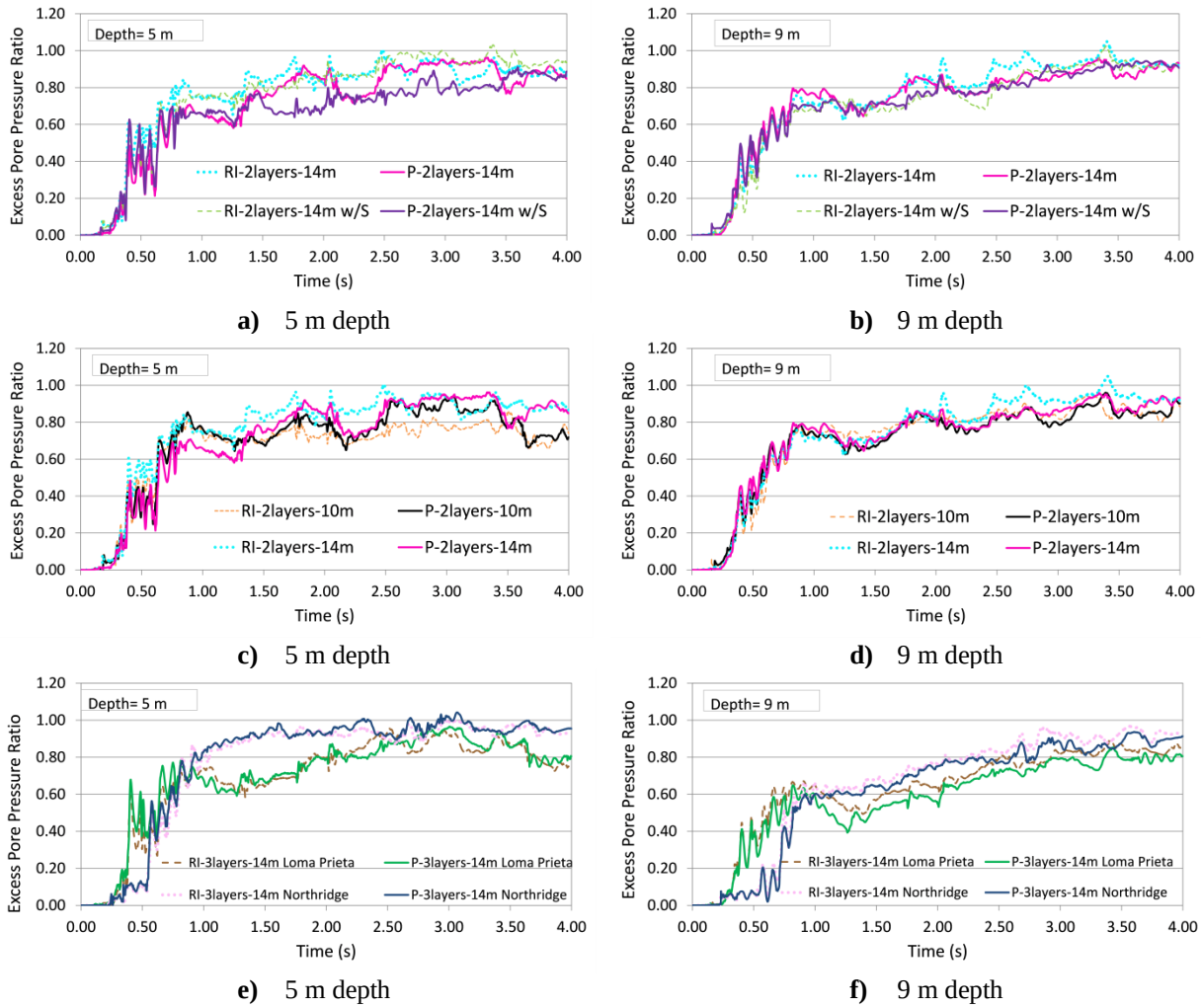

a) 5 m depth **b)** 9 m depth

c) 5 m depth **d)** 9 m depth

e) 5 m depth **f)** 9 m depth

Fig. 6.9 Excess pore pressure ratio time histories in the analyzed systems at different depths and earthquakes

The rigid element length has a slight influence on the pore pressure development in the systems with the 2 layers soil profile (Fig. 6.9c, d). However, the frequency, amplitude and duration of the motion have a great influence in the excess pore pressure ratio time histories as showed by Montoya-Noguera and Lopez-Caballero (2016). In fact, in Fig. 6.9e, f, the effect of the frequency of the excitation in the development of liquefaction at different depths is illustrated. In this case, the r_u values of the system using the Northridge earthquake (4 Hz) are lower (until 1 s calculation) than the system excited by the Loma Prieta earthquake (1.35 Hz). After 1 s, the pore pressure values are greater. It can also be noted that the system shaken with the Northridge earthquake induced the liquefaction later (2.2 s) than the system with Loma Prieta earthquake (1 s). This can be explained because the spectral accelerations are greater in the system shaking with Loma Prieta earthquake. The difference between piles and rigid inclusions with the same frequency of excitation is minor with the 3 layers soil profile (Fig. 6.9e, f).

1.6.2.2. Soil Shear Strains

The maximum shear strains values recorded near the rigid elements (see point P in Fig. 6.3) in all the analyzed cases at different depths are presented in Fig. 6.10. The maximum shear strain values in a liquefied layer are importantly influenced by the soil relative density and the peak acceleration. The increase of the soil relative density implies a decrease of the shear strains level. For instance, in the pile systems with the 2 layer soil profile, the maximum shear strain reached is 3% with Dr=40%. In the rigid inclusion cases this value is equal to 2.5%. In the soil layer with Dr=80%, these values are decreased almost 10 times (Fig. 6.10a). The influence of the peak acceleration is noted for small shear strains at 1 m depth where the decrease acceleration occurs.

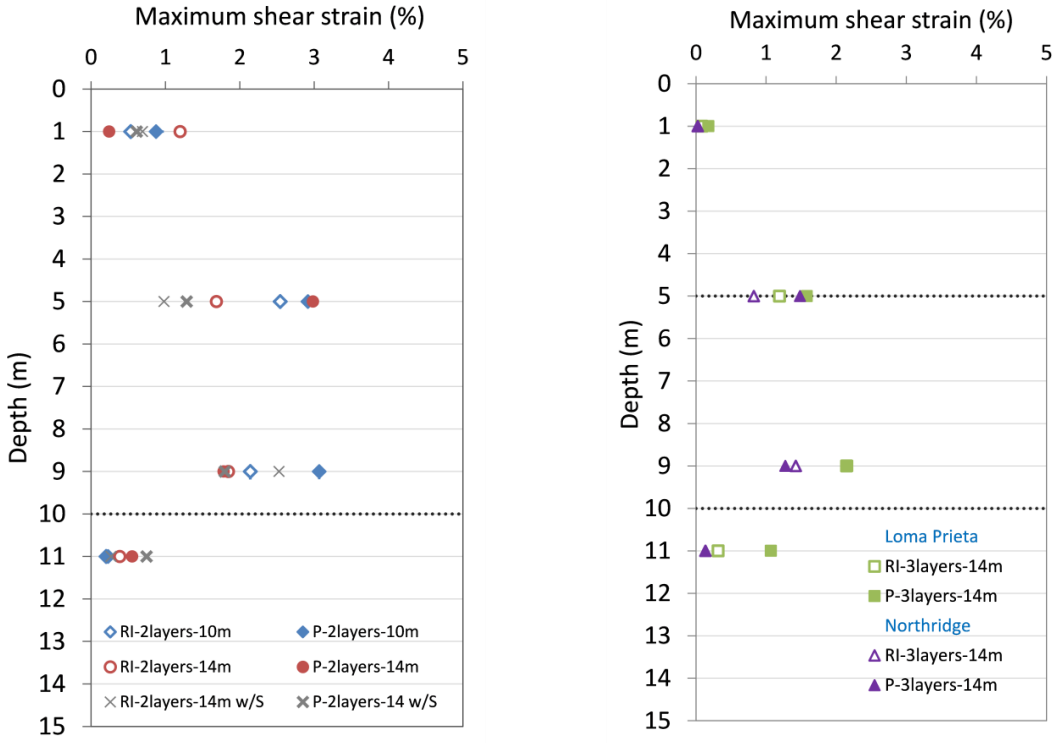

a) 5-storey Building **b)** 3, 5 and 7-storey Buildings

Fig. 6.10 Maximum shear strain in the analyzed systems for different soil profiles and earthquakes.

It can be seen in Fig. 6.10b that the values of shear strain are greater in the liquefiable layer (5 m to 10 m). These values decrease when the predominant earthquake frequency is increased (same peak acceleration) as presented by Haldar and Babu (2010).

1.6.3. Rigid Vertical Element Response

1.6.3.1. Bending Moments

The maximum bending moment values obtained in the pile and rigid inclusion elements with the 2 layers soil profile are shown in Fig. 6.11a. It is noted that the bending moment values in the pile heads

are important due to the fixed connection with the foundation slab. This condition amplifies the inertial forces, which are predominant forces before liquefaction (Ishihara 1997). In the inclusion cases, these values are null because of the presence of the earth platform.

As expected, high moments near the piles head of the piles are not present in the systems that do not consider a superstructure. However, the values in the bottom part remain almost equal, which means that the kinematic forces developed in the systems with and without structure are similar as confirmed by Rahmani and Pak (2012).

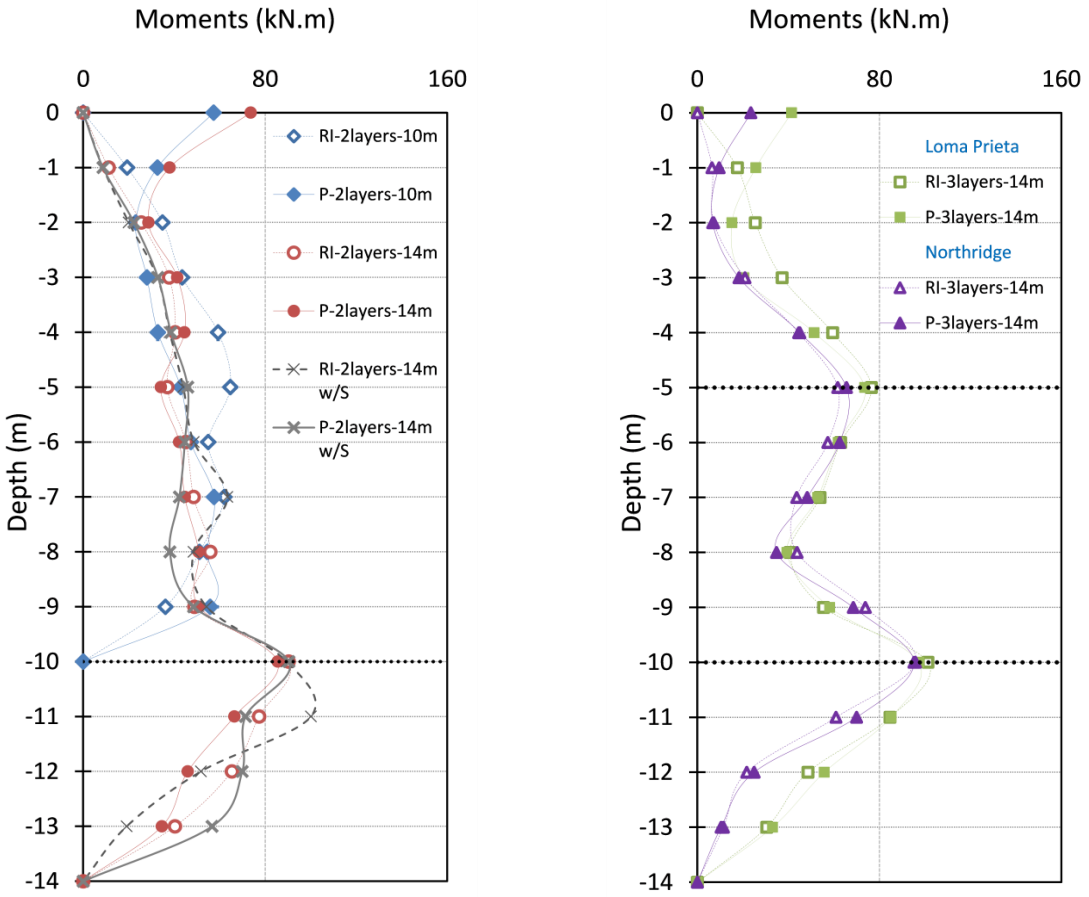

a) 5-storey Building **b)** 5-storey Building

Fig. 6.11 Bending moments in rigid inclusion and pile systems for different soil profiles and earthquakes.

Fig. 6.11a shows the systems considering the 14 m long rigid elements in the 2 layers soil profile. The maximum bending moment values are obtained at the intersection of the liquefiable and non-liquefiable soil (at 10 m depth). This is in good agreement with the results presented by Finn and Fujita (2002), Rahmani and Pak (2012), Phanikanth et al. (2013), Choudhury et al. (2014) and Janalizadeh and Zahmatkesh (2015). The bending moments presented at the intersection are equal to 91 kN.m for both RI-2layers-14m and P-2layers-14m cases. Comparing the systems with 10 m and 14 m element length, it can be concluded that the pile length has a small influence in the position of

bending moments along the rigid elements. However, it can be noted that the values from 2 to 5 m depth in the RI-2layers-10m are greater (of 42% to 55%) than the values in the P-2layers-10m. In the cases of 14 m elements, the maximum difference reaches 50% at 12 m depth (Fig. 6.11a).

For the 14 m length pile elements in the three layers soil profile, as the thickness of the liquefiable layer (5 m) is greater than one-third but less than two-thirds of the total thickness (15 m) of the soil deposit, the maximum moments are presented (in most of the cases) at the interface of liquefiable and non-liquefiable soil layers otherwise the maximum moment is in the head of the element (Liyanapathirana and Poulos 2005). When the pile head is free, the maximum bending moment is always located at the interface of soil layers. These peak values are mainly due to the kinematic forces and are similar in the pile and inclusion cases (Fig. 6.11b). Comparing the bending moments along the rigid inclusion and pile systems, Fig. 6.11b shows that the P-3layers-14m system induces smaller values (from 22% to 51%) than the RI-3layers-14m with the Loma Prieta earthquake at 2 to 4 m depth. The other values are similar along the elements.

It is noted that the frequency of excitation has an important effect on the response of the rigid elements. The increase of the frequency implies a decrease of respectively 17% to 45% in the bending moment values for the RI-3layers-14m and P-3layers-14m. Analogous results were obtained by Liyanapathirana and Poulos (2005) and Rahmani and Pak (2012).

1.6.3.2. Normal Forces

Fig. 6.12 shows the maximum normal forces in the rigid elements computed for all the analyzed cases. The normal forces in the rigid element decrease with depth. The normal forces in the pile cases are greater than the rigid inclusion ones at the head of the elements. The inertial forces are reduced in the rigid inclusion systems because there is no connection with the foundation slab. For instance, the normal force in the P-2layers-10m case is 14% greater than the RI-2layers-10m case. In the systems with 14m long elements, this difference reaches 32%. As expected and due to the inertial forces, in the system without the superstructure the normal forces are smaller.

It can be observed that a longer foundation element produces larger normal forces (Fig. 6.12a). Longer rigid elements have higher contact surface with the surrounding soil which enables them to absorb more energy, mainly when the liquefaction occurs. In the liquefiable soil, the values along the elements in the RI-2layers-10m case are approximately 26% larger than in the P-2layers-10m case. However, in the cases with the 14 m rigid element cases the values of the piles cases are greater than the ones of the rigid inclusion systems. The normal forces along the P-2layers-14m case are 5% greater than RI-2layers-14m at 2 m depth and reduced of 1% at 10 m depth.

Such as in the case of bending moments, as the input motion frequency increases, the normal forces are reduced in both pile and rigid inclusions cases (Fig. 6.12b). In the RI-3layers-14m case, the difference is almost uniform (26%) from the rigid inclusion head to 10 m depth for the Loma Prieta and Northridge earthquakes. For the P-3layers-14m case, the same difference is 74% in the pile head and is reduced to 46% at 10 m. Therefore, the natural frequency of an earthquake can be considered as an important parameter for characterizing the pile behavior.

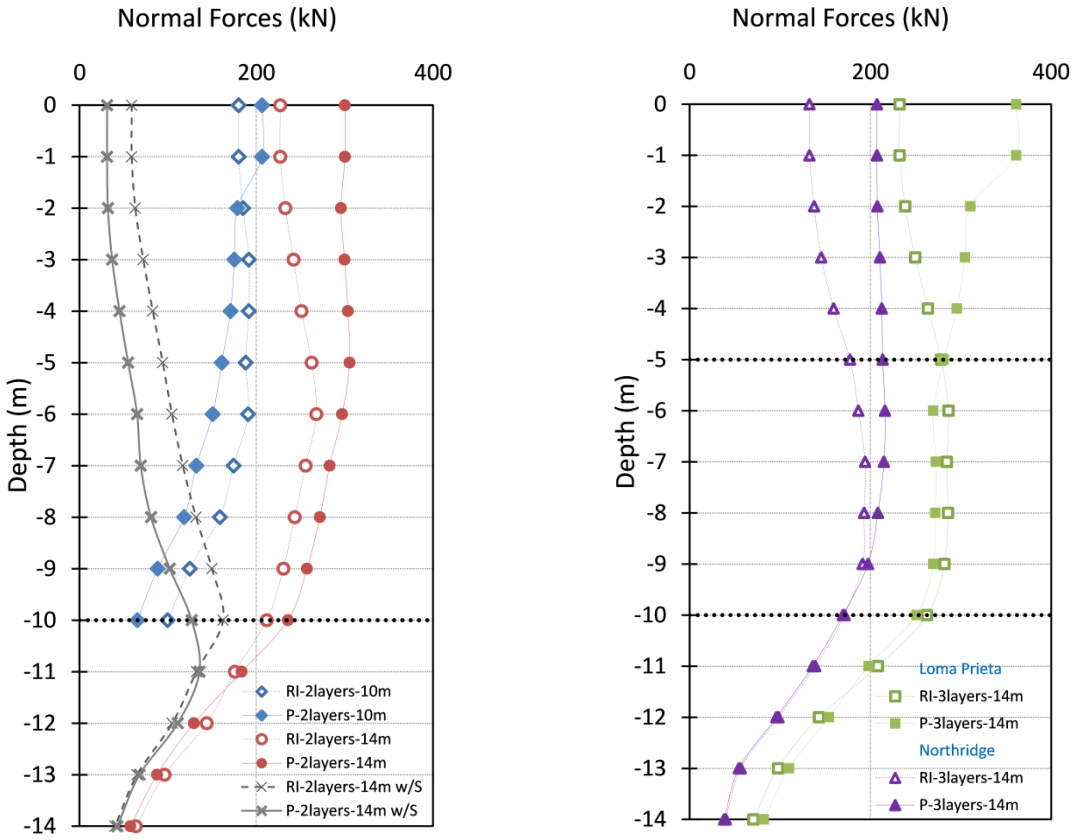

a) 5-storey Building **b)** 5-storey Building

Fig. 6.12 Normal forces in rigid inclusion and pile systems for different soil profiles and earthquakes.

1.6.3.3. Pile Failure Modes

Based on the efforts presented in the previous section, the bending and buckling failure modes are presented. The bending failure takes place when the maximum bending moment in the pile exceeds the yield moment of the pile section ($M_{max}/M_y \geq 1.0$). The considered yield bending moment value of the pile section is equal to 78 kN.m (calculated from the moment curvature relationship of the reinforced concrete section). On the other side, the buckling failure occurs when $P/P_{cr} \geq 0.33$.

Fig. 6.13 shows the relation of M_{max}/M_y and P/P_{cr} ratios for all cases. The figure is divided in four zones as showed in Table 6.7 depending on the type of failure: bending, buckling, or combined effects. It is important to mention that the liquefiable soil thickness and the pile boundary condition have a great influence in the failure mode developed in the rigid elements. For instance, the rigid inclusion cases analyzed in the 2 layers soil profile are more susceptible to create a buckling instability compare to the pile systems. The free-head boundary conditions increase the effective length of the inclusions in a liquefiable zone. Despite the fact that the P/P_{cr} ratio is high enough to produce buckling in the RI-2layers-14m case with and without superstructure, the rigid elements present greater moments than the yield bending moments which makes it susceptible to fail in combined bending-buckling failure modes.

Table 6.7 Rigid element failure modes

Cases		Failure type
$M_{max}/M_y \geq 1.0$	$P/P_{cr} < 0.33$	Bending
	$P/P_{cr} \geq 0.33$	Bending-buckling interaction
$M_{max}/M_y < 1.0$		Buckling instability
	$P/P_{cr} < 0.33$	Safe

As in the 3 layers soil profile, the thickness of the liquefiable soil layer is reduced to 5 m, the elements do not present buckling instability. However, pile and rigid inclusion foundation may collapse by forming a plastic collapse mechanism. This failure takes place due to the imposed moment exceeding pile bending strength (yield bending moment) of the element under consideration. This inability of the rigid elements to sustain such large bending moments may trigger failure during important earthquakes (Kagawa 1992). The P-2layers-10m case is the only system that lies in the safe zone.

To know if pile are unsafe against bending mode or buckling instability, a limit analysis can be made, however, it does not provide any information about the dominant failure mode as presented by Abdoun et al. (2003).

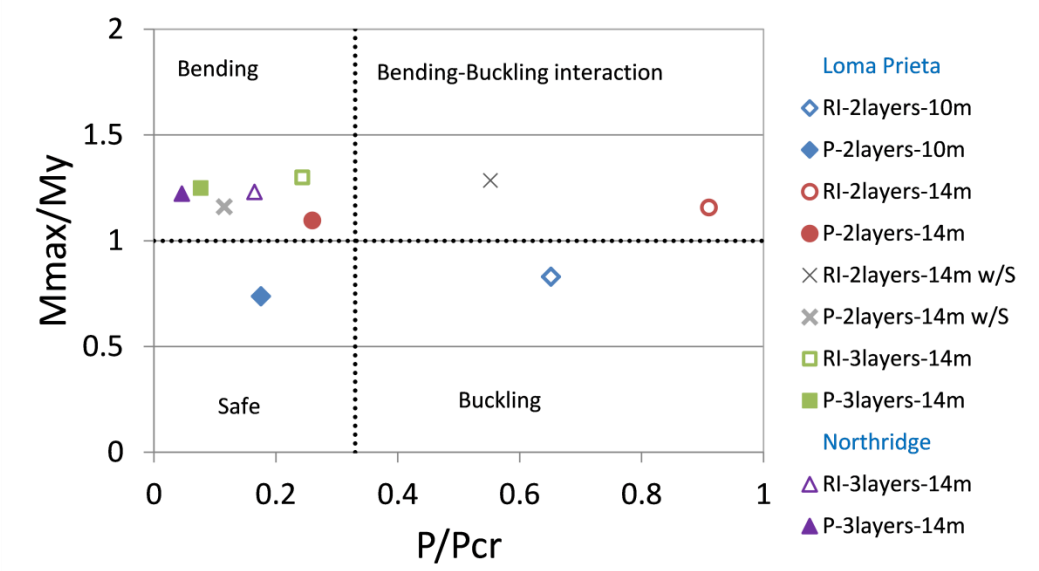

Fig. 6.13 Pile failure modes in the analyzed systems for different soil profiles and earthquakes

1.6.3.4. Displacements

Fig. 6.14 shows the horizontal displacements in the rigid elements for all the analyzed cases. The maximum displacement in the inclusion and pile head is respectively equal to 0.29 m and 0.27 m. It can be noted that the displacements decrease with depth in the rigid elements as stated by other authors (Liyanapathirana and Poulos 2005, Choudhury et al. 2014). Due to the similarity of results for the maximum displacements along the piles and rigid inclusions systems in the 2 layers soil profile, it can be concluded that the pile length and the consideration of the superstructure has no influence on the level of displacements when the liquefaction is developed in the soil.

In accordance with the bending moments developed in the rigid elements, the displacements in the RI-3layers-14m and P-3layers-14m systems decrease as the frequency of excitation increases (Fig. 6.14b). The displacements in the upper part of the RI-3layers-14m are 5% greater than in the RI-3layers-14m ones. When the analyzes are carry out with the Northridge earthquake, the values in the RI-3layers-14m case are reduced of 71% and of 68% in the P-3layers-14m system (Loma Prieta earthquake).

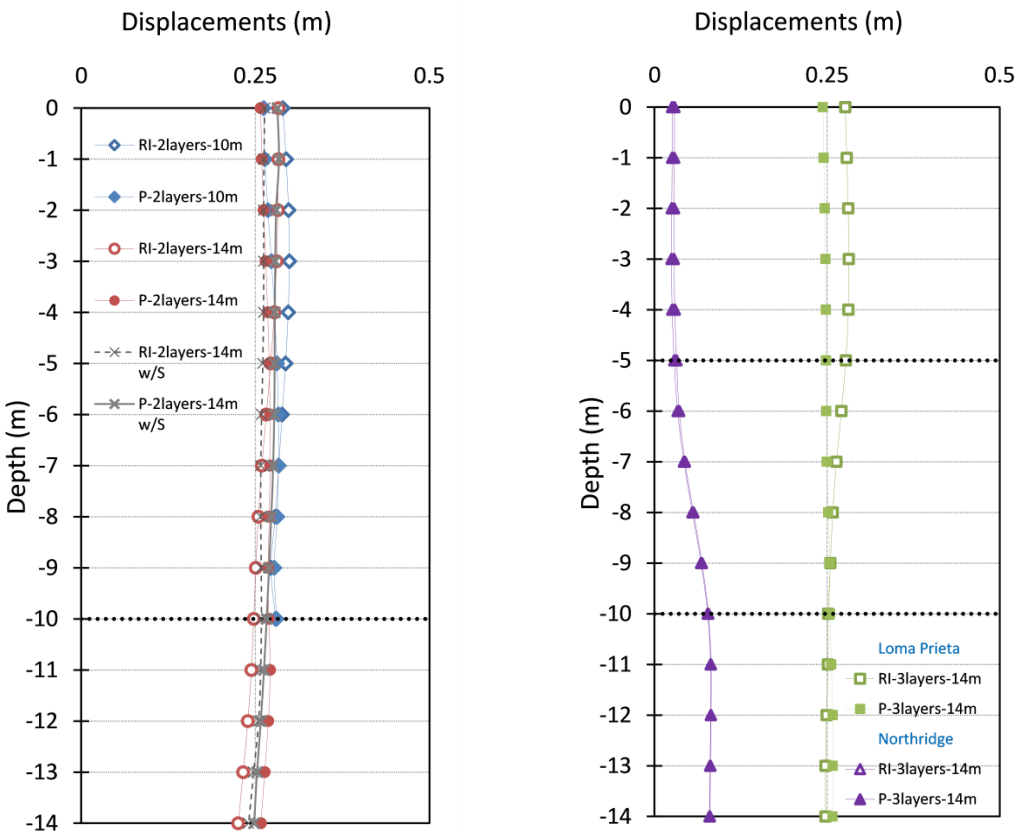

a) 5-storey Building **b)** 5-storey Building

Fig. 6.14 Displacements in the rigid inclusion and pile systems for different soil profiles and earthquakes.

1.7. Preliminary Conclusions

The first part of this Chapter examines the seismic response of soil-inclusion-platform-structure and soil-pile-structure systems under some important parameters (soil profile, pile length and frequency of input motion) considering liquefiable and non-liquefiable sand layers. Two different soil profiles and pile lengths were considered. The behavior of the Nevada sand is represented by the Finn constitutive model. The analysis was carrying out using dynamic coupled fluid-mechanical simulations. Two benchmark earthquakes were used to study the influence of the different frequency excitations.

The response spectra of the analyzed systems are reduced because there is a decrement of the surface accelerations records respect to the input record applied in the bottom. The liquefied soil layer attenuates the energy as the motion propagates to the surface.

The consideration of the SSI reduces the shear forces in the superstructure compare to the fixed-base case. The shear forces in the building with pile systems are greater than the rigid inclusion ones with the same soil profile and pile length.

In general, the values of excess pore water pressure ratio in the systems with rigid inclusions are greater than in the pile systems. The consideration of the building increases the excess pore pressure values at the top of the model compare to the model without superstructure. However, this influence decreases for deeper areas. As the frequency of excitation increases, the values of the excess pore pressure ratio increase.

The bending moments and normal forces values in the pile heads are important due to the fixed connection with the foundation slab that amplifies the inertial forces. They are predominant forces before liquefaction. An advantage of the rigid inclusion cases is that these values are importantly decreased because of the presence of the earth platform. The high values of moments near the pile heads are not present in the systems which do not consider a superstructure. However, due to the kinematic forces, these values remain almost equal in the bottom part, considering or not the structure. The increase of the frequency of excitation implies a decrease of the bending moments, normal forces and displacements.

For the 2 layers soil profile, the effective length of the rigid elements in a liquefiable layer is increased in the rigid inclusion systems (due to the pile tip and head boundary conditions) making possible to reach the buckling instability easily compare to the pile cases, When the liquefiable soil thickness is reduced such as in the 3 layers soil profile, the failure takes place due to the fact that the resulting moments exceed the pile bending strength.

2. Effect of the Soil Relative Density and Frequency of Input Motion

2.1. General

As a complement of Section 1, this section is principally devoted to study the effect of relative density in the seismic analysis of pile and inclusions systems. The influence of the frequency of the seismic loading and pile length are also considered. In this part, the SANISAND constitutive model was utilized to represent the behavior of the liquefiable soil layer. This model predicts with accuracy the soil response for various soil densities, stress levels and loading conditions. Undrained analysis and water level at ground surface were considered. Different relative density values of the sand layer were considered. The linear elastic perfectly plastic constitutive model with a Mohr-Coulomb failure criterion was used to represent the behavior of the non-liquefiable soil layers. Different relative density values of the sand layer were considered. The same two earthquake signals considered in the Section 1 of this Chapter were used to compare the response with different earthquake frequencies.

2.2. Characteristics of the Numerical Model

The soil volume, platform and superstructure dimensions, boundary conditions and soil mesh are considered the same as in Section 1 of this Chapter. However, the analyses are carried out considering a soil profile that is composed of 3 layers of 5 m each, where the layer in between corresponds to the liquefiable sand and the other layers are not liquefiable layers (Fig. 6.15). The upper layer corresponds to an alluvial soil and the lower layer corresponds to the bedrock (Barrero, Taiebat, and Lizcano 2015). The water table is located at the surface ground level. The properties of the different layers are shown in Table 6.8. The behavior of the non-liquefiable soils is represented by the elastic perfectly plastic model with a Mohr-Coulomb failure criterion and the one of the liquefiable soil with the SANISAND constitutive model (Dafalias and Manzari 2004). This model has shown the ability to reproduce a series of monotonic and cyclic tests on Nevada sand (Arulmoli et al. 1992, Shahir and Pak 2010). The material parameters of the Nevada sand required by the model are displayed in Table 6.9 (Taiebat et al. 2010, Rahmani et al. 2012), divided into six categories based in their different functions. Relative densities (Dr) of 40%, 55% and 80% are considered as input parameters of the Sanisand constitutive model (liquefiable sand).

The liquefiable layer (SANISAND model) is considered using a low Rayleigh damping of 0.5% to reduce the high frequency noises (Cheng et al. 2013, Barrero et al. 2015). However, for the elements where the Mohr-Coulomb constitutive model is implemented a Rayleigh damping with a ratio of 5% for a central frequency equal to 2.75 Hz is used. This frequency corresponds to the first soil deposit mode (Idriss et al. 1975, Suwal et al. 2014).

Table 6.8 Soil material properties (Haldar and Babu 2010, Barrero et al. 2015)

Soil Layer	Alluvial	Liquefiable Sand	Bedrock
Density, ρ_{sat} (kg/m³)	2020	1962	2373
Poisson's ratio, ν	0.26	0.45	0.31
Shear modulus, *G* (kPa)	1.99 x10^5	2.7 x10^4	1.15 x10^6
Cohesion, c (kPa)	0	0	0
Friction angle, ϕ (°)	35°	33°	40°

Table 6.9 Material parameters used in SANISAND constitutive model of the Nevada Sand (Taiebat et al. 2010, Rahmani et al. 2012)

Parameter function	Elasticity		Critical state					Dilatancy		Kine matic	Hardening		Fabric dilatancy	
Index	G_0	ν	M	c	λ_c	e_0	ξ	A_0	n^d	n^b	h_0	c_h	Z_{max}	c_z
Value	150	0.05	1.14	0.78	0.027	0.83	0.45	0.81	1.05	2.56	9.7	1.02	5.0	800

The 12 rigid elements (pile or rigid inclusions) embedded in the soil deposits were modelled in the same way as in Section 1.2.2 of this Chapter. However, in this section any mesh refinement around the pile was considered accepting some loose of accuracy (stresses and strains). With the purpose of comparing how the physical cross section influences the generation of pore pressure in the analyzed systems, some calculations were developed with the hybrid technique described in Section 1.4.2 Chapter 3. The consideration of this modelling technique to model the pile or rigid inclusion elements implies a reduction of the time step, leading to a computation time increase.

The use of the SANISAND constitutive model is compared in some calculations with the simpler Finn constitutive model (Martin et al. 1975). The details of the Sanisand and Finn model formulation are displayed in Section 4.3 and 4.4 Chapter 2. The material properties for the Nevada sand (Dr=40%) to use the Finn constitutive model are displayed in Table 6.1 (Section 1.2.1 of this Chapter).

The analyzed systems were subjected to the same records (Loma Prieta 1989 and Northridge 1994 earthquake motions) with the same characteristics as in Section 1.3 of this Chapter.

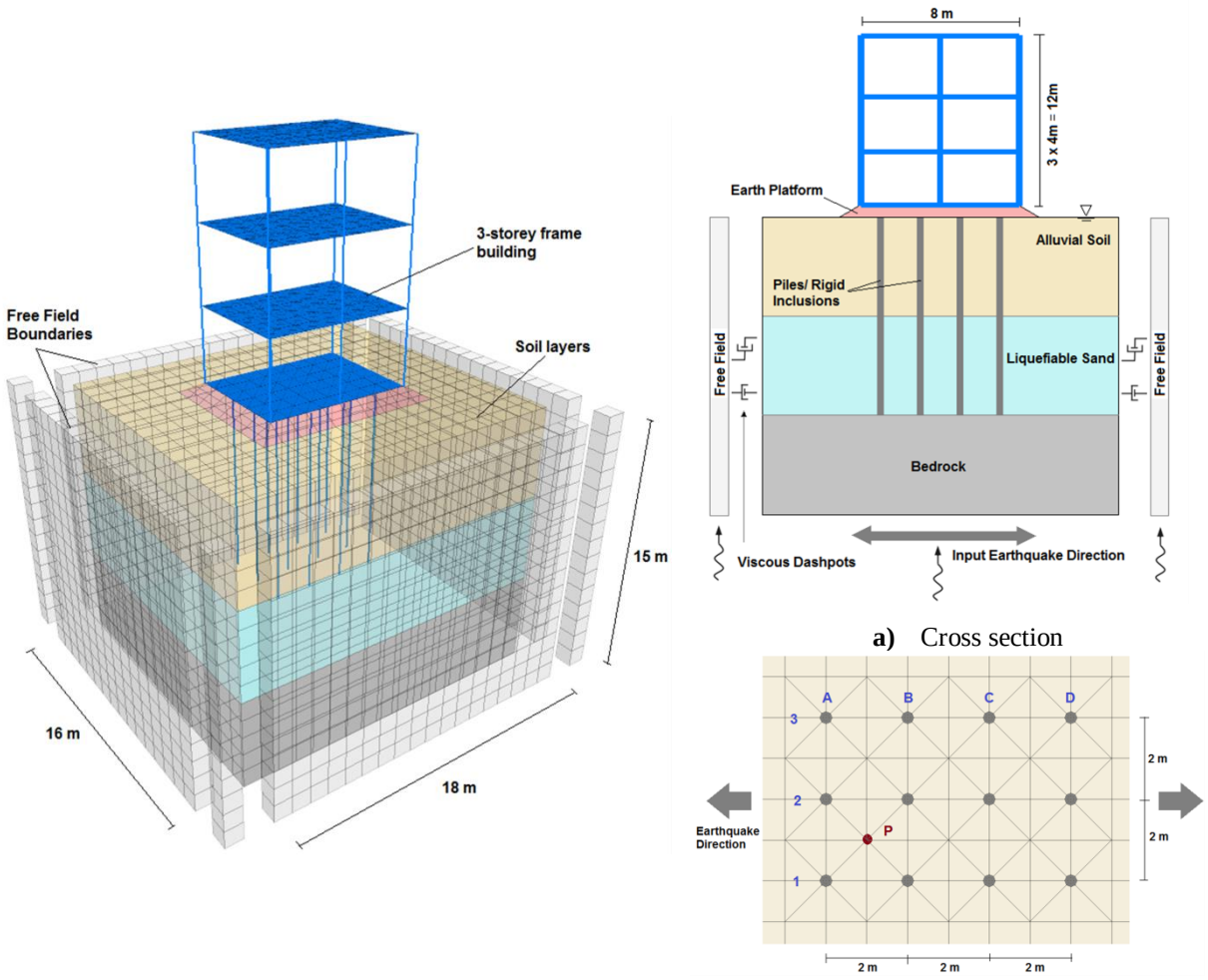

a) Cross section

b) 3D view

c) Plan view of the location of the rigid elements

Fig. 6.15 Geometry of the numerical model

2.3. Numerical Cases

Table 6.10 displays the soil-pile-structure and soil-inclusion-platform-structure cases analyzed. The cases are represented schematically in Fig. 6.16 and Fig. 6.17. The name of each case has two terms, the first term (RI or P) refers to Rigid Inclusion or Pile case, the second one indicates the rigid element length (10 m or 14 m). The term w/S refers to cases without structure. For comparison, a case with the Finn constitutive model for the liquefiable sand layer was also analyzed. This case will be identified with an additional term (F) in its name. As mentioned before, the modeling of reinforced elements was developed with the only beam structural element technique for all cases. Additionally, some cases were analyzed with the hybrid technique (*). The time calculation for the first one is around 23 hours and for the systems that consider hybrid modelling was around 180 hours for each case. Section 1.5 Chapter 3 to consult the computer characteristics.

Table 6.10 Characteristics of the analyzed cases

Rigid elements	Name of Case	Pile Length (m)	Structure	Liquefiable soil		Earthquake
				Constitutive model	Dr	
Rigid inclusions systems	RI-10m*	10	Yes	SANISAND	40, 55, 80%	Loma Prieta/Northridge
	RI-10m w/S	10	No		40%	Loma Prieta
	RI-14m*	14	Yes		40%	Loma Prieta/Northridge
	RI-10m-F	10	Yes	Finn	40%	Loma Prieta
Pile systems	P-10m*	10	Yes	SANISAND	40, 55, 80%	Loma Prieta/Northridge
	P-10m w/S	10	No		40%	Loma Prieta
	P-14m*	14	Yes		40%	Loma Prieta/Northridge
	P-10m-F	10	Yes	Finn	40%	Loma Prieta

* Cases analyzed additionally with the hybrid technique to model the pile or inclusion.

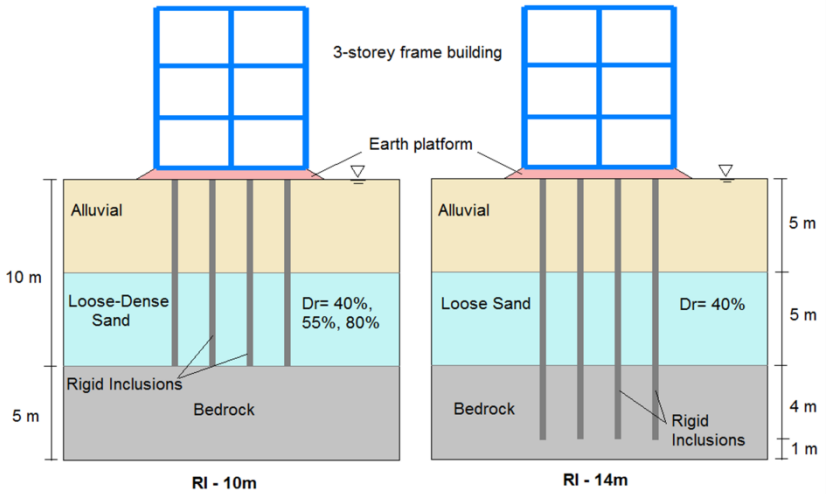

Fig. 6.16 Soil - rigid inclusions - earth platform - structure analyzed systems

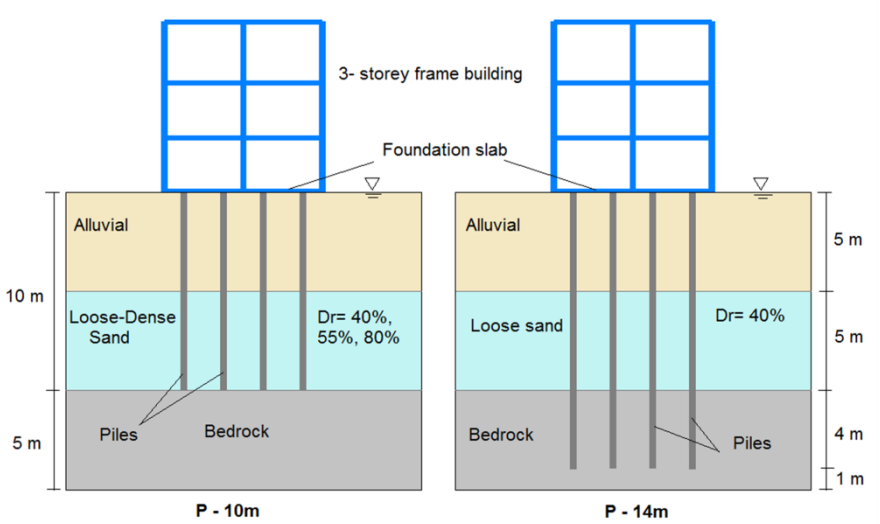

Fig. 6.17 Soil - piles - structure analyzed systems

2.4. Procedure of Analysis

The procedure of analyses is similar to the one of Section 1.5 of this Chapter. The dynamic analysis is performed as a coupled simulation (fluid and mechanical interaction). At this stage, a realistic value of the water bulk modulus (2 GPa) and realistic permeability coefficient are given. These coefficients are $6.6x10^{-5}$, $6.05x10^{-5}$ and $3.7x10^{-5}$ m/s for the Dr=40%, 55% and 80% respectively.

2.5. Results and Comparisons

Similar as in Section 1 of this Chapter, the response of the soil, structure and pile or inclusion foundation was evaluated displaying maximum strains, pore pressure, accelerations, effort and displacements recorded during dynamic calculation. The response of the soil is referred to the point P and the one of the rigid elements to the element positioned in the axes A-1. Both axes and point can be consulted in Fig. 6.15c.

2.5.1. Structure Response

2.5.1.1. Response Spectrum

Confirming the results of the Section 1.6.1.1 of this Chapter and the results obtained by Tokimatsu et al. (2005), Montoya-Noguera and Lopez-Caballero (2016) and Ramirez et al. (2018), Fig. 6.18a shows a reduction of acceleration spectra (due to the energy attenuation in the liquefied layer) as the motion travel from the base (bottom of the model) to the ground surface in all analyzed cases. It is noticeable in Fig. 6.18a that the response spectrum of the systems evaluated with the Finn models are greatly decreased in lower and large periods compare to the systems that use Sanisand model.

The response spectrum increases when the relative density of the sand layer is increased and the attenuation given by the liquefaction triggering is reduced (Fig. 6.18b). However, there is still some attenuation caused by the soil resistance degradation due to the induced shear strains (Kramer et al. 2011).

For the soil deposit considered in this section and in accordance to the results shown in the Section 1, the increment of the earthquake frequency implies a decrease in the response spectrum (Fig. 6.18c).

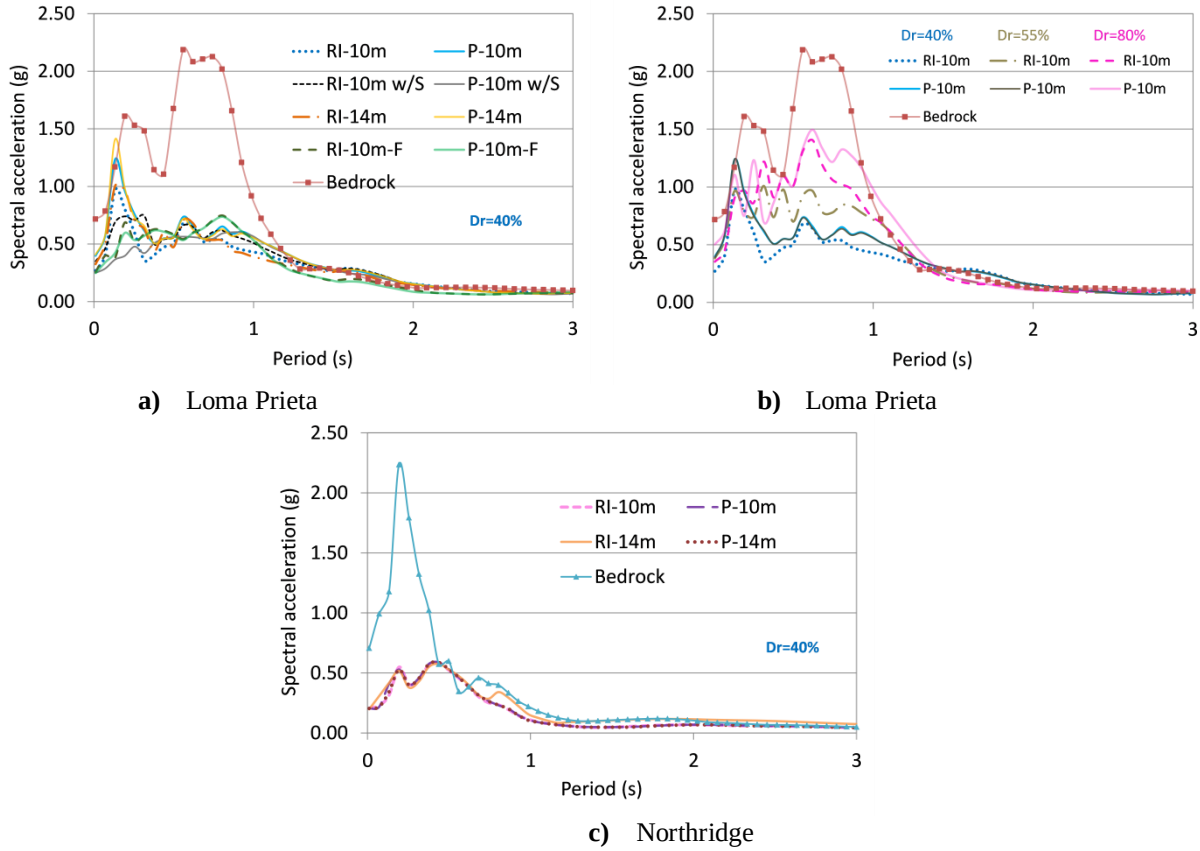

a) Loma Prieta **b)** Loma Prieta

c) Northridge

Fig. 6.18 Acceleration response spectrum of the analyzed systems for different conditions and earthquakes.

2.5.1.2. Shear Forces in the Superstructure

To examine how the pile or rigid inclusion foundations influence the amount of energy absorbed by the structure, the structural shear forces are compared for the different cases in Fig. 6.19. The shear forces in the building were obtained as in Section 1.5.2 Chapter 5. The building founded on piles absorbs more seismic energy than the one founded in rigid inclusions due to the fixed-head connection with the slab foundation (Fig. 6.19a).

The shear forces in the building of the systems analyzed with the Loma Prieta earthquake are larger than the ones with the Northridge earthquake using the same characteristics (Fig. 6.19a, b). The

spectrum accelerations in the Loma Prieta case are larger than the calculation with Northridge earthquake for any period.

As expected and in accordance with the spectrum responses, the shear forces are increased as the relative density increases in the pile cases (Fig. 6.19c). However, for the rigid inclusion cases, the shear forces are less influenced by the relative density. The RI-10m case with Dr=40% shows the greater values.

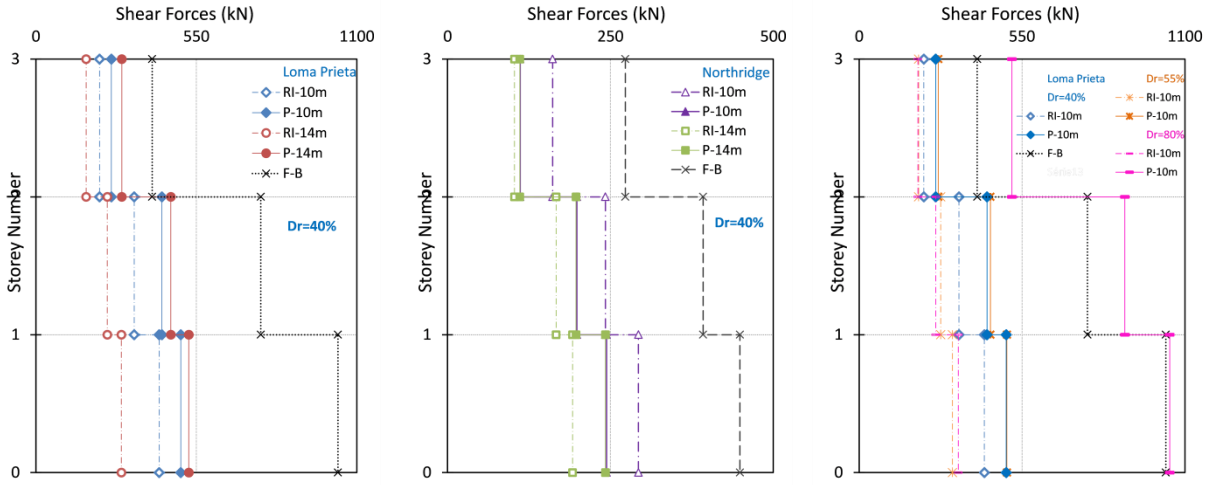

a) Loma Prieta b) Northridge c) Loma Prieta

Fig. 6.19 Maximum shear force distribution on the analyzed systems for different conditions and earthquakes

2.5.1.3. Rocking of Foundation

Considering the definition of rocking as in Section 1.5.3 Chapter 5, Fig. 6.20 displays the maximum rocking in the analyzed systems. The amount of rocking depends on the foundation type supporting the superstructure. The rigid elements are placed or anchored on the bedrock, the axial deformation of the elements and the deformation of the surrounding soil are the main factors which can cause rocking. There is no rocking in the fixed-base structure (F-B). In general, the rocking values in the rigid inclusion cases are greater than in the pile systems with the same pile length and relative density. For instance, the maximum rocking values in the P-10m are respectively equal to 0.15° and 0.47° for the RI-10m with a 40% relative density. For Dr=80%, the same values are obtained, respectively 0.19° and 0.82°. This is because in the pile systems, the building is directly connected to the slab foundation and in the rigid inclusion systems, there is the presence of the earth platform. The rocking in the P-10m system (0.15°) is greater than in the P-14m case (0.11°) with a 40% relative density and the Loma Prieta earthquake. The anchorage on bedrock of the P-14m case reduces the foundation uplift and the settlement values when the compression forces act on the other side of the foundation. A similar behavior is obtained for the systems with the Northridge earthquake. However,

the rocking of the P-10m and P-14m cases analyzed with the Loma Prieta earthquake are 67% and 54% greater than with the Northridge earthquake one.

The rocking values decrease in the systems as the values of relative density decrease. For instance, the rocking values for the RI-10m case with 80%, 55% and 40% of relative density are respectively equal to 0.82°, 0.65° and 0.47°.

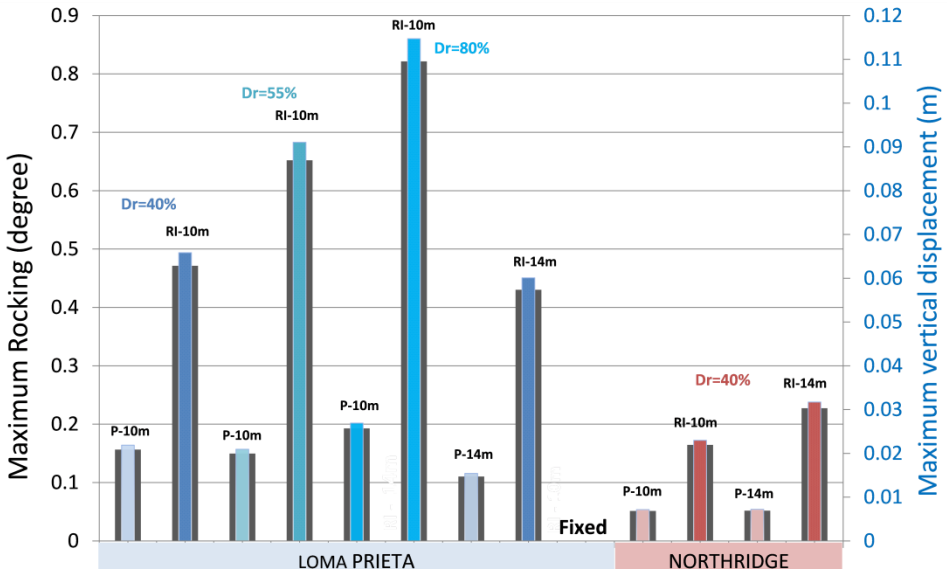

Fig. 6.20 Maximum rocking and vertical displacements for different conditions.

2.5.2. Soil Response

2.5.2.1. Pore Pressure

To study the soil response, the pore pressure time histories computed between the rigid vertical elements at point P (Fig. 6.15c) at two depths (7 m and 9 m) are displayed in Fig. 6.21. Except for the Fig. 6.21e, all the plots shown in this section consider 40% of relative density for the sand layer (at 5-10m depth). The presence of the loose layer causes a stronger contractive response during the dynamic loading which in turns produces a faster increase of the excess pore pressure and a decrement of the vertical effective stress and stiffness. The excess pore water pressure ratio (r_u) and the triggering liquefaction are assumed as in Section 1.6.2.1 of this Chapter

The pile and inclusion cases analyzed with Dr=40% for the liquefiable soil layer under the Loma Prieta earthquake are shown in Fig. 6.21a, b. It is clear from these figures that there is a greater increment in excess pore pressure in the P-14m case compared to the P-10m one. It is also noticeable that this increment is more pronounced in the rigid inclusion cases than in the pile ones. After the first second of calculation, all the systems experience an important drop of the r_u values even to negative

values (R-10m case in Fig. 6.21a). These drops in excess pore pressure are due to the excessive dilatation tendency of the SANISAND model (Taiebat et al. 2010, Ramirez et al. 2018).

Fig. 6.21c, d show the impact of the excitation frequency in the development of liquefaction at different depths. It can be noted that the excess pore pressure ratio values of the pile or inclusion systems with the Northridge earthquake (4 Hz) are smaller than with the Loma Prieta earthquake (1.35 Hz), except for the RI-10m case at 7m depth (Fig. 6.21c)). For all the analyzed cases under the Northridge earthquake, the drops in r_u values are importantly reduced compare to the ones with the Loma Prieta earthquake. It is important to note that in the cases analyzed with the Northridge earthquake, the drops in excess pore pressure were highly decreased.

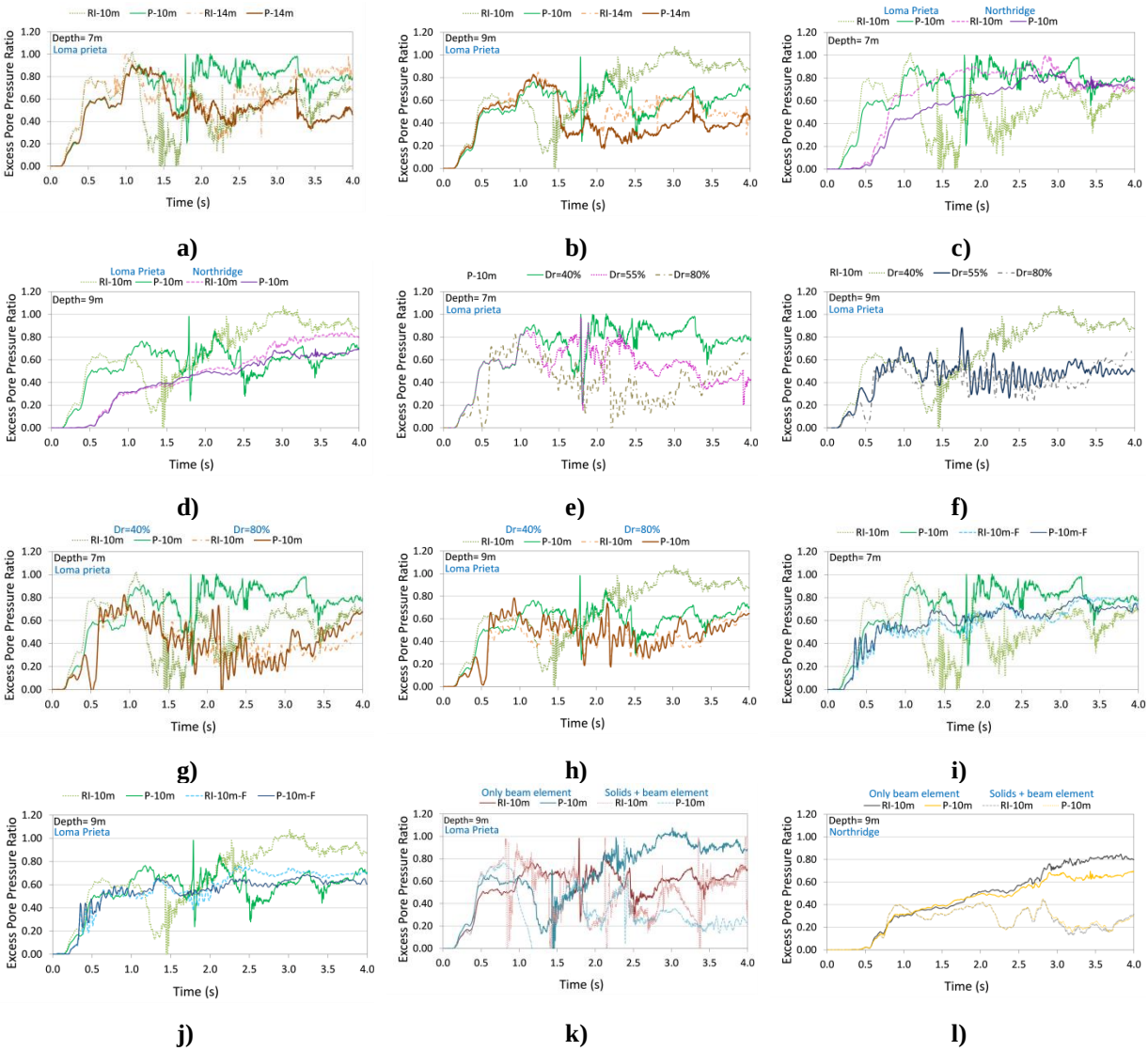

Fig. 6.21 Excess pore pressure ratio time histories in the analyzed systems at different depths.

Fig. 6.21e presents the excess pore pressure ratio histories for the P-10m case with different Dr values of the sand layer (at 7 m depth). As expected, the r_u values increase as the relative density

value decreases. Only the cases analyzed with Dr=40% and 55% induce a true liquefaction. The system analyzed with Dr= 80% shows an important delay in the pore pressure development compared to the cases with lower relative densities. A similar behavior is shown in Fig. 6.21f for the RI-10m at 9 m depth. In this case, only the Dr=40% case implies a true liquefaction. Other comparisons of pile and rigid inclusion systems with the 40% and 80% relative density at 7 m and 9 m depth are respectively displayed in Fig. 6.21g and h.

The generation of excess pore pressure in the numerical calculations developed with the SANISAND model are compared to the ones obtained with Finn model in Fig. 6.21i, j. The generated results of excess pore pressure in the P-10m system at 9 m depth with the SANISAND and Finn model are similar, but not for the RI-10m case (Fig. 6.21j). Nevertheless, for the analyzed cases at 7 m depth, the systems analyzed with the SANISAND model got true liquefaction while the cases analyzed with the Finn model get a maximum value of r_u equal to 0.8 (Fig. 6.21i). This could be due to the limitations of the Finn model which cannot correctly reproduce the cyclic mobility response mechanisms and the associated pattern of shear strain accumulation or due to the fact that the rearrangement of particles cannot be considered (Elgamal et al. 2002, Boulanger and Ziotopoulou 2013, Wang et al. 2014, Tasiopoulou and Gerolymos 2016). It can be noted that at the beginning of the curves in Fig. 6.21h, j, the generation of excess pore pressure (around 0.2 to 0.4 s) with the SANISAND model is gradual; whereas with the Finn model the rapid changing in pore pressure results in steeper curves which occurs because the pore pressure in this model is updated when a half-cycle is completed (Daftari 2015).

Fig. 6.21k, l show how the consideration of the physical cross section of piles affects the development of excess pore pressures. It is noticeable that during the first second of calculation, the systems in which the piles were modeled with the hybrid method got smaller r_u values compare to the same systems where piles were modelled with only beam elements. However, as the analysis continues, the excess pore pressure values of the cases analyzed with the hybrid method are larger. This could be explained by the fact that the physical cross section of the pile increases the confining pressure.

2.5.2.2. Soil Shear Strain

Fig. 6.22 shows the maximum shear strains values recorded at point P (Fig. 6.15c) at different depths. The maximum values are increase a lot in the two upper layers compare to the values in bedrock. In the upper layer (0-5m depth), the shear strains increase for the rigid inclusion cases compared to the pile cases under the Loma Prieta earthquake (Fig. 6.22a, b). The rigid connection of the piles with the slab foundation or the free condition at the inclusion head seems to have an

important influence on the development of shear strains in the upper part of the model. The shear strains in the liquefiable soil layer analyzed with a 40% relative density are greater for the rigid inclusion cases than for the pile ones (Fig. 6.22a).

It is noticeable from Fig. 6.22b that the increase of soil relative density implies a decrease of the shear strain level. Similar results were obtained by Haldar and Babu (2010). For instance the maximum shear strain reached in the RI-10m with a Dr=40% is around 3%, which is reduced of 1.1% for the case with Dr=80%. For the P-10m case the values are respectively reduced from 2.3% to 0.85% for Dr=40% and Dr=80%.

As in the Section 1.6.2.2 of this chapter, it is evident that the shear strain values decrease when the predominant frequency of the input motion is increased (Fig. 6.22a,c).

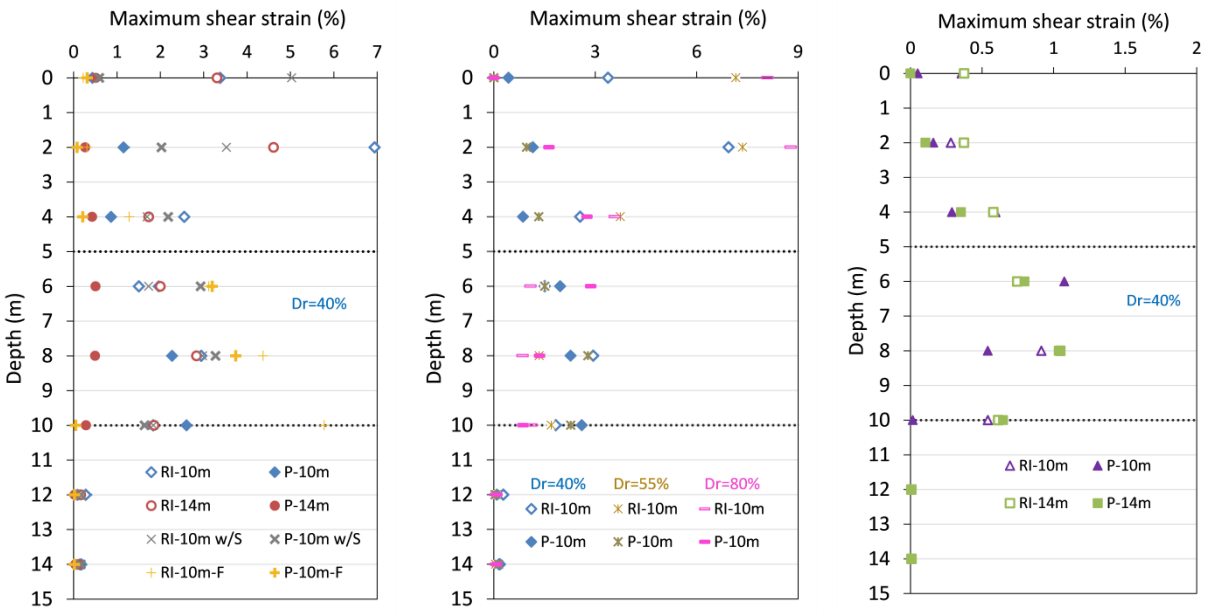

a) Loma Prieta **b)** Loma Prieta **c)** Northridge

Fig. 6.22 Maximum shear strain in the analyzed systems for different conditions and earthquakes.

2.5.3. Rigid Vertical Element Response

2.5.3.1. Bending Moments

Fig. 6.23 displays the maximum bending moment distribution obtained in the pile and rigid inclusion elements. The influence of the fixed or free-head condition and the consideration of superstructure in the systems is shown in Fig. 6.23a and can be explained in the same way as in Section 1.6.3.1 of this Chapter.

The pile length has a small influence on the repartition of bending moments along the rigid elements in the upper layer (0-5 m depth). However, it can be noted that the moments from 5 to 10 m

depth (except at 6 m depth) are greater for the systems with 14 m rigid elements length (Fig. 6.23a). For instance, at 7 m depth, the moments in the RI-14m are 59% greater than the RI-10m ones. In the pile cases, a difference of 37% is obtained. Similar results can be obtained for the systems analyzed with the Northridge earthquake.

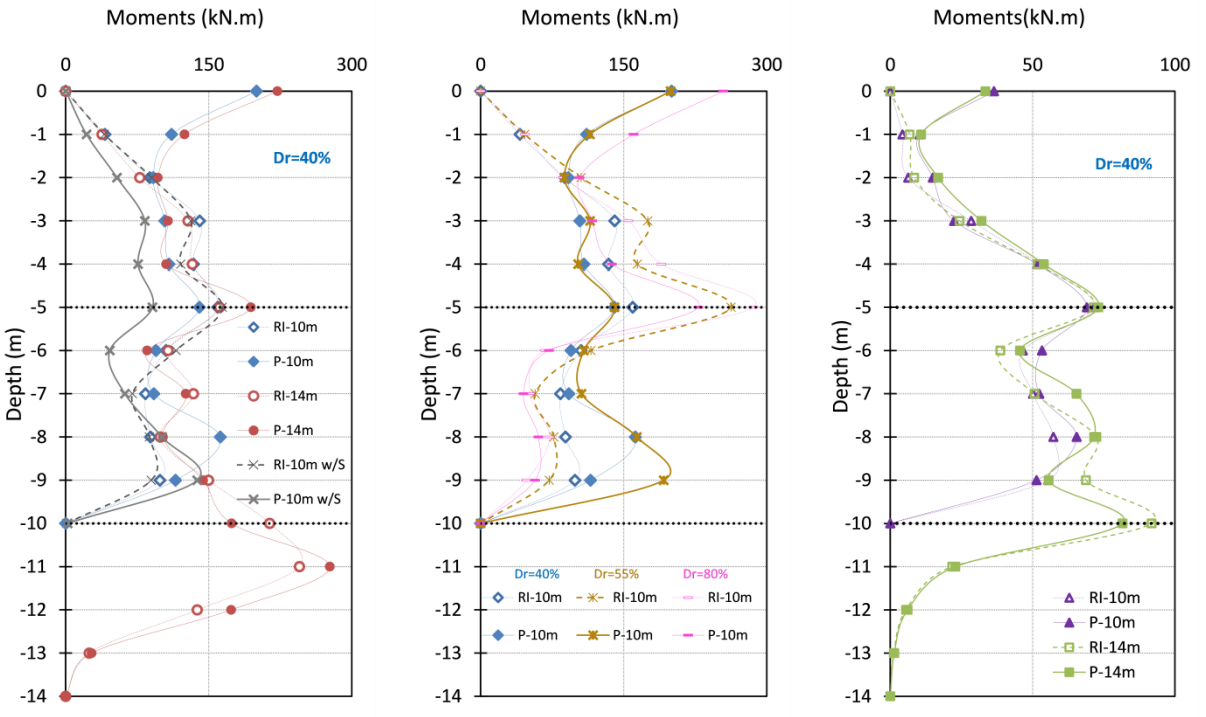

a) Loma Prieta **b)** Loma Prieta **c)** Northridge

Fig. 6.23 Normal forces in rigid inclusion and pile systems for different soil profiles and earthquakes.

For the same reasons as it was presented in Section 1.6.3.1 of this Chapter, the maximum moment (in most of the cases) are located at the interface of the liquefiable and non-liquefiable soils (5 m and 10 m levels). For example, for the case with 14 m rigid elements length, the maximum moments are respectively equal to 245 kN.m and 276 kN.m for the RI-14m and P-14m at 11 m depth in the systems with Dr=40% (Fig. 6.23a). A similar behavior is presented for the cases analyzed with the Northridge earthquake (Fig. 6.23c).

Fig. 6.23b compares the systems analyzed with different relative densities under the Loma Prieta earthquake. In the liquefiable soil layer, the bending moments in the rigid inclusion cases decrease as the relative density value increases. For instance, the moment (88 kN.m) in the inclusion case at 8 m depth with Dr=40% is respectively reduced by 13% and 18% compared to the cases Dr= 55% and 80%. These values are also in accordance with the pore pressure results (Fig. 6.21), which indicates that the pore pressure decrease tends to reduce the pile bending moments (Liyanapathirana and Poulos 2005). However, in the pile case, the bending moments are greater in the system with Dr=55% compare to the cases with other relative density. For example at the 8m depth, the moment (164 kN.m)

in the pile case with Dr=55% is reduced 1% and 62% against the values with 40% and 80% relative density respectively. This tendency is contrary in the upper layer, where the moments in the pile or inclusion systems are greater for a higher relative density. The great influence of the inertial forces in the superstructure increases the shear forces at the base of the building, when the relative density increases (Fig. 6.19b).

The increase of the frequency implies an average decrease of respectively 69% and 67% in the bending moment values for the RI-14m and P-14m cases at different depths. For the RI-10m and P-10m cases, the same differences are respectively of 67% and 65% (Fig. 6.23b, c).

2.5.3.2. Normal Forces

The maximum normal forces along the in the rigid elements are shown in Fig. 6.24. The results displayed in this figure illustrate the impact of the pile type, pile length and the building presence in the development of normal forces in the rigid elements. The normal force distributions and explanations are referred to Section 1.6.3.2 of this Chapter due to the similarity of results.

According to the shear forces developed in the superstructure, the normal forces in the pile cases are greater when the relative density of the liquefiable layer is higher. For instance at 6 m depth, the moment of the P-10m with Dr=80% is reduced of 28% in respect to the systems with 55% and 40% relative density (Fig. 6.24b). This is contrary for the rigid inclusion cases in the liquefiable soil layer. The moment of the RI-10m with Dr=40% is increased of 18% and 32% in respect to the systems with Dr=55% and Dr=80%.

The normal forces are reduced in both pile and rigid inclusions as the input motion frequency increases (Fig. 6.24c). For example, the bending moments along the P-10m with the Northridge earthquake are increased of 36% to 51% compare to the Loma Prieta earthquake. A similar behavior is displayed for the RI-14m case where the increment is from 16% to 29%.

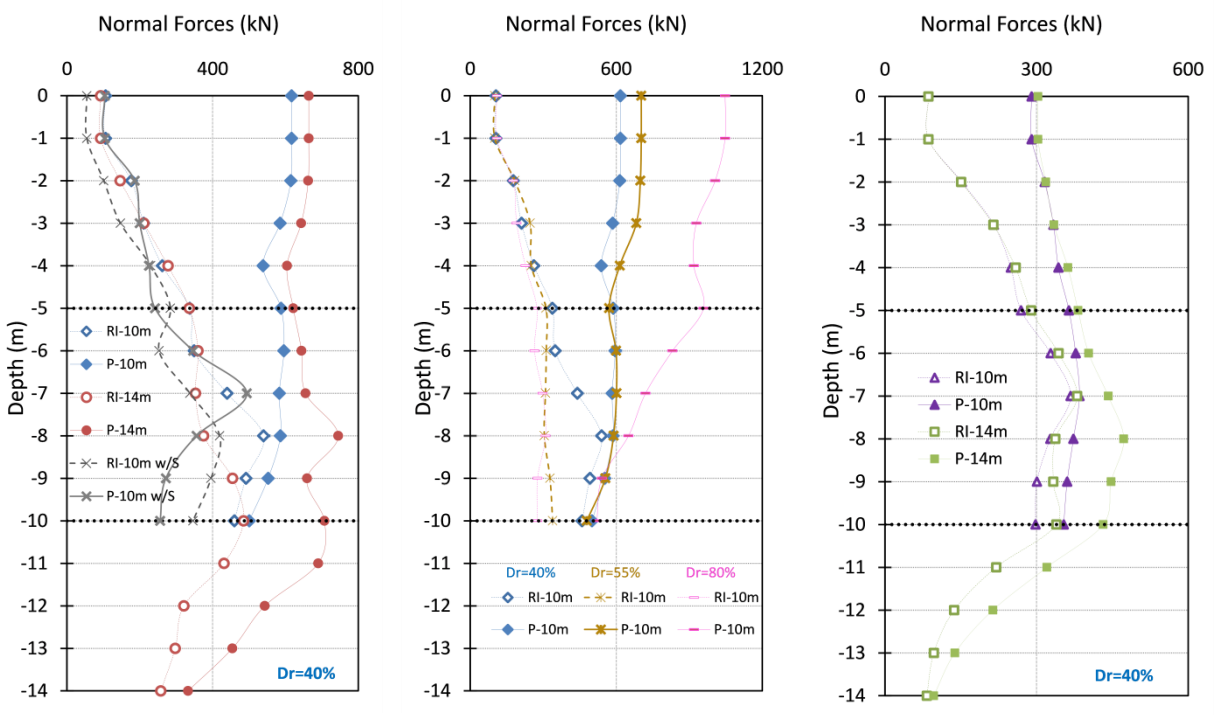

a) Loma Prieta **b)** Loma Prieta **c)** Northridge

Fig. 6.24 Normal forces in rigid inclusion and pile systems for different conditions and earthquakes.

2.5.3.3. Displacements

Fig. 6.25 shows the horizontal displacements in the rigid elements. For all the cases with Dr=40% and the Loma Prieta earthquake (Fig. 6.25a), the displacements are almost similar (0.18 m).

Fig. 6.25b depicts the displacements for different relative densities. The maximum displacement in the pile head are 0.24 m and 0.18 m considering Dr=80% and 40% respectively in the P-10m case. It can be noted that the displacements decreases with depth in the rigid elements as stated by other authors (Liyanapathirana and Poulos 2005, Choudhury et al. 2014).

The displacements in the pile and inclusion systems increased as the frequency of excitation is decreased (Fig. 6.25c). A maximum displacement (0.08 m) of the rigid elements under the Northridge earthquake is obtained in the liquefiable layer. This implies a decrement of about 55% in the Loma Prieta earthquake case for systems with the same characteristics.

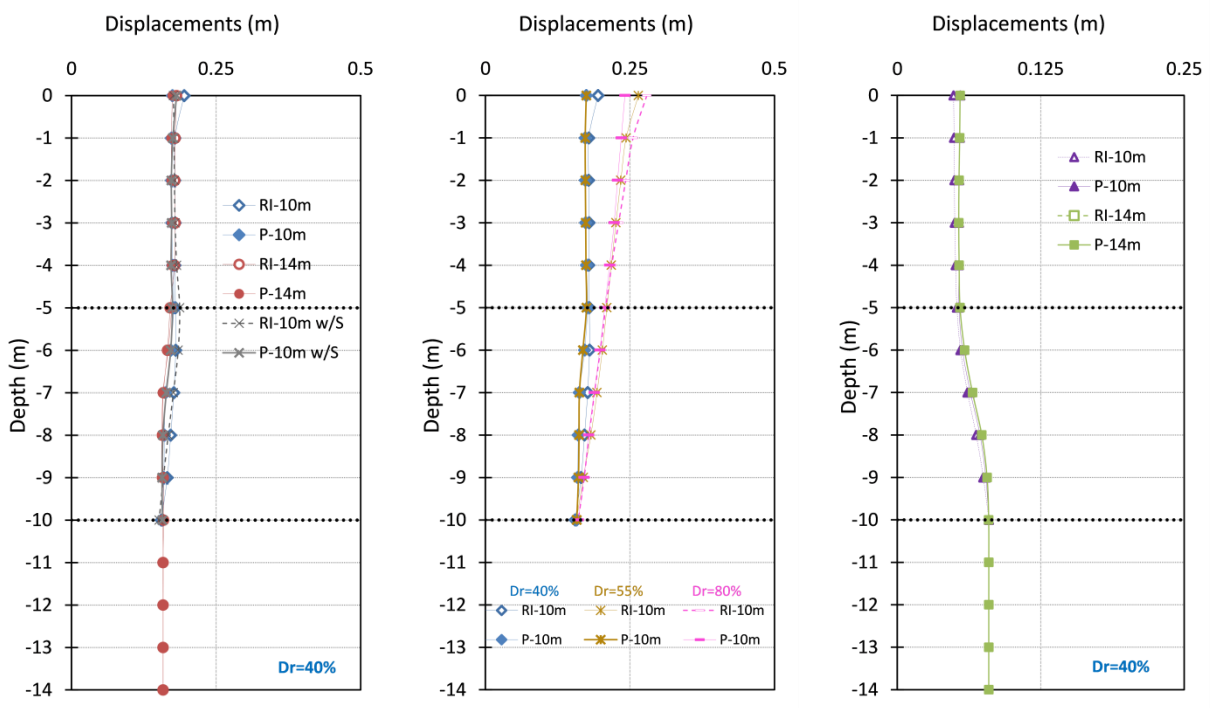

a) Loma Prieta **b)** Loma Prieta **c)** Northridge

Fig. 6.25 Horizontal displacements in rigid inclusion and pile systems for different conditions and earthquakes.

2.6. General Conclusions

The results of this Chapter show the effect of the soil relative density, soil profile, pile length, pile modelling type and earthquake predominant frequency on pile and rigid inclusion systems in the presence of liquefiable soils. Three-dimensional analyses of these systems were developed. A 3-storey concrete building resting on the pile or inclusion foundations was considered. The Finn constitutive model was utilized in the first part of this chapter to represent the behavior of a liquefiable soil layer. Then, in the second part, the comprehensive Sanisand constitutive model was utilized. This model is useful to consider different soil densities, stress levels and loading conditions. All the analyses were carried out using dynamic coupled mechanical/groundwater simulations. Two well know earthquakes (Loma Prieta and Northridge) with different fundamental frequencies were applied to the models.

The response spectra at ground surface in all the analyzed cases are reduced compared to the input motion spectra due to the attenuation of energy in the liquefied soil layer. The increment of the relative density in the sand layer implies greater accelerations at the ground surface. The response spectrum increases when the frequency of the excitation is decreased.

The building shear forces using pile systems are greater than with rigid inclusion systems because the fixed-head connection with the slab foundation. Longer piles impose extra shear forces to columns of the building. In accordance to the response spectrum, the shear forces are reduced as the relative density of the sand layer decreases, in the pile cases.

The increment in excess pore pressure ratio is more pronounced in the rigid inclusion cases than in pile cases. The inertial forces generated in the superstructure affect importantly the excess pore pressure ratio values in the upper part the model. When Sanisand constitutive model is utilized, the excess pore pressure curves show important drops due to the excessive soil dilatation tendency of this constitutive model. However, these pore pressure variations are reduced for the systems analyzed with the Northridge earthquake. The increment of the fundamental input motion frequency and relative density in the sand layer decrease the excess pore pressure ratio values. The consideration of the physical pile cross section increases the excess pore pressure values.

The increase of soil relative density and predominant earthquake frequency produce a decrement of the shear strain level. The free-head connection of the rigid inclusions produces greater strains in the upper part of the model compare to the pile cases.

The maximum bending moments, normal forces and displacements in the rigid elements are increased with the increment of the sand layer relative density. However, they are reduced as the frequency of the earthquake increases. The maximum bending moments are located at the intersection of liquefiable and non-liquefiable soil layers. Longer rigid elements experiment greater normal forces due to the greater energy absorbed from the contact surface with the surrounding soil. However, the rigid element length has a minor effect in the distribution of the bending moments along the elements.

GENERAL CONCLUSIONS AND RECOMMENDATIONS

This research work studies the behavior of rigid inclusion reinforced- and pile structure systems resting on soft soils, under dynamic loadings. To achieve this goal, three-dimensional numerical analyses in a continuum media of both soil-inclusion-platform-structure and soil-pile-structure systems were developed considering different types of soils and constitutive models. Several soil profiles and pile/inclusion groups were considered. Soils in drained and undrained conditions were studied. For the undrained cases, the analyses were carrying out using dynamic coupled fluid-mechanical simulations to analyze the liquefaction phenomenon. The Rayleigh formulation was utilized to represent the appropriate damping in the soil and in the superstructure. The damping constants used to simulate the structural damping were based on the first and second model of frequencies of the building. Local damping was utilized for the rigid elements when modeled by hybrid methods (*i.e* simulated by both volume and structure elements) to avoid zones with high velocity of dynamic wave propagation. In general, the interface elements were not considered; however, the influence of soil-pile interfaces was studied in some cases. Factor such as the foundation type (inclusions or piles), the rigid element basal support conditions, the frequency of the input motion, the dynamic characteristics of the structure, the damping parameters, the soil profile and the relative density were investigated. Other important aspects as pile flexural rigidity, pile group configuration with the same cover ratio, pile length, embedment of the foundation slab or earth platform and structural mass were also studied. The main results divided in soil, superstructure and rigid element responses are reminded below.

Soil response

The results displayed that the properties of the soil and the input motion importantly influence the ground motions recorded at the base of the structure (ground surface motion). Considering soft soils, the results showed a great amplification in the response spectrum compared to the input motion applied at the bottom of the model. When the plastic behavior of soil was considered, the peaks of the spectra decreased importantly in amplitude compared to the response obtained with a linear elastic soil behavior. In the rigid inclusion cases, the accelerations recorded at the top of the soft soil were a little greater than the one recorded at the top of the earth platform. This highlights the advantage of the earth platform to dissipate energy. The input motion frequency greatly influenced the response spectra. When the input motion frequency is close to the fundamental frequency of the system, the amplification of the response spectra is higher due to the resonance phenomenon. The embedment of the slab foundation or earth platform reduces the response spectrum due to the kinematic effects. Small differences in response spectra are noticed in pile or inclusion systems with different pile group configuration.

Dealing with liquefiable soils, the response spectrum at ground surface is reduced due to the attenuation of energy in the liquefied soil layers. The increase of relative density in liquefiable soils implies an increase of the response spectra. Two constitutive models were used to attempt to account for pore pressure build-up ranging from relatively simple to elaborate in terms of complexity and model parameters determination. Thus, the choice of a constitutive model to estimate the potential deformations associated with liquefaction in numerical analyses is very important. In practical engineering, the use of a complicated model is sometimes hard to justify due to the lack of input parameters. The geotechnical investigations to define with accuracy the soil parameters should be reinforced to obtain more reliable designs of reinforced geotechnical structures.

In general, the excess pore pressure values in the time histories in the rigid inclusion systems are greater than in the pile systems. The frequency, amplitude and the duration of the input motion have a great influence in the development of excess pore pressure. In the analyzed cases, the increment of the input motion frequency implies an augmentation of the pore pressure values. The rigid element length has a slight influence. The values of excess pore pressure increase as the soil relative density decreased. The excess pore pressure values considering a structure in the surface are greater than in the systems that do not consider it. This difference is less perceptible in deeper areas. The consideration of the physical cross section of the rigid elements (hybrid modelling) increases the excess pore pressure values in soil compare to the systems where the rigid elements are modelled by beam structural finite elements. This could be explained by the fact that the consideration of the physical cross section of the rigid elements increases the confining pressure which in turns implies a decrease in the resistance to liquefaction.

The distribution of the maximum shear amplitude in the soil is large at the top of the model, where the maximum damping ratio and minimum shear stiffness are attained and small at the bottom. The maximum shear strain values in a liquefiable soil are importantly influenced by the relative density. The increase of soil relative density implies a decrease in the level of shear strain. The shear strains values in the soil decrease when the predominant earthquake frequency is increased. The shear strains in the pile systems are lower than the values in the rigid inclusion systems in the upper part of the models. The rigid connection of pile systems or the free condition at the top of the inclusion cases have a great effect in the development of shear strains in the upper part of the model and less influence in the deeper part. As expected, there is more energy dissipation for the systems with lower target damping. Thus, the decrement in damping ratio implies an increase of shear strains values. In the pile systems, this difference in values is less perceptible than in the rigid inclusion cases. To avoid overdamping in the systems, a correct selection of the central frequency for the Rayleigh damping formulation is important.

Superstructure response

As expected, the shear forces along the building with the fixed-base condition (*i.e* without considering the presence of the soil) are larger when the building height is increased. However, considering soil-structure interaction, the dynamic characteristics of the building plays an important role in the shear forces generated in the superstructure. In this case, the shear forces in the building are reduced compare to the building considering fixed-base condition. The values and trend of variation in these shear forces in the building differ at every level. The foundation type influence the way the shear forces are distributed along the superstructure. The anchored pile or rigid inclusion systems induce higher shear forces than the systems with placed or anchored elements. The anchored elements absorb extra energy from the toe connection with hard soil. The rigid inclusion and pile systems with floating elements present the greater reduction of the maximum base shear force in the building compared to the building in fixed-base case. The shear forces along the building are greater in pile systems compared to the rigid inclusion systems with the same soil profile and pile length. This happens because the inertial forces increase due to the fixed connection between the slab foundation and the pile elements.

The displacements in the structure are increased with the consideration of SSI. This is due to the translation (shear forces) and rotation of the foundation system. In general, the maximum rocking values are lower in the inclusion systems than in pile systems with the same pile length and soil relative density. The systems with placed and anchored in hard soil elements induce a lower rocking compared to the floating elements, because the hard soil reduces the foundation uplift and the settlement values when the rigid elements are subjected to compression and tension forces. In fixed-condition, it is assumed that there is no rocking (excluding rotation of the foundation). The displacements and inter-storey drifts are amplified considering SSI compared to the building in fixed-base condition.

Rigid vertical elements response

In the pile cases, due to the rigid connection with the foundation slab, the bending moments and shear forces at the pile head are great, independently of the type of pile basal support, whereas they are respectively null and importantly reduced in the rigid inclusions cases. Thus, the free head condition of the rigid inclusion system implies an advantage in seismic areas. The high moments near to the head of the piles are not present in the systems that do not consider a surface structure. Due to kinematic forces, the efforts in the rigid elements remain almost the same with and without structure. The increment of the structural mass increases the efforts in the rigid elements. The embedment of

foundation or earth platform produces an important decrease of efforts and displacements in the pile and inclusion elements. The systems anchored on hard soil are greatly affected by the lateral deformation of the surrounding soil, which increases the bending moments and shear forces at the connection level with the hard soil. As the number of pile increases (but keeping the same cover ratio), the moments and normal forces in the rigid elements increase, due to the kinematic interaction between the piles and the surrounding soil. The decrement of the pile modulus produces reduced efforts and displacements in the rigid elements. The bending moments and normal forces in the rigid element are reduced with the increment of the target damping ratio; however, this reduction is less perceptible as the damping ratio is decreased.

The maximum bending moments, normal forces and displacements in the rigid elements are increased with the augmentation of the relative density in the liquefiable soils. This happens because the pore pressure generation and deformations in the soil are reduced as the relative density increases. The cases with low relative density value induce liquefaction. Longer rigid elements experiment greater normal forces due to the greater energy absorbed from the contact surface with the surrounding soil. The characteristics of the liquefiable soil layer and the tip and head boundary conditions of the rigid elements have a great effect in the development of buckling instability, bending failure or a combination of both.

RECOMMENDATIONS TO PRACTICE

Based on the results obtained in this research work, some aspects should be considered by practical engineers. Although the influence of various parameters and configurations of soil-foundation-structure systems were considered, these recommendations can however be altered in some other specific cases.

- The natural period of a superstructure is increased considering the SSI.
- Despite the fact that the shear forces in the building are reduced when taking SSI into account compared to the structure fixed-base case, the dynamic characteristic of the building can modify the shear base force. Dealing with pile systems, special care should be taken at the pile head in the connection with the foundation slab because of the great bending moments and shear forces.
- The increment of displacements in the buildings considering SSI would require a structure more ductile to undergo these large deformations without collapsing. Pile failure at the head level in piles due to the excessive displacements can occur.
- Consider the rocking of foundation in the designs, to avoid tensile pull-out, settlement or punching failure in piles.

- Special care should be taken in pile and inclusion systems with soil profile considering layer with stiffness contrast in the soil layers or in liquefiable and non-liquefiable layers. The efforts developed in the rigid elements at the intersection of the different layer are significantly incremented. Slender ratio of piles can present buckling failure.
- Greater increment of shear forces and moments are presented in the pile elements when they are anchored in a hard soil or bedrock at the level of anchorage.

SUGGESTIONS FOR FURTHER RESEARCH WORKS

- Carry out dynamic experimental tests to validate the developed numerical analyses.
- Consider other types of structures in the numerical model such as shear wall structures which are very effective under lateral loadings and could greatly impact the soil-structure interaction. Bridges simplified as a single degree of freedom structure with short and long pier could be considered to study deeply the inertial interaction effects in the pile systems. Additionally, the nonlinear behavior of the structure could be contemplated.
- Extend the numerical modelling considering other factors such as foundations with different characteristics.
- Inclined piles can be considered.
- Consider the shadow effect (influence of pile spacing) in the response of the pile groups.
- Studied in detail the response of the pile systems considering other constitutive models to properly represent the behavior of soil. For instance, Hardening Soil Model and Hardening Small Strain Soil Model.
- Introduce damping using other way such as the Hysteretic damping when simple constitutive models are utilized.
- Consider the variation of permeability coefficient during liquefaction in the pile systems and the effect of the depth of the liquefying soil.
- Consider techniques such as the stone columns as liquefaction mitigation method.

REFERENCES

Abdoun, T. and Dobry, R., 2002. Evaluation of pile foundation response to lateral spreading. Soil Dynamics and Earthquake Engineering, 22(9–12), pp.1051–1058.

Abdoun, T. et al., 2003. Pile Response to Lateral Spreads: Centrifuge Modeling. Journal of Geotechnical and Geoenvironmental Engineering, 129(10), pp.869–878.

Al Fach, M., 2009. Modélisation tridimensionnelle du Comportement sismique du système sol-pieux-pont : Prise en compte des non-linéarités du sol et du béton. PhD thesis. Université des Sciences et Technologies de Lille. In french.

Allotey, N. and El Naggar, M.H., 2008. Generalized dynamic Winkler model for nonlinear soil–structure interaction analysis. Canadian Geotechnical Journal, 45(4), pp.560–573.

Alsaleh, H. and Shahrour, I., 2009. Influence of plasticity on the seismic soil-micropiles-structure interaction. Soil Dynamics and Earthquake Engineering, 29(3), pp.574–578.

Alsaleh, H., 2007. Modélisation non-linéaire en trois dimensions de l'interaction Sol-Micropieux-Pont sous chargements sismiques. PhD thesis. Université des Sciences et Technologies de Lille. In French.

Ambrosini, R.D., 2006. Material damping vs. radiation damping in soil-structure interaction analysis. Computers and Geotechnics, 33(2), pp.86–92.

Amorosi, A., Boldini, D. and Elia, G., 2010. Parametric study on seismic ground response by finite element modelling. Computers and Geotechnics, 37(4), pp.515–528.

Andersen, K.H., 2009. Bearing capacity under cyclic loading — offshore, along the coast, and on land. The 21st Bjerrum Lecture presented in Oslo, 23 November 2007. Canadian Geotechnical Journal, 46(5), pp.513–535.

Arulmoli, K. et al., 1992. VELACS laboratory testinf program, soil data report. Technical report 90-0562. The Earth Technology Corporation, Irvine, CA, report to the National Science Foundation., Washington, DC.

Ashour, M. and Norris, G., 2003. Lateral Loaded Pile Response in Liquefiable Soil. Journal of Geotechnical and Geoenvironmental Engineering, 129(6), pp.404–414.

Badry, P. and Satyam, N., 2016. An efficient approach for assessing the seismic soil structure interaction effect for the asymmetrical pile group. Innovative Infrastructure Solutions, 1(1), p.8.

Balfour, B., 2013. Vibro Concrete Columns. Available at: http://www.balfourbeatty.com/media/28611/vcp-bbge-web.pdf.

Banerjee, S., Goh, S.H. and Lee, F.H., 2014. Earthquake-induced bending moment in fixed-head piles in soft clay. Géotechnique, 64(6), pp.431–446.

Bao, Y. et al., 2012. Seismic evaluation of soil-foundation-superstructure system considering geometry and material nonlinearities of both soils and structures. Soils and Foundations, 52(2), pp.257–278.

Barrero, A.R., Taiebat, M. and Lizcano, A., 2015. Application of an advanced constitutive model in nonlinear dynamic analysis of tailings dam. GEOQuebec 2015, pp.1–7.

Been, K. and Jefferies, M.G., 1985. A state parameter for sands. Géotechnique, 35(2), pp.99–112.

Benz, T., 2007. Small-Strain Stiffness of Soils and its Numerical Consequences. PhD Thesis. Univesity of Stuttgart.

Berrill, J.B. et al., 2001. Case study of lateral spreading forces on a piled foundation. Geotechnique, 51(6),

pp.501–517.

Berthelot, P., Pezot, B. and Liausu, P., 2003. Amélioration des sols naturels ou anthropiques par colonnes semi-rigides : Le procédé CMC. Eds. Proc. of the 13th European Conf. on Soil Mechanics and geotechnical Engineering (XIII ECSMGE), Praga., pp.25–29.

Bhattacharya, S. and Goda, K., 2013. Probabilistic buckling analysis of axially loaded piles in liquefiable soils. Soil Dynamics and Earthquake Engineering, 45, pp.13–24.

Bhattacharya, S. and Tokimatsu, K., 2004. Essential criteria for design of piled foundations in seismically liquefiable areas. In Proceedings of the 39th Japan National Conference on Geotechnical Engineering, Niigata, 7th-9th July. pp. 1805–1806.

Bhattacharya, S., 2003. Pile Instability during Earthquake Liquefaction. PhD thesis. University of Cambridge.

Bhattacharya, S., Adhikari, S. and Alexander, N.A., 2009. A simplified method for unified buckling and free vibration analysis of pile-supported structures in seismically liquefiable soils. Soil Dynamics and Earthquake Engineering, 29(8), pp.1220–1235.

Bhattacharya, S., Madabhushi, S.P.G. and Bolton, M.D., 2004. An alternative mechanism of pile failure in liquefiable deposits during earthquakes. Géotechnique, 54(3), pp.203–213.

Bohn, C. 2015. Serviceability and Safety in the Design of Rigid Inclusions and Combined Pile-Raft Foundations. PhD thesis. Thechnical University Darmstadt.

Boulanger, R. and Ziotopoulou, K., 2013. Formulation of a sand plasticity model for earthquake engineering applications. Soil Dynamics and Earthquake Engineering, 53(May), pp.254–267.

Boulanger, R.W. and Idriss, I.M., 2006. Liquefaction Susceptibility Criteria for Silts and Clays. Journal of Geotechnical and Geoenvironmental Engineering, 132(11), pp.1413–1426.

Boulanger, R.W. et al., 1999. Seismic Soil-Pile-Structure Interaction Experiments And Analyses. Journal of Geotechnical And Geoenvironmental Engineering, 125 (9)(September), pp.750–759.

Briançon, L. et al., 2004. État Des Connaissances : Amélioration Des Sols Par Inclusions Rigides. Proc. Int. Symp. on Ground Improvevement, Presses de l'ENPC, Paris, pp.15–44.

Briançon, L., Dias, D. and Simon, C., 2015. Monitoring and numerical investigation of a rigid inclusions–reinforced industrial building. Canadian Geotechnical Journal, 52(10), pp.1592–1604.

Brown, D.A. and Shie, C., 1990. Three-dimensional finite element model of laterally loaded piles. Computers and Geotechnics, 10, pp.59–79.

BS 8006, 1995. Code of Practice for Strengthened /Reinforced Soils and Other Fills British Standard Institution, UK,

BSSC, 2009. NEHRP Recommended Seismic Provisions for New Buildings and Other Structures. Fema P-750 Building Seismic Safety Council, Washington, D.C., II, p.388.

Byrne, P.M., 1991. A Cyclic Shear-Volume Coupling and Pore-Pressure Model for Sand. Second International Conference on Recent Advances in Geotechnical Engineering and Soil Dynamics, 1, pp.47–55.

Caltrana, 2006. Seismic Design Criteria. California Department of transportation, Sacramento, CA. , pp.1–33.

Carbonari, S., Dezi, F. and Leoni, G., 2011. Linear soil-structure interaction of coupled wall-frame structures on pile foundations. Soil Dynamics and Earthquake Engineering, 31(9), pp.1296–1309.

Carlsson, B., 1987. Reinforced soil, Principles for Calculation Terratema A. B., Linkoping, Sweden.

Castro, G. and Poulos, S., 1977. Factors Affecting Liquefaction and Cyclic Mobility. Journal of Geotechnical

Engineering, ASCE, 103(June 1977), pp.501–516.

CESMD, Center for Engineering strong Motion Data. US Geological suervey and the California Geological Survey.

Chen, Y., Ma, J. and Qin, X., 2011. Influence of pile embankment sopporing high-speed railways. Porc. of the 1st International Workshop on High-speed and Intercity Raylways, Shenzhen and Hong Kong., 2, pp.155–165.

Cheng, Z. and Jeremić, B., 2009. Numerical modeling and simulation of pile in liquefiable soil. Soil Dynamics and Earthquake Engineering, 29(11–12), pp.1405–1416.

Cheng, Z., Dafalias, Y.F. and Manzari, M.T., 2013. Application of SANISAND Dafalias-Manzari model in FLAC3D. Continuum and Distinct Element Numerical Modeling in Geomechanics, (October 2013).

Chopra, AK. 1995. Dynamics of Structures-Theory and Applications to Earthquake Engineering. Second Edi. Prentice Hall.

Choudhury, D. et al., 2014. Pile Foundations during Earthquakes in Liquefiable Soils – Theory to Practice. 15SEE, pp.327–342.

Chu, D. and Truman, K.Z., 2004. Effects of pile foundation configurations in seismic soil-pile-structure interaction. 13th World Conference on Earthquake Engineering Vancouver, B.C., Canada, (1551).

Clough, R. W., and J. Penzien. 1975. Dynamics Of Structures. Second Edi. McGraw-Hill.

Collin, J.G., Watson, C.H. and Han, J., 2005. Column-supported embankments solves time constraint for new road construction. Contemporary Issues in Foundation Engineering, (724), pp.1–25.

Combault, J. and Pecker, A., 2000. Rion-Antirion Bridge, Greece – Concept, Design, and Construction. Structural Engineering International, pp.22–27.

Comodromos, Emilios M., Mello C. Papadopoulou, and Ioannis K. Rentzeperis. 2009. Pile Foundation Analysis and Design Using Experimental Data and 3-D Numerical Analysis. Computers and Geotechnics 36(5), 819–36.

Dafalias, Y.F. and Manzari, M.T., 2004. Simple Plasticity Sand Model Accounting for Fabric Change Effects. Journal of Engineering Mechanics ASCE, 130, pp.622–634.

Dafalias, Y.F., Papadimitriou, A.G. and Li, X.S., 2004. Sand Plasticity Model Accounting for Inherent Fabric Anisotropy. Journal of Engineering Mechanics, 130(11), pp.1319–1333.

Daftari, A., 2015. New Approach in Prediction of Soil Liquefaction. PhD thesis. Technische Universität Bergakademie Freiberg.

Darendeli, M.B., 2001. Development of a new family of normalized modulus reduction and material damping curves. PhD thesis. The University of Texas at Austin.

Deb, K. 2010. A Mathematical Model to Study the Soil Arching Effect in Stone Column-Supported Embankment Resting on Soft Foundation Soil. Applied Mathematical Modelling 34(12), 3871–83.

de Groot, M.B. et al., 2006. Physics of Liquefaction Phenomena around Marine Structures. Journal of Waterway, Port, Coastal, and Ocean Engineering, 132(4), pp.227–243.

Di Laora, R. et al., 2015. Importance of seismic site response and soil–structure interaction in dynamic behaviour of a tall building. Geotechnique, 65(5), pp.391–400.

Do, N.A., Dias, D. and Oreste, P., 2014. 2D seismic numerical analysis of segmental tunnel lining behaviour. Bulletin of the New Zealand Society for Earthquake Engineering, 47(3), pp.206–216.

Elgamal, A. et al., 2008. Three-Dimensional Seismic Response of Humboldt Bay Bridge-Foundation-Ground System. Journal of Structural Engineering, 134(7), pp.1165–1176.

Elgamal, A., Yang, Z. and Parra, E., 2002. Computational modeling of cyclic mobility and post liquefaction site response. Soil Dynamics and Earthquake Engineering, 22(4), pp.259–271.

Eurocode 8, 1998. Design of structures for earthquake resistance - Part 5: Foundations, retaining structures and geotechnical aspects.

Fan, Z. et al., 2007. Analytical method of load-transfer of single pile under expansive soil swelling. Journal of Central South University, 14(4), pp.575–579.

Finn, W.D.L. and Fujita, N., 2002. Piles in liquefiable soils: seismic analysis and design issues. Soil Dynamics and Earthquake Engineering, 22(9), pp.731–742.

Frank, R., 2006. FOREVER The French national project on micropiles. 14th Prague Geotechnical Lecture.

Gao, X. et al., 2011. Soil-pile-bridge structure interaction in liquefying ground using shake table testing. Soil Dynamics and Earthquake Engineering, 31(7), pp.1009–1017.

Gazetas, G. and Mylonakis, G., 1998. Seismic soil-structure interaction: new evidence and emerging issues. Geotechnical Special Publication, 2(75), pp.1119–1174.

Gazetas, G., 1984. Seismic response of end-bearing piles seismic response of end-bearing single piles. International Journal of Soil Dynamics and Earthquake Engineering, 3, pp.82–93.

Gennaro, V. De et al., 2004. Influence of loading path on the undrained behaviour of a medium loose sand. Canadian Geotechnical Journal, 41(1), pp.166–180.

Ghionna, V.N. and Porcino, D., 2006. Liquefaction Resistance of Undisturbed and Reconstituted Samples of a Natural Coarse Sand from Undrained Cyclic Triaxial Tests. Journal of Geotechnical and Geoenvironmental Engineering, 132(2), pp.194–202.

Girault, P. 1986. Analysis of Foundation Failures in The Mexico Earthquake, 1985 - Factors Involved and Lessons Learned. ASCE: 178–92.

Goh, S.H. and Zhang, L., 2017. Estimation of Peak Acceleration and Bending Moment for Pile-Raft Systems Embedded in Soft Clay Subjected to Far-Field Seismic Excitation. Journal of Geotechnical and Geoenvironmental Engineering, 143(11), p.04017082.

González, L., Abdoun, T. and Dobry, R., 2009. Effect of Soil Permeability on Centrifuge Modeling of Pile Response to Lateral Spreading. Journal of Geotechnical and Geoenviromental Engineering ASCE, (January), pp.50–60.

Grange, S., 2008. Modélisation simplifiée 3D de l'interaction sol-structure: application au génie parasismique. PhD thesis. Institut Polytechnique de Grenoble. In french.

Guido, V.A., Kneuppel, J.D. and Sweeney, M.A., 1987. Plate loading test on geogrid reinforced earth slabs. In: Proceedings Geosynthetics'87 Conference, New Orleans, pp.216–225.

Haeri, S.M. et al., 2012. Response of a group of piles to liquefaction-induced lateral spreading by large scale shake table testing. Soil Dynamics and Earthquake Engineering, 38, pp.25–45.

Haldar, S. and Babu, S.G.L., 2010. Failure Mechanisms of Pile Foundations in Liquefiable Soil: Parametric Study. International Journal of Geomechanics, 10(2), pp.74–84.

Hamada, M., 1992. Large ground deformations and their effects on lifelines: 1964 Niigata earthquake. Case Studies of liquefaction and lifelines performance during past earthquake. Technical Report NCEER-92-

0001, Volume-1, Japanese case studies., Buffalo, NY.

Han, J. and Gabr, M., 2002. Numerical Analysis of Geosynthetic-Reinforced and Pile-Supported Earth Platforms over Soft Soil. Journal of Geotechnical and Geoenvironmental Engineering, 128(1), pp.44–53.

Han, Y., 2001. Dynamic soil-pile-structure interaction. International Conferences on Recent Advances in Geotechnical Earthquake Engineering and Soil Dynamics, Paper 11, pp.1–6.

Hashash, Y.M.A. and Park, D., 2002. Viscous damping formulation and high frequency motion propagation in non-linear site response analysis. Soil Dynamics and Earthquake Engineering, 22(7), pp.611–624.

Hatem, A., 2009. Comportement en zone sismique des inclusions rigides Analyse de l'interaction sol-inclusion-matelas de répartition-structure. Université des Sciences et Technologies de Lille I, Lille, France.

Hazzar, L., Hussien, M.N. and Karray, M., 2017. Influence of vertical loads on lateral response of pile foundations in sands and clays. Journal of Rock Mechanics and Geotechnical Engineering, 9(2), pp.291–304.

Hetenyi, M. 1946. Beams on Elastic Foundations. The University of Michigan Press.

Hewlett, W.J. and Randolph, M.A., 1988. Analysis of piled embankments. Ground Engineering, 21 (3), pp.12–18.

Hokmabadi, A.S. and Fatahi, B., 2016. Influence of foundation type on seismic performance of buildings considering soil-structure interaction. International Journal of Structural Stability and Dynamics, 16, pp.1–29.

Hokmabadi, A.S., 2014. Effect of Dynamic Soil-Pile-Structure Interaction on Seismic Response of Mid-Rise Moment Resisting Frames. PhD thesis. University of Technology Sidney (UTS).

Hokmabadi, A.S., Fatahi, B. and Samali, B., 2014. Assessment of soil-pile-structure interaction influencing seismic response of mid-rise buildings sitting on floating pile foundations. Computers and Geotechnics, 55(January), pp.172–186.

Houda, M., 2016. Comportement sous chargement cyclique des massifs de sol renforcés par inclusions rigides : expérimentation en laboratoire et modélisation numérique. PhD thesis. Université de Grenoble. In french.

Hudson, M., Idriss, I.M. and Beikae, M., 1994. QUAD4M – A computer program to evaluate the seismic response of soil structures using finite element procedures and incorporating a compliant base. Center for Geotechnical Modeling, Dept. of Civil and Environmental Engineering, UC, Davis.

Hussien, M.N., Tobita, T. and Iai, S., 2011. Non-linear response of coupled soil-pile-structure system under sinusoidal excitations with various frequencies. In Civil Society Proceedings A2 (Applied Mechanics). pp. 471–480.

Hyodo, M., Hyde, A.F.L. and Aramaki, N., 1998. Liquefaction of crushable soils. Géotechnique, 48(4), pp.527–543.

Idriss, I.M. and Boulanger, R.W., 2008. Soil liquefaction during earthquakes Earthquake., Oakland, California, USA.

Idriss, I.M. et al., 1975. QUAD-4 - A computer program for evaluating the seismic response of soil structures by variable damping finite element procedures. EERC Report 73-16.

Ishibashi, I. and Zhang, X., 1993. Unified Dynamic shear moduli and damping ratios of sand and clay. Soils and Foundations, 33(1), pp.182–191.

Ishihara, K., 1993. Liquefaction and flow failure during earthquakes. Géotechnique, 43(3), pp.351–451.

Ishihara, K., 1996. Soil Behavior in Earthquake Geotechnics, Oxford Engineering Science Series.

Ishihara, K., 1997. Terzaghi oration : Geotechnical aspects of the 1995 Kobe earthquake. In Preceedings of ICSMFE. Hamburg, pp. 2047–2073.

Ishihara, K., Tatsuoka, F. and Yasuda, S., 1975. Undrained Deformation and Liquefaction of Sand under Cyclic stresses. Soils and Foundations, 15(1), pp.29–44.

Itasca, F. 3D, 2012. Fast lagrangian analysis of continya in 3-dimentions, version 5.0, manual. , pp.1–108.

Jakrapiyanun, W., 2002. Physical modeling of dynamics soil-foundationstructure- interaction using a laminar container. PhD thesis. University of California, San Diego.

Janalizadeh, A. and Zahmatkesh, A., 2015. Lateral response of pile foundations in liquefiable soils. Journal of Rock Mechanics and Geotechnical Engineering, 7(5), pp.532–539.

Japan Society of Civil Engineers, 2005. Standard specifications for concrete structures-2002: Seismic performance verification. JSCE Guidelines for concret No.5(15).

Kagawa, T., 1992. Lateral pile response in liquefying sand. In Proc. 10th World Conference on Earthquake Engineering. Balkema, Rotterdam.

Kausel, E. and Roesse, J.M., 1974. Soil–structure interaction problems for nuclear containment structures. In Proceedings of the ASCE Power Division Conferen ce, Boulder, Colorado.

Kelly, P., 2013. Solid Mechanics Part II: Engineering Solid Mechanics- small strains. The University of Auckland.

Kempfert, H.G., Stadel, M. and Zaeske, D., 1997. Calculation of geotextile-reinforced base courses over pile elements. Bautechnik 74, (12), p.818–825 (in Deutsch).

Kim, Y.S. and Roesset, J.M., 2004. Effect of Nonlinear Soil Behavior on Inelastic Seismic Response of Structures Using Bounding Surface Model. International Journal of Geomechanics, (June), pp.104–114.

Kitiyodom, P., Masumoto, T. and Kawaguchi, K., 2006. Analyses of piled foundations subjected to ground movements induced by tunnelling. In T. and Francis, ed. Geotechnical Aspects of Underground Construction in Soft Ground 5th International Symposium (IS Amsterdam). Amsterdam, Netherlands, pp. 551–557.

Kourkoulis, R. et al., 2012. Hybrid Method for Analysis and Design of Slope Stabilizing Piles. Journal of Geotechnical and Geoenvironmental Engineering, 138(January).

Koutsourelakis, S., Prévost, J.H. and Deodatis, G., 2002. Risk assessment of an interacting structure-soil system due to liquefaction. Earthquake Engineering and Structural Dynamics, 31(4), pp.851–879.

Kramer, S.L. et al., 2011. Site Response Modeling in Liquefiable Soil Deposits. In 4th IASPE/IAEE International Symposium: Effects of Surface Geology on Seismic Motion. University of California Santa Barbara, pp. 1–12.

Kramer, S.L., 1996. Geotechnical Earthquake Engineering Prentice-Hall, ed., New Jersey.

Kuhlemeyer, R.L. and Lysmer, J., 1973. Finite element method accuracy for wave propagation problems. Journal of the Soil Mechanics and Foundation Division ASCE, 99 (SM5), pp.421–7.

Kuhlemeyerr, L.R., 1979. Static and dynamic laterally loaded floating piles. Journal of the Geotechnical Engineering Division ASCE, 105, pp.289–304.

Kumar, A., Choudhury, D. and Katzenbach, R., 2016. Effect of Earthquake on Combined Pile – Raft Foundation. International Jounral of Geomechanics ASCE, ISSN 1532-3641, pp.1–16.

Kwok, A.O.L. et al., 2007. Use of Exact Solutions of Wave Propagation Problems to Guide Implementation of Nonlinear Seismic Ground Response Analysis Procedures. Journal Geotechnical and Geoenvironmental Engineering, ASCE, 133(11), pp.1385–1398.

Labuz, J.F. and Zang, A., 2012. Mohr-Coulomb failure criterion. Rock Mechanics and Rock Engineering, 45(6), pp.975–979.

Ladhane, K.B. and Sawant, V.A., 2012. Dynamic response of pile groups in series and parallel arrangement. Structural Engineering and Mechanics, 41(3), pp.395–406.

Li, X.S. and Dafalias, Y.F., 2012. Anisotropic Critical State Theory: Role of Fabric. Journal of Engineering Mechanics, 138(3), pp.263–275.

Li, X.S. and Wang, Y., 1998. Linear Representation of Steady-State Line for Sand. Journal of Geotechnical and Geoenvironmental Engineering, 124(12), pp.1215–1217.

Liyanapathirana, D.S. and Poulos, H.G., 2005. Seismic Lateral Response of Piles in Liquefying Soil. Journal of Geotechnical and Geoenvironmental Engineering, 131(12), pp.1466–1479.

Liyanapathirana, D.S. and Poulos, H.G., 2006. Behaviour of Pile Groups in Liquefying Soil. GeoCongress 2006, pp.1–6.

Lu, X. et al., 2005. Computer simulation of the dynamic layered soil-pile-structure interaction system. Canadian Geotechnical Journal, 42(3), pp.742–751.

Lu, X., P. Li, Y. Chen, and B. Chen. 2004. Shaking Table Model Testing on Dynamic Soil-Structure Interaction System. 13th World Conference on Earthquake Engineering Vancouver, B.C., Canada 3231(194).

Luo, C. et al., 2016. Nonlinear 3D finite element analysis of soil-pile-structure interaction system subjected to horizontal earthquake excitation. Soil Dynamics and Earthquake Engineering, 84(May 2016), pp.145–156.

Luong, M.P., 1980. Stress strain aspect of cohesionless soil under cyclic and transient loading. In Proceedings of the International Symposium on Soils under cyclic and transient loading. pp. 39–53.

Lysmer, J. and Kuhlemeyer, R.L., 1969. Finite dynamic model for infinite media. Journal of Engineering Mechanics Division ASCE, 95, pp.859–878.

Maheshwari, B.K. and Sarkar, R., 2011. Seismic Behavior of Soil-Pile-Structure Interaction in Liquefiable Soils: Parametric Study. International Journal of Geomechanics ASCE, 11, pp.335–347.

Maheshwari, B.K. and Watanabe, H., 2006. Nonlinear Dynamic Analysis of Pile Foundation : Effect of Separation At Soil-Pile Interface. Soils and Foundations, 46(4), pp.437–448.

Maheshwari, B.K. et al., 2004. Three-dimensional nonlinear analysis for seismic soil – pile-structure interaction. Soil Dynamics and Earthquake Engineering, 24, pp.343–356.

Mánica, M., Ovando, E. and Botero, E., 2014. Assessment of damping models in FLAC. Computers and Geotechnics, 59, pp.12–20.

Manica-Malcom, M.A., 2013. Comportamiento Dinamico de Inclusiones Rigidas. PhD thesis. Universidad Nacional Autonoma de Mexico. In Spanish.

Mánica-Malcom, M.A., Ovando-Shelley, E. and Botero Jaramillo, E., 2016. Numerical study of the seismic behavior of rigid inclusions in soft Mexico City clay. Journal of Earthquake Engineering, 20(3), pp.447–475.

Manzari, M.T. and Dafalias, Y.F., 1997. A critical state two-surface plasticity model for sands. Géotechnique, 47(2), pp.255–272.

Marti, J. and Cundall, P., 1982. Mixed discretization procedure for accurate modelling of plastic collapse. International Journal for Numerical and Analytical Methods in Geomechanics, 6(November), pp.129–139.

Martin, G.R., Finn, W.D.L. and Seed, H.B., 1975. Funadmentals of liquefqction under cyclic loading. Journal of the Geotechnical Engineering Division, 101, pp.423–438.

Mayoral, J.M. et al., 2006. Effect of layered clay deposits on the seismic behavior of a rigid inclusion. Proceedings of the Symposium of Rigid Inclusions in Difficult Subsoil Conditions, ISSMGE TC36, Sociedad Mexicana de Mecanica de Suelos., pp.11–12.

Leclaire, F. et al., 2017. Application of Controlled Modulus Columns for Refinery and Petrochemical Tank Farm. Journal of Earth Engineering. 2 (1), pp. 13-26.

Mendoza, M.J. and Auvinet, G., 1988. The Mexico Earthquake of September 19, 1985- Behavior of Building Foundations in Mexico City. Earthquake Spectra, 4(No.4), pp.835–853.

Messioud, S. et al., 2016. Dynamic response of pile reinforced soils and piled foundations. Geotechnical and Geological Engineering, 34(3), pp.789–805.

Messioud, S., Sbartai, B. and Dias, D., 2016. Estimation of dynamic impedance of the soil-pile-slab and soil-pile-mattress-slab systems. International Journal of Structural Stability and Dynamics, 17(6), p.17.

Meymand, P., 1994. Shaking Table Scale Model Tests of Nonlinear Soil-Pile-Superstructure Interaction In Soft Clay. PhD thesis. University of California, Berkeley.

Mitchell, J.K. and Soga, K., 2005. Fundamentals of Soil Behavior Third Edit., John Wiley and Sons.

Mogami, T. and Kubo, K., 1953. The Behaviour of Soil During Vibration. In Procedings of the Third International Conference on Soil Mechanics and Foundation Engineering. pp. 152–155.

Montoya-Noguera, S. and Lopez-Caballero, F., 2016. Effect of coupling excess pore pressure and deformation on nonlinear seismic soil response. Acta Geotechnica, 11(1), pp.191–207.

Muthucumarasamy, Y., 1988. Dynamic Soil-Structire Interaction: Theory and Verification. PhD thesis. The University of British Columbia.

Neagoe, I. V., 2013. Soft soils reinforced by rigid vertical inclusions. Constructions (2), pp.48–55.

Nghiem, H. and Nien-Yin, C., 2008. Soil-structure interaction effects of high rise buildings. 6th International Conference on Case Histories in Geotechnical Engineering, pp.11–16.

Nguyen, Q. V., Fatahi, B. and Hokmabadi, A.S., 2017. Influence of size and load-bearing mechanism of piles on seismic performance of buildings considering soil-pile-structure interaction. International Journal of Geomechanics, 1(January), pp.1–22.

Nowak, P., 2013. M74 Motorway , Glasgow – Geotechnical Aspects of Design and Construction. Seventh International Conference on Case Histories in Geotechnical Engineering, pp.1–9.

Okyay, U.S., 2015. Sols renforcés par inclusions rigides: etude expérimentale et numérique des transferts de charge. Editions Universitaires Europeennes (ISBN-10: 6131566054).

Okyay, U. S. et al. 2012. Impedance Functions of Slab Foundations with Rigid Piles. Geotechnical and Geological Engineering 30(4): 1013–24.

Park, D. and Hashash, Y.M.A., 2004. Soil damping formulation in nonlinear time domain site response analysis. Journal of Earthquake Engineering, 8(2), pp.249–274.

Pecker, A., 1984. Dynamique des sols P. de l'école nationale des ponts et Chaussées., ed., Paris.

Peiris, L.M.N., 1998. Seismic Modelling of rock-fill embankments on deep loose saturated sand deposits. PhD

thesis. University of Cambridge U.K.

Phanikanth, V.S., Choudhury, D. and Reddy, G.R., 2013. Behavior of Single Pile in Liquefied Deposits during Earthquakes. Technical Note, 13(August), pp.454–462.

Phillips, C. and Hashash, Y.M.A., 2009. Damping formulation for nonlinear 1D site response analyses. Soil Dynamics and Earthquake Engineering, 29(7), pp.1143–1158.

Phillips, C. et al., 2012. Significance of small strain damping and dilation parameters in numerical modeling of free-field lateral spreading centrifuge tests. Soil Dynamics and Earthquake Engineering, 42, pp.161–176.

Pinto, A., Tomásio, R. and Marques, G., 2016. Ground Improvement with Jet Grouting Solutions at the New Cruise Terminal in Lisbon, Portugal. In Proc. of the 16th Int. Conf. on Soil Mechanics and Geotechnical Engineering (ICSMGE), 12- 16 septembre 2005. Osaka, Japon: Elsevier B.V., pp. 1495–1502.

Pinto, P.A., 2012. Study of constitutive models for soils under cyclic loading. Master thesis. Technic University of Lisbon.

Pitilakis, K.D. and Anastasiadis, A.J., 1998. Soil and site characterization for seismic response analysis. Proc. of the Eleventh European Conference on Earthquake Engineering., pp.65–89.

Popescu, R. et al., 2006. Dynamics of nonlinear porous media with applications to soil liquefaction. Soil Dynamics and Earthquake Engineering, 26(6–7), pp.648–665.

Poulos, H.G. and Davis, E.H., 1980. Pile Foundation Analysis and Design, The University of Sydney. Ed. Rainbow-Bridge Book Co.

Priestley, M.J.N. and Grant, D.N., 2005. Viscous damping in seismic design and analysis. Journal of Earthquake Engineering, 9(2), pp.229–255.

Rahmani, A. and Pak, A., 2012. Dynamic behavior of pile foundations under cyclic loading in liquefiable soils. Computers and Geotechnics, 40, pp.114–126.

Rahmani, A., Ghasemi Fare, O. and Pak, A., 2012. Investigation of the influence of permeability coefficient on the numerical modeling of the liquefaction phenomenon. Scientia Iranica, 19(2), pp.179–187.

Ramirez, J. et al., 2018. Site Response in a Layered Liquefiable Deposit: Evaluation of Different Numerical Tools and Methodologies with Centrifuge Experimental Results. Journal of Geotechnical and Geoenvironmental Engineering, 144(10), p.04018073.

Rangel-Núñez, J.L. et al., 2008. Dynamic response of soft soil deposits improved with rigid inclusions. 14th World Conference on Earthquake Engineering (14WCEE), pp.1–8.

Rascol, E., 2009. Cyclic Properties of Sand : Dynamic Behaviour for Seismic Applications. PhD thesis. Ecole Polytechnique Fédérale de Lausanne.

Rathje, E.M. and Bray, J.D., 2001. One- and two-dimensional seismic analysis of solid-waste landfills. Canadian Geotechnical Journal, 38(4), pp.850–862.

Rayhani, M.H. and El Naggar, M.H., 2008. Numerical Modeling of Seismic Response of Rigid Foundation on Soft Soil. International Journal of Geomechanics, 8(6), pp.336–346.

Rees, S., 2013. Part Two: Advanced triaxial testing. Published on the GDS website www.gdsinstruments.com, 2, pp.1–5.

Ren, H., Lu, X. and Li, P., 2008. Computer simulation on dynamic soil-pile-superstructure interaction system considering liquefiable foundation. The 14th World Conference on Earthquake Engineering.

Rodriguez, J. and Auvinet, G., 2006. Rigid inclusions in Mexico City soft soils. In Symposium Rigid inclusions

in Difficult Subsoil conditions. ISSMGE TC36, UNAM.

Rodriguez, J., 2001. Uso de Inclusiones Rigidas para el Control de Asentamientos en Suelos Blandos.

Romo, M.P., 1995. Clay Behavior , Ground Response and Soil- Structure Interaction Studies in Mexico City. In International Conferences on Recent Advances in Geotechnical Earthquake Engineering and Soil Dynamics. pp. 1039–1051.

Roscoe, K.H., Schofield, A.N. and Wroth, C.P., 1958. On The Yielding of Soils. Géotechnique, 8(1), pp.22–53.

Rovithis, E.N., Pitilakis, K.D. and Mylonakis, G.E., 2009. Seismic analysis of coupled soil-pile-structure systems leading to the definition of a pseudo -natural SSI frequency. Soil Dynamics and Earthquake Engineering, 29, pp.1005–1015.

Sadek, M. and Shahrour, I., 2004. A three dimensional embedded beam element for reinforced geomaterials. International Journal for Numerical and Analytical Methods in Geomechanics, 28(9), pp.931–946.

Santamarina, J. C., K. A. Klein, and M. A. Fam. 2001. Soils and Waves, Particulate Materials Behavior, Characterization and Process Monitoring. ed. John Wiley & Sons Ltd. Chichester, England, UK.

Sarkar, R. and Maheshwari, B.K., 2012. Effects of Separation on the Behavior of Soil-Pile Interaction in Liquefiable Soils. International Journal of Geomechanics, 12(1), pp.1–13.

Sato, M., Ogasawara, M. and Tazoh, T., 2001. Reproduction of Lateral Ground Displacements and Lateral-Flow Earth Pressures Acting on Pile Foundations Using Centrifuge Modeling. In International Conferences on Recent Advances in Geotechnical Earthquake Engineering and Soil Dynamics. p. 6.

Seed, H.B. and Lee, K.L., 1966. Liquefaction of Saturated sands during cyclic loading. Journal of the Soil Mechanics and Foundations Division, 92(6), pp.105–134.

Seed, H.B. et al., 1985. Influence of SPT Procedures in Soil Liquefaction Resistance Evaluations. Journal of Geotechnical Engineering, 111(12), pp.1425–1445.

Seed, H.B. et al., 1988. The Mexico Eathquake of September 19,1985- Relationships between soil conditions ans earthquake ground motions. Earthquke Spectra, 4(No. 4), pp.687–729.

Seed, H.B., 1979. Soil Liquefaction and Cyclic Mobility Evaluation for Level Ground during Earthquakes. Journal of the Geotechnical Engineering Division ASCE, 105(February), pp.201–255.

Seed, R.B., Cetin, K.O. and Moss, R.E.S., 2001. Recent advances in soil liquefaction engineering and seismic site response evaluation. Fourth International Conference on Recent Advances in Geotechnical Earthquake Engineering and Soil Dynamics and Symposium in Honor of Professor W.D. Liam Finn, pp.1–45.

Shahir, H. and Pak, A., 2010. Estimating liquefaction-induced settlement of shallow foundations by numerical approach. Computers and Geotechnics, 37(3), pp.267–279.

Shahrour, I., Alsaleh, H. and Souli, M., 2012. 3D elastoplastic analysis of the seismic performance of inclined micropiles. Computers and Geotechnics, 39, pp.1–7.

Shahrour, I., Sadek, M. and Ousta, R., 2001. Seismic behavior of micropiles used as foundation support elements three-dimensional finite element analysis. Transportation Research Record 1772, (01), pp.84–90.

Shajarati, A. et al., 2012. Behaviour of Cohesionless Soils During Cyclic Loading. DCE Technical Memorandum No. 14 Aalborg University, pp.1–11.

SINTEF, 2002. A computer program for designing reinforced embankments. In: Proc. 7th International Conference on Geotextiles, Nice 2002, France, 1, pp.201–204.

Sladen, J.A., D'Hollander, R.D. and Krahn, J., 1985. The liquefaction of sands, a collapse surface approach.

Canadian Geotechnical Journal, 22(4), pp.564–578.

Spears, R.E. and Jensen, S.R., 2012. Approach for Selection of Rayleigh Damping Parameters Used for Time History Analysis. Journal of Pressure Vessel Technology, 134(December 2012), pp.1–7.

Stewart, J.P., Fenves, G.L. and Seed, R.B., 1999. Seismic Soil-Structure Interaction in Buildings. I: Analytical Methods. Journal of Geotechnical and Geoenvironmental Engineering, 125(1), pp.26–37.

Stewart, M.E., Navin, M.P. and Filz, G.M., 2004. Analysis of a column-suported test embankment at the I-95/Route 1 Interchange. Geotechnical Engineering for Transportation Projects, pp.1337–1346.

Su, D. and Li, X.S., 2006. Effect of Shaking Intensity on Seismic Response of Single-pile Foundation in Liquefiable Soil. In Ground Modification and Seismic Mitigation(GSP 152). pp. 97–102.

Suwal, S., Pagliaroli, A. and Lanzo, G., 2014. Comparative study of 1D codes for Site Response Analyses. International Journal of Landslide and Environment, 2(1), pp.24–31.

Tabatabaiefar, H.R. et al., 2015. Evaluation of numerical procedures to determine seismic response of structures under influence of soil-structure interaction. Structural Engineering and Mechanics, 56(1), pp.27–47.

Tabatabaiefar, H.R., Fatahi, B. and Samali, B., 2013. Lateral seismic response of building frames considering dynamic soil-structure interaction effects. Structural Engineering and Mechanics, 45(No.3), pp.311–321.

Taiebat, M. and Dafalias, Y.F., 2008. SANISAND: Simple anisotropic sand plasticity model. International Journal for Numerical and Analytical Methods in Geomechanics, 32 (8), pp.915–948.

Taiebat, M. et al., 2010. Propagation of seismic waves through liquefied soils. Soil Dynamics and Earthquake Engineering, 30(4), pp.236–257.

Takahashi, A. et al., 2002. Lateral resistance of buried cylinder in liquefied sand. In Proceedings of the International Conference on Physical Modelling in Geotechnics.

Tamura, S. and Tokimatsu, K., 2006. Seismic Earth Pressure Acting on Embedded Footing Based on Large-scale Shaking Table Test. In Seismic Performance and Simulation of Pile Foundations in Liquefied and Laterally Spreading Ground. pp. 83–96.

Tasiopoulou, P. and Gerolymos, N., 2016. Constitutive modeling of sand: Formulation of a new plasticity approach. Soil Dynamics and Earthquake Engineering, 82, pp.205–221.

Terzaghi, K., 1943. Theoretical Soil Mechanics Wiley, ed., New York.

Timoshenko, S.P. and Gere, J.M., 1961. Theory of elastic stability McGraw-Hill, ed., New York.

Tokimatsu, K., Suzuki, H. and Sato, M., 2005. Effects of inertial and kinematic interaction on seismic behavior of pile with embedded foundation. Soil Dynamics and Earthquake Engineering, 25, pp.753–762.

Tokimatsu, K., Suzuki, H. and Suzuki, Y., 2001. Back-Calculated p-y Relation of Liquefied Soils from large Shaking Table Tests. In International Conferences on Recent Advances in Geotechnical Earthquake Engineering and Soil Dynamics. pp. 1–6.

Towhata, I., 2008. Geotechnical Earthquake Engineering First Edit., Springer (Series in Geomechanic and Geoengineering).

Trochanis, A.M., Bieiak, J. and Christiano, P., 1988. A three-dimensional nonlinear study of piles leading to the development of a simplified model. A Technical Report of Research Sponsored by The NSF, Grant No. ECE-86/1060

Tsai, C.C., Park, D. and Chen, C.W., 2014. Selection of the optimal frequencies of viscous damping formulation in nonlinear time-domain site response analysis. Soil Dynamics and Earthquake Engineering, 67, pp.353–

358.

Van Eekelen, S.J.M., Bezuijen, A. and Van Tol, A.F., 2013. An analytical model for arching in piled embankments. Geotextiles and Geomembranes, 39, pp.78–102.

Vucetic, M. and Dobry, R., 1991. Efect of soil plasticity on cyclic response. Journal of Geotechnical Engineering, 117(1), pp.89–107.

Wang, J.T., 2011. Investigation of damping in arch dam-water-foundation rock system of Mauvoisin arch dam. Soil Dynamics and Earthquake Engineering, 31(1), pp.33–44.

Wang, M., Chen, G. and Iai, S., 2013. Seismic performances of dyke on liquefiable soils. Journal of Rock Mechanics and Geotechnical Engineering, 5(4), pp.294–305.

Wang, R., Liu, X. and Zhang, J.M., 2017. Numerical analysis of the seismic inertial and kinematic effects on pile bending moment in liquefiable soils. Acta Geotechnica, 12(4), pp.773–791.

Wang, R., Zhang, J.M. and Wang, G., 2014. A unified plasticity model for large post-liquefaction shear deformation of sand. Computers and Geotechnics, 59, pp.54–66.

Wilson, D.W., 1998. Soil-pile-superstructure interaction in liquefying sand and soft clay. PhD thesis. University of California at Davis.

Winkler, E. 1876. Die Lehre von Der Elastizitat Und Festigkeit. Verlag, 182.

Wolf, J.P., 1985. Dynamic Soil-Structure Interaction I. Prentice-Hall, ed., New Jersey: Englewood Cliffs.

Woodward, P.K. and Griffith, D. V., 1996. Influence of Viscous Damping in the Dynamic Analysis of an Earth Dam Using Simple Constitutive Models. Computers and Geotechnics, 19(3), pp.245–263.

Wotherspoon, L.M. and Pender, M.J., 2011. Integrated modelling of the seismic response of a multi-storey framed structure supported on pile foundations. Proceedings of the Ninth Pacific Conference on Earthquake Engineering Building an Earthquake-Resilient Society, Auckland, New Zealand, 5(088), pp.1–8.

Wotherspoon, L.M., 2006. Three dimensional pile finite element modelling using OpenSees. NZSEE Conference Proceedings, (Napier).

Wu, G. and Finn, W.D.L., 1997. Dynamic nonlinear analysis of pile foundations using finite element method in the time domain. Canadian Geotechnical Journal, 3(Crouse 1992), pp.44–52.

Wu, J.J. et al., 2016. A simplified method for the determination of vertically loaded pile-soil interface parameters in layered soil based on FLAC3D. Frontiers of Structural and Civil Engineering, 10(1), pp.103–111.

Xie, Q. et al., 2013. A parametric study of interface characteristics in a buttress retaining wall. Electronic Journal of Geotechnical Engineering, 18 G, pp.1477–1492.

Xu, R. and Fatahi, B., 2018. Effects of Pile Group Configuration on the Seismic Response of Buildings Considering Soil-Pile-Structure Interaction. Proceedings of GeoShanghai 2018 International Conference: Advances in Soil Dynamics and Foundation Engineering. GSIC 2018. Springer, Singapore

Youd, T.L. et al., 2001. Liquefaction Resistance Of Soils: Summary Report From The 1996 Nceer And 1998 Nceer/Nsf Workshops On Evaluation Of Liquefaction Resistance Of Soils. Jounral of Geotechnical and Geoenvironmental Engineering, 127(April), pp.297–313